UNCLASSIFIED

AD NUMBER
AD801897
LIMITATION CHANGES

TO:

Approved for public release; distribution is unlimited.

FROM:

Distribution authorized to U.S. Gov't. agencies and their contractors; Administrative/Operational Use; SEP 1966. Other requests shall be referred to Air Force Rocket Propulsion Lab., Edwards AFB, CA.

AUTHORITY

AFRPL ltr 20 Dec 1971

THIS PAGE IS UNCLASSIFIED

34

AFRPL-TR-66-229

801897

COMBUSTION STABILITY RATING TECHNIQUES

Final Report

L. P. Combs
F. W. Hoehn
S. R. Webb
et al.

Rocketdyne
A Division of North American Aviation, Inc.
Canoga Park, California

September 1966

This document is subject to special export controls and each trans-
mittal to foreign governments or foreign nationals may be made only
with prior approval of AFRPL (RPPR/STINFO), Edwards, California
93523.

Air Force Rocket Propulsion Laboratory
Research and Technology Division
Edwards Air Force Base, California
Air Force Systems Command
United States Air Force

5

DISCLAIMER NOTICE
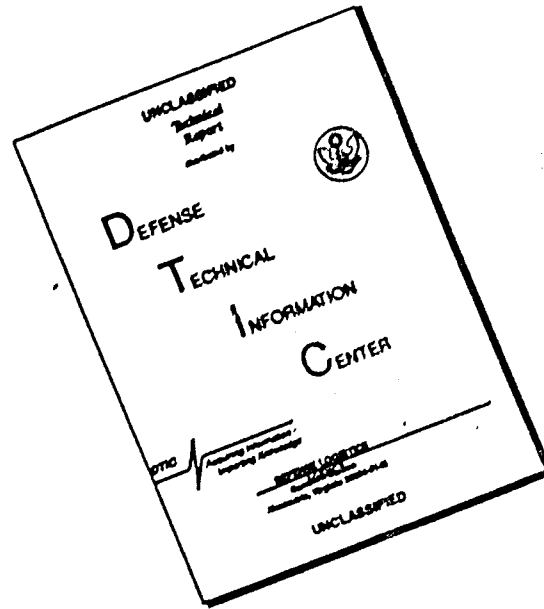
THIS DOCUMENT IS BEST
QUALITY AVAILABLE. THE COPY
FURNISHED TO DTIC CONTAINED
A SIGNIFICANT NUMBER OF
PAGES WHICH DO NOT
REPRODUCE LEGIBLY.

COMBUSTION STABILITY RATING TECHNIQUES

Final Report

L. P. Combs
F. W. Hoehn
S. R. Webb
et al.

Rocketdyne
A Division of North American Aviation, Inc.,
Canoga Park, California

September 1966

This document is subject to special export controls and each transmittal to foreign governments or foreign nationals may be made only with prior approval of AFRPL (RPPR/STINFO), Edwards, California 93523.

Air Force Rocket Propulsion Laboratory
Research and Technology Division
Edwards Air Force Base, California
Air Force Systems Command
United States Air Force

FOREWORD

This report was prepared in compliance with Contract
AF04(611)-10811, PN 3058, PSN 750G, BPSN 623058.

Mr. Thomas J. C. Chew was the project officer for
the Air Force Rocket Propulsion Laboratory.

Dr. R. B. Lawhead was Rocketdyne's program manager,
and Mr. L. P. Combs was project engineer. Additional
Rocketdyne Research Division personnel who contri-
buted to this report were: E. E. Lockwood, J. A.
Murphy, and M. J. Olsasky in cold-flow characteriza-
tion; D. T. Campbell in hot-firing evaluation;
Madeline Alexander and H. Kaspar in analysis and
correlation; and S. Zeldin in technical
photography.

This report has been assigned the Rocketdyne Report
No. 6355-4.

This technical report has been reviewed and is
approved.

<div align="center">

THOMAS J. C. CHEW
Sr. Project Engineer, RPRRC

</div>

ii

ABSTRACT

The objectives of a comprehensive investigation of three techniques for rating the combustion stability of liquid-propellant rocket engines were the establishment of the characteristics of the techniques and of their intercorrelations. The techniques studied were: (1) nondirected explosive bombs, (2) directed explosive pulse guns, and (3) directed flows of inert gases. Characterization was accomplished through cold-flow experiments; each rating device's output pressure, impulse, velocity, etc., were quantitatively correlated to variations of its descriptive parameters, e.g., explosive charge weight, explosive type, burst diaphragm strength, bomb case thickness, etc. Correlating equations are given.

Correlations among techniques were sought by applying them at various positions and directions to an operating rocket and measuring the combustor's stability response. Two different propellant injectors were tested with N_2O_4/N_2H_4-UDMH (50-50) propellants; one of the injectors was tested with N_2O_4/UDMH propellants. The nominal operating conditions were 150-psia chamber pressure and 1.6 mixture ratio. It was discovered that combustion with these propellants and operating conditions is insensitive to transverse velocity or displacement perturbations; the gas-flow technique initiated no chamber pressure disturbances. However, considerable sensitivity to pressure disturbances from bombs and pulse guns was observed.

The combustor's ultimate stability following a pressure perturbation could not be correlated to either bomb or pulse gun parameters or characteristics; recovery to stable operation occurred randomly. The amplitude of the initial pressure wave was correlated quantitatively to both the rating devices' parameters and characteristics. The best correlations were with the parameters, so direct comparison of the techniques through their output characteristics was not possible. The initial modes of instability were qualitatively related to the techniques and their application positions.

By reviewing the determined merits and limitations of the rating techniques, recommendations for selecting a rating method for particular rocket engine programs were developed. The preferred method of rating for general applicability is seen to be a complementary combination of bombs and pulse guns. Recommendations for development of improved rating techniques also are given.

iii/iv

CONTENTS

ILLUSTRATIONS

xiii/xiv

TABLES

SUMMARY AND CONCLUSIONS

Results are reported from a comprehensive study of three techniques for
rating the combustion stability of liquid propellant rocket engines:
(1) nondirected explosive bombs positioned within the combustion chamber,
(2) pulse gun blast wave and explosion products directed into the combus-
tion chamber, and (3) metered flows of inert gases directed into the com-
bustion chamber. The objectives of the study were to characterize the
techniques by means of cold-flow fluid dynamic experiments and to estab-
lish correlations among them through hot-firing determination of a particu-
lar combustor's stability responses to them.

BOMB CHARACTERIZATION

Cold-flow characterization of explosive bombs consisted of exploding them
in the open air and measuring specific characteristics of the resultant
air blast waves. High-explosive charges were encased in closed-end cylin-
drical nylon and Micarta shells and variations of charge weight, charge
length-to-diameter ratio and case thickness were made. Some low-explosive
(fast burning, double-base pistol powder), nylon-case bombs were also
tested.

A Beckman and Whitley Model 200 camera was employed to obtain simultaneous
high-speed streak and framing photographs of the blast waves and Kistler
Model 603A pressure transducers were used for measuring blast-wave pressure-
time histories at specific distances from the bombs. Blast-wave over-
pressures were obtained in three ways, viz., by direct transducer measure-
ment and by calculation with the normal air shock relationships using both
transducer-transit-time-derived velocities and streak-photograph-derived
velocities. The direct transducer overpressure data were less reproducible
and had consistently lower values than the corresponding velocity-derived
overpressures. Direct transducer data were used, therefore, primarily for
measuring blast-wave unit positive-impulse values.

1

Velocity-derived overpressure data were compared with correlations from the literature for blast waves from large, bare, high-explosive charges. Data from two bare charges agreed well with the literature correlations, but overpressures were considerably reduced by encasing the explosives. Overpressures near the bombs were one to two orders of magnitude low, depending upon the case thickness. Blast-wave overpressures from the bombs did not decay as rapidly with increasing distance as do those from bare charges so the bare charge values were reached at some distance from the bomb. Again, that distance depended upon the case thickness.

The initial overpressure data (i.e., at the outer surface of the bomb) were quite well correlated by multiple regression techniques to the high-explosive charge weight and case thickness by an initial velocity correlation:

$$\ln (c_s)_0 = -4.507 + 0.186 \ln W - 0.557 \ln T_c$$

$$(\Delta P)_0 = \frac{7 P_0}{6} \left\{ \left[\frac{(c_s)_0}{a_0} \right]^2 - 1 \right\}$$

Neither changes in charge length-to-diameter ratio nor from nylon to Micarta case material affected the correlation.

Blast-wave velocities measured at distances of 5 to 10 inches from the bomb were similarly correlated with time from the explosion as an additional variable:

$$\ln c_s = \text{constant} + 5.21 \, t - 4.82 \, t^2 + 0.186 \ln W -$$

$$1.05 \, t^2 \ln W - 0.557 \ln T_c + 1.86 \, t \ln T_c - 1.19 \, t^2 \ln T_c$$

A different value of the constant was required, however, for each method or position of data acquisition so this correlation is not nearly as useful as the one for initial blast-wave velocity or overpressure.

2

Blast-wave unit positive-impulse values were obtained by planimeter integrations of the area under the pressure-time records measured with a transducer 10.0 inches from the bombs. These data were well correlated by:

$$\ln I_u = 3.62 + 1.04 \ln W - 0.074 (\ln W)^2 - 0.377 \ln T_c +$$

$$+0.112 \ln (L/D)$$

While the unit positive impulse is specific to the 10.0-inch transducer location, it is still a valid and useful comparative bomb characteristic.

Durations of blast-wave positive overpressures were nearly constant and were only weakly correlated to charge weight. This is, therefore, not a useful characteristic of a bomb.

The low-explosive bombs tested exhibit greater scatter in their pressure amplitude-charge weight-case thickness relationships than did the high-explosive bombs. Further, with thin cases, multiple pressure waves were irreproducibly observed and there was evidence of incomplete powder combustion. Thus, high-explosive charges are preferred.

Cold Characterization of Bombs

The cold characterization of explosive bombs resulted in the following conclusions:

1. High-explosive charges are better for this application than are low-explosive charges. The low-explosive tested exhibited greater scatter in explosion time-delay (fire signal to case rupture) and pressure amplitude- charge weight- case thickness relationships, irreproducible production of multiple pressure waves, and evidence of incomplete powder combustion. Among charges variously composed of PETN, RDX, and Composition C-4, it did not seem to matter which high explosive is used.

3

2. The duration of the first positive overpressure portion of the blast wave is not a valid output characteristic; its value at 10.0 inches from the bomb was nearly constant and was only weakly related to the charge weight.

3. Maximum blast wave overpressure is a valid and useful output characteristic. Its value in ambient air was found to be uniquely determined by the charge weight and confining case thickness. It was found not to vary significantly with the charge shape parameter, cylindrical length/diameter ratio. Overpressures immediately adjacent to the outer surface of the bomb case were those best correlated. Overpressures in the interval 5 to 10 inches away from the bomb surface were quite well correlated by the same expression only if a variable constant were introduced to account for the source of the data. This seriously limits the general usefulness of the correlation; the form based on overpressures at the bomb surface is preferred for calculating this bomb characteristic.

4. Unit impulse of the bomb is a valid characteristic. Its value, as determined at 10.0 inches from the bomb, was correlated well with explosive charge weight, bomb case thickness, and, somewhat, with charge length/diameter ratio. A graphical correlation of overpressure and a reduced distance parameter suggests that the obtained correlation is specific to the 10.0-inch location, and that values at greater distances would presumably be less dependent on the bomb parameters.

5. The characteristic overpressure and impulse correlations obtained for high explosives were not affected by a change of bomb case material from nylon to Micarta. Substantially fewer spurious signals were recorded in the transducer-measured pressure-time data, however, when Micarta was used.

PULSE GUN CHARACTERIZATION

Pulse guns were cold characterized by firing them into a pressurized tank
and measuring some blast-wave characteristics with two Kistler Model 607L
pressure transducers in the gun's discharge barrel. These guns character-
istically produce blast waves having two distinct pressure fronts. The
initial front results from the burst diaphragm rupture and is usually steep-
fronted or shock-like. The second pressure rise, resulting from continued
burning of the explosive charge, is not steep-fronted at first but ampli-
fies the blast wave to its maximum value. This second pressure front prop-
agates at a higher velocity than the initial shock wave and, as it progresses
down the gun barrel, steepens into a second shock wave.

The pressure amplitudes of both of these waves are related to the explosive
charge weight, the burst diaphragm strength, the backpressure in the
receiving tank, and the transducer position downstream of the burst dia-
phragm. The multiple regression correlating equation for the maximum
blast wave pressure is:

$$\ln P_{max} = 8.32 - 1.54 \ln W + 0.32 \, (\ln W)^2 + 0.15 \ln W \ln D -$$
$$0.06 \, (\ln W)^2 \ln D + 0.19 \ln W \ln P_{db} + 0.008 \, (\ln P_b)^2$$

The positive impulse of the pulse gun blast wave was primarily determined
by the charge weight, with tank backpressure exerting only a weak effect
and burst diaphragm strength not even entering the correlation:

$$\ln I_+ = -6.43 + 1.73 \ln W - 0.11 \, (\ln W)^2 - 0.28 \ln D + 0.123 \ln P_b$$

The positive durations of the blast waves, much as found with explosive
bombs, were found to be nearly constant and were not considered to be a
useful characteristic. Blast-wave velocity was correlated but there was
so much scatter in the data that little confidence can be placed in the
correlation.

Several pulse gun charges were fired in which the fast-burning pistol powder (Hercules Bullseye No. 2) was replaced with a slower burning military rifle powder (duPont Military 3031). Very similar trends in initial shock-wave amplitude, maximum blast pressure and impulse were observed although the values were approximately halved by using the less energetic, slower burning powder. Repeatability did not seem to be improved so there was no indication that a change from the "standard" Bullseye powder would be beneficial.

Cold Characterization of Pulse Guns

The cold characterization of explosive pulse guns resulted in the following conclusions:

1. The blast wave produced by the pulse gun characteristically has two pressure spikes. The first is a shock wave resulting from the burst diaphragm rupture. Its amplitude varies both with burst diaphragm pressure rating and charge weight. The second wave is frequently not steep-fronted; it is believed to result from continued combustion, at a high rate, of explosive that had not yet burned when the diaphragm burst. Its amplitude also varies with burst diaphragm strength and charge weight.

2. There was considerable scatter in the pressure data, but valid mean values were obtained by firing replicate charges. Correlation of characteristics to the input parameters made use of those mean values.

3. The maximum blast wave overpressure was correlated with the charge weight, burst diaphragm strength, transducer location (distance from the diaphragm) and pressure of the vessel into which the guns were fired, and was found to be a valid and useful pulse gun characteristic.

4. The blast wave impulse was found to be a valid and useful pulse gun characteristic related primarily to the charge weight and transducer location.

6

5. Initial shock wave velocity, while correlated to the pulse gun parameters, is of questionable validity as a characteristic because of excessive scatter, even in the averaged data.

6. Maximum blast wave overpressures were only slightly influenced by downstream pressure; values at 250 psig were approximately 5 percent higher than values at 150 psig.

7. Values of initial shock wave overpressure, maximum blast wave overpressure, and impulse were approximately halved by replacing the normal fast-burning Hercules Bullseye double-base pistol powder with a lower-burning (by approximately 5:1), less-energetic (by approximately 70 percent), duPont Military 3031, double-base rifle powder.

8. Blast wave positive duration was not a valid pulse gun characteristic, since it exhibited only random variations even when the powder burning rate was changed.

GAS FLOW CHARACTERIZATION

Cold characterization of the gas flow technique consisted mainly of demonstrating that the apparatus assembled could be operated in a manner that would give reproducibly controlled flowrate vs time profiles. The approach taken was: (1) measure the gas flowrate delivered from a fixed gaseous supply system as a function of flow control valve position and downstream pressure, and (2) preprogram the valve position as a function of time so that a particular desired flowrate vs time profile could be produced. This approach permitted selection of any arbitrary flow profile; it was anticipated that linear rates of increase in gas flowrate, momentum or kinetic energy might be used at various times during the rocket engine test program.

Preprogramming of valve position vs time made use of a Donner Model 3750 diode function generator. Satisfactory control was demonstrated by generating ramp flows with linear flowrate increases ranging from approximately

4 to 25 lb/sec^2 with nitrogen and approximately 1.8 to 5.9 lb/sec^2 with helium. At the higher rates, full flow was reached in approximately 250 milliseconds.

The system originally assembled had maximum flowrates of approximately 5 and 1.5 lb/sec with nitrogen and helium, respectively. Higher values were desired for engine pulsing, so an additional surge tank was intalled in the gas flow generation system without re-evaluating its characteristics.

ENGINE STABILITY EVALUATION

The relative effectiveness of the stability rating techniques in determining a rocket combustor's stability traits was investigated by applying the techniques at various positions in an operating rocket and observing their effects on its stability. The nominal 10,000-pound-thrust, cylindrical rocket combustor employed was operated at fixed conditions of 150-psia chamber pressure and 1.5 to 1.6 mixture ratio with N_2O_4/N_2H_4-UDMH(50-50) propellants. Straight UDMH was also used as the fuel during some tests. Two different injectors were tested: one had an unlike triplet injection element pattern, the other had a pattern composed of both self-impinging doublet and unlike doublet elements. The injection end of the combustion chamber was fitted with a three-radial vane, uniformly spaced baffle assembly that had provided dynamic combustion stability in an earlier ablative chamber use of these injectors. During the current studies, a metal-walled chamber was used to better accommodate a multiplicity of rating technique positions and instability-monitoring pressure transducers.

The response of the combustor to each disturbance was measured by three or more flush-mounted Photocon Model 1325 pressure transducers. The transient pressure data were reduced and recorded in sufficiently detailed form that the rating techniques could be correlated successively to: (1) the initial response of the combustion processes, (2) the initial mode of combustion instability triggered, (3) transitions to other instability modes, and (4) whether recovery to stable operation or a sustained instability was experienced.

8

Quantitative correlations were obtained which relate the initial response
of the combustor, as indicated by the amplitude of the first observed
pressure wave, to the parameters and characteristics of the rating tech-
nique. The initially triggered mode(s) of combustion instability · ld
be related only qualitatively to the position and orientation of th· rat-
ing device; quantitative correlations broke down at this step.

Response of Combustor to Gas Flow Rating Technique

From the hot-firing tests in which directed flows of gaseous nitrogen
and helium were admitted to the combustion chamber, the following
conclusions have been drawn:

1. Steady-state combustion of the storable N_2O_4/N_2H_4-UDMH (50-50)
   propellant combination, under the conditions tested, is insen-
   sitive to transverse gaseous displacement disturbances; i.e.,
   such disturbances do not result in measurable pressure
   disturbances.

2. Inert gas flowrates ranged up to about 25 percent of the main
   propellant flowrates and were injected at velocities up to the
   inert gas stream sound velocities with no apparent change in
   the lack of displacement sensitivity. Even quite high rates of
   flowrate changes (which may be comparable with the transient
   propellant spray gasification and combustion triggered by a
   pressure wave's passage) were not able to affect the spray
   combustion enough to generate a pressure wave.

3. Among tests with tangential, chordal and radial directions
   of gas injection, no apparent differences in the lack of dis-
   placement sensitivity were discerned.

4. The tangential and chordal gas injection established vigorous
   transverse eddy flow patterns near the injector on a scale
   that is large compared to the spacing between injection elements.
   Observation of events within the chamber by means of high speed
   motion cameras looking up the exhaust nozzle was invaluable in
   determining this fact.

9

Initial Combustor Response to Explosive
Bomb Rating Technique

The attempts to correlate observed initial pressure wave amplitude data
to the cold-flow characteristics and/or input parameters of non-directional
explosive bombs resulted in the following conclusions:

1. The initial combustor response to pressure disturbances from
   bombs, as indicated by the amplitude of the initial pressure
   wave, can be successfully correlated to the device's character-
   istics and/or design parameters and its location in the combustor.
   Bomb charge weight and case thickness are very influential param-
   eters, while charge shape (L/D) is unimportant. The case thick-
   ness had a strong residual effect in correlations using bomb
   output characteristics that is unexplained. Of the bomb position
   variables, the distance from the injector is clearly the most
   influential.

2. The initial pressure wave data, as recorded, can be used as an
   adequate measure of the combustor's stability response. The
   resultant correlation models are very complex, however, and
   cross-comparisons among injectors, chambers, rating devices or
   other variables are made very difficult and qualitative. Ad-
   justment of the data by means of an incidence coefficient, which
   accounts for variations in pressure wave incidence among the
   transducers, may remove much of the complexity and improve the
   ease and validity of comparing correlations.

3. Measureable pressure waves resulted from detonation of every
   bomb used in the hot-firing tests. High-explosive charge weights
   from 3.2 to 25 grains were used.

4. Increased amplitudes of the initial pressure waves resulted
   from increased charge weights. This effect had an upper limit,
   however, since 25 grain charges resulted in amplitudes com-
   parable to those from 13.5 grain charges. Reasons for the effect
   and for its upper limit were not determined.

10

5. The pressure wave amplitudes, as adjusted by an approximate incidence coefficient, remained essentially invariant with transverse distance from bombs in the triplet injector tests and increased slowly in the doublet injector tests. The response which the propellant spray combustion field is capable of exhibiting is apparently a direct function of the disturbance amplitude, otherwise each wave would continue to grow in time to the same equilibrium amplitude. Some fundamental investigation of this phenomenon appears to be needed.

6. The spray combustion field established by the doublet injector was distributed over a longer portion of the combustion chamber and contained more spray than that from the triplet injector. This was deduced from observation with the doublet injector of: (a) higher initial wave amplitudes, (b) smaller effect of bomb distance downstream from the injector, (c) continued wave growth in the transverse directions, and (d) lower combustion efficiency, than with the triplet injector.

7. Similar observations for N_2H_4–UDMH(50-50) fuel as compared with neat UDMH fuel suggest that the combustion process is more distributed with the former, mixed fuel. Considering the higher latent heat of vaporization and surface tension of hydrazine, this is a physically realistic result.

8. Bomb orientation effects were not included in the data correlations, which were based wholly on cylindrical bombs whose axes were parallel to the chamber's cylindrical axis. Results from a few bombs installed with their axes normal to the chamber's axis indicated appreciable effects which deserve continued investigation.

9. Similarly, bombs installed in or near the converging section of the exhaust nozzle gave inexplicably high initial wave amplitudes and should be investigated further.

11

Initial Combustor Response to Explosive Pulse
Gun Rating Technique

The attempts to correlate observed initial pressure wave amplitude data
to the cold-flow characteristics and/or input parameters of the directed
pulse guns led to the following conclusions:

1. The initial combustor response to blast waves from pulse guns,
    as indicated by the amplitude of the initial pressure wave, was
    correlated successfully to the device's parameters and character-
    istics and to the position and direction of application to the
    combustor. Charge weight, burst diaphragm strength, barrel
    diameter and barrel length were all influential parameters but
    were overshadowed by application effects.

2. The correlation models were complicated by a number of chamber
    distance terms which, unlike the bomb models, were not particu-
    larly simplified by adjusting the initial wave amplitude data
    with incidence coefficients. This probably resulted from a
    directional, rather than simply spherical, wave propagation.

3. The initial pressure wave propagated with an apparently pseudo-
    spherical expansion from the pulse entry point. Its front
    appeared to be more like a shock wave and propagated faster in
    the direction of pulse gun orientation than in other directions.

4. The initial pressure wave amplitudes, near the pulse gun entry
    point, generally increased with increasing charge weight, burst
    diaphragm strength and barrel diameter and decreased with in-
    creasing distance of the entry point from the injector.

5. The amplitudes at greater distances from the entry point con-
    tinued to depend upon the parameters when the pulses were
    directed radially or chordally. Tangentially directed pulses,
    however, tended to give higher and nearly equal initial wave
    amplitudes on the opposite side of the chamber from the entry
    point.

6. With tangentially directed pulses, the initial wave amplitude
    near the entry point may be primarily controlled by burst
    diaphragm strength.

7. Waves whose initial amplitudes near the entry point were less
    than 40 psi were attenuated rather than amplified.

8. Higher initial wave amplitudes resulted from using the doublet,
    rather than the triplet, injector and from using N_2H_4-UDMH (50-50)
    fuel, rather than neat UDMH fuel. These observations are con-
    sistent with the bomb ratings.

Ultimate Combustion Stability

The ultimate stability appeared to be only remotely related to the rating
techniques. Rather, it seemed to be determined by a complex interaction
among the initial acoustic mode(s), a low-frequency chug, and the transi-
tion to subsequent instability modes. Sustained instabilities were almost
invariably a coexistent combination of the third tangential and first radial
acoustic modes. Driving of the third tangential, or first transverse baf-
fle compartment mode, appeared to be the key to a sustained instability.
That mode was rarely observed in the first 3 to 5 milliseconds after the
initial pressure wave. That time period included an initial surge in mean
chamber pressure and a decay to the lowest pressure portion of the frequency
chug. The appearance of the third tangential mode depended upon appreciable
amplification of the first tangential acoustic mode during the period of
recovery from the depth of the chug. These phenomena were not successfully
correlated to the trigger devices.

The sustained instability was the second tangential mode during several
tests with the doublet injector, notably those in which a bomb was inserted
radially through the chamber wall and approximately one-half of those in
which UDMH was the fuel. This difference was not explained.

13

COMPREHENSIVE COMPARISON AND RECOMMENDATIONS

A comprehensive comparison is drawn among the rating techniques by considering their relative merits and limitations for engine application and other attributes such as effectiveness, repeatability, reliability, and handling characteristics. A summarization of the relative merits and limitations is presented on the following page.

The fact that the correlations derived from bomb data were best described by a linear model and the pulse gun data were best described by a logarithmic model makes it difficult to make a direct comparison of the effects of the techniques. It was apparent that variations in charge weight had a much stronger influence on the resultant pressure disturbance with bombs than with pulse guns. The other variables cannot be directly compared.

Aside from the complexity of the models, an additional difficulty is that the characteristics of the techniques, though related, were not absolutely comparable. The initial cold-flow blast-wave pressures produced by a given bomb charge weight, for example, were lower than the maximum blast-wave pressures measured in the pulse gun barrel by factors ranging from approximately 2 to 50, depending upon case thickness and diaphragm strength. A more directly comparable characteristic of the pulse gun might be the blast-wave pressure amplitude immediately downstream of the termination of the barrel in the combustion chamber wall.

This study has yielded considerable detailed information on the effectiveness and applicability of stability rating techniques to liquid rockets. The ultimate stability of the combustor could not be correlated to either bomb or pulse gun parameters or characteristics; recovery to stable operation occurred randomly. The amplitude of the initial overpressure was correlated quantitatively to both the parameters and characteristics of the rating devices. Generalized correlations between techniques were not established, however. The initial modes of instability were qualitatively related to the techniques and their position of application.

MERITS AND LIMITATIONS OF RATING TECHNIQUES

	Bombs	Pulse Guns	Gas Flows
Merits	Rate pressure sensitivity	Rate pressure sensitivity	Rate displacement sensitivity
	Best correlated technique	Charges protected from heat	Potential for quick rating in a few tests
	Small size	Multiple guns per test possible	Does not disrupt chamber flow
	Minimum external access required	Charges not fired in a test are not discarded	Limited hazard to chamber (no shrapnel)
	Voids permit many positions from a port	Precise fire control (timing)	Possibility of chemical effects
	Best access for regeneratively cooled combustion chambers	Modest size	Precise control
	Materials readily available at modest cost	Directionality permits forcing particular modes	Good reproducibility
	Position versatility, i.e., not restricted to wall	Handling hazards are minimized	Limited handling hazards
	Disturbances are nondirectional	No chamber flow disruption	
Limitations	Shrapnel damage to engine parts	Require access to positions external to engine	Does not rate pressure sensitivity
	Initiation needs electrical circuit with external access	Multiple bosses are required for multiple pulses or varying location	Not known to simulate natural triggering mechanisms
	May disrupt normal chamber flow	Limited to chamber wall application	Multiple bosses required for varying location
	Heat transfer to case may change structural and explosive characteristics	Limited availability of some components	Limited to chamber wall application
	Liable to thermal detonation	Complex wave form is produced	Extensive supply and flow control system may be required
	Subject to structural failure; limited to one per test	Poor reproducibility (cold flow)	Large quantities of gas may be needed for triggering
	Orientation effects sensitivity	Ports may affect stability or acoustic cavities	Ports may affect stability or acoustic cavities
	Hazardous to handle		
	Must dispose of live bombs not exploded during a test		
	Possibility of ejecting live bombs from chamber		

15

The current effort with the explosive bomb and pulse gun rating devices
has shown that although both are capable of producing a disturbance which
in turn may cause a sustained combustion instability, each of the methods
has certain operational disadvantages. An additional effort is required
to investigate improvements on these two basic methods of combustion insta-
bility rating devices as well as new rating devices.

It is expected that a relatively simple modification of the design of
these devices would partially overcome some of their shortcomings. For
instance, either the use of a high-burning-rate powder or modification
of the barrel length of the pulse gun should introduce a more definite
and steep-fronted wave into the chamber. Modification of the bomb case
material would produce less shrapnel than the nylon or Micarta cases
which are currently used.

Although the existing rating devices can be improved to the point of
increased versatility, it is doubtful that a particular technique can be
made into a universally applicable device.

INTRODUCTION

BACKGROUND

Experience has shown that liquid propellant rocket engines occasionally
operate unstably, with moderate to high amplitude oscillations in pro-
pellant burning rates and, therefore, in combustion chamber pressure.
While several types of combustion instability have been identified and
studied extensively, the most difficult to control and eliminate have
been those destructive oscillations corresponding to the cross-sectional
acoustic resonances of the rocket combustion chamber. Because the fre-
quencies, pressure distributions, and phases exhibited by these insta-
bilities are similar to those obtained from linear solution of the wave
equations, they are commonly referred to as "acoustic instabilities,"
even though they are usually nonlinear and sometimes resemble detonation
waves.

The sources of energy for driving acoustic instabilities are predominantly
the propellant atomization, mixing, gasification, and combustion processes*,
i.e., those processes that are confined within the combustion chamber.
Pressure wave motion within the chamber interacts with the propellant
spray combustion process and effects transient changes in the local pro-
pellant burning rates. For the wave motion to be sustained (i.e., the
pressure wave amplitude increased or maintained), a proper phase relation-
ship must exist between the oscillating pressure and the oscillating burn-
ing rate. In most cases of acoustic instability, the coupling appears
to be quite direct because each wave affects the propellant combustion
strongly enough that sustaining combustion energy is added directly to
that wave. A single, finite-amplitude pressure disturbance thus can be
amplified and result in oscillatory combustion. Additionally, however,

---

*It is possible, even probable, that propellant injection rate oscillations
occur during an acoustic instability and thus influence the instability
driving processes. This may be an important factor in the establishment
of a sustained instability. Once an instability is established, however,
injection rate oscillation is usually considered to be a second-order
effect, resulting in a somewhat higher or lower pressure oscillation
amplitude than if the injection rates were invariant.

sustaining an acoustic instability requires that the altered spray combustion field must be capable of responding positively to successive wave passages, adding at least as much or more energy to each wave as the damping processes remove.

The initiation of acoustic instabilities is frequently a nonlinear phenomenon, (i.e., a weak disturbance or oscillation in the combustion chamber may not be capable of affecting the combustion processes enough for the disturbance to be amplified), while a somewhat larger disturbance may be amplified very rapidly. It has long been believed that a relationship exists between a rocket's inherent stability of combustion and its ability to absorb large disturbances yet maintain its steady-state operation. This belief forms the basis for combustion stability rating.

Rating Combustion Stability

The objective of stability rating testing is the determination, in as few tests as possible, of the relative resistance of candidate engine systems or components to the initiation and sustaining of destructive or otherwise objectional oscillatory combustion. Rating techniques may be divided into two broad categories: (1) those that rely upon the spontaneous occurrence of unstable combustion, and (2) those that introduce finite disturbances into the combustion chamber in attempts to initiate instabilities artificially. Techniques in each category have definite advantages as well as some specific shortcomings.

Disturbances that are large enough to trigger an instability may occur naturally during normal rocket engine operation. If they occur frequently, every test may be unstable; if infrequently, only an occasional test may be unstable. One method for rating a system's inherent stability, then, has been the observation of the percentage of tests that are spontaneously unstable during normal operation. This approach is obviously prohibitively expensive for evaluating the effects on system stability of seemingly minor component variations or improvements. An alternate spontaneous rating method that has occasionally been used involves a systematic

18

variation of operating conditions until a region of spontaneous instability is found and its boundary at least partially mapped out. The rating then consists of determining how the instability boundary shifts when an engine component change is made. Distance of the normal or design operating conditions from the boundary of an unstable region is presumed to be synonymous with resistance to spontaneously occurring instabilities.

Parameters that have been varied in this kind of stability rating are the injection mixture ratio, the chamber pressure (by variation of either propellant flowrates or chamber contraction ratio), and propellant temperature. The majority of such rating has been carried out in research-scale rocket motors designed for relatively inexpensive and frequent testing. This method has been used only infrequently for large engine ratings; by far the greatest use in this regard has been in the rating of LO_2/H_2 engines by varying the hydrogen injection temperature.

The following advantages may be ascribed to rating techniques that rely on spontaneous occurrence of instability:

1. The ratings are associated with naturally-occurring disturbances.

2. Application of the technique does not disrupt the normal combustion chamber flow patterns by foreign bodies or substances.

3. The ratings may be quite reproducible.

Conversely, some disadvantages may be:

1. A relatively large number of tests may be required for obtaining a single rating.

2. The instability rated may not be the one most likely to be initiated by an occasional large disturbance at the normal operating conditions.

19

3. No indication is obtained of the initial disturbance magnitudes experienced in obtaining ratings. (The amplitude of the resultant pressure wave, however, may be related to that magnitude.)

4. If operating conditions are varied, the rating may be obtained at conditions far removed from normal or realistically useful operating conditions.

5. If, operating conditions are varied, determined boundaries may be associated with driving mechanisms which are different than those experienced under normal operating conditions (e.g., a region may be encountered where instability is driven by feed-system-coupled injection rate oscillations).

The second category—the introduction of a finite amplitude disturbance for artificial instability initiation—provides a means of rating at the normal operating point. Advantages are:

1. The disturbance can nominally be controlled as to time of initiation so that limited hardware exposure to a destructive condition may be scheduled.

2. Disturbances can be sequenced in graduated sizes to provide quantitative relative magnitudes.

3. More than one disturbance can sometimes be introduced in a single test.

4. The mode of instability initiated may be controlled by proper selection and positioning of the disturbance source.

Disadvantages are imposed by the disruption of normal propellant flow if a device is inserted in the chamber, by irreproducible device behavior or combustion response from test to test, and by uncertainties as to whether the artificial disturbance bears any relationship to naturally occurring triggers that might occasionally be encountered. These disadvantages are so outweighed by the advantages and by the need for valid stability ratings that the rating techniques based on artificial initiation of instability have been employed in a large number of engine development and research programs during the past 10 to 12 years.

Three basic techniques have been used for the majority of the ratings obtained or sought using artificial instability initiation:

1. Nondirected explosive bombs placed at various locations within the combustion chamber

2. Explosive blast waves from pulse guns directed into the combustion chamber through the chamber sidewall

3. Directed flows of inert or reactive gases similarly introduced near the injector

Various investigators have preferred one or another technique, and different rocket systems (with variations of size, combustor configuration, injector concept, operating conditions, propellant combination, etc.) have exhibited varying degrees of sensitivity to a particular technique. Since ratings have been sought with all three methods only in a few isolated and incomplete studies, meaningful comparisons among the stability traits of systems or the applicability of techniques have not been possible.

The investigation that is the subject of this report was conducted in an attempt to establish generalized correlations among rating techniques and their effects in initiating unstable combustion.

Recorded Pressure Terminology

The cold-flow characterization of the explosive bombs were obtained in ambient surroundings. Such terms as blast wave peak overpressure, peak ove. pressure, blast wave pressure, shock wave overpressure, etc. refer to the amplitude of steep-fronted shock waves measured at a finite distance from the center of the explosion. The magnitude was obtained from either direct pressure transducer recordings or calculated from Rankine-Hugoniot shock relationships. The initial shock wave overpressure, however, refers to the amplitude measured at the bomb-case surface.

21

The cold-flow characteristics of the pulse guns were obtained by firing them into a pressurized vessel. Pressure transducers were located within the gun barrel at two different positions. All records, with one exception, were obtained photographically from an oscilloscope trace. A point of similarity among the various pressure traces was the apparent occurrence of two shock waves. The initial steep-fronted pressure rise was undoubtedly a shock wave resulting from the burst-diaphragm rupture. The magnitude of this recorded pressure is referred to as the initial overpressure or initial shock wave pressure. The secondary shock wave usually propagated faster than the initial wave and thus tended to overtake it. It is identified as the second pressure rise or front, maximum blast overpressure, maximum blast wave pressure, or simply as the peak pressure.

Pressure transducer outputs during the hot-firing program were recorded on a seven-channel tape recorder. The response of the combustor to the device disturbance was indicated by the amplitude of the first observed pressure wave. This wave is interchangeably referred to as the initial peak pressure, initial overpressure, initial peak overpressure, peak pressure and initial pressure wave.

COLD-FLOW CHARACTERIZATION

EXPLOSIVE BOMBS

In rating rocket combustion stability with explosive bombs, small explosive charges are detonated at strategic locations within an operating rocket combustion chamber, and the response of the propellant combustion processes to the bomb disturbances are observed. Bomb charges must be insulated from the combustion gases to avoid premature thermal detonation. Protective cases made of Micarta, Teflon, nylon, and composite ablative materials have been used in previous investigations. If thermal detonation is to be avoided for more than 2 to 3 seconds of mainstage operation, it may be necessary to use such protective assemblies as a spun fiberglass heat shield slipped over a machined nylon bomb case.

Bomb disturbances are usually intended to be nondirectional, i.e., to produce a blast wave which propagates spherically from the bomb location. An ideal bomb configuration, then, might be a spherical explosive charge, containing an electrically initiated detonator, tightly confined in a spherical insulating shell. Production of the ideally spherical blast has not been emphasized however, because of great practical advantages in making cylindrical, rather than spherical, charges, viz., lower case machining costs, ability to firmly pack different charge weights into one size of case, easier explosive loading, conformity to the cylindrical shape of most electrical initiators, and easier design for supporting the bomb.

Most previous rating studies employed a simple cylindrical bomb design; this design was used exclusively in this program, as well. Each bomb case was machined from a solid piece of a single material. The explosive charges were packed into the closed end of the protective cases and made to conform, as nearly as practicable, to a cylindrical shape. The bomb assemblies were attached or supported from the opposite, or open end.

23

Experimental Program

Cold-characterization experiments provided data for relating bomb output
characteristics to bomb descriptive parameters. The experiments con-
sisted of exploding a large number of bombs in the open air and measuring
specific characteristics of the resultant air blast waves, e.g., velocity,
peak pressure amplitude, the duration of the positive pressure portion
of the wave, and positive unit impulse. The characteristics were measured
by simultaneous use of pressure transducer and high-speed photographic
instrumentation. To get satisfactory records, particularly from the
pressure transducers, some development of the experimental arrangement
was necessary. In this section, the experimental approach taken, the
instrumentation used, and the various modifications made are discussed.

Experimental Approach. A schematic diagram of the experimental apparatus
is shown in Fig. 1; a bomb is shown mounted near the edge of a large
metal plate in which two pressure transducers are mounted. In an edge
view (Fig. 1a), it can be seen that the center of the explosive charge
is in the same plane as the top surface of the plate. The transducers
are thus oriented to measure the pressure-time history of the bomb blast
wave in "side-on" or grazing incidence as it propagates across the plate.
This orientation was chosen to minimize the possibilities for spurious
pressure signals and transducer damage resulting from bomb fragments
impacting the transducers. The use of two transducers gives data regard-
ing the average wave velocity, and changes in wave shape and amplitude
between the two positions.

Photographic equipment is shown in Fig. 1b as being aligned with a trans-
ducer station to obtain simultaneous streak and framing photographic
records of the blast wave traversing that position. From the wave velocity
determined from the streak film, together with knowledge of the ambient
air properties, the peak pressure associated with the wave can be calcu-
lated from Rankine-Hugoniot shock relationships. In some experiments,
streak photography was used to obtain peak pressure measurements at the
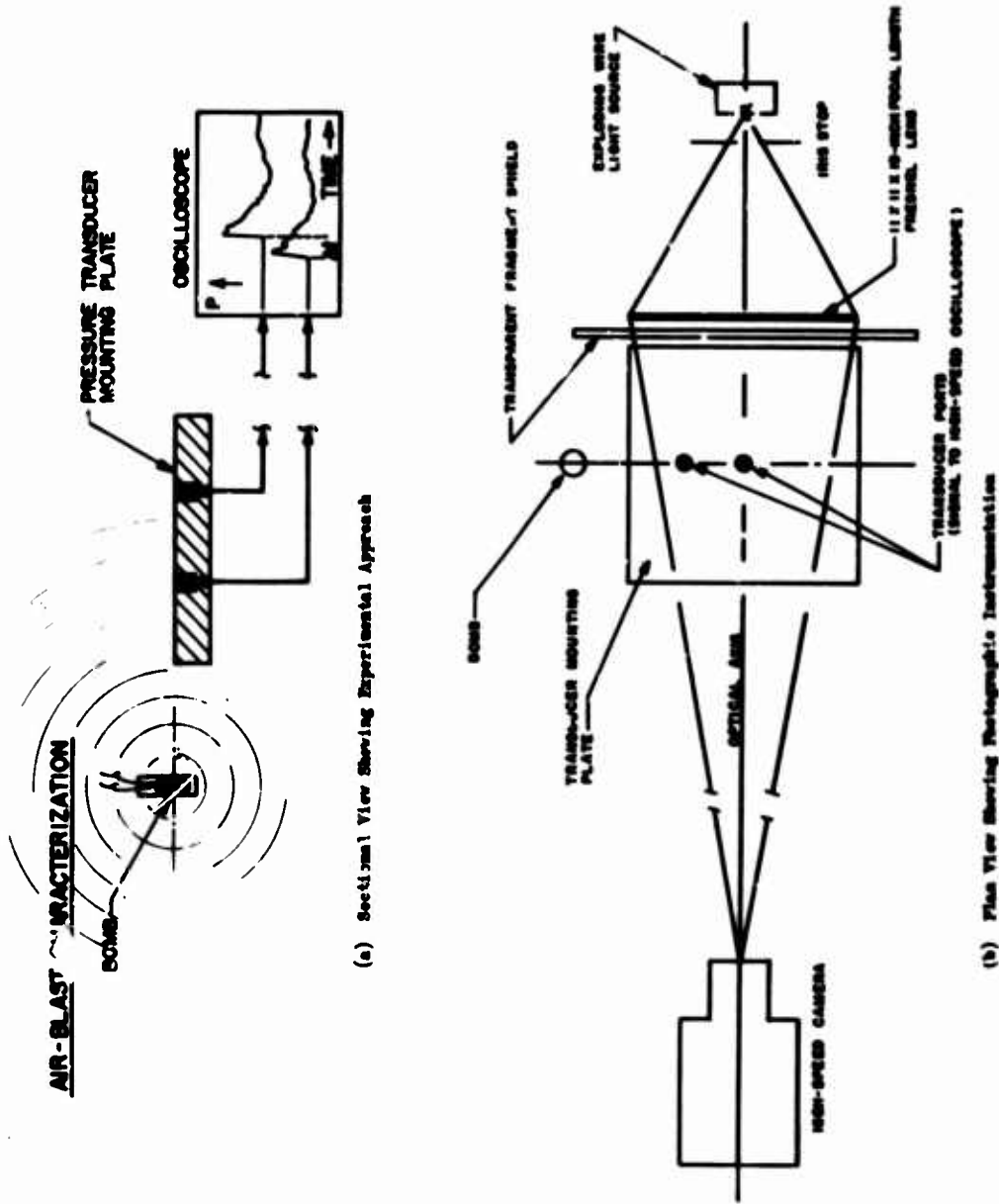
Figure 1. Apparatus for Cold-Characterization of Explosive Bombs

transducer locations for comparison with the direct transducer pressure data. In other tests, the photographic equipment was aligned with the bomb to provide data on the peak pressure at the bomb surface. The sequence of framing photographs provided a visual record of the shock wave and particle motion as an aid to interpreting the pressure data.

Photographic Instrumentation. Simultaneous streak and framing photographs of the blast waves were obtained with a Beckman and Whitley Model 200 camera. That air-turbine-driven, rotating-mirror camera had previously been used in a study of detonator fragmentation and so was essentially already set up and checked out. The camera control circuitry includes an event-initiating (fire-control) circuit which signaled bomb detonation when the camera achieved a preselected speed. For all but a few of the initial checkout experiments, the camera was set to record at a turbine (mirror) speed of 333 revolutions per second. At that speed, the streak film writing rate was 0.9206 mm/microsec and the framing pictures were taken at 73,260 pictures per second. With the framing stop used, exposure times were 3.23 microseconds per picture. A total of seven pictures were obtained in each sequence.

The photographs, both framing and streak, were shadowgraphs, having been obtained with a focused backlight beam. The light source was a 0.75-inch-long, 5-mil exploding tungsten wire; the duration of usable light was approximately 100 microseconds. An 11-1/2 by 11-1/2-inch plastic Fresnel lens with a 19-inch focal length was used to converge the light into the camera lens. The bomb was fired between the Fresnel lens and the camera. The effective field of view was approximately 8 inches high by 10 inches wide.

Pressure Instrumentation. A review of commercially available transducers led to selection of the Kistler Model 603A piezoelectric transducer as the one most likely to be suitable for obtaining satisfactory pressure-time records from bomb explosions. Since costly transducer damage could

26

result from direct impingement of bomb fragments on the transducer sensing diaphragm, mounting the transducer for side-on, rather than face-on, wave incidence was selected. Side-on incidence was also expected to permit direct comparison between the transducer-derived and wave-velocity-derived peak pressure data without need for considering wave-reflection coefficients.

Preliminary Evaluation. Before ordering transducers for this experimental work, a series of development tests was conducted to determine whether adequate transducer mounting and placement could be achieved, and whether fragment damage might be a major or a minor problem. An early version of the Kistler Model 603A transducer (on loan from another program) was flush-mounted, off-center in a 24-inch by 24-inch by 1-inch-thick aluminum plate. This transducer mounting plate was placed on a 6-inch-deep bed of sand for dampening plate vibrations. Initially, no attempt was made to shock mount the transducer; the available unit was neither acceleration compensated nor supplied in a shock-resistant adapter.

Available surplus 13.5-grain, plastic-cased detonators were used (without protective bomb cases) to provide blast waves. Tests were made initially with the center of each detonator located 18 inches horizontally from and 4 inches above the transducer. When no evidence of transducer damage was observed, those distances were reduced in successive tests. Some sketches of bomb and transducer locations, and examples of the recorded signals are summarized in Fig. 2.

Two undesirable characteristics were recorded in the transducer output signal: (1) A low-frequency (< 5000 cps) oscillation or wandering about the ambient pressure line occurred before the arrival of the air-blast wave (Fig. 2b and 2c), and (2) a high-frequency (~ 150,000 cps) oscillation followed the passage of the shock wave. By striking the plate at the bomb position with a hammer, the low-frequency oscillation

was determined to be resonant ringing of the transducer mounting plate (Fig. 2d). Three changes were made which helped to minimize this spurious signal:

1. The transducer was floated in a mass of RTV rubber.

2. The detonator was moved off the edge of the transducer mounting plate and lowered so that the center of the explosion was in the plane of the plate surface.

3. The edge of the plate nearest the bomb was shielded from direct bomb fragment and blast wave impact by a separate, isolated reflection member (Fig. 2h). The bed of sand was replaced with a wooden mounting block when this isolation shield was added.

The high-frequency oscillation was identified as a resonant frequency of the particular pressure transducer. This oscillation was reduced to a satisfactorily low amplitude by electronic compensation using a Rocketdyne Dynamic Analog Differential Equation Equalizer (DADEE). The resonant frequency of this transducer is just at the upper limit of the DADEE which was available, so precise matching was not accomplished. The amplitude of the resonance in the recorded signal was reduced acceptably in most cases; however, the DADEE electronics introduced a noise at about 1 megacycle which was removed by using a 200-kilocycle cutoff filter. Some typical results using this unit and conditions comparable with Fig. 2i are shown in Fig. 3. The pressure calibration for Fig. 3 is uncertain because of undetermined gain introduced by the DADEE. That preliminary evaluation demonstrated that satisfactory pressure-time data could be obtained with transducers as close as 11 inches to the plastic-cased detonators. This evaluation was terminated after firing a 50-grain bomb in a 3/16-inch-thick nylon case, and observing no transducer damage or adverse degradation of the pressure measurement.

Continued Transducer Evaluation. Discussion with Kistler representatives disclosed that the newer Model 603A transducers are acceleration

28
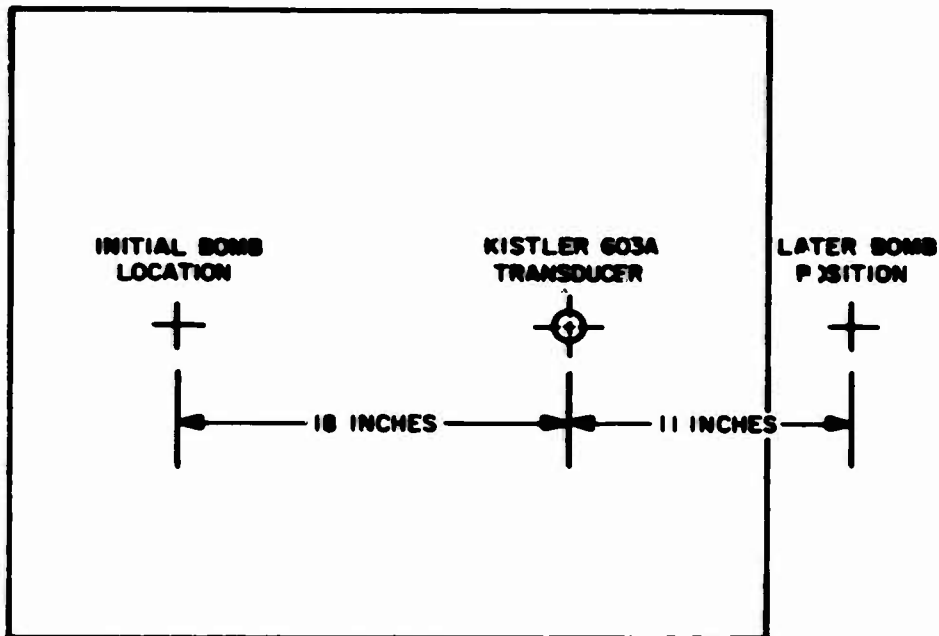
(a) Plan View of Transducer Mounting Plate

(c) Detonator 4 Inches Above Bomb Position With 1/2-In Under Detonator

(b) Detonator 4 Inches Above Plate in Initial Bomb Position

(d) Plate Struck at Initial With a Hammer

A

20μ - SEC/CM

ater 4 Inches Above Plate in Initial
Position With 1/2-Inch Foam Rubber
Detonator

20μ - SEC/CM
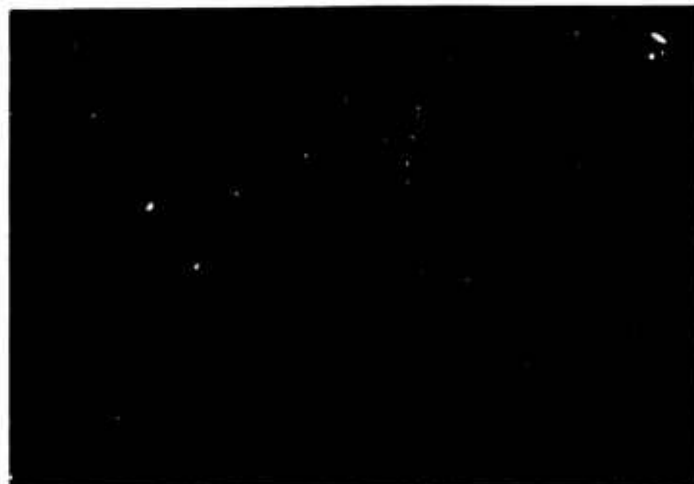
(e) Detonator Level With Plate in Later Bomb
Position

I MILLISEC/CM

te Struck at Initial Bomb Position
a Hammer

NOTE: All oscilloscope photographs in
Fig. 2 and 3 have equal vertical
sensitivities equivalent to
approximately 5 psi/cm.

Figure 2. Summary of Kistler Model 603A (Early
Version) Transducer Evaluation
Experiments

29

β

ᴧ
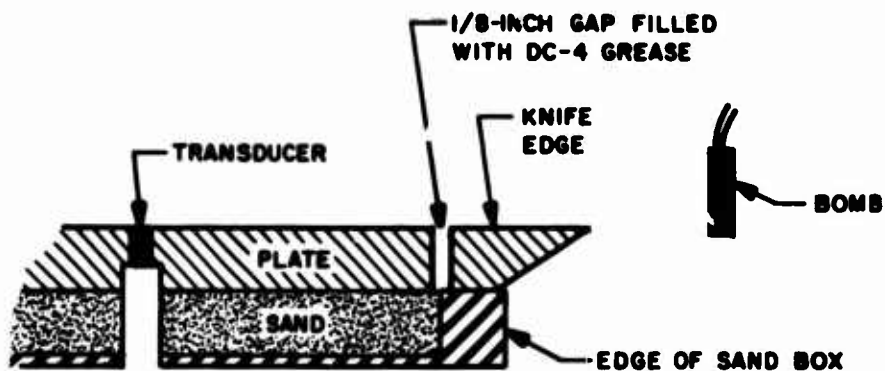
(f) Sectional View of Transducer Mounting
     Plate With Knife-Edge Isolator
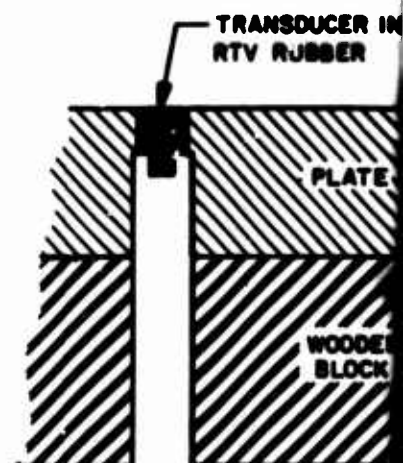
(h) Sectional View of Mod
     Transducer Mounting

20μ - SEC/CM

50μ - SEC/CM

(g) Detonator 18 Inches From Transducer, In
     Plane of Plate With Knife-Edge Isolator

(i) Detonator 11 Inches From
     Plane of Plate of Fig. 2

A
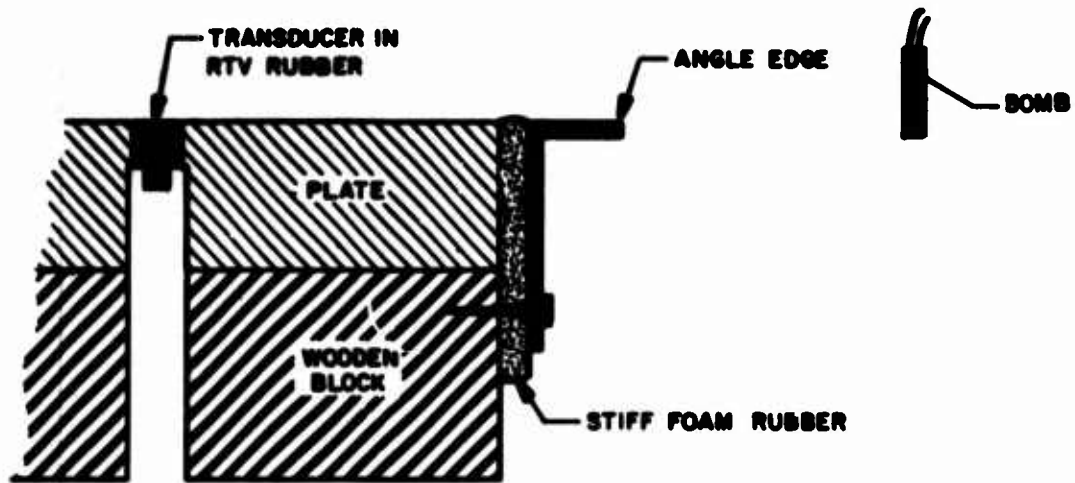
(h) Sectional View of Modified Configuration for
     Transducer Mounting Plate

50μ - SEC/CM
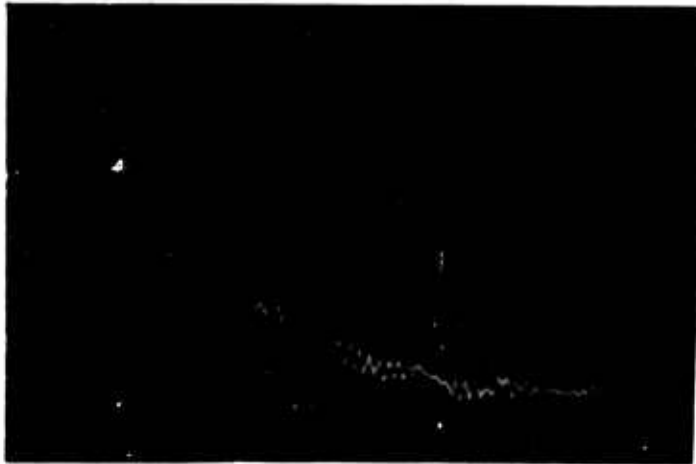
(i) Detonator 11 Inches From Transducer In
     Plane of Plate of Fig. 2h

Figure 2. (Concluded)

TRANSDUCER

CHARGE
AMPLIFIER

A

DADEE

BAND-PASS FILTER

20 CYCLES
TO 200 KILOCYCLES

OSCILLOSCOPE
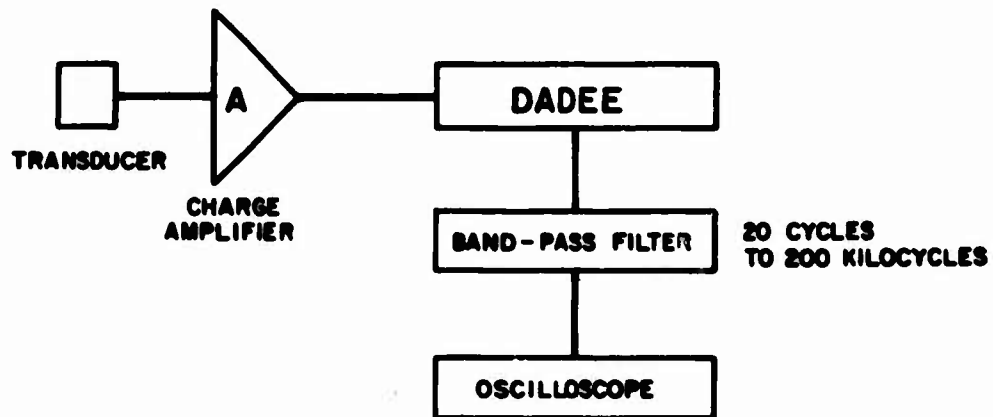
(a)   Block Diagram of Transducer Electronic Circuit

(c)   Same
      Cuto

50μ - SEC/CM
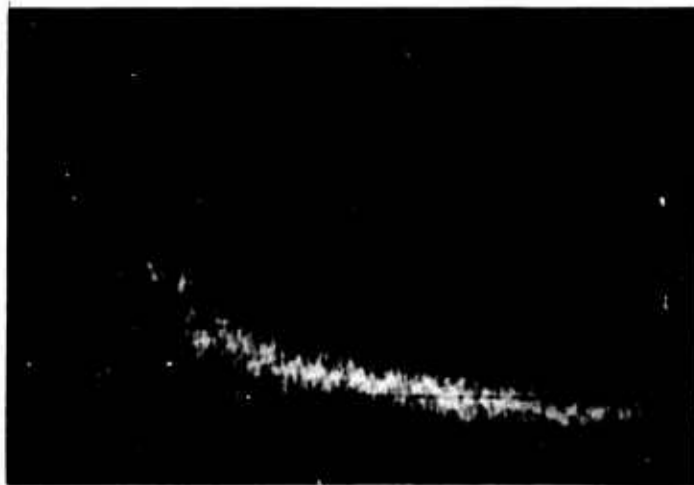
(b)   Detonator and Transducer Configuration
      Same as Fig. 2i but With DADEE,
      Unfiltered

(d)   R

A

$80\mu - SEC/CM$
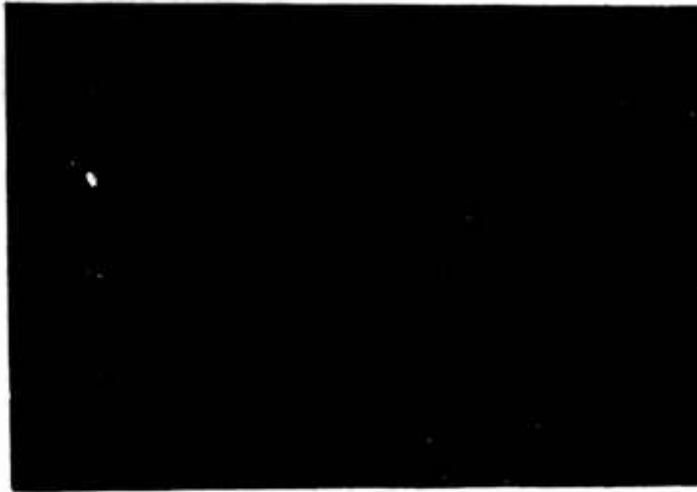
(c) Same as Fig. 3b but with 200,000 cps Cutoff Filter

$80\mu - SEC/CM$

NOTE: All oscilloscope photographs in Fig. 2 and 3 have equal vertical sensitivities equivalent to approximately 5 psi/cm.
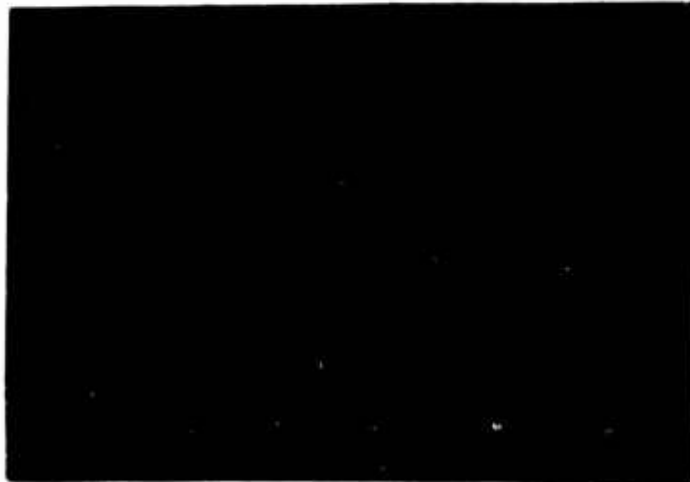
(d) Replicate of Fig. 3c Conditions

Figure 3. Summary of Results for Kistler Model 603A Transducer With DADEE

B

compensated and are obtainable in a special shock mount; one was purchased for measuring the blast wave pressure. Its response and resonance characteristics were evaluated in a manner similar to that just described for the transducer which was not acceleration compensated. The transducer was flush mounted in the transducer mounting plate, and subjected to the blasts from 13.5-grain and 5.5-grain plastic-cased detonators. As before, the detonators were placed 11 inches from the transducer, and were oriented so that the center of the explosion occurred in the plane of the upper surface of the mounting plate. The electrical output of the charge amplifier of the transducer was fed directly, without compensation or filtering, to a Hewlett-Packard Model 175A single-beam oscilloscope equipped with a Polaroid camera.

In addition to its acceleration compensation, the new transducer was obtained with a Delrin (plastic) shock-mount adapter. It was found that appreciable disturbances were transmitted through the mounting plate and through the adapter before the air shock arrived. These disturbances were eliminated by removing the adapter and potting the transducer into the mounting plate with RTV rubber. A typical pressure-time record obtained with a bare detonator is shown in Fig. 4.

Multiple Pressure Transducers. To obtain backup data on blast-wave velocity, both Kistler Model 603A transducers were installed in the mounting plate. They were placed in line with the bomb and spaced 3 inches apart. Their nominal distances from the bomb were 7 inches for the uncompensated transducer and 10 inches for the new transducer. The external DADEE and filtering previously used with the uncompensated transducer were not used; that transducer was merely used to indicate the time of arrival of the blast wave at its position.

The outputs from both transducers were recorded on a Tektronix Model 555 dual-beam oscilloscope to obtain an accurate value of the blast-wave transit time between their locations. The output of the new compensated transducer was recorded also with the Hewlett-Packard oscilloscope noted

50 microsèc/cm

5 psi/cm

P_{10}
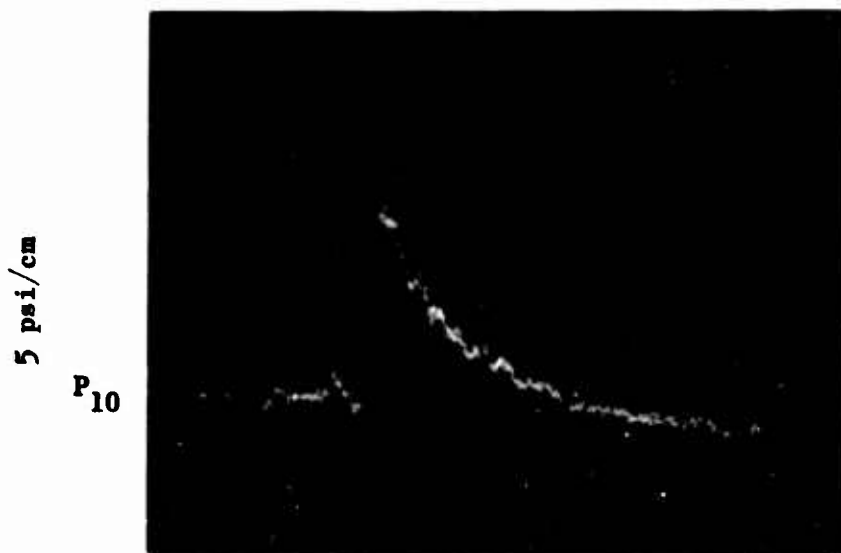
Direct Oscilloscope Photo of the Output of
an Acceleration-Compensated Kistler 603A
Transducer

Figure 4. Pressure Record From Explosion of a Bare
Olin Plasticap (5.5 Grains RDX)

earlier. Both oscilloscopes were voltage calibrated daily, and the sweep rates were checked weekly to ensure accurate determination of time.

Simultaneously with this transducer change, the bomb fragment deflector plate was mounted differently from that shown in Fig. 2h to obtain better isolation of the transducers from transmission of extraneous signals through the mounting plate. The configuration finally used is shown in Fig. 5. This change allowed the transducers to be positioned 1 inch closer to the bomb than the earlier position.

Overall Checkout of Experimental Methods. Before undertaking the bomb test series, the complete system was checked out by firing explosive charges having known blast-wave characteristics. Bare spherical charges of 50/50 Pentolite (50-percent PETN, 50-percent TNT) were selected for this purpose because free-air blast data for this explosive have been compiled (Ref. 1).

Two cast charges weighing 108 grains each were made available from another program. Plastic-cased, 5.5-grain detonators were used to initiate the charges, which were cast with a detonator well that extended to the center of the charge. Thus, an explosion having a blast wave as spherical as practically possible, and having essentially no fragments to affect the measurements, was available to check out the system.

The charges were fired from the same location as the bombs would be in subsequent tests. The centerline of the charge was in the plane of the transducer mounting plate in both tests, but the detonator orientation was varied. In the first test, the detonator axis was normal to the plane of the mounting plate (detonator above the plate), while in the second test the detonator was in the plane of the mounting plate and extended from the charge diametrically opposite from the transducers.

When the first charge was fired, the delay time from fire signal to oscilloscope sweep signal was set at 150 microseconds. As a result, the
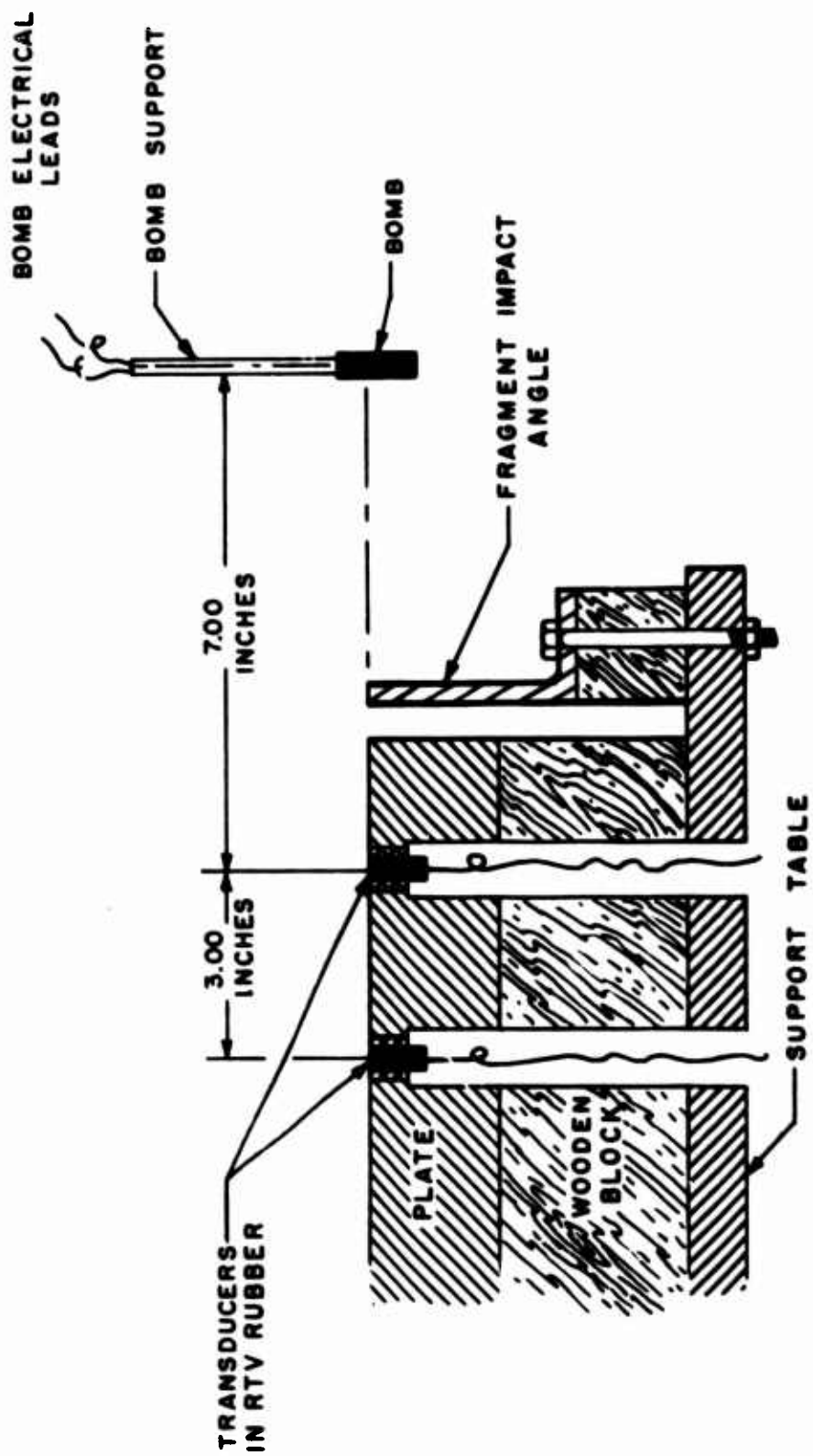
Figure 5. Sectional View of Final Configuration for Transducer Mounting Plate

passage of the blast wave over the first transducer was not recorded, nor was the wave front observed on the streak film. That delay was shortened to 100 microseconds for the second test, and adequate data were obtained. Second-test data are shown in Fig. 6 and 7. Figure 6 is a framing camera sequence showing the nearly spherical blast wave propagating over the transducer mounting plate and Fig. 7 shows the pressure time records displayed on the two oscilloscopes. The pressure scale noted there is based upon the factory-supplied calibration for the acceleration-compensated transducer.

The appearance of the pressure records is excellent. The total time elapsed from the beginning of the pressure rise to the peak pressure is on the order of 3 to 4 microseconds, a value that is hardly noticeable on photographs taken at the 50 microsec/cm sweep rate used in Fig. 7. There is a very minimal indication of transducer ringing (at a resonant frequency of 330,000 cps). The indicated pressure decay following the front of the blast wave appears to be a faithful reproduction.

Data reduced from the two 108-grain Pentolite tests are tabulated in Table 1, and, as indicated, loss of transit time and streak data greatly limits the usefulness of the first test. The tabulation for the second test is divided into pressure-transducer-derived and streak-photograph-derived information. From the blast-wave transit time between the two transducers, a wave velocity was calculated:

$$(c_s)_{7-10} = \frac{10-7}{(t_{10} - t_7)} = \frac{3}{\Delta t_{7-10}} \tag{1}$$

The shock Mach number:

$$M_{7-10} = \frac{(c_s)_{7-10}}{c_0} \tag{2}$$
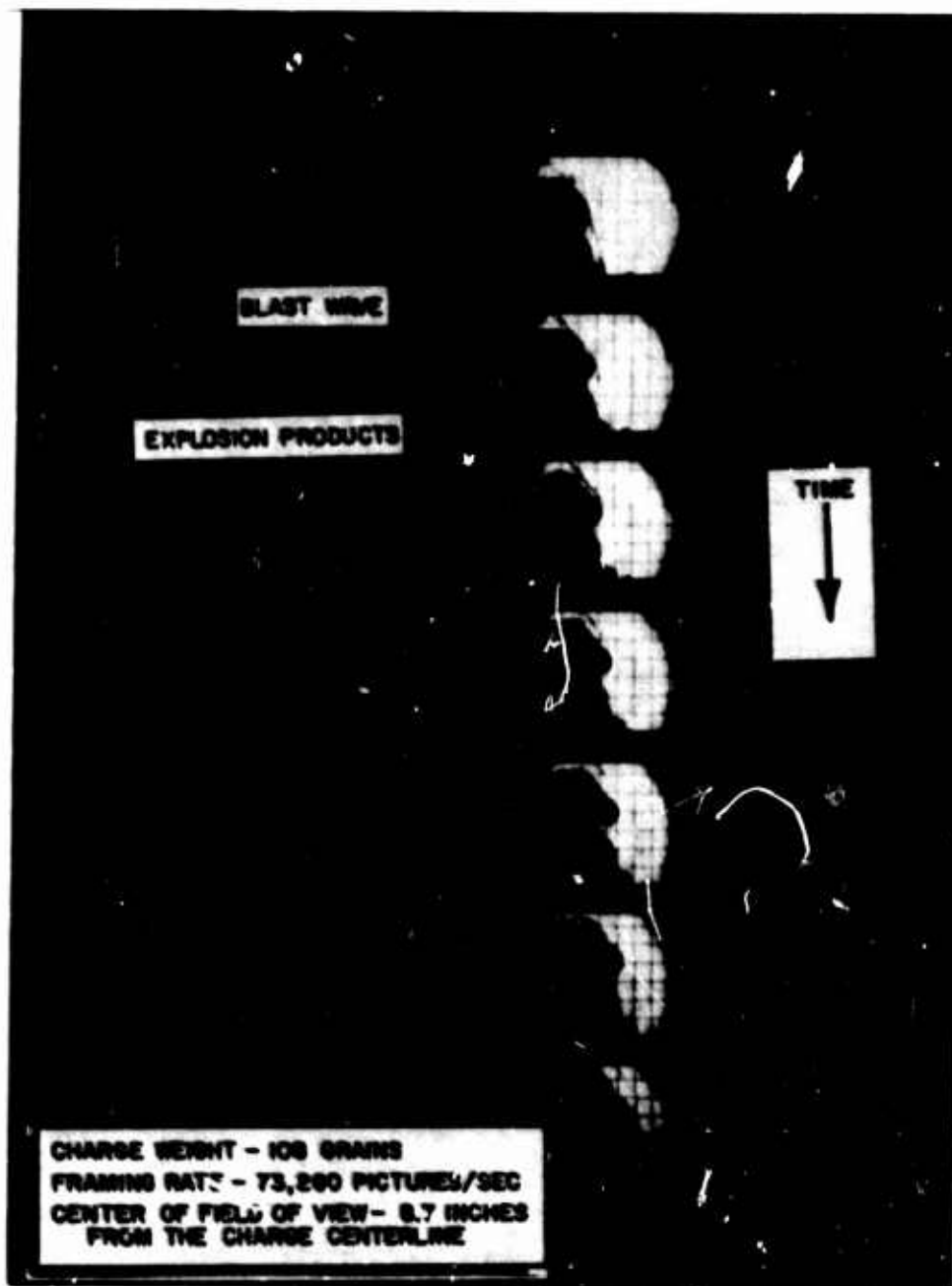
Figure 6. Sequence of Framing Photographs From Explosion of a Bare 50/50 Pentolite Charge

P_7

20 psi/cm

P_{10}

t_7 t_{10}
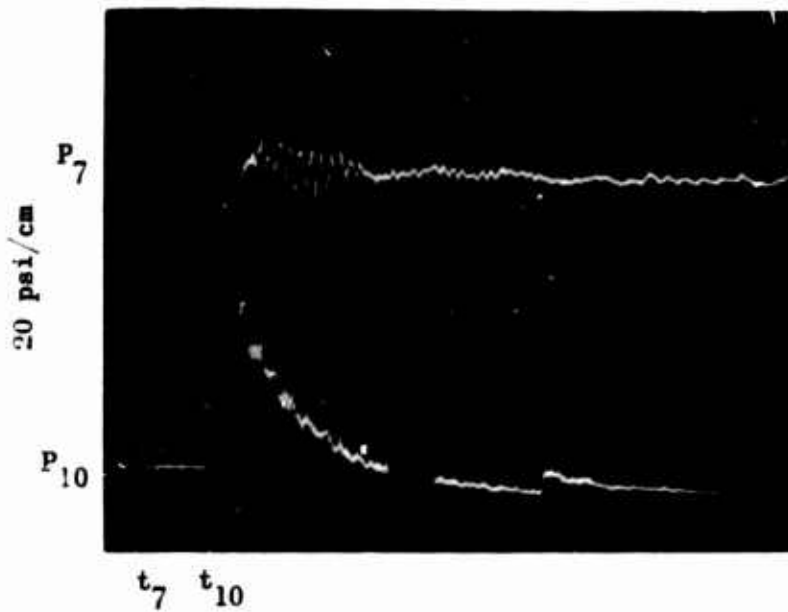
a. Photo for Obtaining Wave Transit Time

50 microsec/cm

20 psi/cm

P_{10}
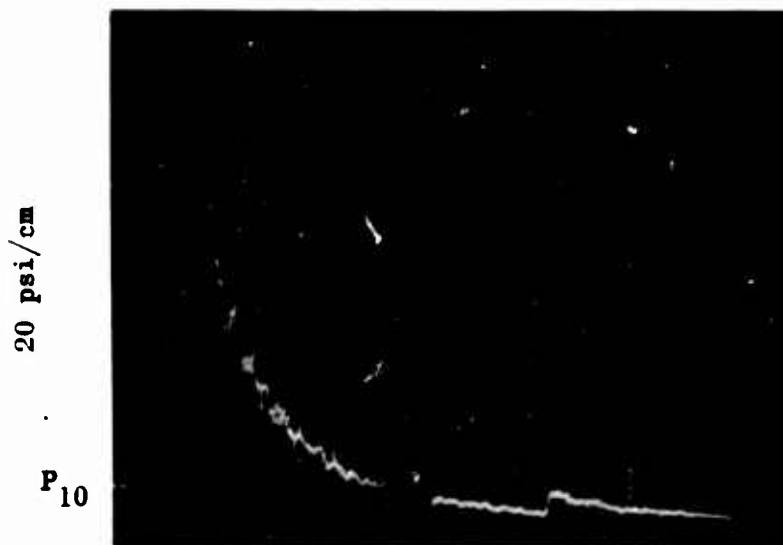
b. Output of Acceleration Compensated Kistler 603A Transducer

Figure 7. Pressure Records From Explosion of a Bare Spherical Charge of 50/50 Pentolite (108 Grains)

TABLE 1

AIR BLAST DATA FROM EXPLOSION OF BARE
SPHERICAL PENTOLITE CHARGES

Variable	Units	Test Number 1	Test Number 2	Average
Transducer Data				
t_7	Microseconds	--	72	--
t_{10}	Microseconds	157	133	147
Δt	Microseconds	--	61	--
M_{7-10}	None	--	3.62	--
ΔP_{7-10} (calc)	psig	--	210	--
ΔP_{10}	psig	92	100	96
$I_{10}/4\,\pi\,R^2$	psi-microsec	3365	3343	3354
T_+	Microseconds	160	141	151
Streak Camera Data				
$M_{8.5}$	None		3.40	
$\Delta P_{8.5}$ (calc)	psig		172	
M_{10}	None		3.09	
ΔP_{10} (calc)	psig		139	

39

was then substituted in the Rankine-Hugoniot relation for air shock waves:

$$\Delta P_{7-10} = \frac{7P_o}{6} \left[(M_{7-10})^2 - 1 \right] \tag{3}$$

to obtain a calculated value of the shock-wave overpressure. This value is followed in the table by the measured peak pressure at 10 inches from the charge. Next are listed the impulse per unit area and the duration of the positive pressure portion of the record measured at the 10-inch station. The unit impulse was obtained by planimeter measurement of the area under the pressure record for time $t_{10} < t < (t_{10} + T_+)$. That is:

$$\frac{I_{10}}{4\pi R^2} = \int_{t_{10}}^{t_{10}+T_+} p \, dt \tag{4}$$

From the streak record, wave velocities were reduced at 8.5 and 10 inches from the bomb, and were used to calculate peak shock-wave overpressure by relations equivalent to Eq. 2 and 3. The calculated value of 172 psig at 8.5 inches is approximately 18 percent below the value of ΔP calculated from blast-wave transit time. However, the 8.5-inch distance measured in the slit plane of the camera is approximately 0.5 inch farther (radially) from the bomb than the midpoint distance between the two transducers. Therefore, the "streak" pressure should be somewhat below the "transducer-derived" pressure, and the agreement is believed to be quite good. The measured peak pressures, ΔP_{10}, for the two tests were only 8 percent different from each other, and their values were approximately 31 percent below the streak-velocity-derived calculated overpressure at 10 inches $(\Delta P_{10}(\text{Calc}) = 139 \text{ psig})$. This discrepancy is believed to be caused primarily by the inability of the transducer to respond faithfully and reproduce the first few microseconds of wave passage. In the following discussion, this discrepancy is further examined by comparing these limited data with those available in the literature.

40

Transducer inability to measure the leading edges of a steep-fronted shock wave and to measure peak pressure if the shock is immediately followed by a rarefaction wave was recognized at the outset of this program. It was intended to calculate peak shock overpressure from velocity measurements, and to use the pressure data of the transducer to obtain positive pressure duration and unit impulse. Aside from general interest in how close the transducer actually comes to indicating true peak pressure, primary interest is in how deficiencies here affect the accuracy of unit impulse measurement.

Goodman (Ref. 1) compiled data on blast-wave properties resulting from detonation of 50/50 Pentolite charges of 0.25-pound and larger. He reported that peak-pressure data could be correlated as a function of radial distance, R, from an explosive charge of weight, W:

$$\Delta P_R = f \ (R, \ W^{-1/3}) \tag{5}$$

His correlating line is reproduced in Fig. 8. In the region of interest to this study, the data were obtained with pressure transducers, and exhibited scatter of about ±25 percent.

Reutenik and Lewis (Ref. 2) detonated large charges (217 and 12,000 pounds) of both 50/50 Pentolite and TNT. Their strain-gage pressure transducer data lie substantially higher than Goodman's curve, however, their data had been treated analytically to obtain an improved estimate of peak over-pressure by extrapolating backward in time along the pressure-decay curve. Their correlating curve is also shown in Fig. 8; values of over-pressure greater than 40 psig were extrapolated by them, based on Goodman's data.

Data points from the current two 50/50 Pentolite tests are also shown in Fig. 8. It is seen that the direct-pressure transducer data agree with Goodman's correlation, while those derived from velocity data agree with the Reutenik and Lewis correlation. The implication of this is that the current measurements are as good as direct-pressure transducer measurements normally are found to be. The data correction technique used by

41
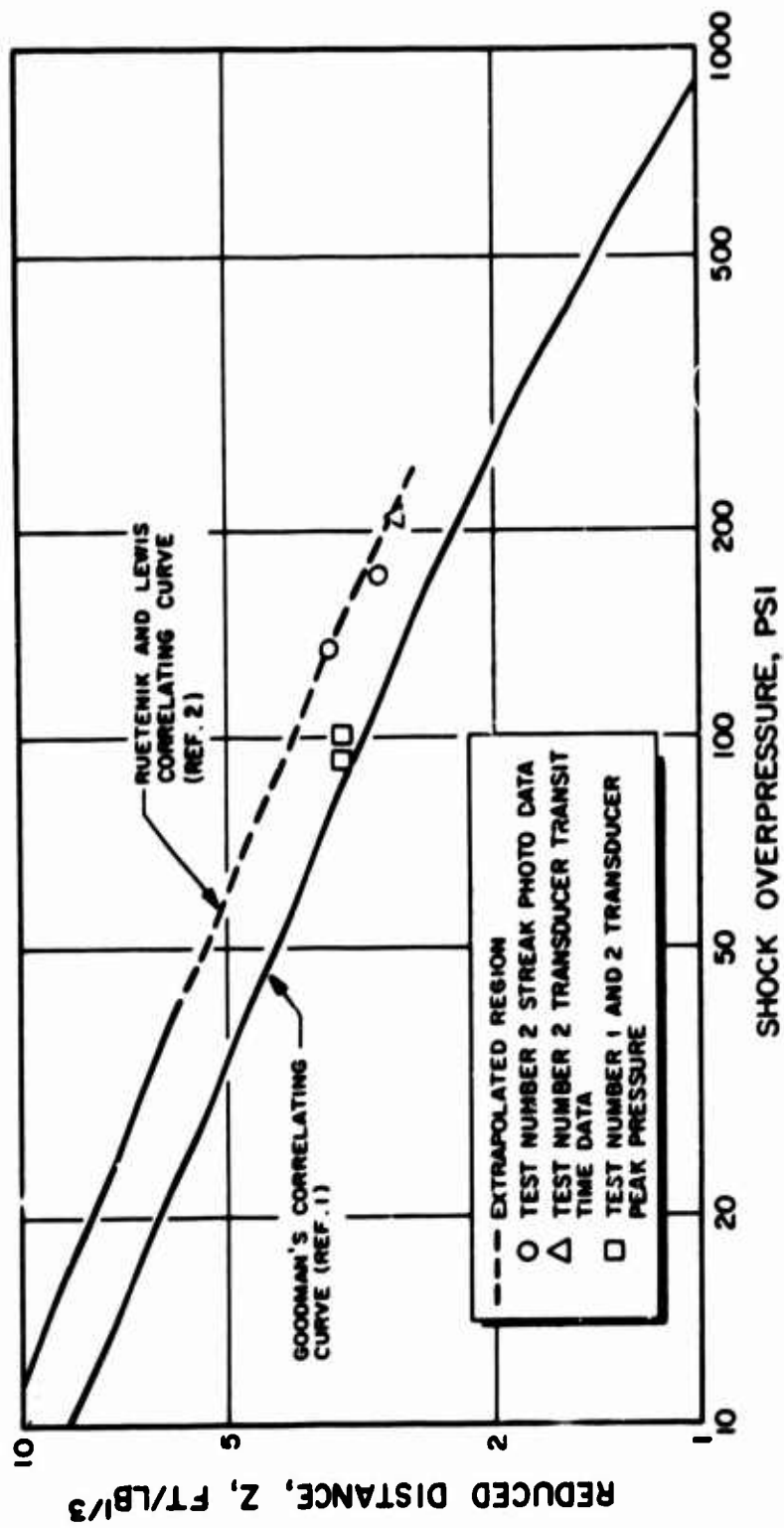
Figure 8. Correlation of Peak Pressure Data From Spherical 50/50 Pentolite Explosions

42

Reutenik and Lewis could not be applied with precision to the current data because Rocketdyne had both considerably higher amplitudes and shorter positive durations.

Another factor demonstrating that the current transducer pressure data are comparable with those of other investigators, is the unit impulse. The measured values in Table 1 are not only less than 1 percent different from each other, but their average is only 1.3 percent higher than a value of 3310 psi-microsec obtained from a unit impulse correlation given by Goodman (Ref. 1).

The error in measuring unit impulse is therefore believed to be just that resulting from the failure of the transducer to reproduce the very steep and very narrow leading edge of the pressure front. Consider the following values:
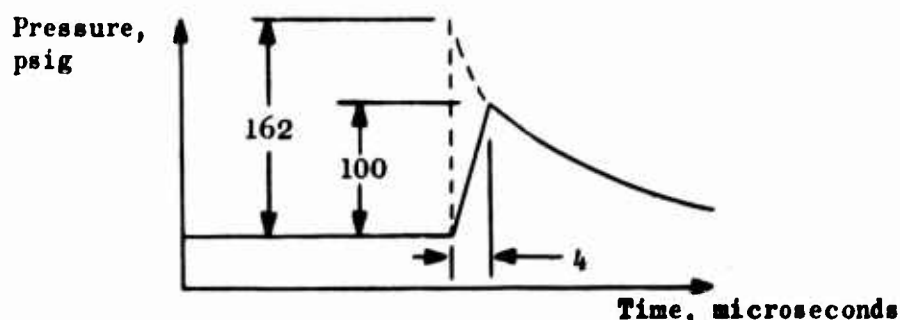
The area between the dotted "true" pressure curve and the solid transducer-indicated pressure curve is approximately 320 psi-microsec; i.e., approximately 9.5 percent of the tabulated unit impulse, and approximately 8.7 percent of the sum of the tabulated and error values. If the total indicated rise time were only 3 microseconds, these errors would be reduced to 7.1 and 6.5 percent, respectively.

43

Bomb Design Parameter Variations

The bomb design parameters which were varied were:

1. Explosive charge weight, W

2. Case thickness, T_c

3. Charge length-to-diameter ratio, L/D

4. Case material

5. Type of explosive

Charge weights of 5.5, 13.5, and 50 grains were selected for the cold-flow characterization studies. Approximately equal intervals of $\ln [W^{1/3}]$ were believed to be desirable because in previous studies blast wave peak pressure and impulse had been correlated on that basis.

Bomb case thicknesses of 0.063, 0.125, 0.250, and 0.500 inch were used. It was thought that this range would certainly include the thinnest cases likely to be used in a hot-firing program, and that the range was broad enough to delineate clearly the effect of thickness on bomb characteristics.

Explosive charge L/D ratios of 1.0 and 4.0 were selected as nominal design values. Whenever a commercial detonator constituted the entire charge, however, the L/D ratio had some intermediate value.

The bomb cases were made of nylon or Micarta. These materials have been observed to break up differently in this application; nylon tends to fragment into moderately large chunks, while Micarta tends to fragment into lighter weight shreds characteristic of the cloth matrix.

High explosive charges were used for the majority of the bombs fired. The design details are listed in Table 2, which shows that three different kinds of high explosive were used: PETN, RDX, and Composition C-4 plastic explosive. RDX and PETN have been found to produce nearly identical air-shock characteristics (Ref. 3). With similar confinement, Composition C-4 is equally as brissant and energetic as PETN; hence, it was

44

TABLE 2

BOMB DESIGN DETAILS FOR HIGH EXPLOSIVE CHARGES

Bomb Code	Total Weight of High Explosive, grains	L/D Ratio of Explosive Charge	Wall Thickness of Bomb Case, inches	Diameter of Explosive Charge, inches	Length of Explosive Charge, inches	Inside Diameter of Bomb Case, inches	Outside Diameter of Bomb Case, inches	Explosive Configuration	Nylon Case, Number Fired	Nicarta Case, Number Fired
1	90	1	0.063	0.540	0.540	0.540	0.665	2-81 and 36.5 grains C-4	3	1
2	90	4	0.063	0.341	1.364	0.341	0.466	2-81 and 36.5 grains C-4	2	1
3	5.5	1.3	0.390	0.500	0.389	0.500	1.280	011n plastioap only	4	1
4	13.5	1	0.063	0.341	0.343	0.341	0.466	011n cap and 8.0 grains PETN	5	1
5	5.5	1.3	0.063	0.500	0.389	0.500	0.405	011n plasticap only	3	1
6	13.5	2.7	0.063	0.500	0.646	0.500	0.405	2-81 cap only	4	1
7	13.5	1	0.185	0.341	0.343	0.341	0.591	011n cap and 8.0 grains PETN	5	1
8	90	1	0.185	0.540	0.540	0.540	0.790	2-81 and 36.5 grains C-4	3	1
9	5.5	1.3	0.185	0.500	0.389	0.500	0.530	011n plasticap only	4	1
10	13.5	2.7	0.185	0.500	0.646	0.500	0.530	2-81 cap only	3	1
11	90	4	0.125	0.341	1.364	0.341	0.591	2-81 and 36.5 grains C-4	3	2
12	13.5	1	0.170	0.341	0.343	0.341	0.681	011n cap and 8.0 grains PETN	5	3
13	90	1	0.250	0.540	0.540	0.540	1.040	2-81 and 36.5 grains C-4	4	5
14	5.5	1.3	0.250	0.500	0.389	0.500	0.700	011n plasticap only	6	1
15	13.5	2.7	0.250	0.500	0.646	0.500	0.700	2-81 cap only	3	1
16	90	4	0.090	0.341	1.364	0.341	0.681	2-81 and 36.5 grains C-4	3	1
17	13.5	1	0.390	0.341	0.343	0.341	1.381	011n cap and 8.0 grains PETN	3	1
18	90	1	0.390	0.540	0.540	0.540	1.540	2-81 and 36.5 grains C-4	3	1
19	13.5	2.7	0.390	0.500	0.646	0.500	1.380	2-81 cap only	3	1
20	90	4	0.390	0.341	1.364	0.341	1.381	2-81 and 36.5 grains C-4	3	1

NOTES:
1. Inside diameter of bomb case differs from diameter of explosive charge for those bombs in which a cap only is used for the explosive charge, to allow for the thickness of the detonator case.
2. Dupont E-81 detonator has a 13.5-grain PETN base charge.
3. 011n Plasticap detonator has a 5.5-grain RDX base charge.
4. Composition C-4 plastic explosive is RDX (91 percent) with plasticizers.

45

not anticipated that the use of different high explosives would influence the characteristics. Composition C-4 was selected mainly because of its plastic properties, i.e., it is easier to handle than granular explosives, and hazardous spills and loss of a portion of a weighed charge during bomb loading are less likely to occur. The bombs were assembled as sketched in Fig. 9, with the initiating detonator either constituting the entire charge or partially immersed in the base charge. For L/D ratio purposes, the equivalent charge length was calculated as:

$$L = \frac{4}{\pi D^2} \left[\frac{W_b}{\rho_b} + \frac{W_d}{\rho_d} \right] \tag{6}$$

where subscripts b and d denote base and detonator charges, respectively. A small amount of foamed polyurethane packing was inserted in the open end of the case to keep the detonator in place.

A series of tests was made with the high explosive replaced by Hercules Bullseye No. 2 (a fast-burning, double-base pistol powder) which was selected because of its previous history of use in stability-rating pulse guns. Explosion of the powder was initiated by a miniature electric match containing 1.5 grains of pyrotechnic, which is little more than a source of heat for igniting the powder charge. The entire charge weight was thus pistol powder. Rather than redesign the bomb cases to account for the lower density of the pistol powder than that of the Composition C-4, the same cases were used, and the L/D ratio was allowed to vary. Bomb design details are listed in Table 3. The number of tests conducted with each bomb design are also indicated.

Experimental Results

Three kinds of raw data were obtained from open-air bomb explosions: (1) framing shadowgraph sequences, (2) streak shadowgraph sequences, and (3) pressure records; all were recorded directly at test time on 3- by 4-inch Polaroid prints. In this section, examples of the raw data and
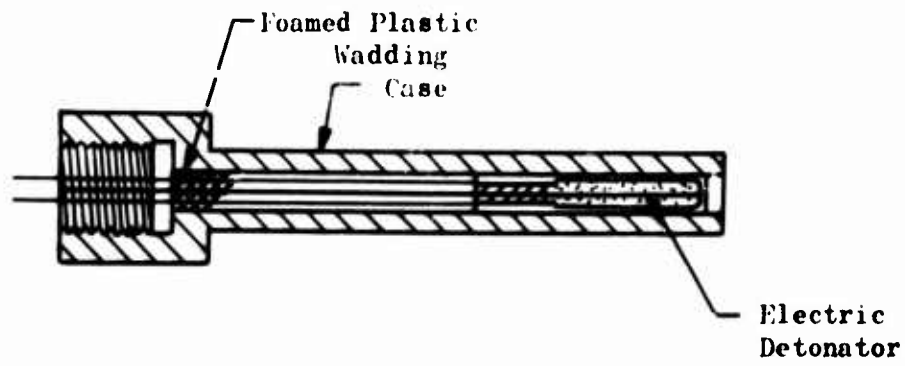
a. Electric Detonator as the Entire Explosive Charge
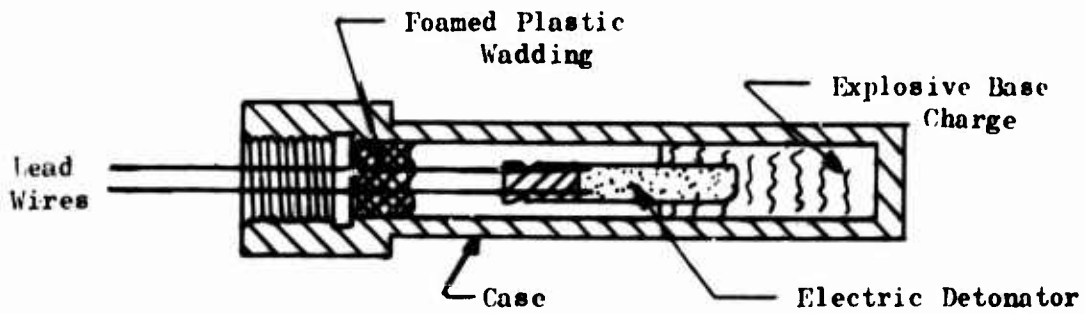
b. Electric Detonator for Initiation of a
High-Explosive Base Charge

Figure 9. Typical Explosive Bomb Assemblies

TABLE 3

BOMB DESIGN DETAILS FOR

HERCULES-BULLSEYE-POWDER CHARGES IN NYLON CASES

Bomb Code	Weight of Explosive, grains	L/D Ratio of Explosive Charge	Wall Thickness of Bomb Case, inches	Diameter of Explosive Charge, inches	Length of Explosive Charge, inches	Outside Diameter of Bomb Case, inches	Number Fired
20HB	50.0	7.3	0.500	0.341	2.5	1.341	2
16HB	50.0	7.3	0.250	0.341	2.5	0.841	2
1HB	50.0	2.0	0.063	0.540	1.1	0.665	3
2HB	50.0	7.3	0.063	0.341	2.5	0.466	2
3HB	50.0	12.0	0.500	0.280	3.5	1.280	1
4HB	13.5	2.1	0.063	0.341	0.7	0.466	3
6HB	13.5	3.9	0.063	0.280	1.1	0.405	3
12HB	13.5	2.1	0.250	0.341	0.7	0.841	3
15HB	13.5	3.9	0.250	0.280	1.1	0.780	2

the methods of their reduction to quantitative data are discussed, and the tabulated data are presented.

Framing Photograph Sequences. An example of the framing shadowgraphs has already been given, Fig. 6, for a 50/50 Pentolite charge. The uncomplicated propagation of a nearly spherical blast wave over the transducer mounting plate shown there is considerably more distinct (because the charge is larger and bare) than similar records with bombs. The blast wave is also more cleanly separated from the explosion products because there was no case debris thrown ahead of the explosion products. Nevertheless, Fig. 6 does present a typical picture of the blast-wave-mounting plate interaction.

No direct quantitative data were taken from the framing shadowgraphs. They were used principally for indications of unusual occurrences that might invalidate the data, and for auxiliary, blast-wave, position-time information in instances where case-particle impacts near a transducer made it difficult to determine when the blast wave crossed that transducer.

Streak Photographs. Streak shadowgraphs were obtained simultaneously with the framing shadowgraph sequences. In those taken in the neighborhood of the transducer mounting plate, the blast waves were usually distinguishable on the original prints, but sometimes just barely. The method of data reduction was identical to that for the streak photographs taken with bombs in the field of view, described below.

A direct streak photograph of a bomb detonation is reproduced in Fig. 10. It was taken by aligning the camera so that its internal slit viewed a 10-inch-long by about 0.020-inch-wide field normal to the axial center-line of the bomb. The bomb was backlighted (Fig. 1) so that its diameter formed a dark shadow near the center of the camera's field of view, which extends upward in time from the bottom of the photograph in Fig. 10. The thin, dark lines parallel with that bomb image are 1.00-inch grid

49
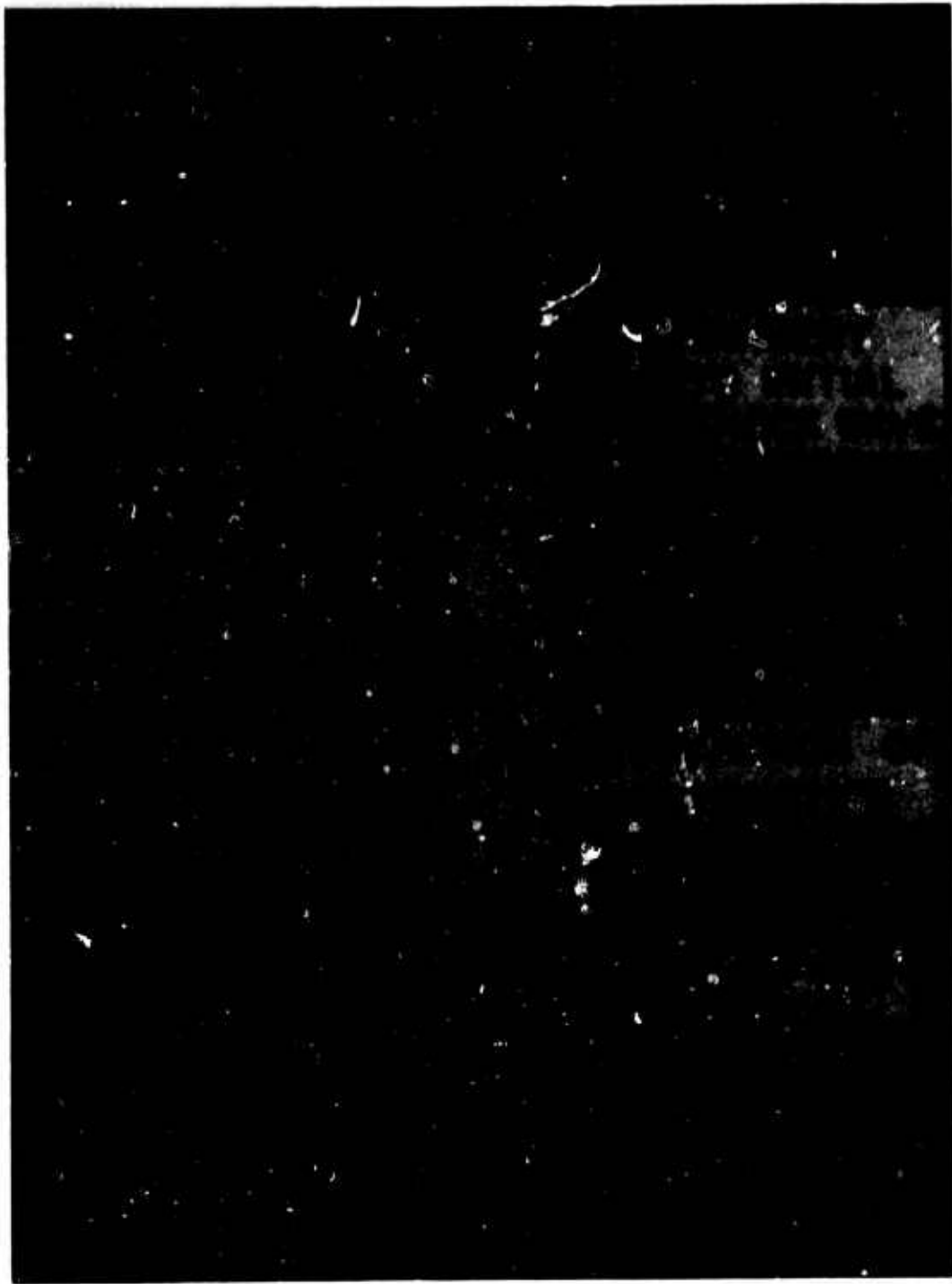
Figure 10.   Streak Photograph of High-Explosive,
Nylon-Case Bomb Detonation

marks (and some scratches from previous tests) on the 1/4-inch-thick Plexiglas fragment shield for the backlighting apparatus.

Detonation of the bomb resulted in simultaneous radial propagation of a blast wave, case debris, and explosion products. At that time, the back-lighted image of the bomb on the streak photograph was replaced by their cumulative backlighted images. The slope of the edge of an image is proportional to the velocity of the material that made the image. Most of the dark "fan" on the photograph is from case debris and explosion products. In most cases, the shock trace quickly separated from and led the material flow. The slope of the shock trace then is proportional to the shock velocity.

These particular photographs were taken to obtain initial velocities of the shock waves. With moderately large charges, the initial wave is readily distinguishable on such a record; as the charge weight is reduced and the bomb case becomes proportionately more massive, the initial shock wave becomes more and more difficult to identify. Many times during these experiments, the only direct evidence of the initial shock was a diffrac-tion of the grid line images as it passed over them. For that reason, each photograph was examined carefully with a stereoscopic microscope, and each shred of evidence of the passage of the initial wave was care-fully marked with a sharp stylus. These marks were subsequently used as the basis for constructing a line tangent to the initial shock wave at the instant of bomb rupture. The slope of the tangent line was converted to initial shock velocity.

Two values of initial shock velocity were obtained from each bomb firing, one from the right side and another from the left side of the streak photograph. Usually, the bomb was not centered in the photograph, but was offset to the left. The left- and right-hand velocities generally agreed within about 5 to 10 percent of each other. In cases of wide disparity between them, it is believed that the right-hand side should be preferred. This is because fragments may have initial velocities higher than the initial shock velocity, so that discrimination of the shock

51

very soon after detonation is not as reliable as it is at later times; the right-hand side has a longer time period through which to examine the photograph and extrapolate backward to the instant of detonation.

Blast-wave overpressure was calculated for each value of wave velocity by means of Eq. (2) and (3).

Transducer-Measured Pressures. A few examples of typical pressure records obtained with the acceleration-compensated Kistler Model 603A located 10 inches from high-explosive, nylon-case bombs are shown in Fig. 11. Measurement difficulties imposed by the shower of bomb-case fragments attending the blast wave are apparent; each pressure trace had from a few to many spurious signals superimposed on the "real" pressure histories. Their interpretation as fragment impacts on or near the transducer was supported by observations of cratering in the RTV rubber potting around the transducers and of occasional complete obscuration of the shock front on the streak photographs by particles traveling both ahead of and behind the front. Such loss of data made it necessary to run a large number of replicate tests; as seen in Table 2, a total of 75 bombs was fired to accomplish characterization for 20 high-explosive, nylon-case configurations.

Several examples of pressure data obtained with high-explosive, Micarta-case bombs are shown in Fig. 12. The pressure traces were considerably less complicated by spurious signals from particle impact than had been experienced with nylon cases. This beneficial result, probably caused by the tendency of the Micarta bomb to fragment into shreds rather than chunks, may be an important effect to consider in selecting bombs for rating engines which have potentially delicate chamber components.

Pressure records from low-explosive, nylon-case bomb explosions are shown in Fig. 13. Here again, there were fewer difficulties with case-fragment impacts giving spurious pressure signals; this was a result of the explosion having been less brissant than with high explosives. With 0.063-inch-thick cases, however, the pressure records were considerably different

52

50 microsec/cm

5 psi/cm

b. Blast Wave Identity Obscured by Multiple Fragment Impacts (A Code 7 Bomb)

50 microsec/cm

5 psi/cm

d. Blast Wave Apparently Degraded by a Dense Shower of Fragments in the Neighborhood of the Pressure Transducer
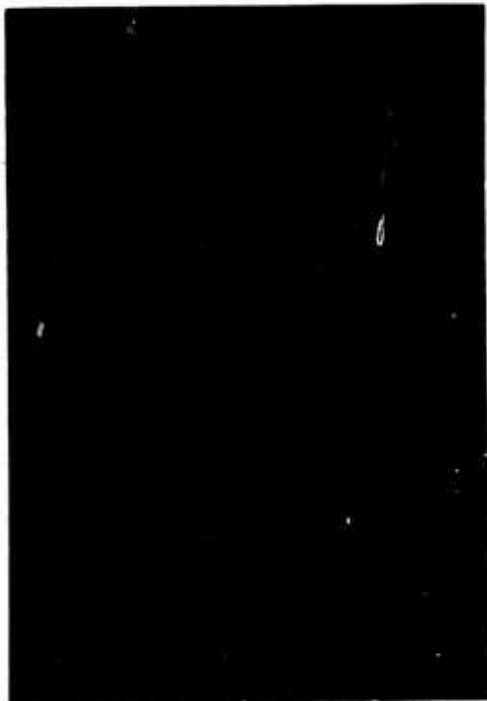
50 microsec/cm

5 psi/cm

a. Satisfactory Blast Wave Record, Appreciable Precursor Disturbances and a Few Particle Impacts During Wave Passage (A Code 6 Bomb)

50 microsec/cm
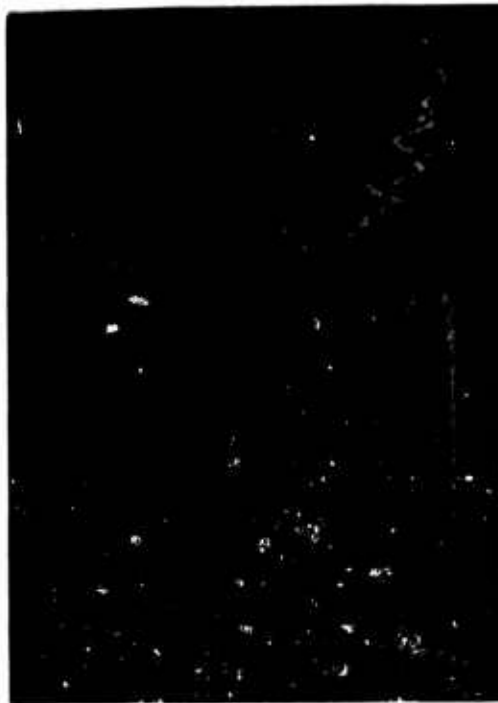
5 psi/cm

c. Satisfactory Blast Wave Record (A Code 13 Bomb)

Figure 11. Some Examples of Pressure Records From Explosion of High-Explosive, Nylon-Case Bombs

50 microsec/cm

5 psi/cm

b. A 5.5-grain, 0.25-in. Wall Code 14 Bomb
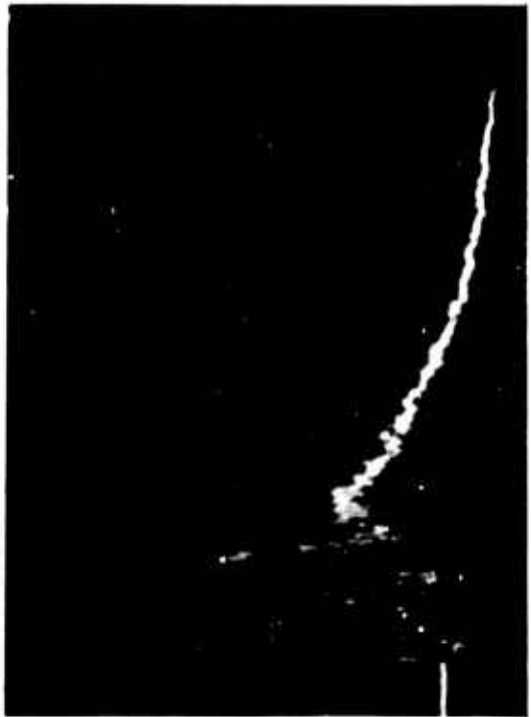
50 microsec/cm

5 psi/cm

d. A 13.5-grain, 0.25-in. Wall Code 12 Bomb

50 microsec/cm

5 psi/cm

a. A 5.5-grain, 0.063-in. Wall Code 5 Bomb

50 microsec/cm

5 psi/cm

c. A 13.5-grain, 0.063-in. Wall Code 4 Bomb

A

d. A 13.5-grain, 0.25-in. Wall Code 12 Bomb

5 psi/cm

50 microsec/cm

f. A 50-grain, 0.25-in. Wall Code 13 Bomb
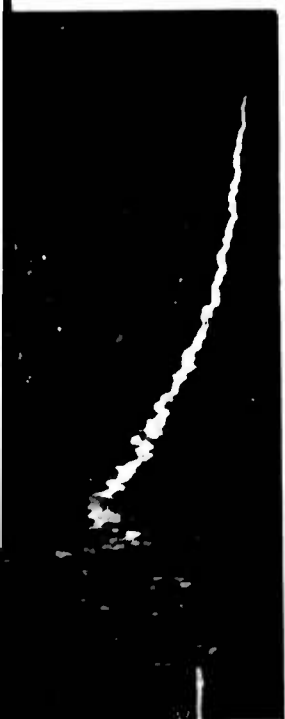
5 psi/cm

c. A 13.5-grain, 0.063-in. Wall Code 4 Bomb

5 psi/cm

50 microsec/cm

e. A 50-grain, 0.063-in. Wall Code 1 Bomb

10 psi/cm

Figure 12. Some Examples of Pressure Records From Explosion of High-Explosive, Micarta-Case Bombs

54
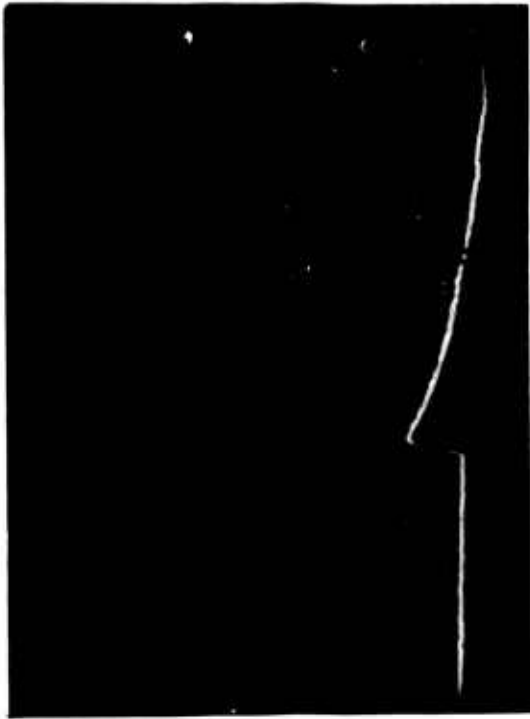
a. Two 50-grain, 0.063-in. Wall Code 2HB Bombs

b. Two 50-grain, 0.063-in. Wall Code 1HB Bombs

b. Two 50-grain, 0.063-in. Wall Code 1HB Bombs

50 microsec/cm
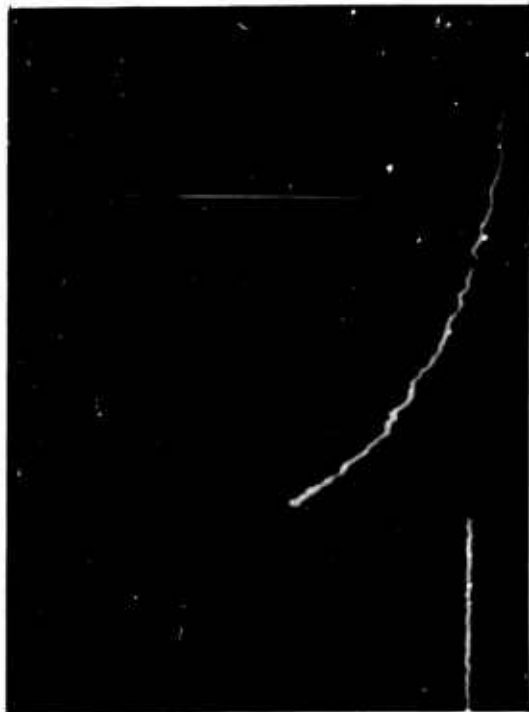
5 psi/cm

c. A 50-grain, 0.50-in. Wall Code 20 HB Bomb

50 microsec/cm

5 psi/cm

d. A 50-grain, 0.25-in. Wall Code 16HB Bomb

50 microsec/cm

e. A 13.5-grain, 0.25-in. Wall Code 15HB Bomb

50 microsec/cm

5 psi/cm

Figure 13. Some Examples of Pressure Records From Explosion of Low-Explosive, Nylon-Case Bombs

55

B

than any that had been observed with previous bombs. There were frequently
two pressure waves (and twice there were three) spaced at irreproducible
time intervals. The first wave was steep fronted and sometimes had only
a moderate amplitude; it apparently resulted from case rupture prior to
complete burning of the powder. The second wave was less steep and had
a peak amplitude that is probably related to charge weight and its time
of appearance after the initial wave. Two of the records appeared remark-
ably similar to pressure records obtained with pressure transducers in
the barrel of the pulse gun, which are discussed later. With 0.250- and
0.500-inch-thick cases, the pressure traces had an appearance much like
those from high-explosive charges. It was initially thought that these
charges were so well confined that a high deflagration rate was achieved,
and the powder was essentially consumed prior to case disintegration. As
is noted later in the correlation of these low-explosive data, the fact
that pressure amplitudes increased with increasing case thickness (as
contrasted with the opposite effect with high explosives) belies such a
conclusion.

The pressure record photographs were analyzed to obtain direct-measured
values of peak overpressure, positive unit impulse, and positive duration
of the blast wave. Additionally, the transit time for wave travel between
the two transducers gave an average wave velocity from which an overpres-
sure was calculated.

Data Tabulations. A complete tabulation of the data concerning the initial
blast wave near high-explosive, nylon-case bombs is given in Table 4.
These data are from the streak photographic records; no pressure transducer
data were recorded during these experiments. Data concerning the blast
wave in the neighborhood of the pressure transducers are tabulated in
Table 5 for the high-explosive, nylon-case bombs, in Table 6 for the high-
explosive, Micarta-case bombs, and in Table 7 for the low-explosive, nylon-
case bombs. The time increment from electrical fire signal to actual rup-
ture of the nylon case was not as reproducible with low explosives as it
had been with high explosives. The variability was several times the

56

TABLE 4

INITIAL SHOCK WAVE DATA (HIGH-EXPLOSIVE, NYLON-CASE BOMB SERIES)

Bomb Code Number	Charge Weight, grains	Case Thickness, inches	Charge L/D Ratio	Left Side of Bomb			Right Side of Bomb			Average of Two Sides		
				Velocity, in./microsec	Mach Number	Shock Overpressure, psig	Velocity, in./microsec	Mach Number	Shock Overpressure, psig	Velocity, in./microsec	Mach Number	Shock Overpressure, psig
1	50	0.063	1.0	0.1817	8.950	1590	0.1198	8.810	1507	0.1208	8.880	1530
2		0.063	4.0	0.1178 / 0.1283	8.659 / 9.000	1380 / 1370	0.1006 / 0.1000	7.400 / 7.355	906 / 895	0.1092	8.035	1080
8		0.125	1.0	0.0946	6.960	811	0.0685	5.035	602	0.0812	6.000	596
11		0.125	4.0	—	—	—	—	—	—	0.0546	4.022	268
13		0.258	1.0	0.0658	3.280	185	0.0476	3.500	184	0.0461	3.310	174
16		0.258	4.0	0.0473	3.478	181	0.0454	3.382	166	0.0464	3.410	175
18		0.500	1.0	0.0365	2.596	93.0	0.0331	2.636	79.6	0.0342	2.515	86.3
20		0.500	4.0	0.0338	2.468	85.5	0.0319	2.345	72.7	0.0329	2.414	78.1
4	13.5	0.063	1.0	0.0920	6.760	730	0.0835	6.140	610	0.0878	6.450	660
6		0.070	2.7	0.0856	6.300	646	0.0799	5.800	542	0.0855	6.090	605
–		0.105	2.7	0.0649	4.773	360	.0636	4.675	344	0.0643	4.720	352
7		0.125	1.0	0.0569	4.182	270	0.0613	4.510	380	0.0591	4.346	294
10		0.138	2.7	0.0692	4.630	398	0.0976	4.239	278	0.0589	4.389	298
–		0.119	2.7	0.0695	4.800	367	0.0652	4.640	344	0.0644	4.730	378
10		0.138	2.7	0.0651	4.780	360	0.0595	4.570	291	0.0623	4.575	328
12		0.258	1.0	0.0371	2.777	106	0.0336	2.474	88.8	0.0354	2.601	93.4
12		0.258	4.0	0.0365	2.666	101	0.0356	2.618	94.9	0.0361	2.651	97.7
15		0.257	2.7	0.0399	2.954	185	0.0421	3.091	139	0.0410	3.013	131
17		0.500	1.0	0.0290	2.130	57.8	0.0272	2.000	52.5	0.0281	2.065	52.8
19		0.507	2.7	0.0254	1.870	40.2	0.0266	1.956	46.3	0.0260	1.913	43.0
–	5.5	0.016	1.3	0.1357	9.100	1400	0.1373	9.400	1490	0.1258	9.25	1460
5		0.077		0.0766	5.190	489	0.0698	4.840	370	0.0682	5.018	400
9		0.111		0.0445	3.271	158	0.0466	3.423	175	0.0456	3.367	166
11		0.266		0.0300	2.306	66.5	0.0537	2.475	82.6	0.0318	2.341	72.7
3		0.516		—	—	—	—	—	—	0.0182	1.339	12.8
3		0.516		—	—	—	—	—	—	0.0202	1.484	19.3

57

TABLE 5

AIR BLAST WAVE DATA (HIGH-EXPLOSIVE, NYLON-CASE BOMB SERIES)

TABLE 5

(Continued)

59

TABLE 5

(Concluded)

TABLE 6

AIR BLAST WAVE DATA (HIGH-EXPLOSIVE, MICARTA-CASE SERIES)

Bomb Code Number	Charge Weight, Grains	Charge L/D Ratio	Case Thickness, inches	Data Derived From Pressure			
				7- to 10-inch Transit Time Information			
				Δ Time (7 to 10 Inches), microsec	Velocity, in./microsec	Mach Number	Overpressure, psig
5	5.5	1.3	0.063	179.7	0.0167	1.227	8.2
*				177.5	0.0169	1.243	8.8
				175.2	0.0171	1.259	9.4
*				172.9	0.0174	1.276	10.0
↓*	↓	↓	↓	--	--	--	--
				--	--	--	--
14			0.250	176.8	0.0170	1.247	9.0
				155.0	0.0194	1.423	16.4
*				153.4	0.0196	1.438	17.2
↓*	↓	↓	↓	152.1	0.0197	1.450	17.7
				150.4	0.0199	1.466	18.5
4	13.5	2.7	0.063	100.0	0.0300	2.206	62.5
		1.0	0.063	113.0	0.0265	1.952	45.2
				--	--	--	--
↓	↓	↓	↓	98.5	0.0305	2.239	64.9
12	13.5	2.7	0.250	121.7	0.0247	1.813	36.8
		1.0		136.2	0.0220	1.619	26.1
↓	↓	↓	↓	142.0	0.0211	1.553	22.7
1	50		0.063	105.8	0.0284	2.085	54.0
				82.6	0.0363	2.670	99.2
				82.6	0.0363	2.670	99.2
↓*			↓	82.7	0.0363	2.670	99.2
13			0.250	124.6	0.0241	1.770	34.4
				137.7	0.0218	1.602	25.2
↓	↓	↓	↓	143.5	0.0209	1.537	22.0
16	50	4.0	0.250	115.9	0.0259	1.903	42.2
2	50	4.0	0.063	92.7	0.0324	2.379	75.4

*Rows marked with an asterisk are data obtained with a second oscilloscope simultaneously with

A

TABLE 6

ST WAVE DATA (HIGH-EXPLOSIVE, MICARTA-CASE SERIES)

Data Derived From Pressure Transducers						
7- to 10-inch Transit Time Information				Measured Overpressure, psig	Positive Duration, microsec	Unit Impulse psi-microsec
e (7 nches), osec	Velocity, in./microsec	Mach Number	Overpressure, psig			
.7	0.0167	1.227	8.2	7.5	199	415
7.5	0.0169	1.243	8.8	7.8	196	428
.2	0.0171	1.259	9.4	7.7	230	--
2.9	0.0174	1.276	10.0	8.1	233	430
--	--	--	--	--	177	--
--	--	--	--	6.3	170	420
.8	0.0170	1.247	9.0	9.0	163	--
.0	0.0194	1.423	16.4	10.6	166	350
.4	0.0196	1.438	17.2	10.5	161	341
.1	0.0197	1.450	17.7	10.0	179	328
.4	0.0199	1.466	18.5	10.2	179	363
.0	0.0300	2.206	62.5	20.5	199	--
.0	0.0265	1.952	45.2	16.9	183	934
--	--	--	--	18.5	169	--
.5	0.0305	2.239	64.9	20.2	179	901
.7	0.0247	1.813	36.8	13.5	194	642
.2	0.0220	1.619	26.1	18.6	173	522
.0	0.0211	1.553	22.7	14.6	170	541
.8	0.0284	2.085	54.0	31.5	184	1436
.6	0.0363	2.670	99.2	35.8	210	1759
.6	0.0363	2.670	99.2	>40	179	--
.7	0.0363	2.670	99.2	55.1	179	2280
.6	0.0241	1.770	34.4	23.5	144	1109
.7	0.0218	1.602	25.2	21.8	171	1057
.5	0.0209	1.537	22.0	22.9	176	980
.9	0.0259	1.903	42.2	34.3	150	1297
.7	0.0324	2.379	75.4	30.6	186	1933

with a second oscilloscope simultaneously with the data in the preceding row.

B

TABLE 7

AIR BLAST WAVE DATA (LOW EXPLOSIVE, NYLON CASE SERIES)

Bomb Code Number	Charge Weight, Grains	Case Thickness, Inches	Charge L/D Ratio	Data Derived From Pressure Tran...				M Ove
				7- to 10-inch Transit Time Information				
				Δ Time (7 to 10 Inches), microsec	Velocity in./microsec	Mach Number	Overpressure, psig	
16HB ▼	50	0.250 ▼	7.3 ▼	149 160	0.02013 0.01875	1.480 1.379	19.2 14.4	
1HB		0.063	2.0	189 186 182 186 183	0.01587 0.01612 0.01648 0.01612 0.01639	1.167 1.185 1.212 1.185 1.205	5.8 6.5 7.5 6.5 7.3	
20HB ▼		0.500 ▼	7.3 ▼	146 162	0.02054 0.01851	1.510 1.361	20.6 13.7	
2HB	50	0.063	7.3	190 181 183 179	0.01578 0.01604 0.01639 0.01675	1.160 1.179 1.205 1.232	5.5 6.3 7.3 8.4	
3HB		0.500	12.0	167	0.01796	1.321	12.0	
4HB	13.5	0.063	2.1	202 199 194	0.01485 0.01507 0.01546	1.092 1.108 1.137	3.1 3.7 4.7	
6HB	13.5	0.063	3.9	196 200 197	0.01530 0.01500 0.01522	1.125 1.103 1.119	4.3 3.5 4.1	
12HB	13.5	0.250	2.1	152 164 161 168 164	0.01973 0.01829 0.01863 0.01785 0.01829	1.451 1.345 1.370 1.313 1.345	17.8 13.0 14.1 11.7 13.0	
15HB	13.5	0.250	3.9	171 167 171 167	0.01754 0.01796 0.01754 0.01796	1.290 1.321 1.290 1.321	10.7 12.0 10.7 12.0	

*Rows marked with an asterisk are data obtained with a second oscilloscope simultaneously with that

A

TABLE 7

IR BLAST WAVE DATA (LOW EXPLOSIVE, NYLON CASE SERIES)

Data Derived From Pressure Transducers						
7- to 10-inch Transit Time Information						
Δ Time (7 10 Inches), microsec	Velocity in./microsec	Mach Number	Overpressure, psig	Measured Overpressure, psig	Positive Duration, microsec	Unit Impulse psi-microsec
149	0.02013	1.480	19.2	13.5	186	910
160	0.01875	1.379	14.4	9.9	172	656
189	0.01587	1.167	5.8	4.4	182	383
186	0.01612	1.185	6.5	5.2	224	364
182	0.01648	1.212	7.5	5.3	223	395
186	0.01612	1.185	6.5	4.3	203	323
183	0.01639	1.205	7.3	4.3	199	362
146	0.02054	1.510	20.6	19.2	199	1410
162	0.01851	1.361	13.7	27.6	193	1640
190	0.01578	1.160	5.5	4.2	182	290
181	0.01604	1.179	6.3	4.3	182	297
183	0.01639	1.205	7.3	4.3	150	274
179	0.01675	1.232	8.4	4.4	158	270
167	0.01796	1.321	12.0	9.0	204	710
202	0.01485	1.092	3.1	2.5	179	195
199	0.01507	1.108	3.7	2.0	205	171
194	0.01546	1.137	4.7	3.7	167	273
196	0.01530	1.125	4.3	2.4	208	225
200	0.01500	1.103	3.5	1.3	160	87.5
197	0.01522	1.119	4.1	2.3	302	168
152	0.01973	1.451	17.8	>8.0	188	Off Scale
164	0.01829	1.345	13.0	8.6	195	591
161	0.01863	1.370	14.1	8.6	197	593
168	0.01785	1.313	11.7	7.6	189	538
164	0.01829	1.345	13.0	7.9	191	563
171	0.01754	1.290	10.7	6.6	195	460
167	0.01796	1.321	12.0	6.8	195	476
171	0.01754	1.290	10.7	8.3	182	505
167	0.01796	1.321	12.0	8.7	182	521

tained with a second oscilloscope simultaneously with that in the preceding row.

B

approximate 100-microsecond duration of a streak film record; therefore, after several attempts, streak photography was abandoned and only pressure transducer data were taken. Streak photography was then also omitted from the high-explosive, Micarta-case experiments so that a larger number might be fired.

Data Correlations

Correlating Method. The experimental data were analyzed to establish correlations between individual output characteristics and the bomb input parameters. The multiple regression correlating techniques used are summarized in Appendix A.

Responses Considered for Characterization. The output parameters which were considered in characterizing the bomb were positive duration, positive impulse, and peak pressure. Positive duration is the time duration of overpressure; i.e., the time interval between the first indication of a pressure rise and the instant that the pressure next falls below its initial level. For each test, unit positive impulse was obtained by integrating the pressure time curve, using a planimeter or photographic records such as those in Fig. 11 through 13. The time base used was the positive duration (Eq. 4). Peak pressure data may be obtained directly from the pressure traces, but the pressures derived from wave velocity data were believed to be more accurate and were the ones correlated.

Positive Duration. The positive duration developed as being of little value in the characterization. From the raw data it appeared that positive duration did not vary significantly over the range of input parameters (explosive weight, explosive shape, and case thickness). Actually, a weak correlation (multiple correlation coefficient of 0.6) with charge weight was found:

$$\ln T_+ = 4.97 + 0.064 \ln W \tag{7}$$

63

where T_+ is positive duration in microseconds measured 10.0 inches from the bomb centerline and W is charge weight in grains. From this fitted equation, the average durations for charge weights of 5.5, 13.5, and 50 grains are, respectively, 161, 171, and 186 microseconds.

Unit Positive Impulse. Conversely, the unit positive impulse was very well correlated to the bomb parameters for characterizing the bomb data. Not only are these data more repeatable, but also most of the variation in impulse can be explained in terms of the input parameters. A model for high-explosive, nylon-case bombs was obtained which had a multiple correlation coefficient of 0.996, thus, the model accounts for more than 99 percent of the variation in impulse. Further, all three input parameters were significant in describing impulse. Case material was found not to be significant when Micarta was used in place of nylon; thus the following single model can be used for high-explosive charges encased with either material:

$$\ln I_u = 3.62 + 1.04 \ln W - 0.074 \ (\ln W)^2 - 0.353 \ln T_c + \qquad (8)$$

$$0.112 \ln (L/D)$$

In this model, I_u is unit positive impulse, measured in psi-microseconds at a location 10.00 inches from the bomb centerline; W, charge weight in grains; T_c, the case thickness in inches; and L/D, the shape factor. The error in unit positive impulse is about 8 percent as measured by the residual standard deviation (see Appendix A).

It should be noted that the term $(\ln W)^2$ is included in the correlation to account for a slight nonlinearity in the effect of bomb weight. Because such a term is included, the correlating equation cannot be used to infer what would happen for charge weights much larger than the 50-grain size used in this program. For larger weights, the square term becomes dominant to give unreasonably low predictions.

64

The data points correlated are shown in Fig. 14 together with correlating lines from Eq. (8). The effect of case thickness, while not as great as that of weight over the range of variation considered for each variable, is still appreciable.

In the bomb data analyzed, the variable weight and case thickness appear to be independent in their effects on unit impulse. That is, the effect of thickness is apparantly the same for each charge weight (and vise versa). Similarly, there is no apparant interaction of shape and case thickness or of charge weight and shape.

When the high explosive was replaced by the low-explosive Hercules Bullseye No. 2 powder, quite different effects were observed. The model for unit impulse became:

$$\ln I_u = 6.08 + 0.560 \ln W + 0.777 \ln T_c - 0.152 \left(\ln L/D\right)^2 \quad (9)$$

It is of the same general form as the model for high explosives, but the signs of two of the terms have been reversed. The most significant reversal is that, with pistol powder, the impulse <u>increased</u>, rather than decreased, with case thickness. Further, the effect of weight is somewhat less important than that of case thickness. These reversals offer positive evidence that low-explosive bomb output characteristics are predominantly controlled by the parameters that control case rupture. This is further substantiated by the observed secondary pressure waves (Fig. 13) which apparently resulted from continued burning of residual explosive after case breakage. Although data were not obtained with low-explosive, Micarta-case bombs, such a change in case material with this explosive should be expected to have a strong influence on the output characteristics.

The error in the fit for the low-explosive bombs was only slightly greater than for high-explosive bombs, being about 13 percent. The increase can be attributed to the fact that there are fewer data in the analysis. For simplicity of analysis, all raw unit-impulse data from bombs of the same

65
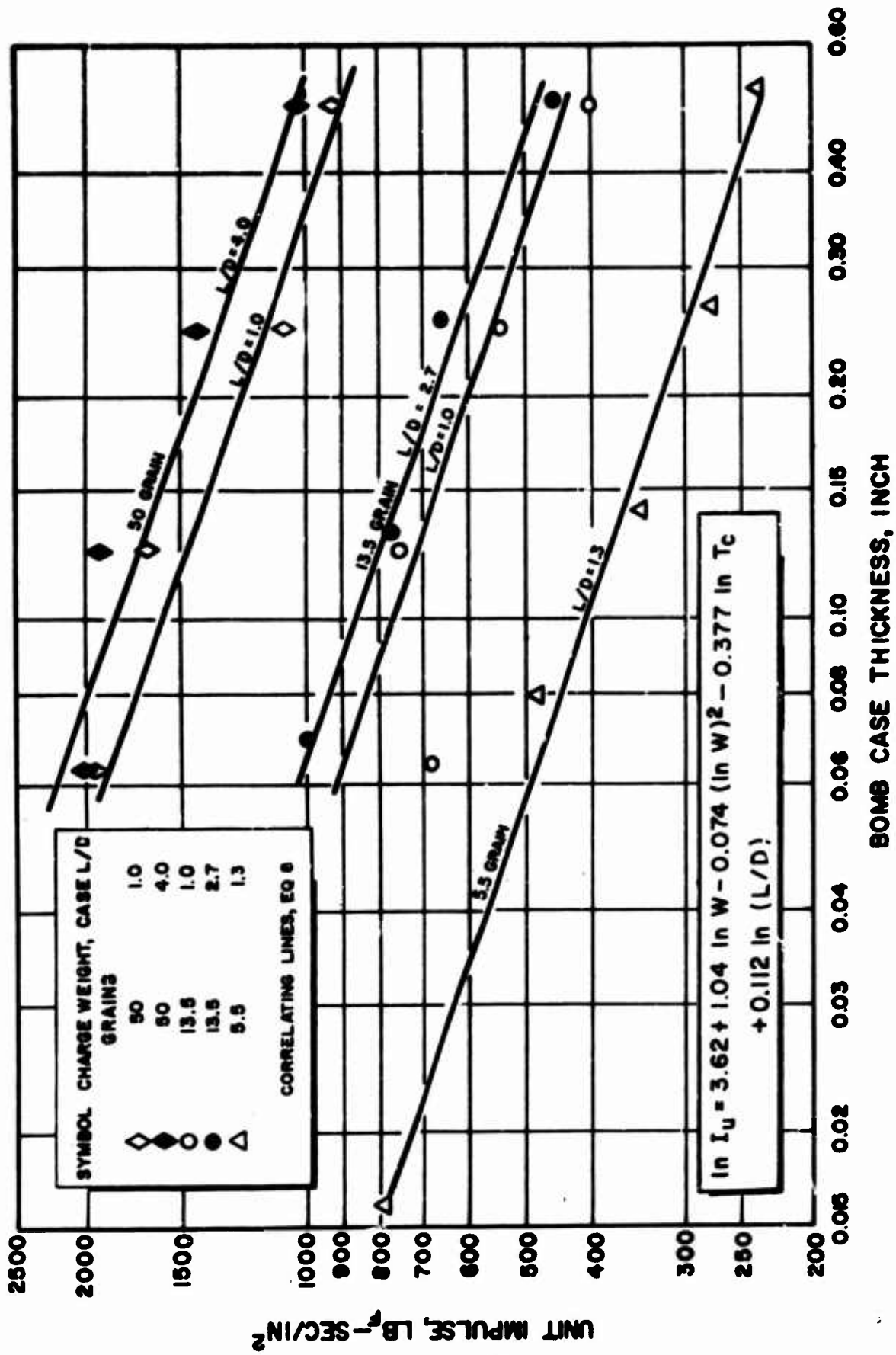
Figure 14. Correlation of Unit Impulse Measured 10.00 Inches From Cylindrical High-Explosive, Nylon-Case Bombs

configuration were averaged before the correlations were computed. Thus, the ln I_u was the logarithm of the average, not the average of the logarithms. It is not expected that this procedure has any significant effect on the values of the coefficients obtained. Since the numbers of observations on the bombs of various configurations varied somewhat (last columns of Tables 2 and 3), some of the data included in the analysis were more stable than others, being averages of a greater number of raw observations. While a more rigorous analysis would take these differences into account, it was not felt that the improved precision of the results was worth the added expense and trouble of analyzing all the data separately. This procedure does not affect the average accuracy of the results.

Peak Pressure. There are four kinds of peak pressure data that have been obtained from these experiments:

1. Direct-pressure transducer data obtained with a Kistler Model 603A transducer, located 10.00 inches from the bomb centerlines

2. Pressure calculated from an average blast-wave velocity as determined by measuring its transit time between two pressure transducers, located 7.00 and 10.00 inches from the bombs, respectively

3. Pressures calculated from local blast-wave velocity as determined by streak photography

    a. In the neighborhood of the bombs

    b. In the neighborhood of the transducers

As indicated earlier, the direct-pressure transducer measurements are believed to provide valid indications of unit impulse, positive duration, and wave shape, and yet give the least reliable measure of peak pressure. The other methods for obtaining peak pressures are all based on calculating shock-wave overpressure from wave velocity data. The correlation of peak pressure was attacked, therefore, through a correlation of wave velocity.

67

The blast-wave velocity data were obtained at various distances from the bombs. Since time from detonation and distance from the bomb are related through the wave velocity, either time or distance may be used in the correlation. It was thought to be reasonable that the wave velocity would decay exponentially with time and in a more complicated manner with distance. Time was selected, therefore, as the correlating variable.

Correlating models of the form

$$(c_s)_o = A \ W^a T_c^{\ b} \ (L/D)^c \tag{10}$$

for the initial wave velocity, and

$$c_s = (c_s)_o \ \exp\left[B \ W^d \ T_c^{\ e} \ t \right] \tag{11}$$

for the data in the neighborhood of the transducers, were attempted. The model for initial wave velocity gave:

$$\ln (c_s)_o = -4.507 + 0.186 \ \ln W - 0.557 \ \ln T_c \tag{12}$$

No significant effect of the charge shape factor (L/D ratio) was found. Curves of initial shock-wave over pressure, calculated from velocities derived from this equation, are shown in Fig. 15 with the individual, velocity-derived. initial-overpressure data points. This graph employs a semi-logarithmic scale, rather than the log-log scale which would be more appropriate for the correlating equation, so as to show that the data can very reasonably be extrapolated to the value of overpressure given in the literature for bare charges of 50/50 Pentolite. It is seen that a confining case around the charge greatly decreases the initial-shock-wave amplitude. The reduction is nearly an order of magnitude even for the thin case of the Olin Plasticap 5.5-grain detonator. This effect is obviously lessened by increasing charge weight, but, within the charge sizes of interest in stability rating, it is a very strong effect.

68
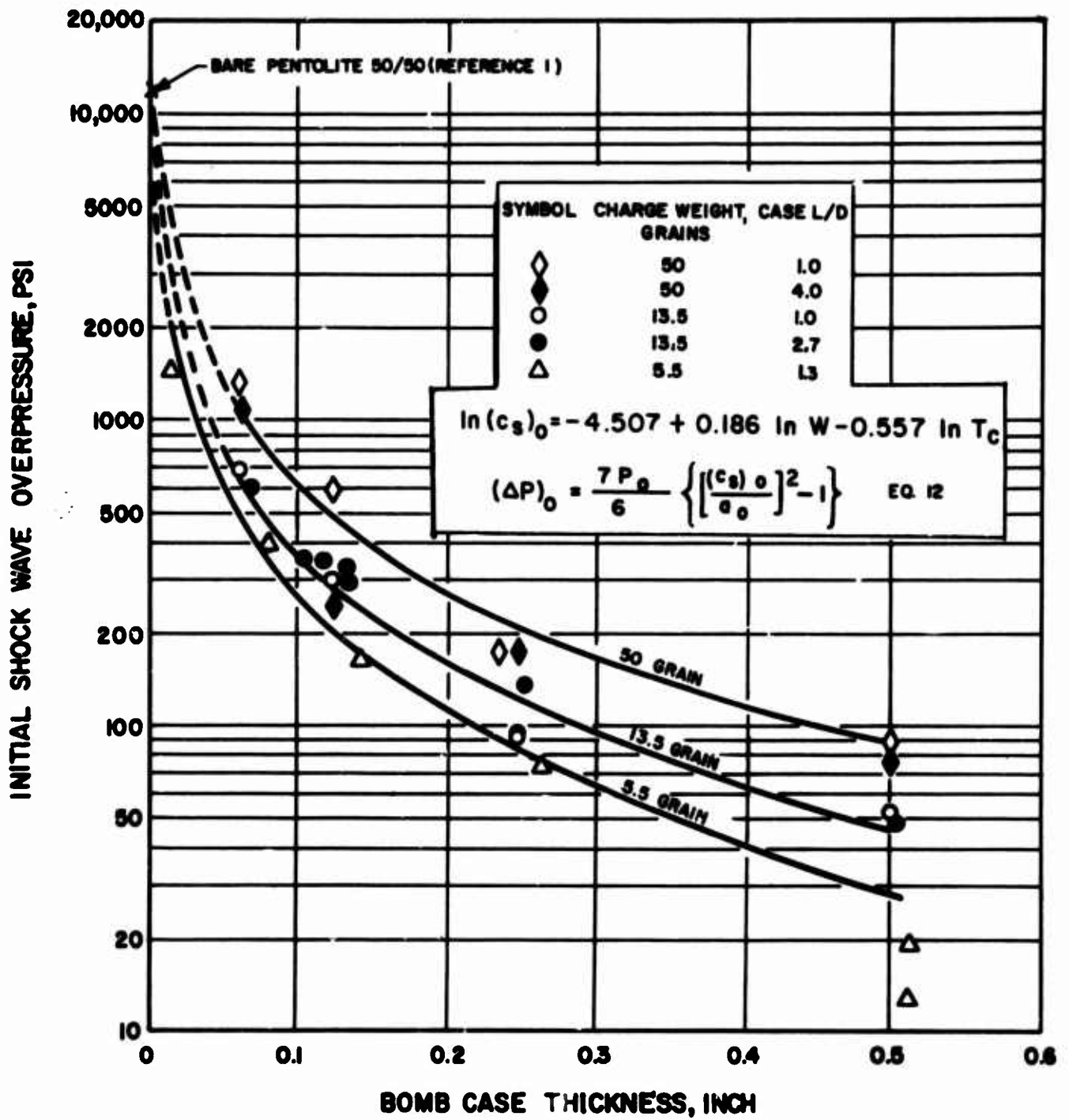
Figure 15. Initial Shock Wave Amplitude Calculated From
Streak Velocity Near the Bomb-Case Surface

69

The model for exponential decay of blast-wave amplitude, Eq. (11), did not yield satisfactory correlations. A more complex model, employing quadratic terms, was found to correlate the data well; the error in velocity was about 8 percent as indicated by the residual standard deviation. This model, however, required a variable constant whose value depended upon the method or position of data acquisition:

$$\ln o_s = \text{constant} + 5.21\ t - 4.82\ t^2 + 0.186\ \ln W -$$

$$1.05\ t^2\ \ln W - 0.557\ \ln T_c + 1.86\ t\ \ln T_c -$$

$$1.19\ t^2\ \ln T_c \tag{13}$$

where t is measured in milliseconds and velocity in in./microsec. The constant term which depends on the type of measurement involved, is as follows:

- 5.286 for streak photograph data taken in vicinity of transducer

- 5.397 for transducer transit-time velocities

- 4.507 for streak photograph data taken in vicinity of bomb.

No significant effect of the shape factor L/D was found. The quadratic terms in time were used to account for what are probably asymptotic effects, such as the wave velocity approaching the sound velocity as time increases.

While the correlation of the data by the model of Eq. (13) was quite good (9.0 percent error based on the standard deviation), the need for a variable constant is not particularly satisfying. It is of interest to note that the two values of this constant which correlated the data from the neighborhood of the transducers were in essential agreement, giving velocities that differed by about 12 percent [exp (5.397 - 5.286) -1].

70

Conversely, the mean value of those constants, inserted in Eq. (13) with
$t = 0$, gives velocities that are smaller by a factor of 2.3 [exp (5.341 -
4.507)] than those given by Eq. (12). This large disparity might partially
be attributed to the fact that the data were obtained from two sets of
experiments (Table 4 and 5), but is more likely a result of the data having
been obtained in two discrete spatial groupings, one at the bomb surface,
and the other in the interval of 5 to 10 inches from the surface, with no
intermediate points to bridge the gap.

The lack of intermediate data is made clearly evident by plotting the data
on an overpressure vs reduced distance basis, such as that used earlier to
show that the instrumentation system gave peak-pressure data in agreement
with other investigators' results (Fig. 8). In Fig. 16, a separate graph
is given for each of the three charge weights tested. The heavy, solid line
that sweeps down to the right across each graph is the mean correlating line
of Goodman (Ref. 1), and the heavy, dashed line is that of Ruetenik and
Lewis (Ref. 2) for large, bare high-explosive charges. As discussed earlier,
small bare charges of 50/50 Pentolite gave direct transducer peak pres-
sures that agreed with Goodman's correlation and wave-velocity-derived
pressures that agreed with Reutenik and Lewis'.

All three sets of velocity-derived data for nylon-case bombs are plotted
in Fig. 16. The initial-shock-wave amplitude data appear at low values
of reduced distance, i.e., the outer radius of the case divided by the
cube root of the charge weight for those data. It is noted that this
convention forces data for a high L/D ratio to move to the left of data
for a low L/D ratio. Data obtained by transducer transit time and streak
photography near the transducers appear at high values of reduced distance,
and are indistinguishable from one another.

The strong attenuating effect that the presence of a confining case has
on the initial-shock-wave overpressure is again seen. In some cases,
the plotted initial-shock values are as much as two orders of magnitude
lower than Goodman's correlation. As compared with Fig. 15, this type

71

of plot comes reasonably close to permitting a single correlating line for all of the initial-shock-wave amplitude data. If one assumes a single straight line, its equation would be of the form

$$\ln P_i = a - b \ln Z \tag{14}$$

or, substituting for Z,

$$\ln P_i = a + 1/3 \; b \; \ln W - b \ln R \tag{15}$$

Recognizing a correspondence of P_i to $(c_s)_0$ and of R to T_c, it is interesting to compare this expression with Eq. 12, and note the precise agreement of the coefficients of the logarithmic terms.

Somewhat arbitrary dashed lines have been sketched in Fig. 16 to connect data points from similar bombs. The shapes of these connecting lines were suggested by one set of streak-velocity-derived data from a single bare 13.5-grain, plastic-cased detonator that was fired in the preliminary transducer evaluation. Those points are plotted as X's in Fig. 16b. There is a strong implication that the blast-wave strength is maintained (or degraded at a much lower rate) for some distance from the bomb, and that the wave amplitude sooner or later becomes asymptotic to the behavior of a wave from a bare charge. Whether or not this effect, which is almost certainly attributable to the behavior of bomb-case fragments, is still appreciable at a distance 10 inches from the bomb, is obviously related to both charge weight and case thickness.

Except for the variable constant, the velocity correlation model could be used to calculate the pressure vs reduced distance curves which were roughly sketched in Fig. 16. An attempt to obtain a fit for all the data with a single constant, however, resulted in a very poor model, and several attempts to obtain a model in terms of velocity and distance were unsuccessful.

It was concluded that the bomb-to-transducer distance had unfortunately been chosen such that a number of the observed blast waves had acheived

72
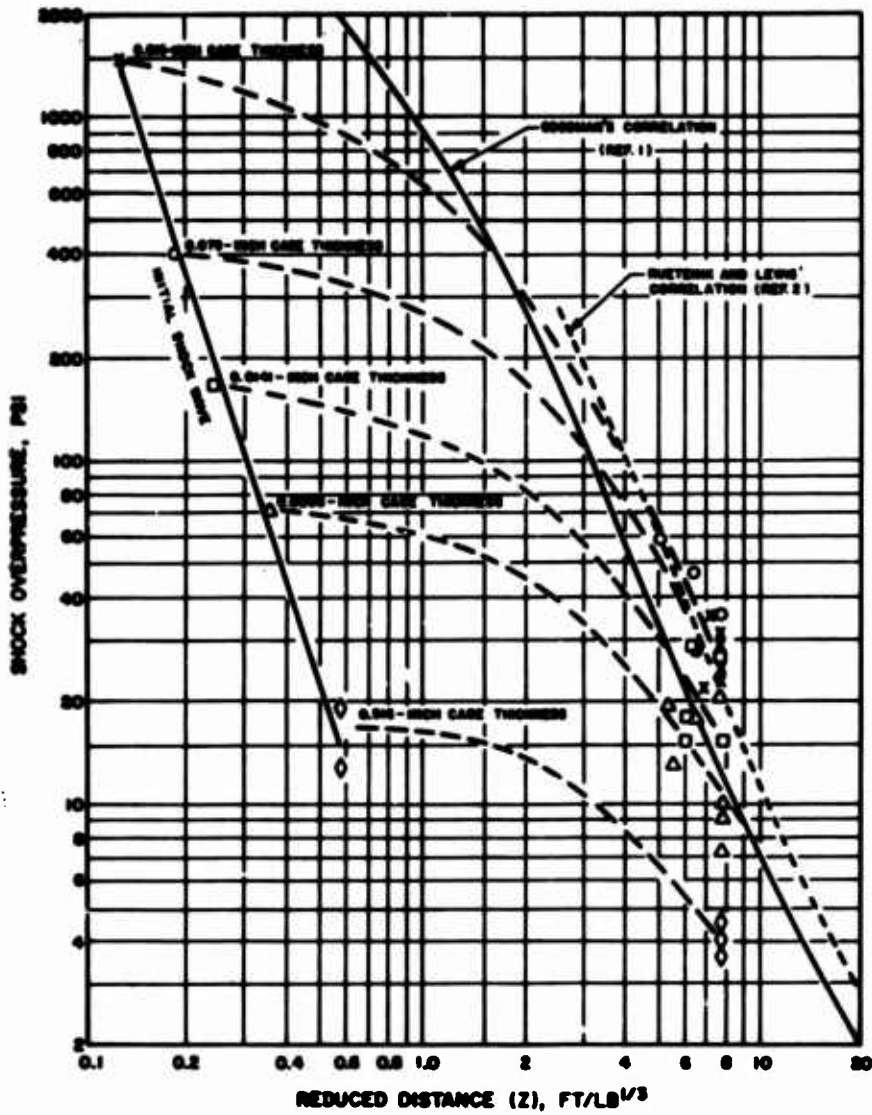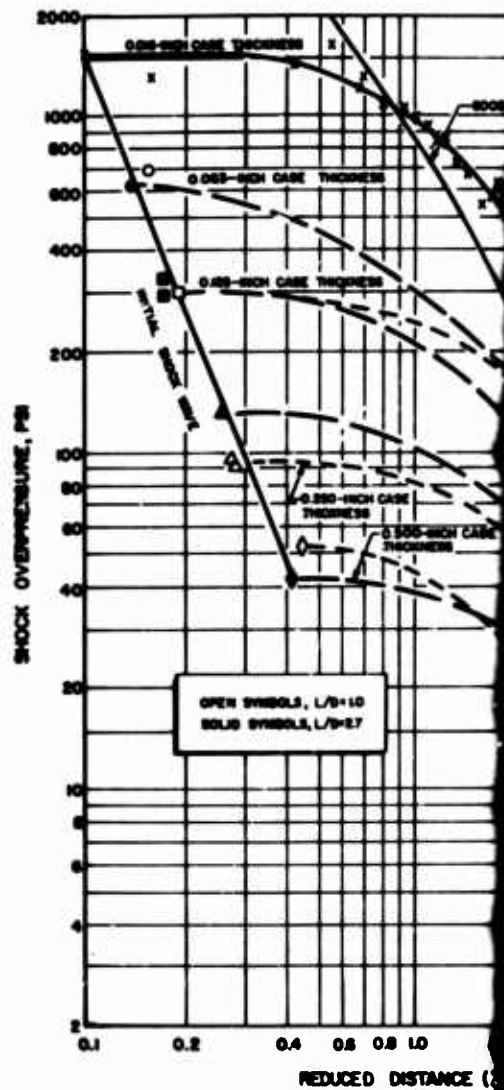
a. 5.5-Grain Bombs

b. 13.5-Grain

A
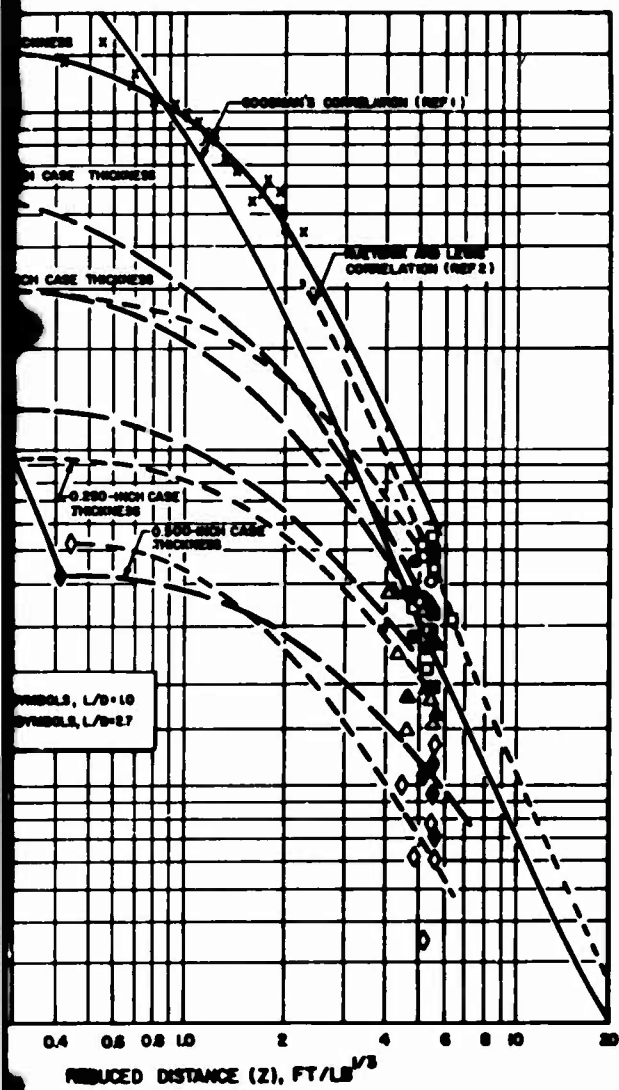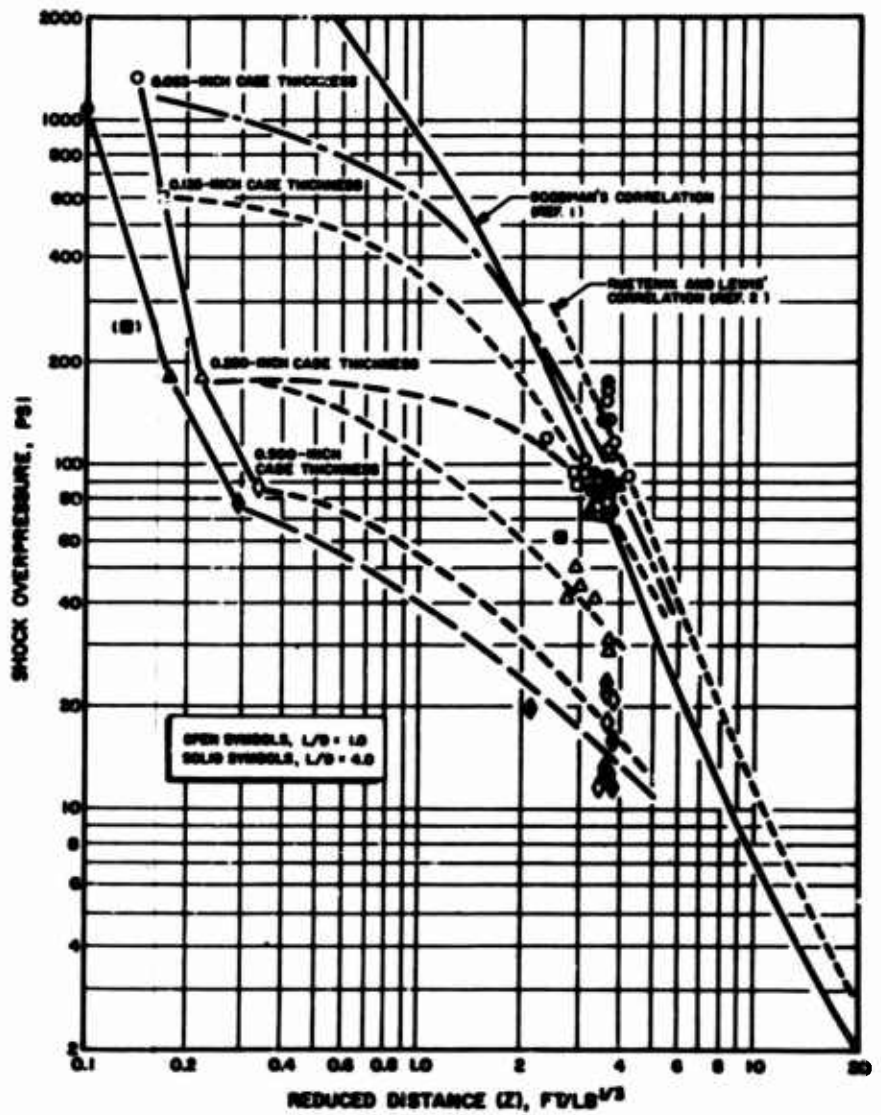
b. 13.5-Grain Bombs

c. 50-Grain Bombs

Figure 16. Air-Shock Wave Overpressures
From High-Explosive, Nylen-
Case Bombs

73

B

asymptotic recovery to bare-charge behavior, while others were at various
stages in the recovery process. The difficulty in obtaining adequate cor-
relation probably stems from mixing data from those two categories. Had
more streak-velocity data been sought in the 0- to 5-inch range, a valid
model for the recovery process probably would have been obtained.

From the available models, however, it is apparent that the initial-shockwave
correlation is the one of most value for characterizing bombs for stability
rating. Even though they did not correlate as well, the direct pressure
and distant velocity data provided useful information on the blastwave
shape, impulse, duration, case material, and explosive-type changes which
could not have been discerned from streak records alone.

Effect of Case Material. The transducer transit-time velocity data
for Micarta and nylon cases are compared in Table 8. These results sug-
gest that the nylon and Micarta cases are quite similar in their behavior.

PULSE GUNS

The combustion stability rating device known as the "pulse gun," introduces
a blast wave into a rocket combustion chamber that is followed by a trans-
ient directed flow of combustion product gases. Pulse guns were cold-flow
characterized in this program by firing them into a 50-gallon tank that
was prepressurized with an inert pressurant, and by measuring various
parameters near the inlet of the gun to the tank.

Experimental Apparatus

Pulse-Gun Hardware. The pulse guns evaluated were fabricated by Rocketdyne
from prints of engineering drawings supplied by AFRPL. The guns are ostensibly
identical to those developed at Aerojet-General Corp., and used for stability
ratings there and at AFRPL. A cross-sectional view of an assembled pulse
gun is shown in Fig. 17a, essentially reproduced from Ref. 4. It consists
of an explosive charge loaded in a center-fire cartridge, contained within
a sealed combustion chamber (breech); a mechanism for initiating explosion
of the charge; a passageway (barrel) for conducting the explosion products

TABLE 8

COMPARISON OF MICARTA AND NYLON CASE TRANSDUCER
TRANSIT TIME VELOCITY DATA

Charge Weight, grains	Case Thickness, inches	Charge L/D Ratio	Wave Velocity, inches/microseconds	
			Micarta	Nylon
5.5	0.063	1.3	0.0170	–
5.5	0.250	1.3	0.0188	–
13.5	0.063	2.7	0.0300	0.0273
13.5	0.250	2.7	0.0247	0.0227
13.5	0.063	1.0	0.0285	0.0314
13.5	0.250	1.0	0.0215	0.0189
50	0.063	4.0	0.0324	0.0408
50	0.250	4.0	0.0259	0.0313
50	0.063	1.0	0.0337	0.0408
50	0.250	1.0	0.0223	–
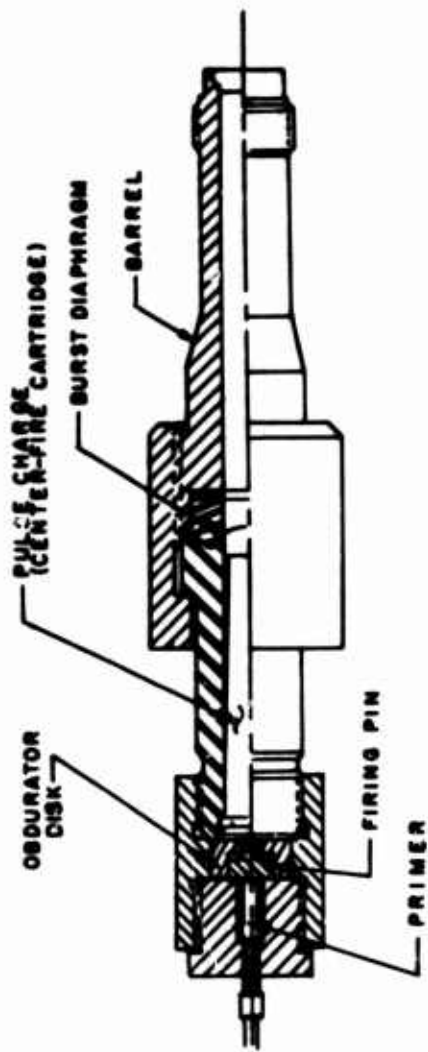
(a) Section View of Assembled Pulse Gun (Ref. 4)
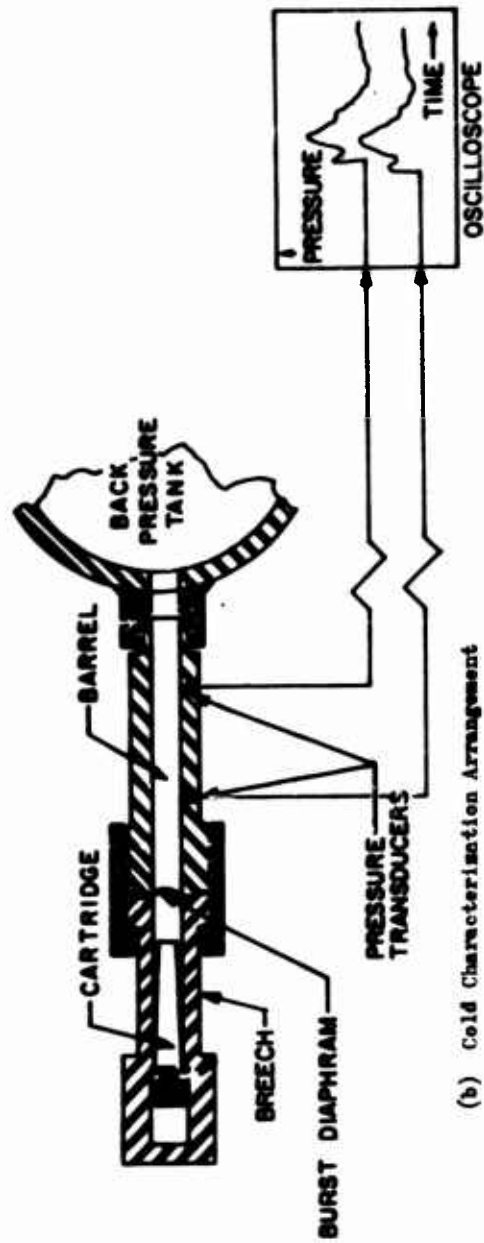
(b) Cold Characterization Arrangement

Figure 17. Pulse Gun Cold-Characterization Apparatus

into the combustor to be perturbed and a burst-diaphragm, pre-explosion closure for that passage. The pulse-gun assembly is attached to the combustor with a threaded connection that has a compression seal. The experimental arrangement used in cold-characterization firings is shown schematically in Fig. 17b.

There are two difference breeches: one accepts caliber .38 Special pistol cartridges which are used for 10- and 15-grain charges the other accepts caliber .300 Magnum rifle cartridges for 20-grain and larger charges*. Standard center-fire primers are used to initiate explosion of the charges; these are fired by impact with a firing pin, which is driven, in turn, by combustion gases from a small, electrically initiated primer**.

The pulse-gun barrel design was modified to accommodate pressure transducers. A modified barrel having the same length as the standard barrel (Fig. 17a) is shown in Fig. 18a. In the first firings, with the gun discharged into the ambient air, the blast wave had not coalesced into a well-defined, steep-fronted shock wave by the time it passed the last transducer location of that barrel. Therefore, a longer barrel was built, having a total length equivalent to the longest blast-wave travel path in the subsequent rocket motor firing program. This longer barrel design is detailed in Fig. 18b. In the barrel, transducer ports were centered at distances of 1.44, 3.72, and 6.00 inches downstream of the seating surface for the burst diaphragm flange.

---

*Maximum charge weights of 80 grains were used in this program. Even larger charges have been used with larger breeches at Aerojet-General Corp. (Ref. 4). The resultant combustion chamber disturbance amplitudes were found, however, to be related to the fraction of the breech volume occupied by the explosive charge so that smaller disturbances resulted from 160-grain charges that filled only 63 percent of the breech than from 80-grain charges that filled 88 percent of the smaller breech. These data were obtained with a single burst-diaphragm rating (20,000 psi).

**The Bermite MK113 Primer designated in the pulse-gun specification obtained from AFRPL, was replaced after about 16 charges were fired with a similar primer that was available as surplus equipment from another program. This change had no observable effect upon the behavior of the gun.

77

(a) Standard Length Modified Barrel With Transducer Ports

(b) Long Modified Barrel With Transducer Ports

Figure 18. Modified Pulse Gun Barrel Details

Burst diaphragms having 7500-, 10,000-, and 20,000-psi pressure ratings were purchased from Fike Mfg. Co. The diaphragms served the triple function of protecting the charges from exposure to combustion-product gas temperatures, prohibiting explosion products to escape from the breech until the charges were nearly completely burned, and forming a shock wave to initiate the pulse.

Pulse Charges. A fast-burning, double-base, smokeless pistol powder (Hercules Bullseye No. 2, or equivalent) is designated in the pulse-gun specification received from AFRPL. This specification was adhered to for the majority of the pulse charges fired, both in the cold-characterization and hot firings. One of the desired evaluations was the effect of explosive type on the characteristics of the gun. Several charges were tested, therefore, with a different explosive.

Some consideration was given to using a high explosive for the change in explosive type. This idea was soon rejected because of the possibility that the breech might be ruptured before the diaphragm could break and provide pressure relief from a highly brissant explosion.

It was desired to evaluate the effect of a substantial change in the explosive burning rate. The characteristics of commercial powders were examined, and it was found that a larger change could be effected by going to slower burning powders. Among Olin powders, for example, WC230 (comparable with Hercules Bullseye No. 2) has a relative quickness of about 5 in comparison with WC846 (a 7.62-millimeter NATO military cartridge powder and Olin's standard of comparison), while their fastest burning powder, WC Blank, has a relative quickness of about 10. There are some rifle powders that burn even more slowly than WC846 so changes by a factor of 5 or more could be made by using slower burning powders and by a factor of only about 2 by using faster burning powders. It was decided, therefore, to select a slower burning powder. A check of those available locally led to the selection of duPont Military 3031 which has characteristics comparable with the Olin WC846 referred to earlier. Because the slower burning rate is partially achieved by reducing the percentage of nitroglycerin, the heat of combustion of the duPont Military powder is only

79

about 70 percent that of Hercules Bullseye powder. For comparable charge weight, therefore, the change in powder should be expected to give reduced pressure amplitudes.

Charge weights tested were the same as those used by other investigators: 10- and 15-grain charges loaded in caliber .38 Special cartridges and 20-, 30-, 40- and 80-grain charges loaded in caliber .300 H&H Magnum cartridges. The blast-wave magnitude may be predominantly controlled by the charge size, but is also influenced by the burst-diaphragm rating, particularly if the powder is only partially burned when the diaphragm ruptures (Ref. 5). For that reason, both charge weight and burst-diaphragm strength are quoted in specifying a pulse charge.

To avoid confusion in presenting and interpreting data, a more completely descriptive charge nomenclature is used in this report: each pulse will be identified by the base charge weight, powder identification, and burst-diaphragm rating. As illustrative examples, 15HB/10K designates a 15-grain charge of Hercules Bullseye powder with a 10,000-psi burst diaphragm, and 40 duPM/20K designates a 40-grain charge of duPont Military powder with a 20,000-psi burst diaphragm.

Instrumentation. Because the transients involved during testing required instrumentation having the highest frequency response available, a search was made to obtain components permitting high-frequency response compatible with good precision and reliability in the explosive environment. This led to the selection of the Kistler 607L pressure transducer which has a range of 0 to 30,000 psi, and good linearity. Its natural frequency is approximately 130 kc.

The output of the transducer was amplified by a charge amplifier flat to 150 kc. Primary data records were obtained by photographing the outputs of two such transducers displayed on an oscilloscope. The two pressure signals, together with an amplified temperature signal were also recorded simultaneously on magnetic tape. The magnetic tape provided backup in case of malfunction of the oscilloscope, and also permitted more versatile analysis and data reduction after the tests.

The frequency response of the primary pressure measurement system was limited by the natural frequency of the pressure transducer (130 kc), since the oscilloscope and charge amplifier have flat responses above that frequency. The tape-recorded data were limited in frequency response to 100 kc by the electronics of the tape system. For this reason, leading edges of pressure traces were analyzed using directly recorded oscilloscope traces only.

The pressure transducers were installed in the outermost two transducer ports of the pulse-gun barrel (Fig. 18) in all tests. A 5-mil, chromel-alumel thermocouple was mounted in the middle port; the thermocouple tip was recessed approximately 1/16 inch to avoid damaging it with burst-diaphragm and charge-cartridge fragments. The response time of the thermocouple was quite long, on the order of 1/4 second; nevertheless, it proved to be useful in identifying explosion product leakage past improperly tightened or cleaned diaphragm seating surfaces.

Experimental Procedure

It was originally planned to fire a total of six charges from each charge category with the six charges distributed as follows: (1) one charge fired into open air, (2) three charges fired into a 50-gallon tank containing gaseous nitrogen at ambient temperature and 150-psig back-pressure, and (3) two charges with a back-pressure of 250 psig. A typical test sequence involved the following steps:

1. The components for a pulse-charge assembly, consisting of one diaphragm, one loaded cartridge, and one squib, were obtained from storage, and the pulse gun was thoroughly examined.

2. The primer chamber, firing pin assembly, and diaphragm seating surfaces of the pulse gun were cleaned, and the hardware was inspected for damage resulting from previous firings.

3. The diaphragm, cartridge, and primer were installed, and the pulse gun assembly was mounted in the receiving tank.

4. The transducer lines were connected, the pressure in the receiving tank was adjusted to the desired value, the electronic instrumentation was checked and the pulse gun was fired.

During the course of the firings, certain difficulties and problem areas were encountered repeatedly. These are listed in some detail to provide information which may prove helpful in future pulse-gun firings.

1. The weakest component in the pulse-gun assembly was the firing pin. Three firing pins were lost because of severe cracks in the body of the pin. Two firing pins jammed within the obdurator disk during the early firings. No solution to the cracking of the firing pins was found, but the jamming was apparently eliminated by a careful cleaning of the pin and holder after each firing, combined with a careful alignment of the pin within its enclosing cylinder during the pulse-gun assembly. Future pulse-gun designs might be improved by lengthening the piston portion of the firing pin to improve the alignment.

2. During the first firing of the larger charges (40 to 80 grains), it was noted that some runs showed leakage of combustion gases under the seating surface of the diaphragm. This was first discovered by examining the thermocouple trace and comparing it with that of the upstream pressure transducer. In cases where leakage occurred before rupture of the diaphragm, a definite output from the thermocouple was noted before the upstream pressure step appeared. In severe leakage cases, the leakage was also visible on the upstream pressure trace as a small pressure pulse visible before the large pressure step caused by diaphragm rupture (Fig. 19). Leakage was practically eliminated by careful attention to the cleaning procedure used on the seating surface and by using a methodical tightening sequence during pulse-gun assembly.

3. Examination of pressure traces from several firings showed considerable ringing in the pressure transducers before rupture of the burst diaphragm. Apparently this was caused by the mechanical shock transmitted to the body of the pulse gun by the actuation of the firing pin. In some runs showing an unusual amount of ringing before diaphragm rupture, it was found by later examination

82
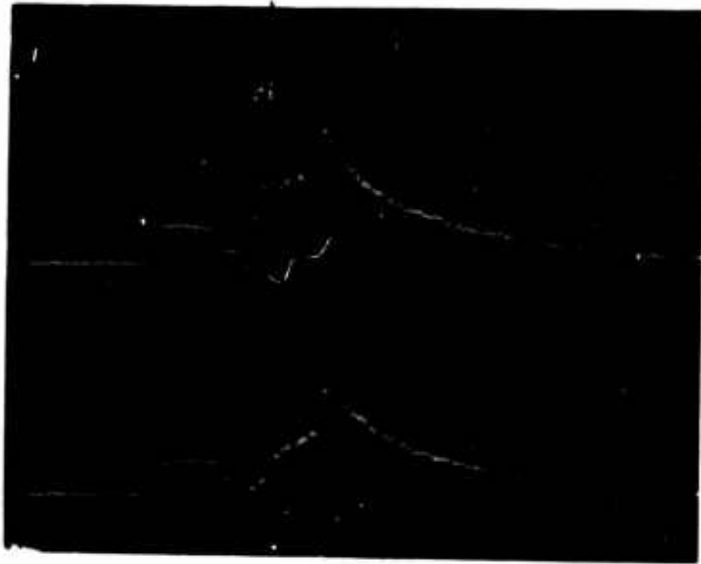
100 microsec/cm

a. An 80 HB/20K Charge

200 microsec/cm
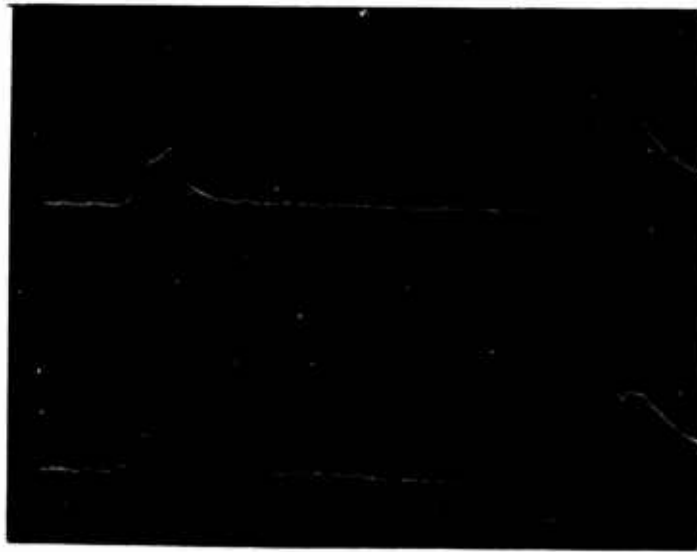
b. A 40 duPM/20K Charge

Figure 19. Examples of Pressure Surges Before
Burst Diaphragm Rupture

of the pulse-gun assembly that the firing pin exhibited considerable friction within its containing cylinder that apparently retarded completion of its normal stroke. Replacement of those firing pins resulted in a smoother preshock trace.

4. Pulse-gun firings into the receiving tank resulted in considerable postrun vibration, which often loosened the pressure transducers in their mounts. It was necessary to check the transducers after every firing to see whether they had become loosened by vibration.

Experimental Results

The majority of the information obtained from pulse-gun firings is derived from the recorded pressure-time data. In this section, examples of these raw data are presented and discussed, and tabulations of the data reduced from them are given.

Typical examples of pressure-time traces obtained with the standard charge categories tested are shown in Fig. 20. With the exception of Fig. 20c, all records were photographed directly from an oscilloscope. The record of Fig. 20c was obtained from playback of tape-recorded data from the same firing as that shown in Fig. 20b. The reduction in response incurred in the tape-recording process, using available equipment, is apparent. Additional examples of nonstandard combinations of charge weight and burst-diaphragm strength appear in Fig. 21, and three of duPont Military powder charges are shown in Fig. 22.

Many points of similarity can be discerned among the oscilloscope data as well as a few points of dissimilarity. There are also some unexplained phenomena. In discussing these data, the same convention will be used as was earlier in presenting bomb data: a numerical subscript of a parameter denotes distance from the source, in this instance, downstream of the burst diaphragm. Thus $P_{1.44}$ is the static pressure at a position 1.44 inches from the diaphragm, and $\Delta t_{1.44-6.0}$ is the blast-wave transit time between transducers located at 1.44 and 6.00 inches from the diaphragm.

200 microsec/cm

1250 psi/cm

b. 15HB/10K Charge

200 microsec/cm

2500 psi/cm

d. 20HB/20K Charge

200 microsec/cm

625 psi/cm

a. 10HB/7.5K Charge

200 microsec/cm

c. Tape-Recorder Data From Same
15HB/10K Charge as b
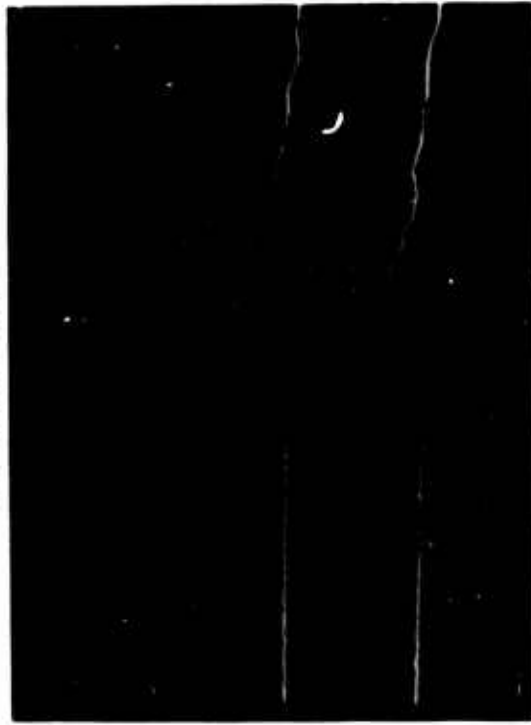
Approximately 1250 psi/cm

200 microsec/cm

A

c. Tape-Recorder Data From Same
15HB/10K Charge as b

200 microsec/cm

2500 psi/cm

e. 30HB/20K Charge

d. 20HB/20K Charge

200 microsec/cm

6250 psi/cm

f. 40HB/20K Charge

20 microsec/cm

12,500 psi/cm

g. 80HB/20K Charge

NOTE: Upper Traces are $P_{1.44}$,
Lower Traces are $P_{6.00}$ in all
Photographs

Figure 20. Pressure Records From Pulse Guns Fired Into a
150-psig Back Pressure Tank

85

B

200 microsec/cm

$P_{1.44}$
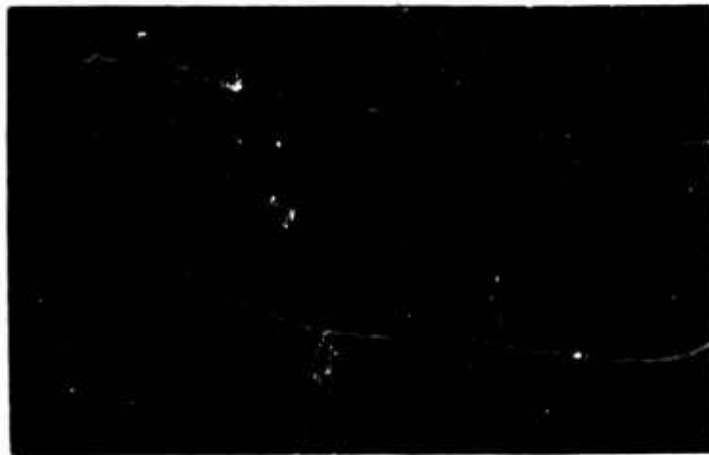
$P_{6.00}$

2500 psi/cm

a. A 20HB/7.5K Charge

200 microsec/cm

$P_{1.44}$

$P_{6.00}$

1250 psi/cm

b. A 20 HB/10K Charge

200 microsec/cm
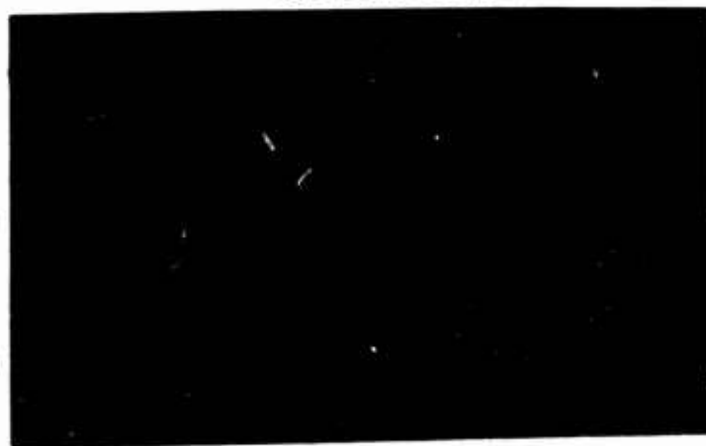
$P_{1.44}$

$P_{6.00}$

2500 psi/cm

c. A 20 HB/20K Charge

Figure 21. Examples of Pulse Gun Blast Waves From Nonstandard Charge
Weight and Diaphragm Strength Combinations

200 microsec/cm

1250 psi/cm

$P_{1.44}$

$P_{6.00}$

b. A 70 duPM/20K Charge

200 microsec/cm

625 psi/cm
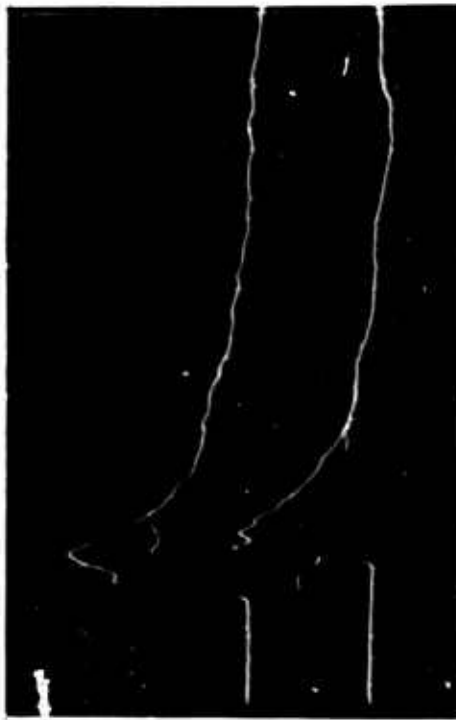
$P_{1.44}$

$P_{6.00}$

a. A 20 duPM/10K Charge

6250 psi/cm

$P_{1.44}$

$P_{6.00}$

d. An 80 duPM/20K Charge

1500 psi/cm

$P_{1.44}$

$P_{6.00}$

c. A 40 duPM/20K Charge

Figure 22. Examples of Pulse Gun Blast Waves From Slower Burning duPont Military 3031 Powder

The most obvious point of similarity among the pressure traces is the
apparent occurrence of two shock waves. This is most clearly seen with
the larger charges, but is readily identified with the smaller charges
as well. The initial steep-fronted pressure rise is undoubtedly a shock
wave resulting from the burst-diaphragm rupture. A second, sometimes less
steep-fronted, pressure wave follows the initial shock wave. The secondary
wave usually propagates faster than the initial wave (and thus tends to
overtake it), and often is seen to steepen between the 1.44- and 6.00-inch
transducer positions.

The mechanism by which this secondary pressure wave is produced, has not
been established; certainly it must come from within the pulse-gun breech,
since the wave propagates in a downstream direction. At first it was
thought that the secondary pressure wave resulted from shock reflections
within the pulse-gun breech, e.g., an initial explosion wave reflected
from the burst diaphragm before it ruptured and subsequently reflected
from the primer end of the effectively empty cartridge. This interpre-
tation could not be supported in attempts at constructing a wave diaphragm
because of the variable time increment between the waves. The appearance
of similar multiple waves, spaced at nonreproduced time intervals, in
the low-explosive-bomb pressure records (Fig. 13) offers a strong clue
to the probable cause, i.e., continued burning of residual powder after
the diaphragm ruptures is at high enough rate to produce a succession
of pressure wavelets which eventually coalesce into a second shock wave
as they propagate down the gun barrel.

Another point of similarity is the essentially constant duration of the
positive pressure portion of the pulses, regardless of charge size,
burst diaphragm strength, or breech volume.

The initial shock wave is recorded with a total rise time of approximately
4 to 5 microseconds. (This is not apparent on the traces reproduced here,
but was observed on direct oscilloscope photographs with faster oscillo-
scope beam sweep rates.) The measured rise time may be limited both by

the natural frequency of the transducer and by the response of the
transducer when a plane pressure wave propagates across the finite width
of its sensing surface. The transducer limiting rise time is only slightly
less than 4 microseconds $([(2)(130,000)]^{-1})$ and, at the measured initial-
wave velocity, the wave takes approximately 5 microseconds to cross the
transducer face. Within the ability of the transducers to resolve it, then,
the initial wave is indicated to be a pressure discontinuity or shock wave.

The precursor disturbances resulting from pressure-wave transmission through
the pulse-gun structure are particularly evident in Fig. 20a and 20d
Transducer ringing at the natural frequency of 130,000 cps appears to be
worse with the smaller charges because of the greater gain used in recording,
but is probably not actually of any different amplitude than with large
charges.

Data reduced from the pressure-time records are: initial-shock amplitude,
maximum-pressure amplitude, positive-pressure duration, total impulse, and
initial-shock-wave transit time between transducers. This latter value is
used to calculate an average wave velocity. These data, for all firings made,
are presented in Table 9.

To give a qualitative feeling for the pulse gun data before proceeding with
the correlation, plots of two complete sets of data are shown in Fig. 23
and 24. Both plots are of the maximum blast wave pressure from "standard"
pulse charge designations, and both show data obtained with three different
downstream backpressures. Figure 23 shows data from the transducer located
1.44 inches downstream of the burst diaphragm, while the data in Fig. 24
are from the 6.00-inch position.

The only correlating line shown in Fig. 23 and 24 is that reported by
Peoples (Ref. 5) at Aerojet General Corporation for data obtained with
pulse guns fired into the open air, using a transducer location comparable
with the 6.00-inch position of Fig. 24. The effect of explosive charge

89

TABLE 9

BLAST WAVE DATA FROM PULSE GUN FIRINGS

Test Number	Charge Description	Barrel Length	Set Pressure, psig Nitrogen	$\Delta P_{1.44}$ Shock Amplitude, psig	$(\Delta P_{1.44})_{max}$ Maximum Pressure, psig	$I_{1.44}$ Total Impulse, lbf-sec	$(t_o)_{1.44}$ Pulse Duration, Microsec	$\Delta P_{6.00}$ Shock Amplitude, psig	$(\Delta P_{6.00})_{max}$ Maximum Pressure, psig	$I_{6.00}$ Total Impulse, lbf-sec	$(t_o)_{6.00}$ Pulse Duration, Microsec	$\Delta t_{1.44-6.00}$, microsec	Initial Shock Velocity, ft/sec
32	10BB/7.5K	Long	150	1440	1440	0.0975	1010	1280	1250	0.0480	790	116	3370
116		Long	150	1440	1560	0.0800	800	2150	2150	0.0775	970	84	4350
117		Long	150	1625	2130	0.0915	760	2160	2160	0.0675	760	98	4380
118		Long	150	1670	2080	0.0932	800	2110	2110	0.0895	900	86	4400
1		Short	Ambient	See Note 2	1095	See note 2	—	—	—	See note 3	—	—	—
2		Short	Ambient	—	1699	—	—	—	—		—	—	—
16	15BB/10K	Short	270	1340	1370	See note 3	—	—	—		—	—	—
18		Short	Ambient	—	1810	—	—	—	—		—	—	—
17		Short	Ambient	—	2330	—	—	—	—		—	—	—
19		Short	Ambient	—	2600	—	—	—	—		—	—	—
46		Long	150	2290	2290	0.165	980	2770	3120	0.105	860	86	4410
45		Long	150	2640	3440	0.161	1050	1050	2000	0.0970	1010	90	4350
33		Long	150	2290	2640	0.163	1020	1075	1875	0.0862	880	88	4370
37		Long	150	1960	2330	0.218	966	2900	3080	0.116	870	88	4370
38		Long	150	2640	3330	0.142	1090	1560	2770	0.104	950	86	4450
44		Long	270	1310	3000	0.190	950	1500	1940	0.0975	870	135	2890
43		Long	270	1750	2220	0.166	1020	—	—	—	1000	116	3500
39		Long	Ambient	—	2640	—	—	—	—	—	—	—	—
36		Long	Ambient	—	2880	—	—	—	—	—	—	—	—
47		Long	Ambient	—	4460	—	—	—	—	—	—	—	—
23	20BB/20K	Long	150	4120	4120	0.216	1050	4000	4250	0.173	810	64	7940
38		Long	150	2770	3940	0.210	1040	3500	4120	0.162	780	72	5200
48		Long	150	4250	4680	0.218	960	4120	4250	0.124	700	72	5200
49		Long	150	3900	4250	0.207	960	3900	4120	0.122	700	70	5430
30		Long	150	3770	4250	0.193	1060	3500	4380	0.121	900	75	5070
28		Long	250	3080	3080	0.187	880	4380	4620	0.182	990	70	5430
51		Long	270	4250	4750	0.281	1060	4500	5000	0.157	810	84	4500
56		Long	Ambient	—	4050	—	—	—	—	—	—	—	—
24	30BB/20K	Long	150	6375	6230	0.364	1100	4000	5000	0.242	1010	72	5200
26		Long	150	4000	6575	0.324	1060	5250	5375	0.232	1000	72	5200
55		Long	150	6375	6125	0.324	1040	3900	5875	0.254	980	68	5590
35		Long	250	6375	6575	0.392	1210	3000	4750	0.210	1150	84	4500
		Long	250	6075	6375	0.362	1140	3770	6500	0.286	800	82	4650

TABLE 9
(Concluded)

Test Number	Charge Description	Barrel Length	Bomb Pressure, psig Nitrogen	$\Delta P_{1.44}$ Shock Amplitude, psig	$(\Delta P_{1.44})_{max}$ Maximum Pressure, psig	$I_{1.44}$ Total Impulse, lbf-sec	$(T_+)_{1.44}$ Pulse Duration, Microsec	$\Delta P_{6.00}$ Shock Amplitude, psig	$(\Delta P_{6.00})_{max}$ Maximum Pressure, psig	$I_{6.00}$ Total Impulse, lbf-sec	$(T_+)_{6.00}$ Pulse Duration, Microsec	$\Delta t_{1.44-6.00}$ Microseconds	Initial Shock Velocity, ft/sec
56	M58/20K	Long	270	3,875	7,125	0.377	1140	5,750	5,750	0.261	1040	84	4520
57		Long	Ambient		10,000								
59		Long	150	7,200	9,560	0.420	1070	6,250	6,250	0.298	980	90	6570
58		Long	150	5,310	8,770	0.445	1150	6,000	6,250	0.334	1070	80	6540
31		Long	150	5,750	8,770	0.495	1160	6,300	5,950	0.322	990	65	5850
30		Long	270	5,250	5,250	0.516	1070	6,060	7,250	0.385	1090	76	5900
60		Short	270	5,000	5,000	0.498	980	5,650	7,300	0.300	960	71	5330
15	Di4K/20K	Ambient	Ambient		21,900								
8		Long	Ambient		26,000								
7		Short	Ambient		24,000								
34		Long	150	12,700	25,000	0.991	1140	8,300	15,000	0.527	1090	53	7170
55		Long	150	13,770	25,000	0.966	1180	7,750	14,000	0.506	910	57	6670
61		Long	150	15,000	25,000	1.016	1080	7,000	13,770	0.533	1000	98	6950
62		Long	270	11,900	25,000	0.978	930	10,000	13,100	0.678	930	54	7000
120		Long	270	11,290	25,000	0.963	980	10,300	13,100	0.595	970	52	7200
130	2064FV/10K	Long	150	1,100	1,400	0.118	1280	1,100	1,250	0.0887	1130	128	3170
100	2068/10K	Long	150	2,300	2,600	0.213	1330	2,130	2,430	0.181	1292	96	3900
102	2068/16K	Long	150	2,090	2,200	0.216	1390	1,600	2,000	0.167	1220	108	3800
119	2068/18K	Long	150	1,600	3,600	0.202	1270	1,350	2,250	0.1265	1080	117	3850
131	2064FV/18K	Long	150	1,430	1,640	0.0980	1300	1,100	1,100	0.0945	920	108	3550
122	2064FV/18K	Long	150	1,100	1,520	0.0815	1070	1,100	1,100	0.0945	800	88	3800
107	2064FV/20K	Long	150	1,977	2,660	0.181	1080	1,780	1,780	0.0995	1040	88	4770
108	2064FV/20K	Long	150	1,810	2,770	0.181	1040	1,700	1,900	0.0970	1070	83	4440
105	2064FV/20K	Long	150	2,050	2,810	0.1475	1310	2,000	2,000	0.125	1150	80	3990
106	2064FV/20K	Long	150	2,050	3,100	0.164	1120	1,770	2,000	0.1215	1200	82	4440
109	2064FV/20K	Long	150	1,562	3,750	0.182	1440	1,910	2,310	0.1135	1080	98	4130
110	2064FV/20K	Long	150	1,760	2,920	0.165	1160	1,950	2,100	0.1180	1040	76	7000
135	2064FV/20K	Long	150	6,690	12,000	0.575	1440	6,300	6,300	0.225	1210	73	4670
124	2064FV/20K	Long	150	4,590	12,000	0.572	1380	5,900	6,060	0.215	1260	68	7790

NOTES:
1. For ambient firings there was no shear-defined shock front at location 1.44 so that data for $\Delta P_{1.44}$, $\Delta t_{1.44-6.00}$, and initial shock velocity could not be obtained.
2. Total impulse data was not obtained for ambient firings.
3. Total impulse data was not obtained for firings using the short barrel.

91
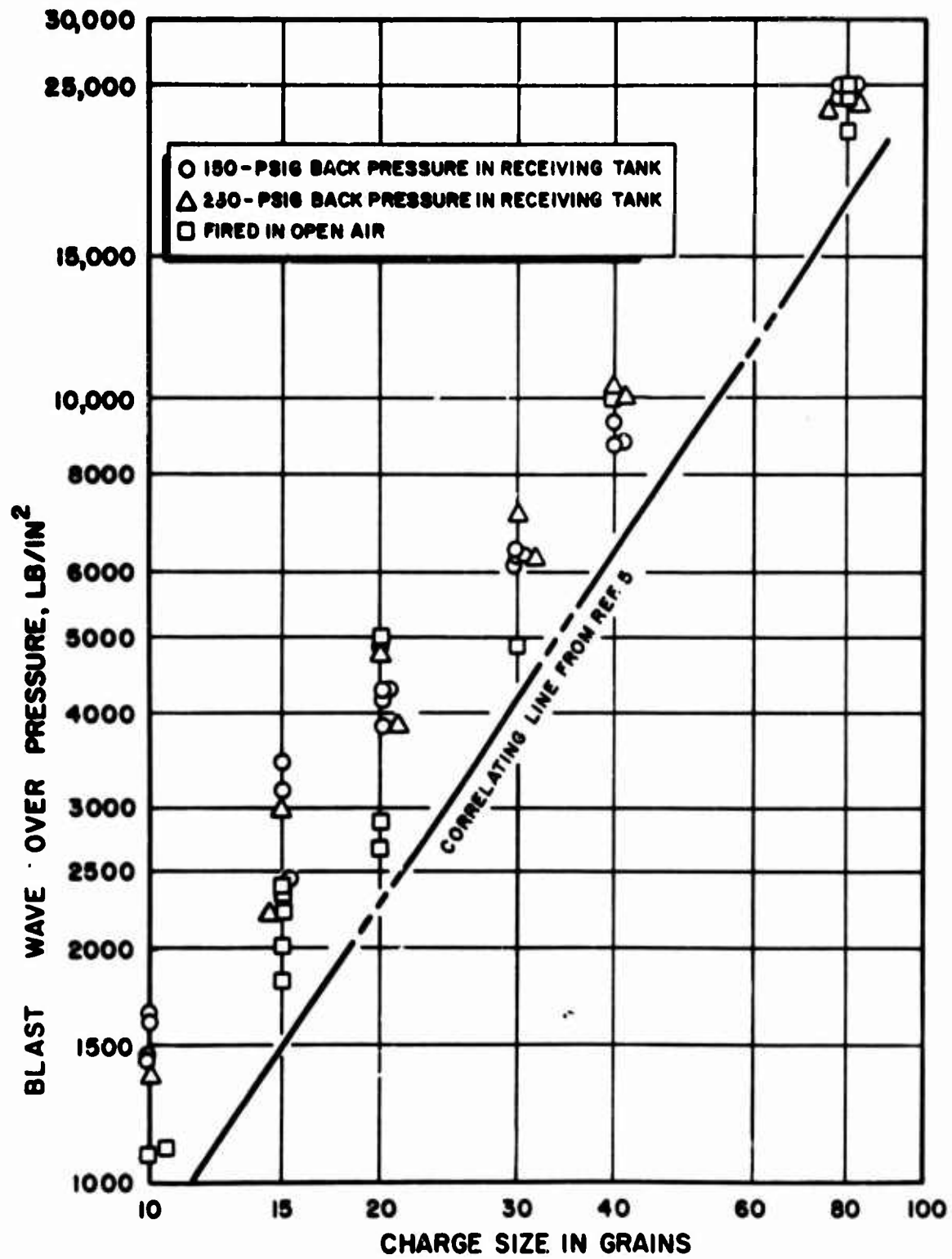
Figure 23. Maximum Blast Pressure Amplitude at 1.44 Inches From Pulse Gun Burst Diaphragm
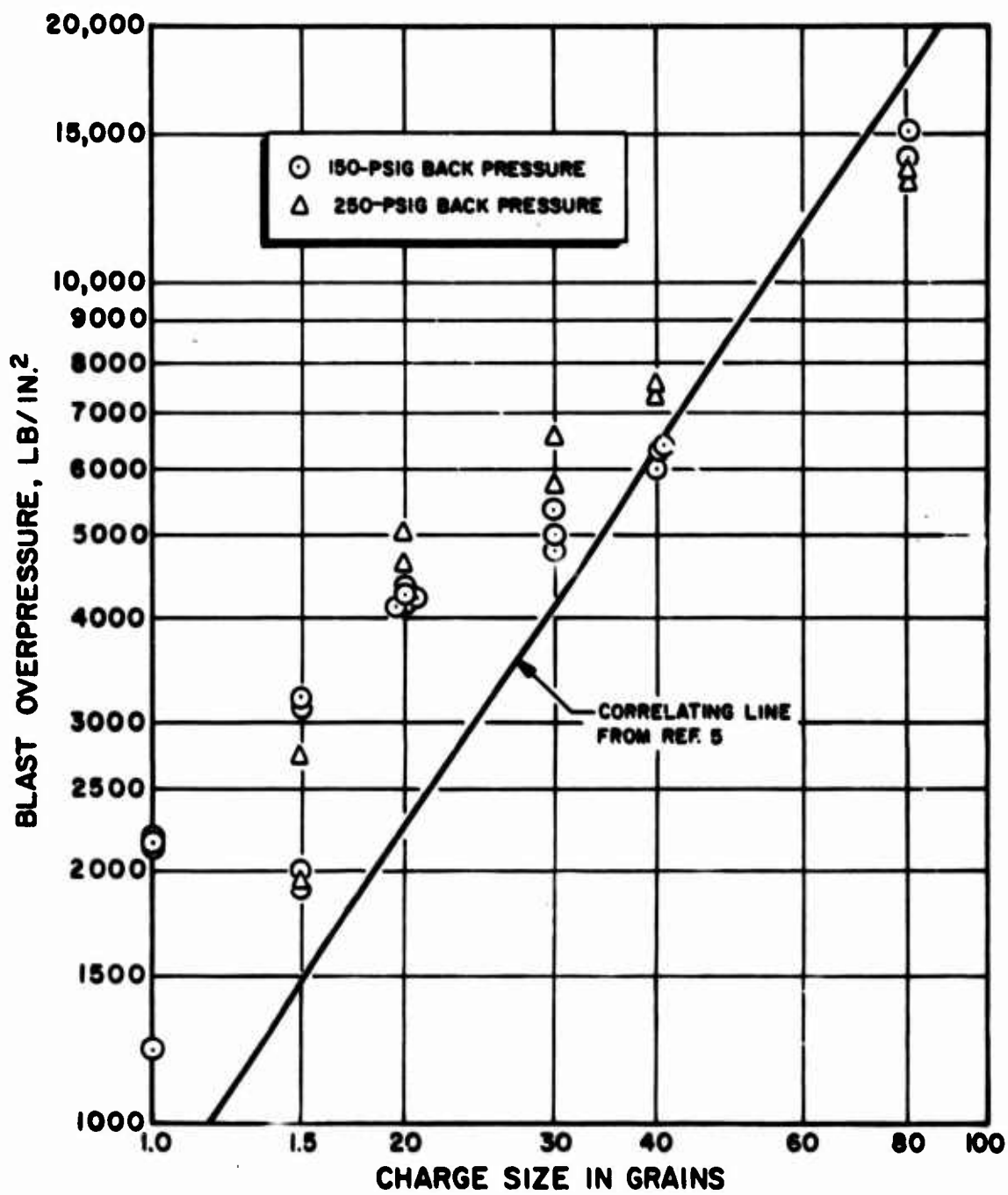
Figure 24. Maximum Blast Pressure Amplitude at 6.00 Inches
From Pulse Gun Burst Diaphragm

93

weight on maximum pressure in the current data from the 1.44-inch position appears to parallel the Aerojet correlation but with about 50 percent higher amplitudes, while the effect at the 6.00-inch position appears to be grossly distorted. This was a surprising result. That appearance was not restricted to the maximum pressure amplitude data, however, because the same type of curvature was seen in similar plots of initial shock wave amplitude and of total impulse.

As a further check of the validity of what seemed to be a discrepancy between the two sets of data, the pressure transducers were recalibrated after all but nine of the firings had been made. The recalibration data fell within three percent of the factory-supplied calibrations and exhibited excellent linearity. It was concluded that the apparent data distortion at the 6.00-inch position was a valid characteristic of the data.

Data Correlations

Variables Considered in the Correlation. The primary pulse gun parameters varied in the cold characterization tests were:

1. Charge Weight, W (grains)

2. Powder Type, PT

3. Diaphragm Burst Pressure, P_{db} (1000's of psi)

4. Pulse Gun Barrel Length, X (inch)

5. Back Pressure, P_b (psi)

The distance D from the diaphragm to each of the two transducers was also considered in the analysis. The output data used as the dependent variables were:

1. Maximum Blast Pressure, P_{max} (psi)

2. Positive Impulse, I_+ (lbf-sec)

3. Velocity of the Initial Shocks, c_s (ft/sec)

94

The response is the amplitude of the higher, and ordinarily the second
of the two pressure peaks measured at the pressure sensors in the pulse
gun barrel. Unit positive impulse was obtained with a planimeter in the
same way as for the bombs. Because the blast waves were confined, rather
than expanding spherically, the integrated values, Eq. 4 , were multiplied
by the cross-sectional area of the pulse gun barrel. The correlated values
were thus total positive impulse. The velocity was obtained from the
transit time between the transducers located at 1.44 and 6.0 inches.

A fourth response parameter, the positive duration, was not analyzed
quantitatively. It is fairly clear that the positive duration data, as
given in Table 9, behave essentially the same as for the bombs; that is,
there is only a very weak correlation with charge weight.

Correlation of Peak Pressure. The multiple linear regression techniques
described in Appendix A were used to obtain empirical models to fit the
peak pressure data. The correlation included all of the available peak
pressure data for Hercules Bullseye powder except the few data obtained
with the short barrel. As for the bomb data, the averages of the responses
for each set of conditions were used, rather than the individual data
points. The final model obtained is the following:

$$\ln P_{max} = 8.32 - 1.54 \ln W + 0.32 \left(\ln W\right)^2 + 0.15 \ln W \ln D -$$

$$0.06 \left(\ln W\right)^2 \ln D + 0.19 \ln W \ln P_{db} + 0.008 \left(\ln P_b\right)^2 \quad (16)$$

A total of more than 98 percent of the variation in $\ln \left(P_{max}\right)$ is now
explained by the right-hand side of Eq. 16 with a standard deviation of
0.093 about the regression line. A cursory examination of the peak pressure
data for fixed transducer distance and back pressure (Fig. 23) shows that
the logarithm of peak pressure is essentially linearly related to the
logarithm of charge weight. This simple apparent relationship leads one

to question the complexity of the model given, and in particular the presence of the terms in $(\ln W)^2$, $(\ln W)^2 \ln D$, and $\ln W \ln P_{db}$. One possible explanation for the appearance of these terms in the model is that the regression is spurious and the extra terms are effectively "explaining" what is in reality random fluctuations in the data. A preponderance of available evidence, however, indicates that the functional relationship between $\ln P_{max}$ and $\ln W$ is actually, though only moderately, curved. Figures 25 and 26 are logarithmic plots of the average values P_{max} against W for the transducers at 1.44 and at 6.00 inches respectively, and for a back pressure of 150 psi. Since three rated strengths of burst diaphragms were used, the data should fall on three different parabolas according to Eq. 16. The fit, especially for the 20,000-pound burst diaphragm rating is excellent. Note that although the quadratic term in $\ln W$ is smaller at $D = 6.00$ than at $D = 1.44$, the linear term changes enough so that the curvature is greater at the longer distance. It now seems clear that the apparent anomaly of the nonlinear behavior at 6.00 inches may be accounted for by the curvature with charge weight and the effect of the burst diaphragm.

The maximum charge weight used in the program was 80 grains due to the limitation in the breech size of the pulse gun. As noted previously, larger charges have been used with larger breeches at Aerojet General Corporation (Ref. 5) which resulted in an apparent relationship between combustion chamber disturbance amplitudes and the fraction of the breech volume occupied by the explosive charge.

Two breech sizes were also used in the current program, but the characterization testing reveals no effect of breech size. The 10- and 15-grain charges were fired in the smaller breech; if there were a breech-volume effect, results using these charge weights would have been higher than would be expected by extrapolating back from the larger charge sizes. Because the results were lower, we conclude that either there is no breech-volume effect or it is completely masked by the effect of diaphragm burst pressure.
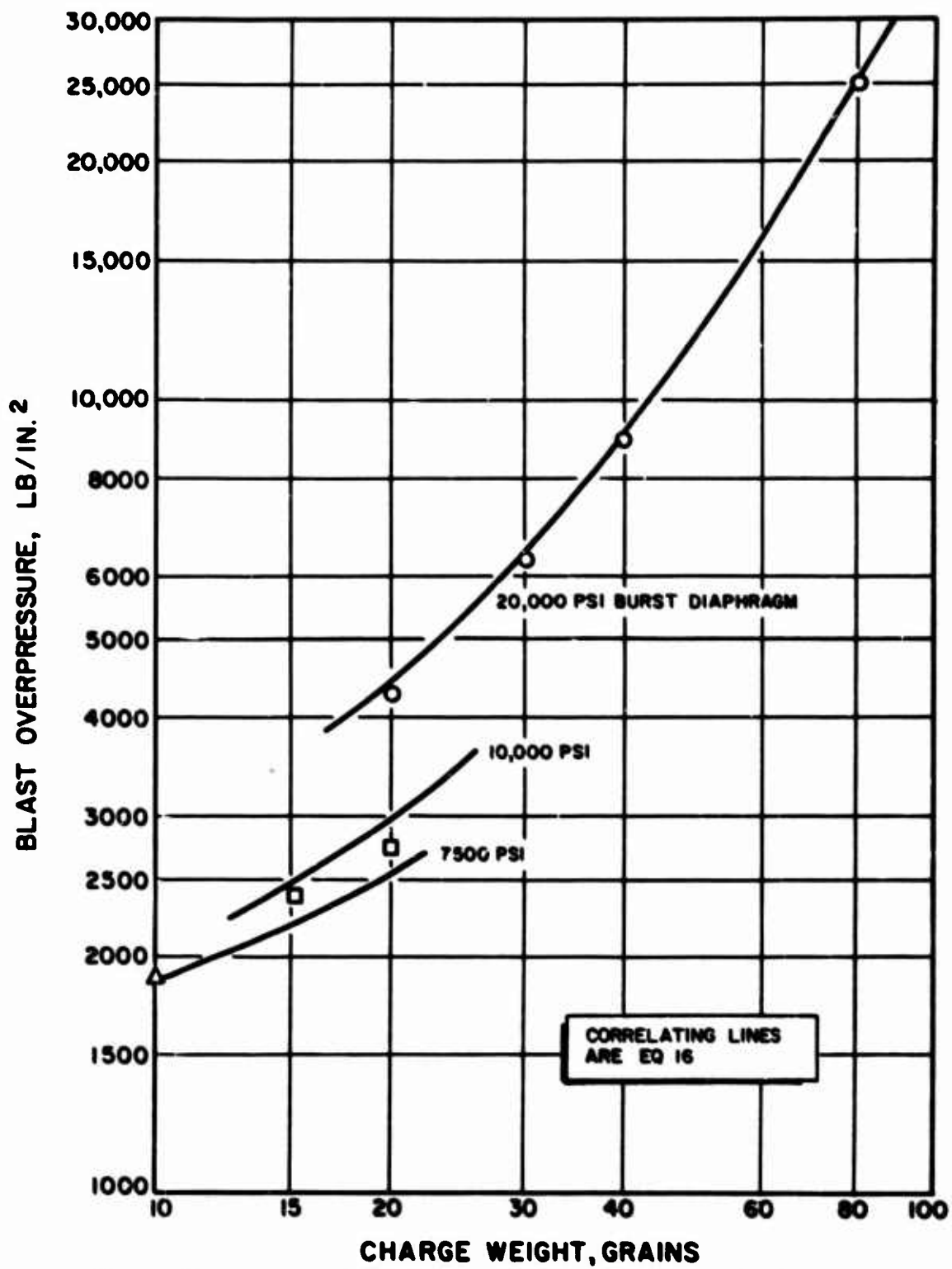
Figure 25.   Maximum Blast Pressure Amplitude at 1.44 Inches From
Pulse Gun Burst Diaphragm.   (Hercules Bullseye Powder)
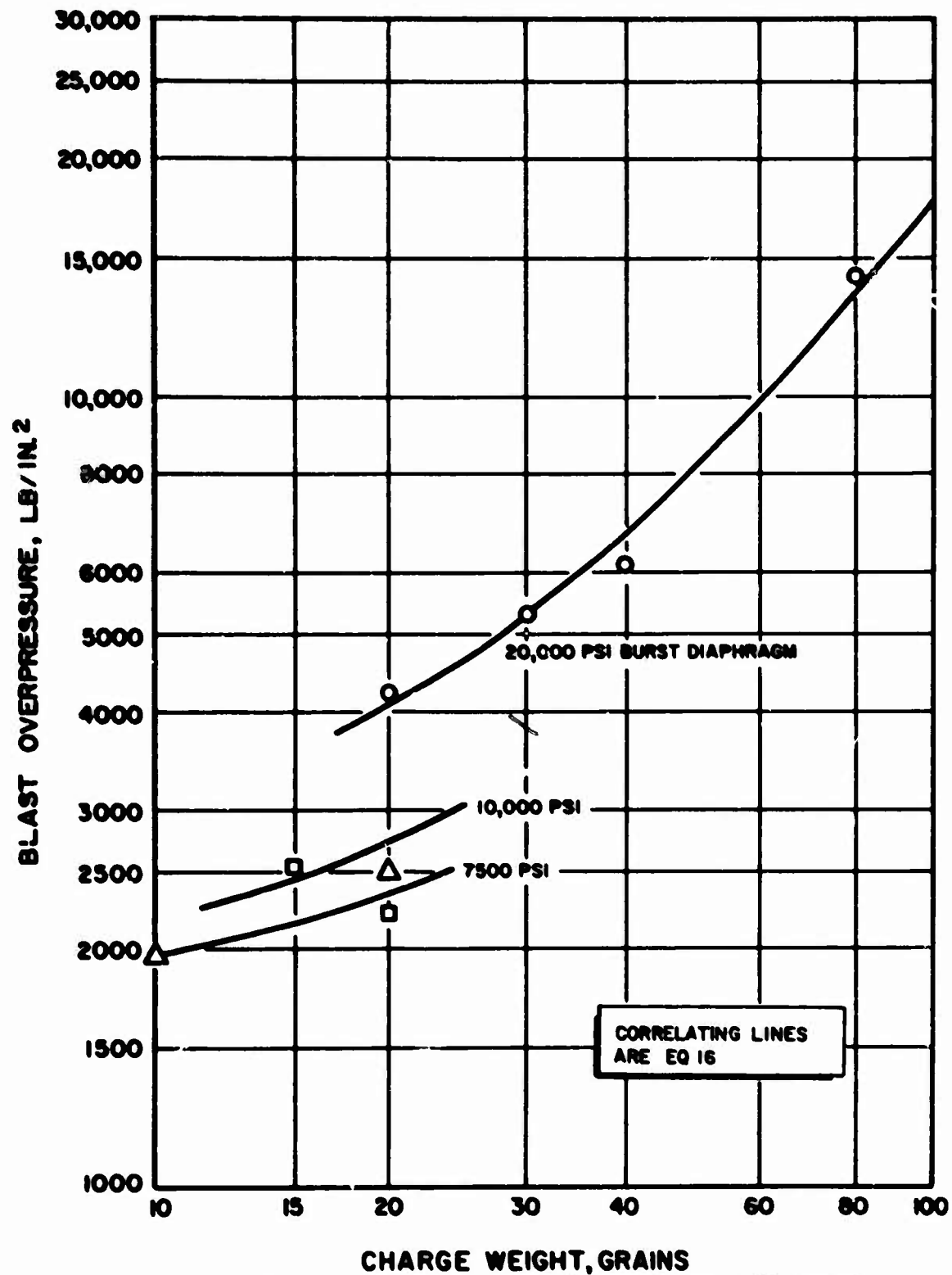
Figure 26. Maximum Blast Pressure Amplitude at 6.00 Inches
From Pulse Gun Diaphragm. (Hercules Bullseye
Powder, 150-psi Backpressure)

98

Correlation of Positive Impulse. A logarithmic model of the form

$$\ln I_+ = -6.43 + 1.78 \ln W - 0.11 (\ln W)^2 - 0.28 \ln D +$$

$$0.123 \ln P_b \qquad\qquad (Eq. 17)$$

was found to be satisfactory for estimating positive impulse. Again over
98 percent of the total variation in $\ln I_+$ is explained by the test input
parameters in Eq. 17. A standard error of 0.067 about the regression line
was obtained.

As was the case with the bombs, a very good fit of positive impulse was
obtained with a very simple model. Particularly striking is the fact that
the effect of charge weight does not interact with tranducer distance.
Unlike the peak pressure data, for which the curves at the two distances
actually cross and have different curvatures, two parallel curves are
sufficient to fit the positive impulse data (Fig. 27)

While the inclusion of the $(\ln W)^2$ term in Eq. 17 improves the overall fit
of the data, there are some indications that this term in the correlation
may be spurious. First, the data at the high and low ends of the curves
are fit just as well by straight lines which can be visually fit to the
data as by the regression curves. Second, the direction of curvature is
opposite that observed for peak pressure. At any rate, the amount of
curvature is so slight that the deviations from linearity are probably
not of any real importance.

Correlation of Velocity. A comparison of Fig. 28 with Fig. 25 through 27
shows that there is much more variability in the velocity data than in the
peak pressure or positive impulse. It is therefore not possible to develop
a model which is physically meaningful and which fits the data well. The
best model obtained fit only the larger charges even approximately:

$$\ln c_s = 11.1 - 1.94 \ln W + 0.130 (\ln W)^2 - 0.149 (\ln P_{db})^2 + \qquad (18)$$

$$0.411 \ln W \ln P_{db} - 0.0549 \ln P_b$$

99
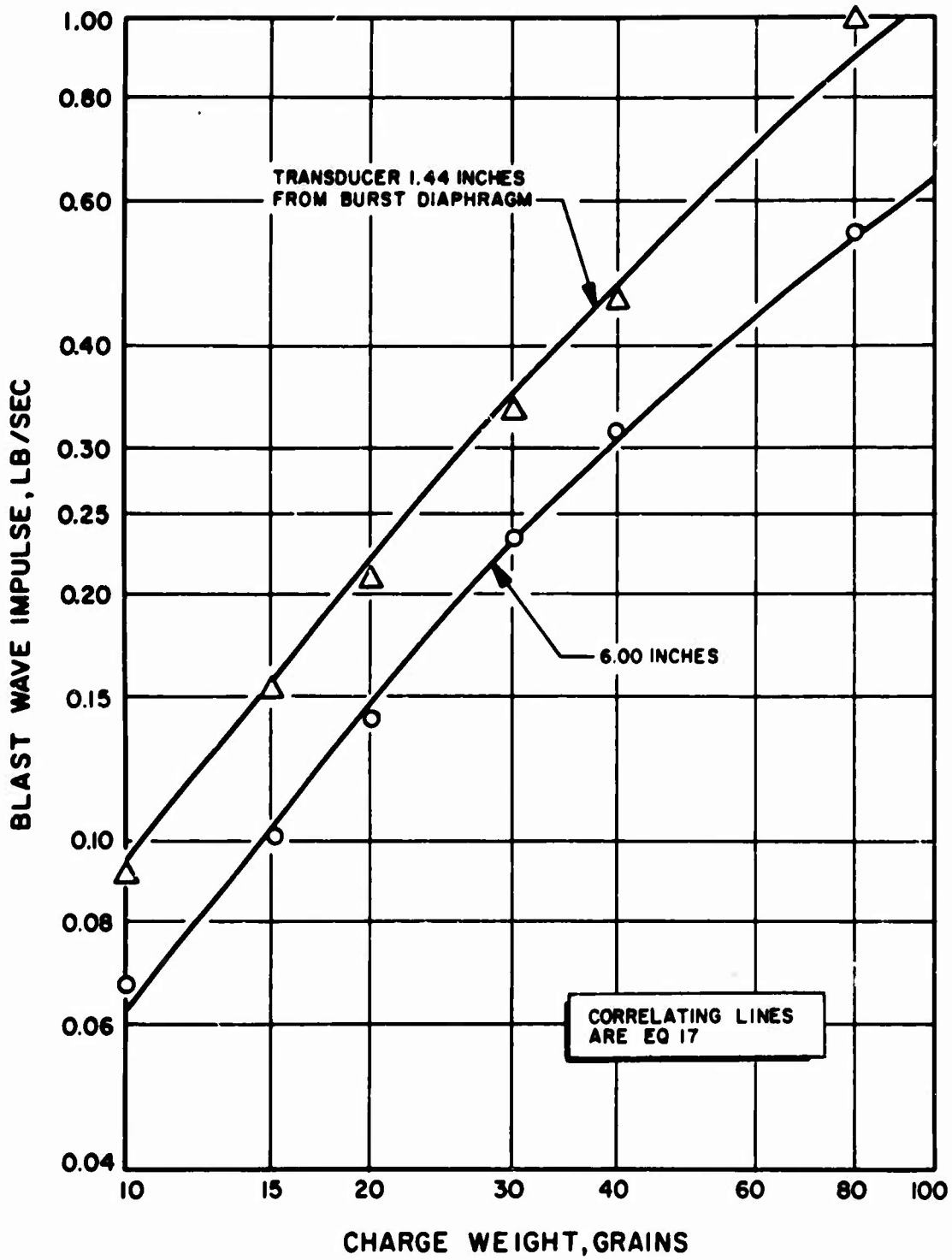
Figure 27. Impulse From Pulse Gun Blast Waves. (Hercules
Bullseye Powder, 150-psi Backpressure)

100
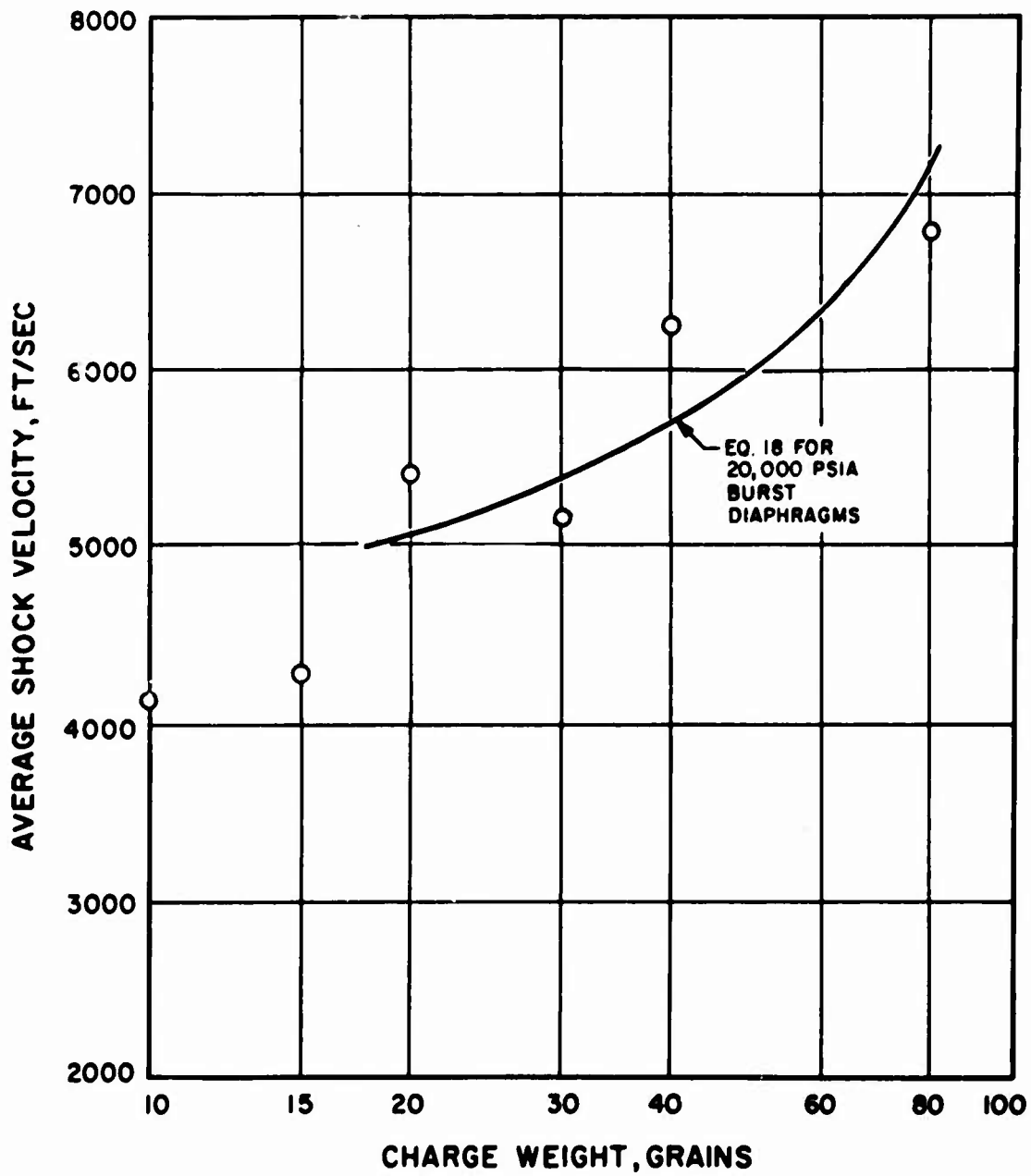
Figure 28.   Average Velocity of Initial Shock Wave
in Pulse Gun Barrel (Hercules Bullseye
Powder, 150-psi Backpressure)

101

<u>Initial Shock Wave Pressure.</u> In addition to the maximum peak pressure
(the amplitude of the second pressure peak), data on the initial shock
wave pressure were reduced from the photographic records. These are
plotted as a function of charge weight in Fig. 29 and 30 for transducers
at 1.44 and 6.00 inches, respectively. Since the initial shock wave
pressure data are so similar to those for secondary (maximum) peak
pressure discussed earlier, no formal correlation was run. Several
points of similarity and dissimilarity will be noted in a qualitative
fashion.

The general functional form of the initial shock wave pressure relation-
ship is obviously quite similar to that for maximum peak pressure. For
small charges, the two pressures are nearly the same; however, for higher
charge weights, the maximum peak is greater by a factor approaching 2 for
150 psi back pressures. The curvature with ln W for fixed P_{db} and P_b is
more pronounced in the initial shock wave pressure data. The effect of
burst diaphragm appears to be about the same. Finally, there is some
evidence that the initial pressures are degraded more by an increase in
back pressure than are the maximum pressures.

<u>Results With duPont Military Powder.</u> A total of 10 pulse gun charges
using the slow-burning powder (duPont Military 3031) were fired during
the cold characterization portion of the program. Because few data were
available, the results were not correlated statistically, but qualitative
observations may be made for plots of the data. Figures 31 through 33,
which are analogous to Fig. 25 through 28, contain individual values in
the resulting data rather than averages. In general, the results were
similar but of appreciably lower magnitude.

With the duPont Military powder, a diaphragm of 10,000 psi rated burst
pressure was used with a 20-grain charge and 20,000 psi diaphragms were
used with charge weights of 30, 40, and 80 grains. Once again the effect
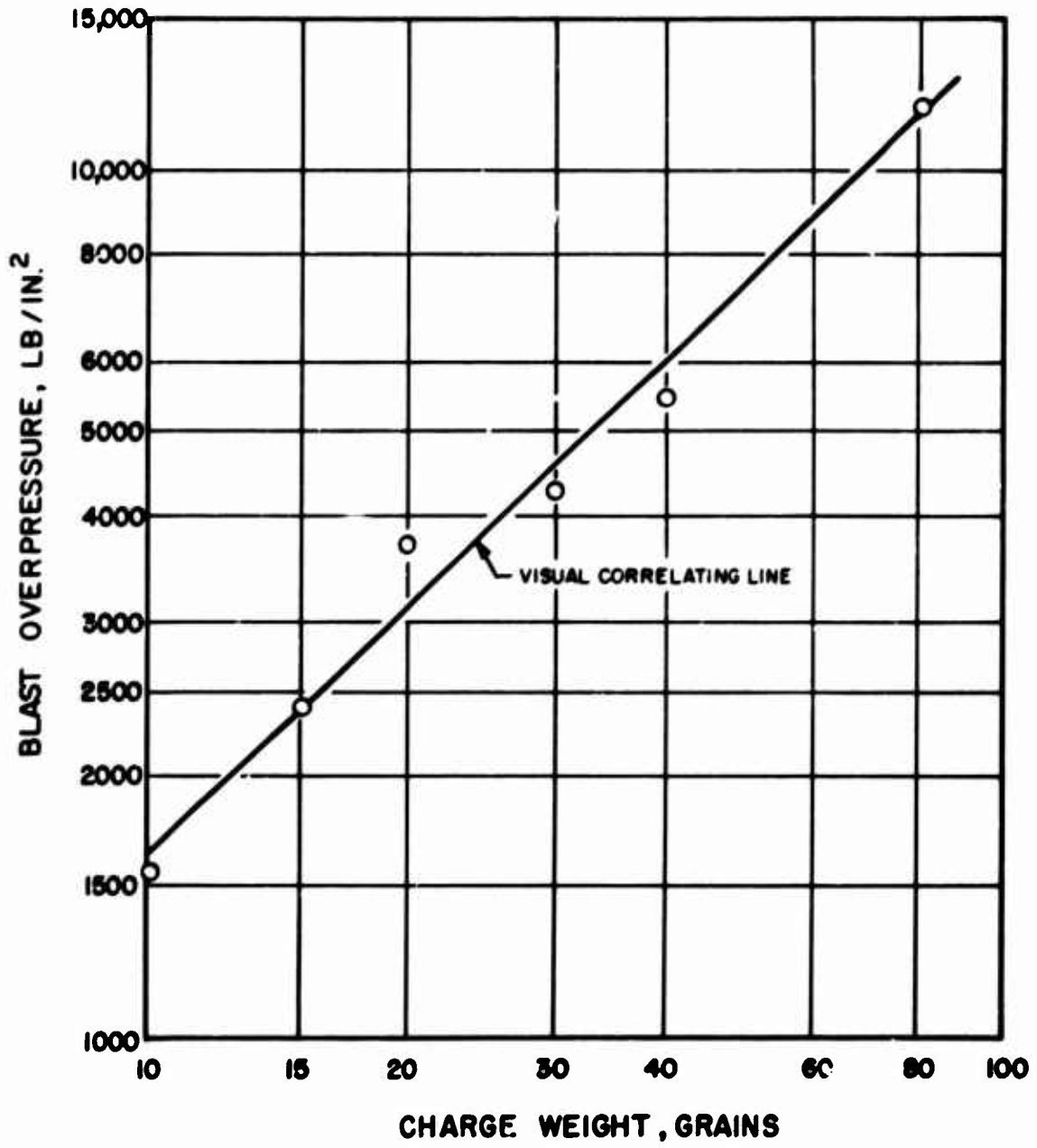
Figure 29.   Initial Shock Wave Pressure Amplitude at 1.44 Inches
From Pulse Gun Burst Diaphragm.   (Hercules Bullseye
Powder, 150-psi Backpressure)
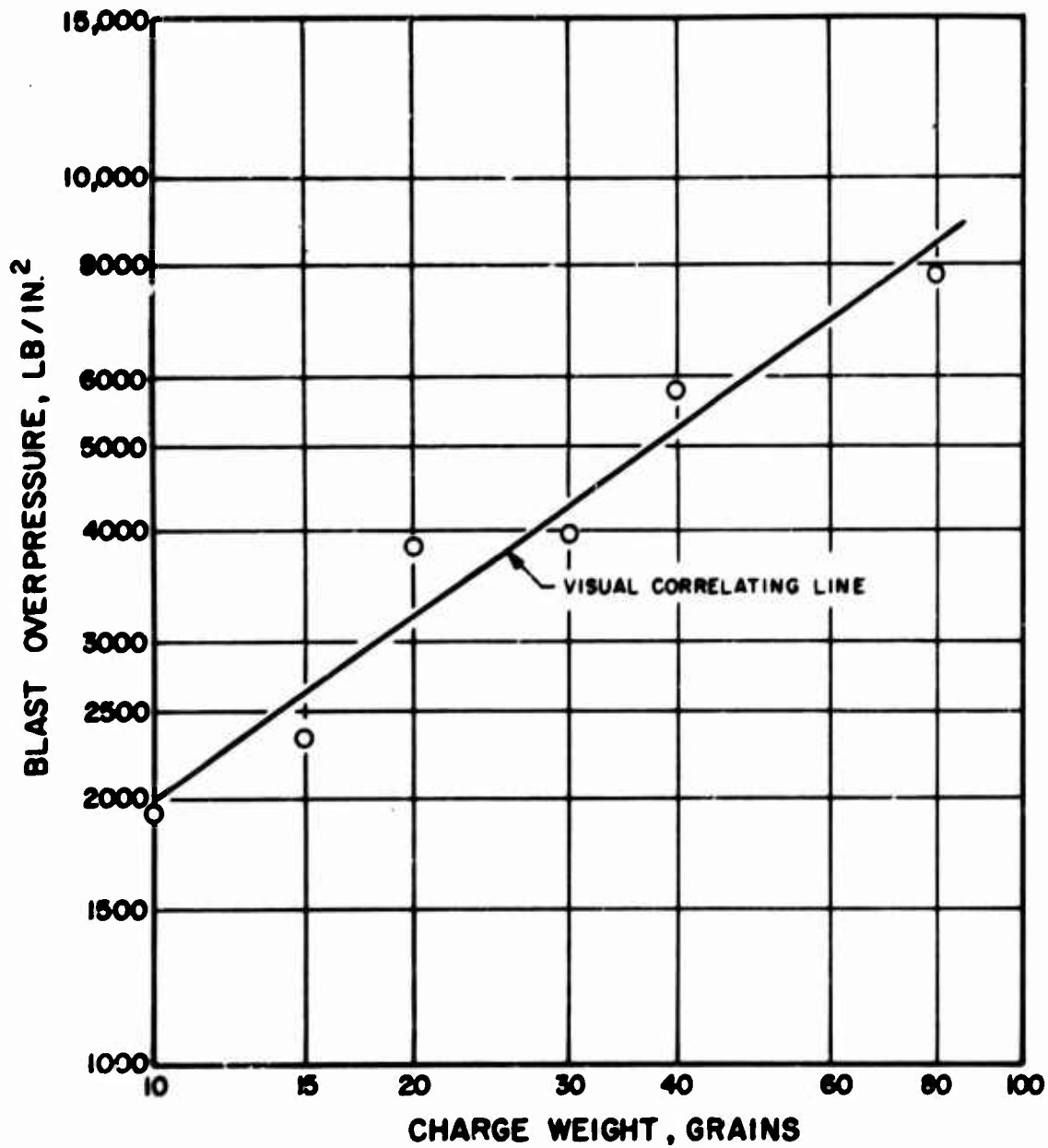
Figure 30. Initial Shock Wave Pressure Amplitude at 6.00 Inches From Pulse Gun Diaphragm (Hercules Bullseye Powder, 150-psi Backpressure)

104
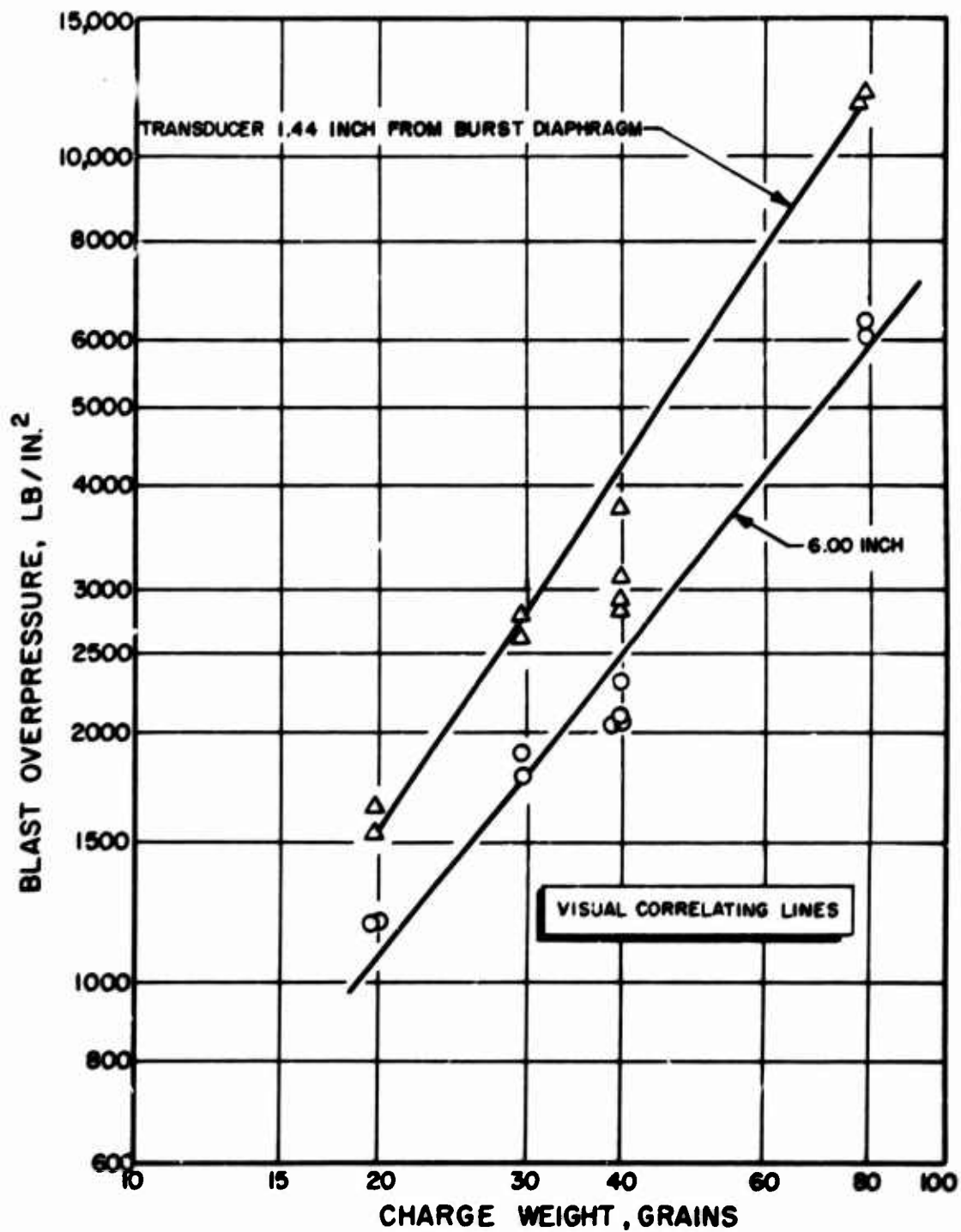
Figure 31. Maximum Pulse Gun Blast Pressure Amplitude
(duPont Military 3031 Powder, 150-psi
Backpressure)

105
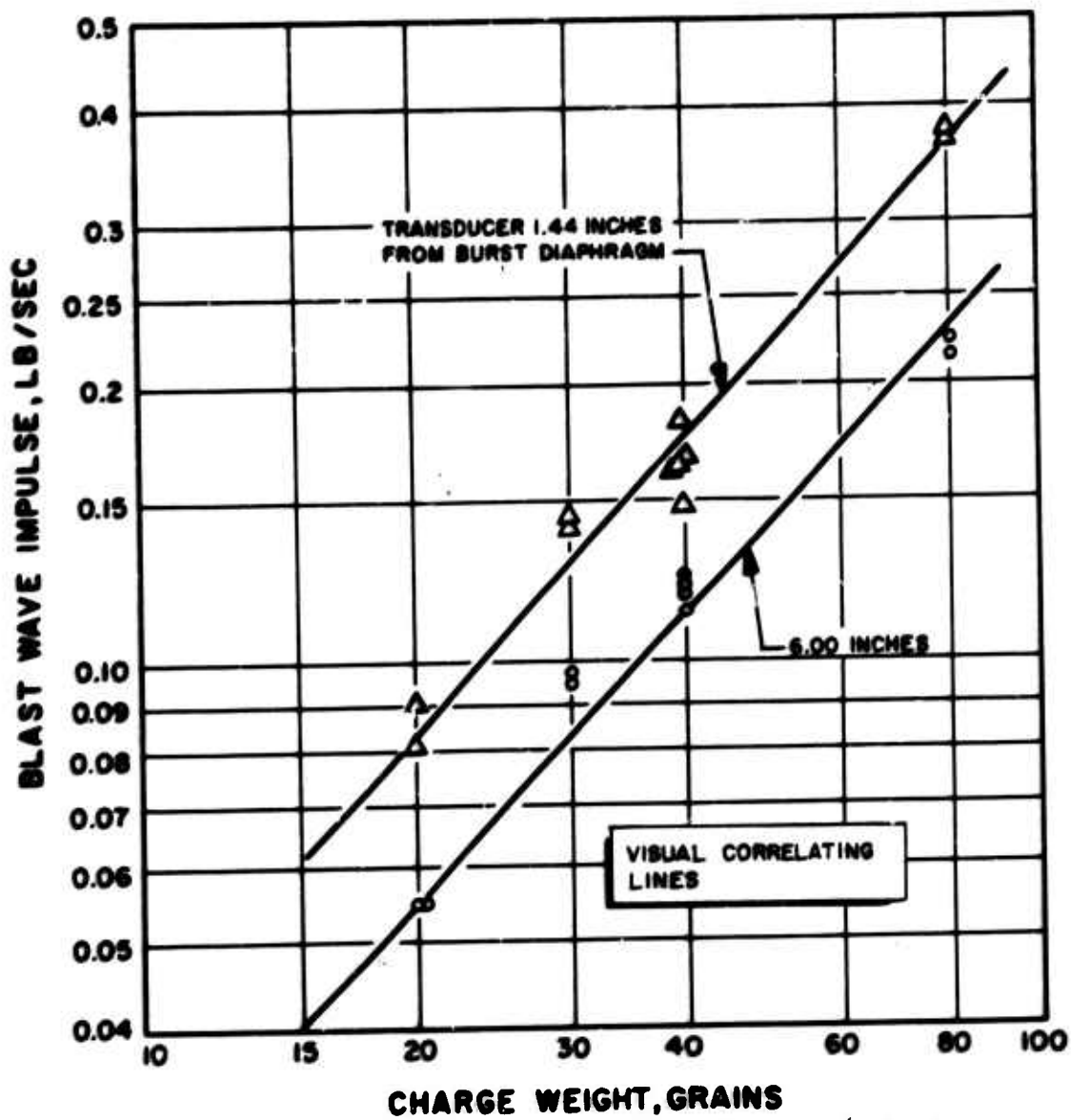
Figure 32.   Impulse From Pulse Gun Blast Waves.   (duPont
Military 3031 Powder, 150-psi Backpressure)

106
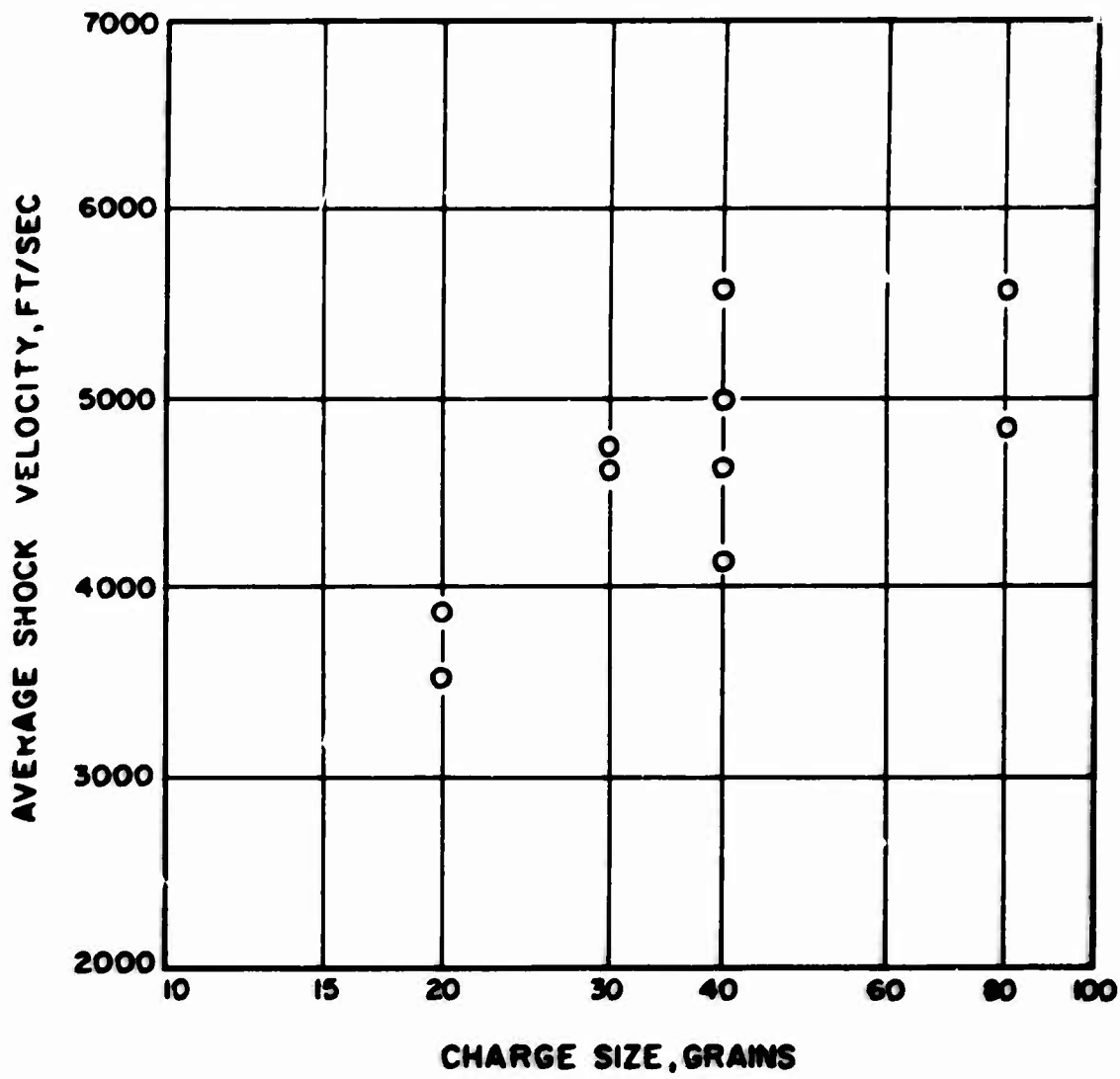
Figure 33. Average Velocity of Initial Shock Wave in Pulse Gun
Barrel (duPont 3031 Powder, 150-psig pressure)

of charge weight on peak pressure for fixed diaphragm rating is slightly curved on a logarithmic plot, and the effect of diaphragm rating is also noticeable. The consistency of the duPont Military powder peak pressure data with that for Hercules Bullseye powder gives a corroboration with independent data of the functional form used earlier. Superposition of the curves for maximum pressure amplitude, Fig. 31 , shows that, as with the Hercules powder, the difference in peak pressure between the transducers at 1.44 and 6.00 inches is appreciably greater at the higher weights. The amplitudes of the pressure waves with the slower burning duPont powder is in general less than half those with the Hercules powder. The slope of the ln W vs ln P_{max} plot is slightly greater, so that the effect of charge weight is slightly greater with the duPont powder.

As before, the impulse data appear to be quite reproducible and easy to interpret, with parallel lines serving to model the impulse at 1.44 and at 6.00 inches. The impulse values are lower by a factor of about 2-1/2 than those for the faster burning powder. There is a slight suggestion of positive curvature of ln I_+ for the largest three weights. The velocity data are once again quite scattered. There is no indication of any effect besides that of weight. The velocities are about 1000 or 1500 ft/sec lower. Finally, initial shock wave pressure plots (not illustrated) show the same relationship to the maximum pressure as was observed with the Hercules powder.

DIRECTED FLOWS OF GASES

The third combustion stability rating method investigated consists of introducing a directed gas flow into the rocket combustion chamber and determining the gas flowrate (or other characteristic) at the instant of instability. The technique has been found to be most effective when applied to the region just downstream of the injector, the gas flow may also be more effective if directed tangentially or chordally rather than radially across the injector. Inert gases have been used almost exclusively, although some limited investigations have made use of both oxidizer and fuel gases (Ref. 6).

108

Several gas flow control methods have been used. Each method contains elements for limiting the ultimate eventual flowrate (e.g., source pressure regulation), and for controlling the transient flowrate (e.g., a flow control valve). The simplest method involves rapid actuation of a simple shutoff valve to effect a more or less impulsively initiated flow having constant flowrate. In an extreme application, the valve may be opened fast enough that a weak shock wave attends the onset of gas flow into the combustor. This method provides a single data point for each rocket engine firing so that multiple firings and staircase testing techniques are required.

A more productive flow control method utilizes slow actuation of a linear or proportioning flow control valve, so that the gas flowrate increases gradually in a controlled and reproducible manner. Most often, linear variation of flowrate with time has been sought; in at least one study, control was for linear variation of momentum flux with time. In this manner a range of rating technique characteristics can be covered in a single engine firing and, potentially, a valid stability rating may be obtained for each firing in which an instability is initiated.

The mechanisms whereby an injected gas flow disturbs the steady-state combustion processes to produce a finite amplitude pressure wave and ultimately initiate a sustained instability are not at all well understood. A concept that this technique affects displacement or velocity-sensitive combustion processes rather than pressure-sensitive processes is rather widely held. This technique probably accomplishes less close simulation of naturally occurring triggering mechanisms than do the bomb and pulse gun techniques. Nevertheless, its potential for accomplishing a quantitative rating in a minimum number of tests makes it an attractive candidate for stability rating work.

Experimental Approach

The method of steadily increasing the gas flowrate was selected for this program. It was anticipated that capabilities for independent time rate of variation of any gas flow characteristic would be desirable in the hot-firing characterization. A gas flow generator system was designed with flow control valve position (or percent open) as the primary control variable. Cold characterization consisted of determining the control settings required to provide a prescribed flow profile, measuring the flowrate, the output gas temperature and pressure, and determining correlations among them when the control valve timing, connecting tube design, and gas species were changed.

The flow generator was initially designed in anticipation of: (1) 10-lbm/sec nitrogen and 3-lbm/sec helium maximum flowrate requirements, and (2) flow durations ranging from 0.25 to 3.0 seconds. The flow system components were size-selected on the basis that gases would be supplied at 2500 psia source pressure to the flow generator and that the maximum flowrate would be determined by sonic (choked) flow through the port or tube connecting the flow generator to the combustion chamber.

The flow generator system initially assembled is shown schematically in Fig. 34 and photographically in Fig. 35. A list of the flow generator components is given in Table 10; the component numbers listed there correspond with those on Fig. 34. The schematic shows that either of two gases could be chosen for testing and that addition of any number of test gases can be achieved simply by duplicating four valves for each additional test gas desired. Flow was measured by observing the pressure drop across a calibrated orifice. (A backup RAMAPO flow transducer was soon determined not to be needed and was removed from the system.) The position of the flow control valve stem was monitored with a linear motion transducer and adjusted by a hydraulic cylinder which was driven by a servovalve. The power required for the hydraulic system was provided by a hydraulic pump. A

110
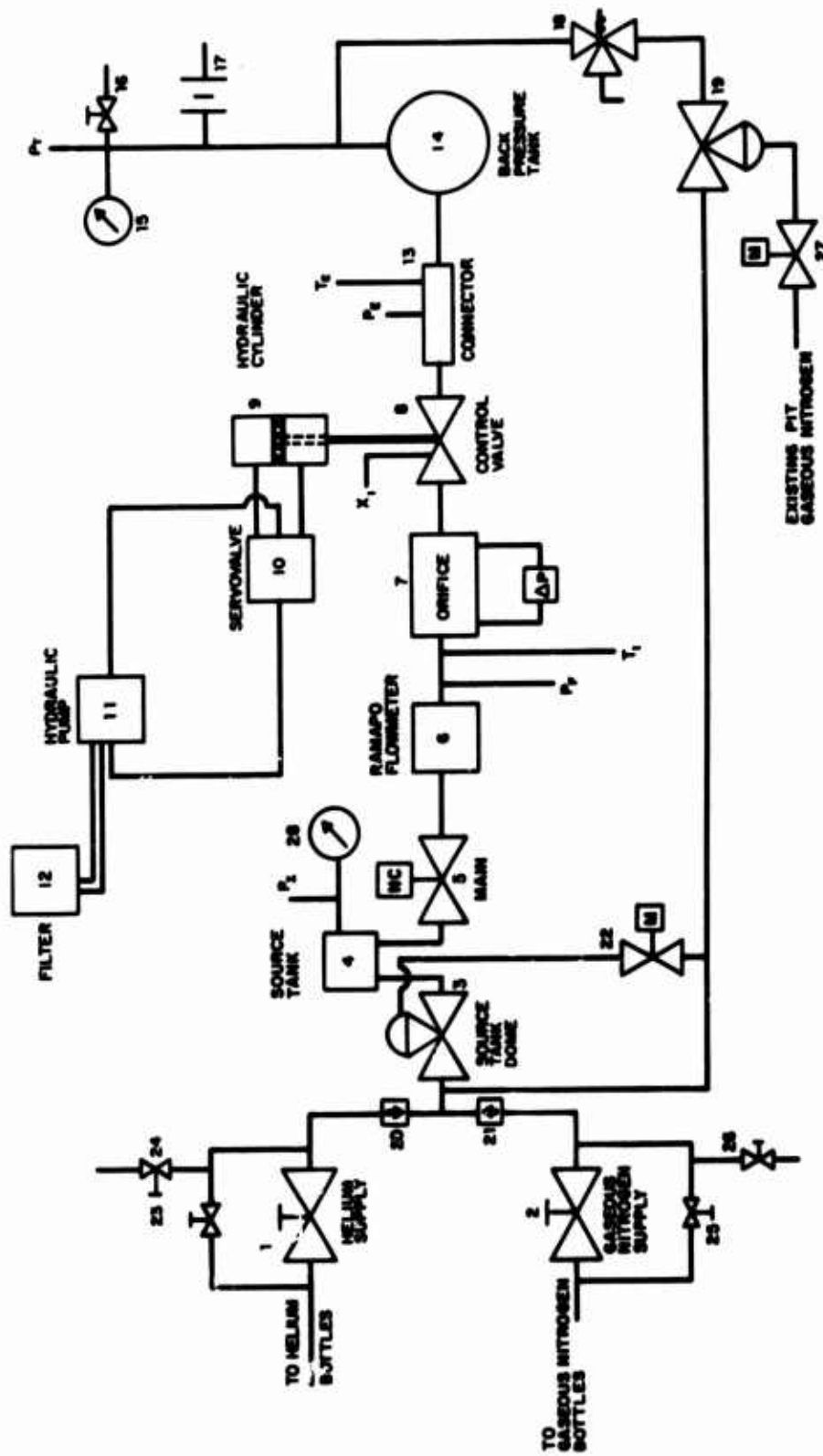
Figure 34. Gas Flow Generator System
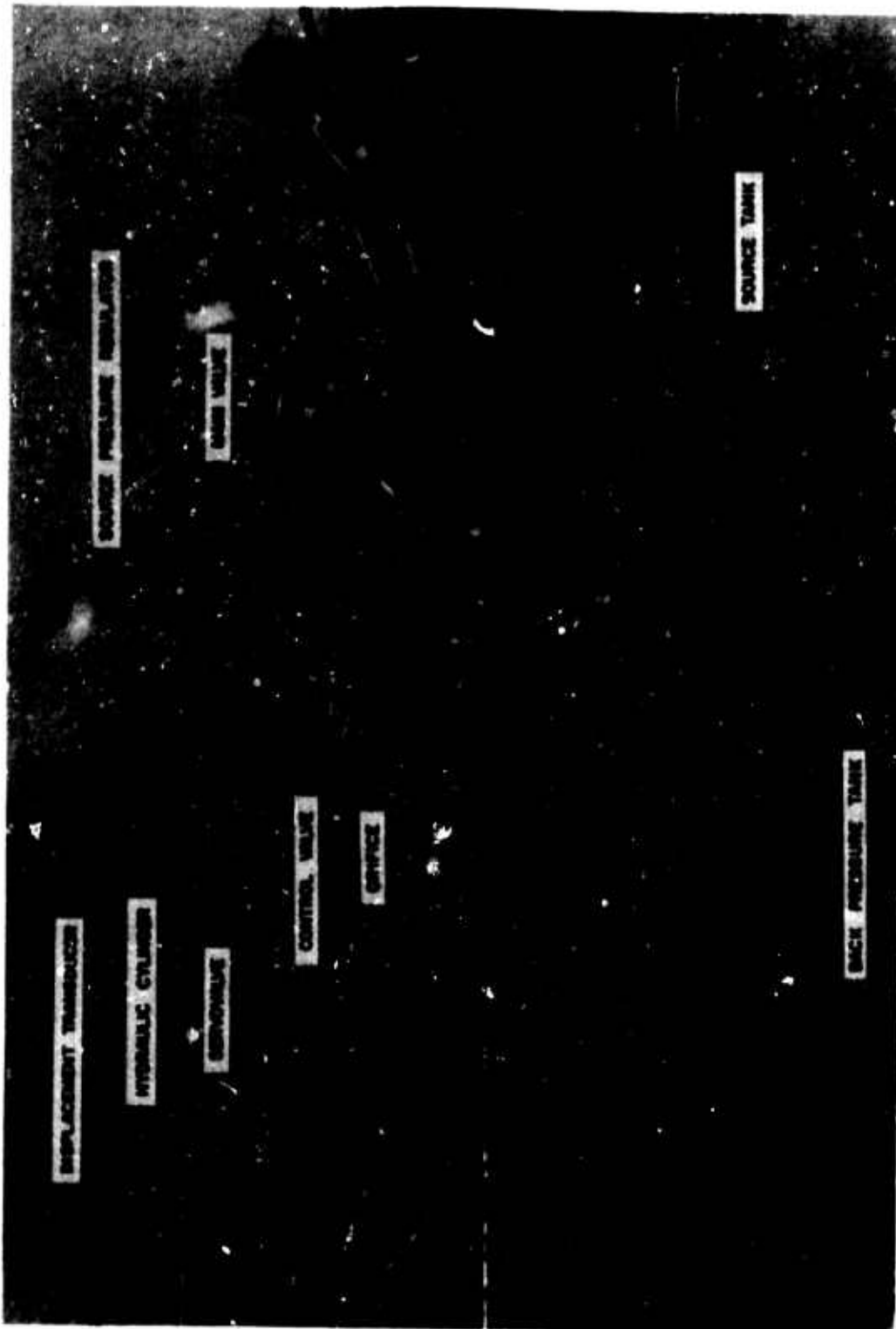
Figure 35. Assembly of Gas Flow Generator

112

TABLE 10

COMPONENTS OF FLOW GENERATOR SYSTEM FOR GAS PULSE RATING DEVICE

Pneumatic System				
Schematic Number[1]	Description	Size	Vendor	Model
1	Helium Supply Valve	1 inch	Annin	M/H 4510
2	Gaseous Nitrogen Supply	1 inch	Annin	M/H 4510
3	Source Tank Regulator	1-1/2 inch	Grove	WH-408-K5
4[2]	Source Tank	2 inch cylinder	NAA	-
5	Main Valve	1 inch	Annin	JB-143670-7
6[3]	Ramapo Flowmeter	1 inch	Ramapo	-
7	Orifice Holder	1 inch	NAA	-
8	Control Valve	1 inch	Fisher	D 1204
9	Hydraulic Cylinder	1 inch	NAA	-
10	Servovalve	1/4 inch	Cadillac	2281
11	Hydraulic Pump	10 GPM	NAA	WR 283478
12	Hydraulic Filter	-	NAA	-
13	Instrumentation Connector	1 inch	NAA	-
14	Back Pressure Tank	50 gallons	Southwest Welding	4513
15	Back Pressure Gauge	1/4 inch	Victor	12933-1
16	Back Pressure Hand Vent	1/2 inch	Grove	224 KX
17	Burst Diaphragm Holder	1-1/2 inch	BMB	2122 U
18	Back Pressure 3-Way Valve	1/2 inch	Marotta	305
19	Back Pressure Regulator	3/8 inch	Grove	GK-206-03
20	Check Valve	1 inch	Marotta	CVM 516
21	Check Valve	1 inch	Kepner	DS 143912-A-400
22	Source Tank Loader	1/4 inch	Grove	-
23	Helium Bypass Valve	1/4 inch	Robbins	SSKO 250-4T
24	Helium Bleed Valve	1/4 inch	Robbins	DS 157005-F
25	Gaseous Nitrogen Bypass Valve	1/4 inch	Robbins	SSKO 250-4T-763
26	Gaseous Nitrogen Bleed Valve	1/4 inch	Robbins	DS 157005-F

Electronic System				
	Analog Computer		Donner	3000
	Diode Function Generator		Donner	3750
	DC Amplifier		Kintel	111 BFO
	Current Amplifier		Photocon	CA 401

(1) Reference: Figure 34
(2) Volume increased to 9 cu ft for final configuration
(3) Omitted for final design

connecting section provided smooth transition between the 1-inch ID system tubing and the 1/2-inch ID exit tube required for entrance into the combustion chamber. This section was equipped with a Kistler 601A pressure transducer. and an unsheathed chromel-alumel thermocouple constructed of 5-mil wire. The thermocouple provided a moderately fast-response temperature measurement, and the pressure transducer was for monitoring the exit flow for spikes and transients. The thermocouple was recessed somewhat to avoid damage to the small-diameter wires during high flows. For cold-flow characterization, a tank simulated the rocket chamber. Back pressure was also remotely controlled.

Programmed control of the gas flow was accomplished through a preprogrammed schedule of desired valve position as a function of time. The actual versus desired valve stem position was compared, and the resulting error was used to drive the valve stem in the proper direction to reduce the error. In this way any desired valve position versus time curve could be obtained within the physical limitations of the equipment.

The electronic equipment used for valve position preprogramming and control also is listed in Table 10.

Experimental Results

Cold characterization of the initially assembled system revealed erratic, irreproducible surges in flowrate, which resulted from the inability of the source tank pressure regulator to follow changes in demand imposed by moderately fast control valve motion. It was recognized that increasing the size of the source tank, which was initially quite small (approximately 0.1 cu ft), could eliminate this problem. It was roughly estimated that between 7 and 10 cu ft of surge capacity would be needed, however, so it was decided to evaluate the gas flow control characteristics with the source tank and its pressure regulating valve removed from the system. The pipelines from the gaseous supply valves were then plumbed directly to the flow generator's main shutoff valve.

114

Calibration Tests. The modified gas flow generator was cold-flowed (in a steady-state flow mode) in a series of calibration tests to obtain flowrate vs valve position data. A nominal supply pressure of 2000 psi was used, and flows of both nitrogen and helium were made through connecting tubes of three different diameters to a tank prepressurized to two pressure levels. Examples of the resultant calibrations are shown in Fig. 36 for nitrogen and in Fig. 37 for helium. The similar shapes of the three curves on each of these figures were interpreted as an indication that the control valve exercised effective control that was not unduly influenced by the gas supply system characteristics. This interpretation was later recognized as being erroneous.

Ramp Flow Tests. One type of flowrate vs time profile thought to be desirable for stability ratings is a linear ramp, i.e., a constant rate of flowrate increase. Achieving such a ramp requires a valve position vs time history that is different than linear in order to remove the nonlinearities of the flowrate vs position calibration. The gas flow generator used a Donner Model 3100 diode function generator to accomplish this control. This device can be used to generate any desired function by approximating it with a sequence of 24 straight line segments. The control circuit compares the output of the function generator with the output of a valve position transducer and varies the hydraulic pressure supply to a hydraulic valve actuator.

Using the calibration curves, function generator settings were adjusted to produce linear flowrate ramps. Both nitrogen and helium flows were evaluated with various values of ramp slope (rate of change of flowrate). Some results of these experiments are shown in Fig. 38 for nitrogen and in Fig. 39 for helium. All three ramps in each of those graphs were produced with a single array of setting of the function generator; only the duration of the ramp was varied. With nitrogen (Fig. 38), the data points were within ±0.2 lbm/sec of the desired linear ramps for all flows having ramp flow durations greater than 0.25 second. Shorter duration ramps can be made with reduced linearity

115
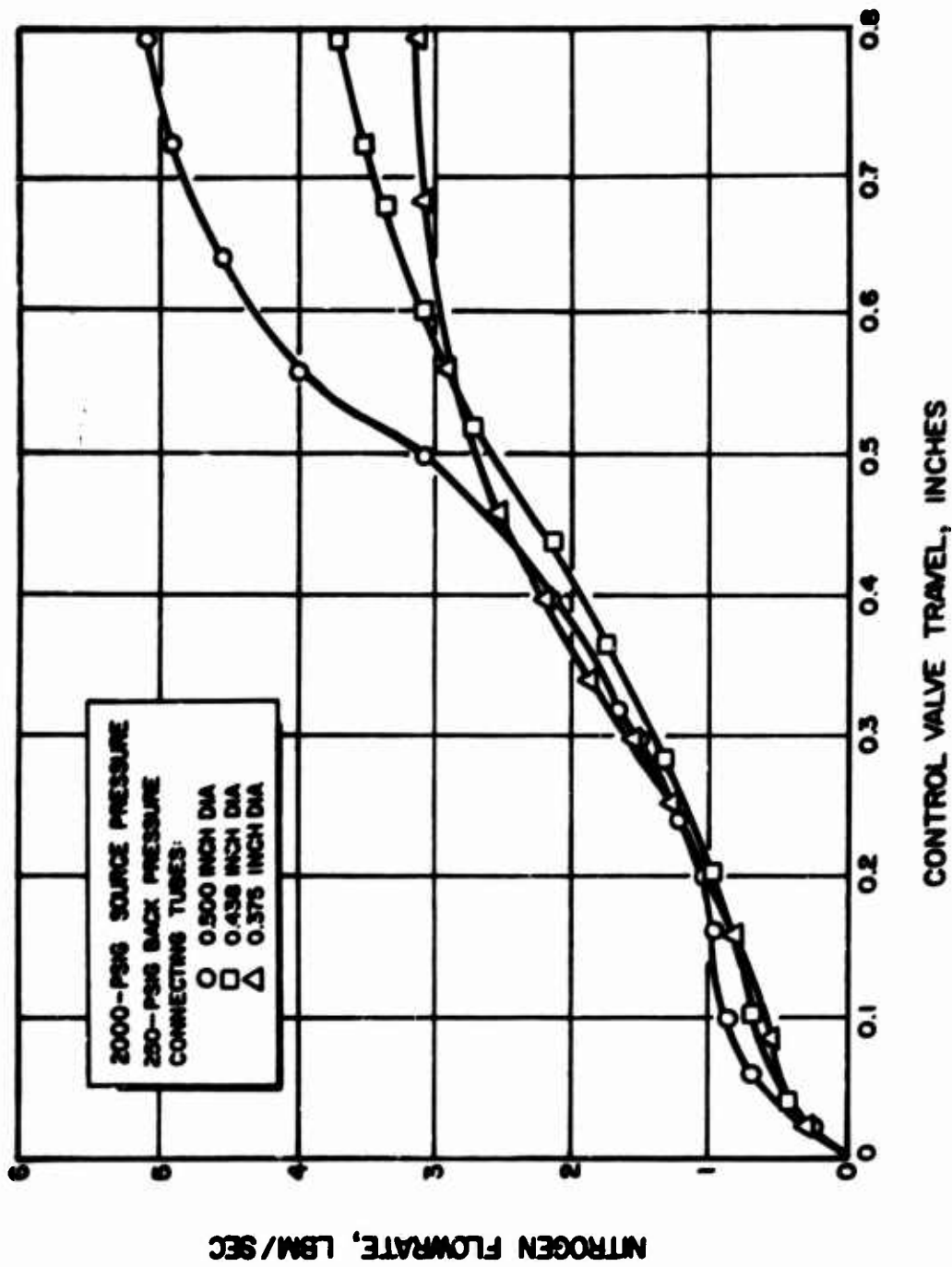
Figure 36. Nitrogen Flowrate vs Valve Position Calibration for Modified Gas Flow Generator

116

CONTROL VALVE TRAVEL, INCHES

HELIUM FLOWRATE, LBM/SEC

2000-PSIG SOURCE PRESSURE
250-PSIG BACK PRESSURE
CONNECTING TUBES:
○ 0.500 INCH DIA
□ 0.438 INCH DIA
△ 0.375 INCH DIA
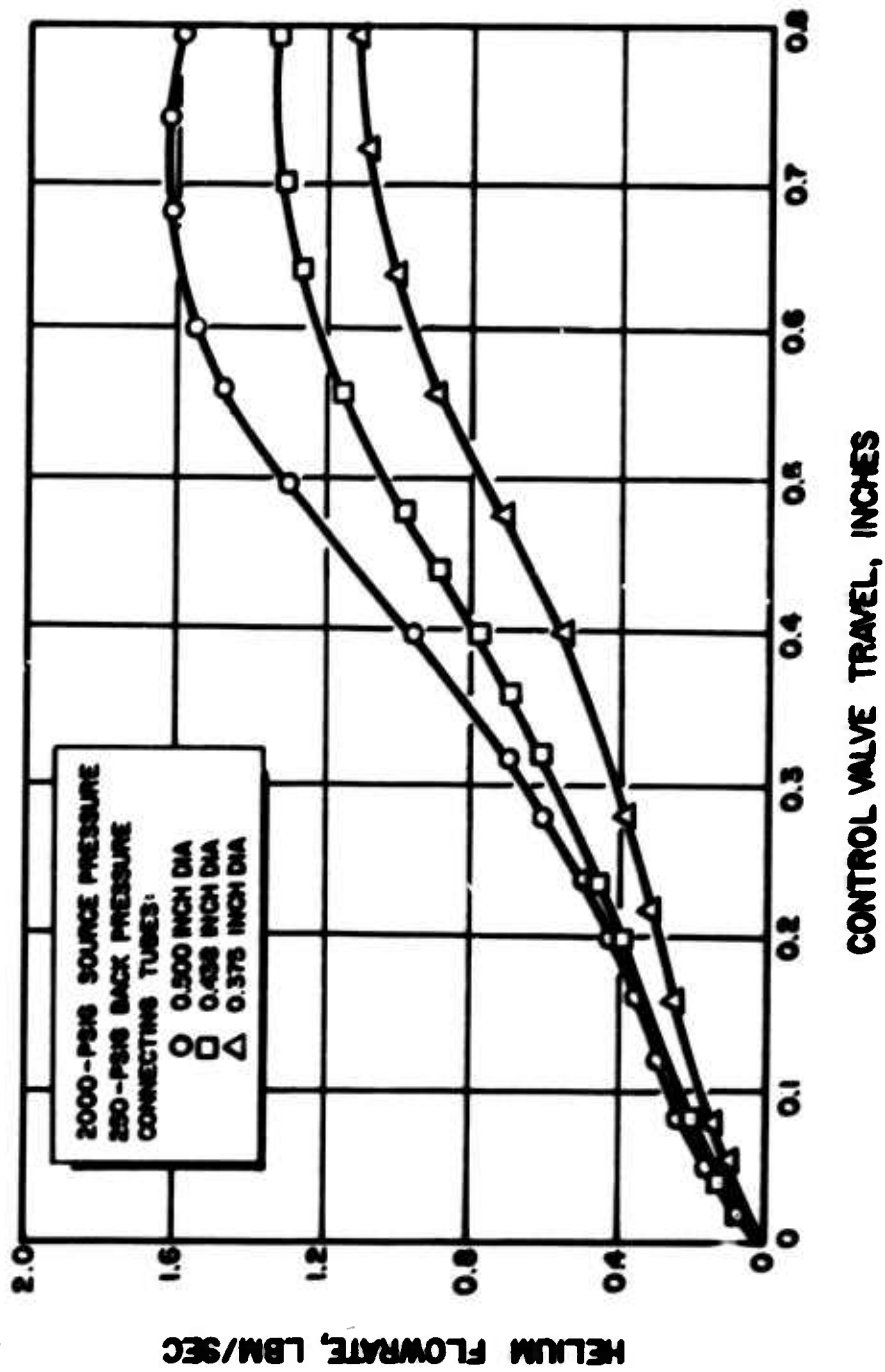
Figure 37. Helium Flowrate vs Valve Position Calibration for Modified
Gas Flow Generator

117
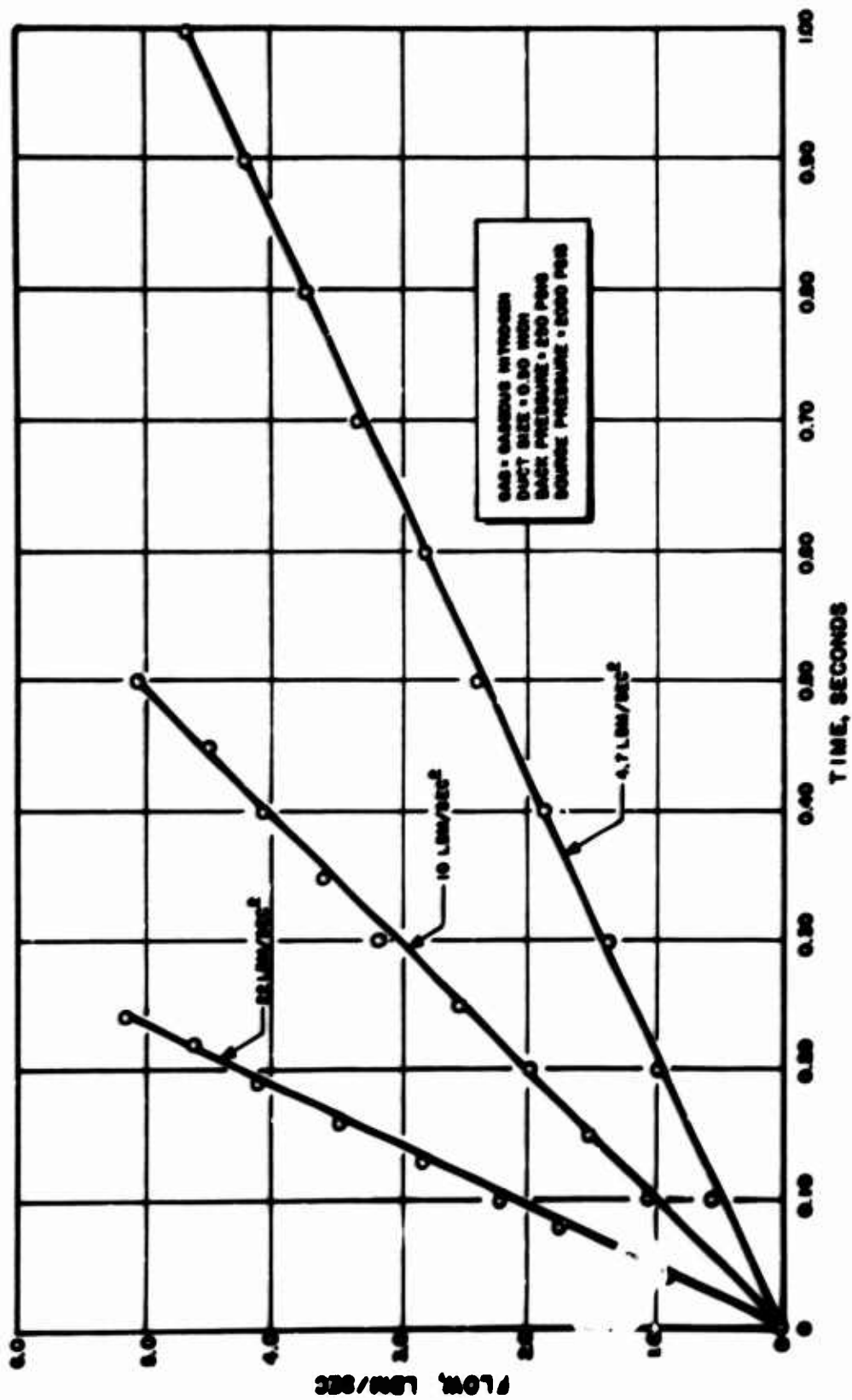
Figure 38. Linear Ramp Nitrogen Flowrates Produced by the Modified Gas Flow Generator
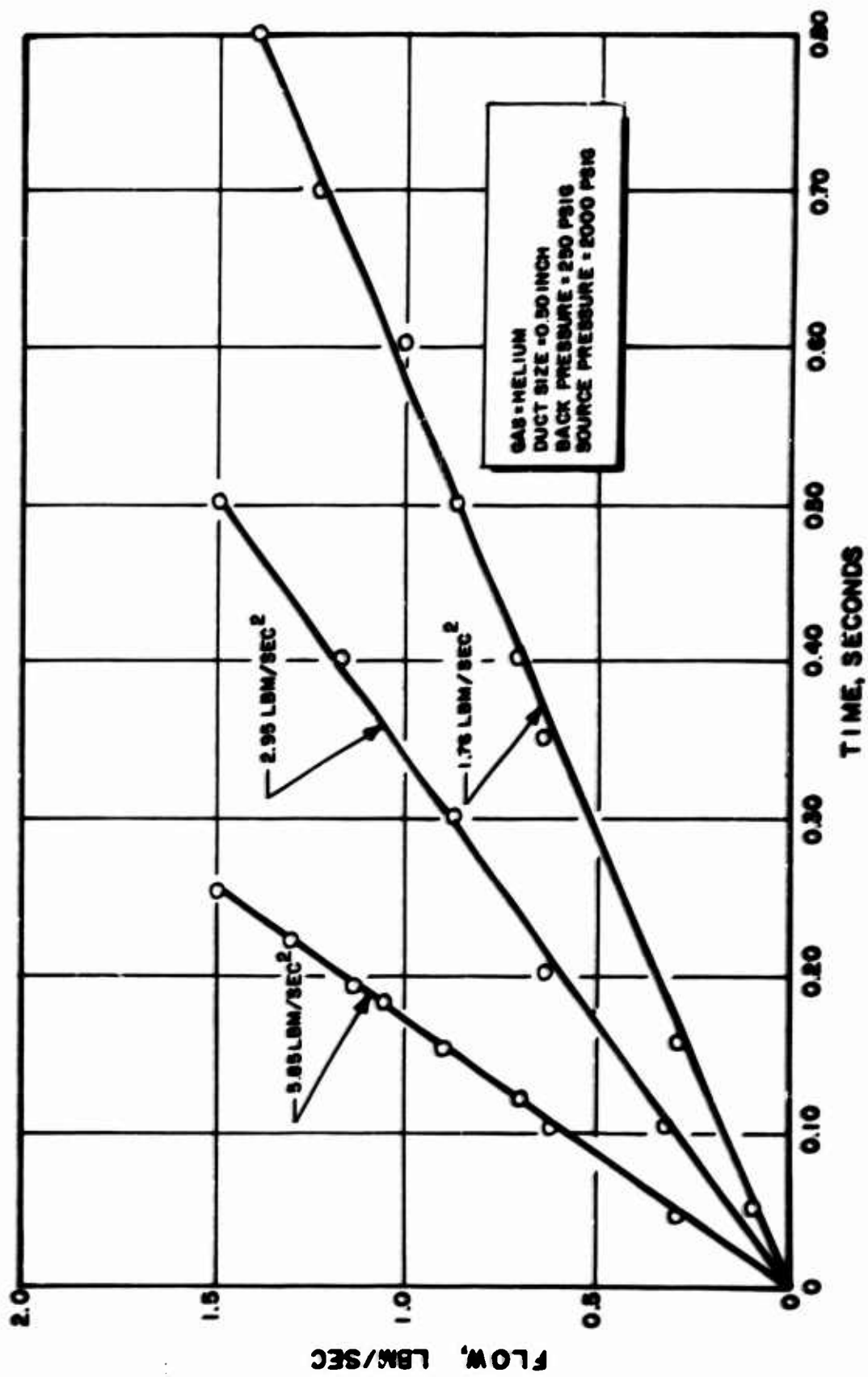
Figure 39. Linear Ramp Helium Flowrates Produced by the Modified Gas Flow Generator

119

using the same array of function generator settings or, given additional cold flows, a corrected array of settings for improved linearity could be developed. Usable ramps with durations as short as 0.1 second are possible, but even shorter durations are limited by imprecision of gas flowrate measurements. The maximum attainable nitrogen flowrate was just over 5 lbm/sec and was somewhat dependent upon the tank back pressure.

With helium, the maximum attainable flowrate was approximately 1.5 lbm/sec, the ramp slopes for particular durations were correspondingly reduced, and the data points were within 0.07 lbm/sec of being linear for ramp durations greater than 0.25 second. These data adequately demonstrated that any desired flow function could be produced by using the function generator flowrate control technique.

The gas temperature in the connecting tube showed little variability during the flow ramps. All values were within 10 degrees Fahrenheit of the supply temperature. No attempt to correlate these small changes to the flow conditions was made.

Similarly, no transient pressure spikes or surges were observed with the Kistler transducer in the connecting tube. The static pressure at that point was not measured.

Additional Flow Generator System Modifications

The foregoing experiments also demonstrated, however, that the maximum flowrate through the modified gas generator is a strong function of the gaseous supply system's pressure drop characteristics as well as a function of that system's initial pressure. The first factor limits the generator's general utility in that every installation would have to be cold-flow characterized individually for the particular gas supply system. The second factor limits the generator's local utility because it would normally be supplied from a gas source that supplies other test stand needs, such as propellant tank pressurization, propellant line purging, and pneumatic valve

120

actuation. A particular value of source gas pressure at the time of the test cannot normally be guaranteed, so the slope of the ramp would be an essentially uncontrolled variable.

Calculations were thus made to determine how much surge tank capacity would be required to make the flow generator independent of the gas supply system and simultaneously increase the maximum attainable flowrates. The calculations were based on using the gas supply system to pressurize a source tank of arbitrary volume, located in the system as shown by tank (4) in Fig. 34, and operating the system in a blowdown manner with no additional gas supplied from the gas supply system. The calculations are somewhat conservative, therefore, in that longer durations or slightly higher maximum flowrates would be possible if additional gas were admitted during the ramp flow.

The previous flowrate calibrations were used to estimate pressure drops of the system downstream of the source tank as functions of maximum gas flowrates. Added to the chamber pressure, this gave a minimum tank pressure which would supply a particular maximum flowrate. The tank volume was then calculated from

$$V_T = \frac{\dot{w}_{max} d}{2(\rho_i - \rho_f)} \tag{19}$$

The calculated results (Fig. 40) show that a surge tank volume of approximately 2 cu ft would have provided adequate isolation of the original generator from the gas systems. The anticipated maximum flowrate requirements of 3 lbm/sec helium and 10 lbm/sec nitrogen could not be met, however; even a moderately large surge tank cannot provide these maximum flowrates. Similar calculations for higher initial pressures and larger diameter tubes connecting the gas flow generator to the combustor revealed that the desired maximum flowrates could be obtained by replacing the 1/2-inch diameter connecting tube with a 3/4-inch tube and providing approximately 8 cu ft of surge tank.
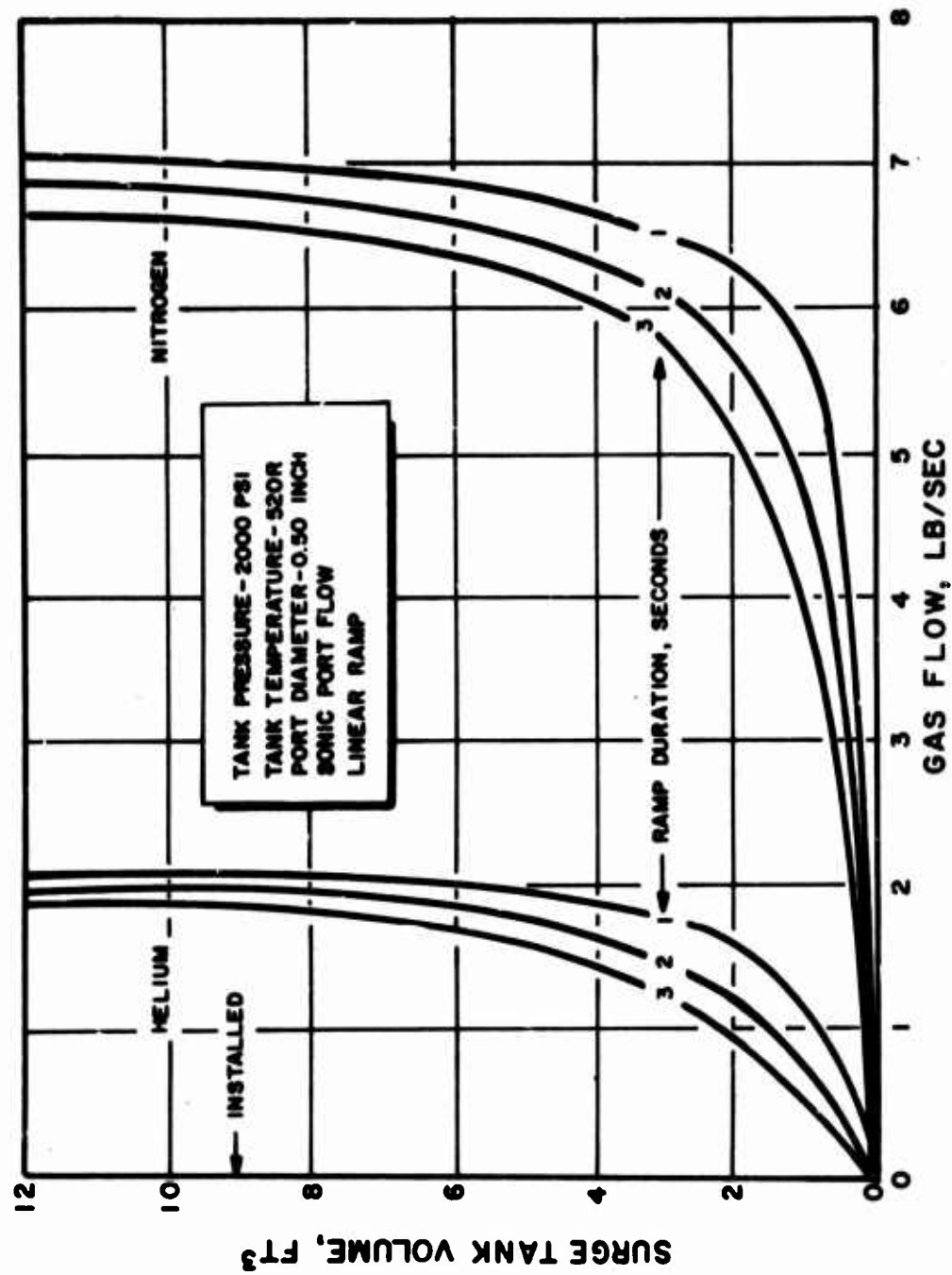
Figure 40. Effects of Surge Tank Volume and Linear Ramp Duration on Maximum Gas Flowrates

122

Accordingly, six 1-1/2 cu ft carbon dioxide cylinders were installed in parallel to provide 9 cu ft of surge capacity. Simultaneously, the flow generator was moved to the hot firing test stand and close-coupled to the rocket motor hardware.

This system was activated on the test stand just as the hot-firing program was ready to be initiated. When the repetition of the flowrate versus valve position calibration tests were begun, it was found that the additional surge volume made it possible to control the gaseous flowrate for a linear ramp by full servo control; i.e., by comparing the actual instantaneous flowrate with the derived flowrate and bypassing the valve position control per se. This mode of control made use of an existing analog computer network which was already partially utilized for preprogrammed valve position function input and for computation of flowrate for direct readout. Linear gas flowrate ramps were scheduled for initial use in the hot-firing program, and, because the cold-flow calibrations would delay starting the hot-firings by approximately a week, it was decided to use the full servo-control of flowrate.

Gas flows with characteristics other than linear flowrate ramps would still require valve position, rather than direct flowrate, control. It was intended, therefore, to conduct the calibration tests at some later, more convenient time in the program. As is discussed later in this report, however, the gas flows were so ineffectual in initiating combustion instabilities that the rating technique was eliminated from further evaluation before this additional work was performed.

SIMULATED CHAMBER STUDY

A chamber assembly from the hot-firing hardware was temporarily modified for examining the effects of the rating devices on sprays formed by one of the injectors during simulated propellant flows using water. The triplet pattern injector, described later, was modified by plugging all orifices

123

except those in the outer three rings in two baffle compartments. All orifices were plugged in the remaining baffle compartment, thus leaving a field of view for a Fastax camera during the water flows. The injector was assembled to the combustion chamber section without the nozzle section. In this manner, all of the chamber pulse boss and bomb mounting positions were made available for use during the simulated propellant flows.

Tests were conducted with water supplied to both propellant manifolds at flowrates such that the nominal mainstage propellant injection velocities were modeled. Blasts from pulse guns and gaseous nitrogen flows were introduced radially and chordally through the chamber wall and bombs were mounted at the 4.95-inch radial position on the downstream edge of a baffle vane. High-speed photographic records were taken with a 16-millimeter Fastax camera having a capacity of 400 feet of film and a maximum framing rate of about 6000 frames/sec. Photofloc lamps were used to illuminate the water sprays in the neighborhood of the injector.

The photographic results were generally less than satisfactory. The blast waves from both the bomb and pulse gun devices so rapidly generated and dispersed a dense fog that the camera's field of view was completely obscured within one to five frames and remained so for several milliseconds. These photographs were dramatic illustrations of the powerful disruption of steady-state conditions that must occur in an operating rocket when one of these devices is discharged, but nothing quantitative could be gained from them. With the gaseous nitrogen flow, spray displacement could be observed to proceed rapidly across the chamber in a sequence of frames, and the camera's field of view remained clear until the first-displaced spray had splashed onto the chamber wall opposite the gas flow's entry point. While it appeared that quantitative spray behavior data could be obtained from continued studies with gaseous flows, the simulated chamber experiments were terminated because they could not (without major modification, at any rate) provide quantitative information to advance the characterization of bombs and pulse guns.

124

HOT-FIRING PROGRAM

The relative effectiveness of the stability rating techniques in establishing a rocket combustor's stability traits was investigated by applying them at various positions in an operating rocket and observing their effects on its stability. Major objectives were the establishment of correlations between the rating techniques' characteristics and the combustor's response and establishment of practical correlations between different rating techniques.

There has been a growing trend under rocket engine development contracts over the past few years toward requiring a more or less definitive demonstration of dynamic stability, i.e., rapid recovery to steady-state operation after a sizeable disturbance. Frequently, one of the stability rating techniques investigated in this program is specified as the disturbance source. For that reason, it seemed appropriate that an engine that had previously been evaluated as dynamically stable, at least under some operating conditions, be used during this program. An engine from an earlier program was determined to have the right combination of thrust level, propellant experience, range of injector experience, and stability characteristics to form a base level for this study of the rating techniques.

A number of modifications were necessary to make existing components from that engine program suitable for use during this program. An ablative-walled combustion chamber was replaced with a metal-walled chamber to permit installation of a multiplicity of pulse bosses and pressure transducer ports. An aluminum baffle assembly, built as an integral part of the injector and cooled by a through-flow of fuel which was then sprayed from the baffles' downstream edges, was replaced by an uncooled copper assembly. Two existing injectors that had not had integral baffles were then reworked to obtain the desired injection patterns.

EXPERIMENTAL PROGRAM

Test Conditions

The hot-firing program was conducted on Pad 3 at the Research Combustion and Heat Transfer Laboratory. Remote control of the motor during the hot firings was accomplished with preset sequenced valve signals. Two Eagle timers were used for this purpose. The first, a 5-second-duration timer, controlled the operating signals for the combustion stability rating devices and the main propellant valves. The second, a 25-second-duration timer sequenced the high-speed cameras and the fuel-side water flushing system. The 2.5-second programmed test firings began with a 100 ±25 millisecond oxidizer lead at start, with a 120 ±25 millisecond fuel-rich cutoff. The fuel valve pneumatic cylinder was orificed to close more slowly than the oxidizer valve to ensure a fuel-rich cutoff in the event of premature test termination. A water flush was sequenced to flow through the fuel side of the injector after the fuel main valve was closed. Gaseous nitrogen purges were applied to each injector propellant supply line during startup and shutdown. The purge was automatically terminated during the start sequence by a check valve as chamber pressure approached the mainstage level.

Nominal operating target conditions for all hot-firing tests were:

      Propellant: N_2O_4 oxidizer, N_2H_4-UDMH(50-50) and UDMH fuels
      Mixture Ratio: 1.6 o/f
      Chamber Pressure: 150 psia

Disturbances from maximum of four rating devices were introduced during each test. The explosive bombs were always signaled first to avoid thermal initiation; each subsequent device was sequenced at 400-millisecond intervals. A total of 148 disturbances by the various rating devices were introduced into the combustion chamber during 86 hot-firing tests.

Test Hardware Description

The motor test hardware consisted of an injector and thrust chamber assembly as shown in Fig. 41. The motor developed 10,500 pounds of thrust at 150-psia chamber pressure.

Combustion Chamber. The combustion chamber was of conventional design, being comprised of a right circular cylindrical section and a deLaval nozzle. The cylindrical portion had an inside diameter of 11.41 inches and extended to 8.00 inches from the flat-faced injector plane; the first 6.25 inches of that length was formed by an uncooled copper section which was fitted with pulse inlet and transducer ports and slotted to receive the baffle assembly as shown in Fig. 42.

The combustor contained nine pulse boss positions, offering chordal, tangential, and radial directions at three different axial distances from the injector face. Each boss position was designed to accept the burst diaphragm holder (barrel) section of the pulse gun apparatus and a machined adapter for the gas flow generator pulsing device. Further, each boss port diameter could be varied to provide a diameter of 0.515, 0.430, and 0.370 inches for these two pulse rating devices. Eight Photocon pressure transducer ports were initially located within the combustion chamber; two additional ports were strategically added during later hot-firing tests.

The explosive bombs were installed at three different radial positions in the chamber by attaching them to the downstream edge of one baffle blade. An attachment method was devised to avoid manual screw thread engagement of the bomb case. The new method, sketched in Fig. 43, employs a slotted end on the bomb case, with a shoulder that engages an enlarged section in the mating baffle hole by snap action. Quick, positive engagement was thus achieved without the risk of breaking the electrical connections by twisting the leads.
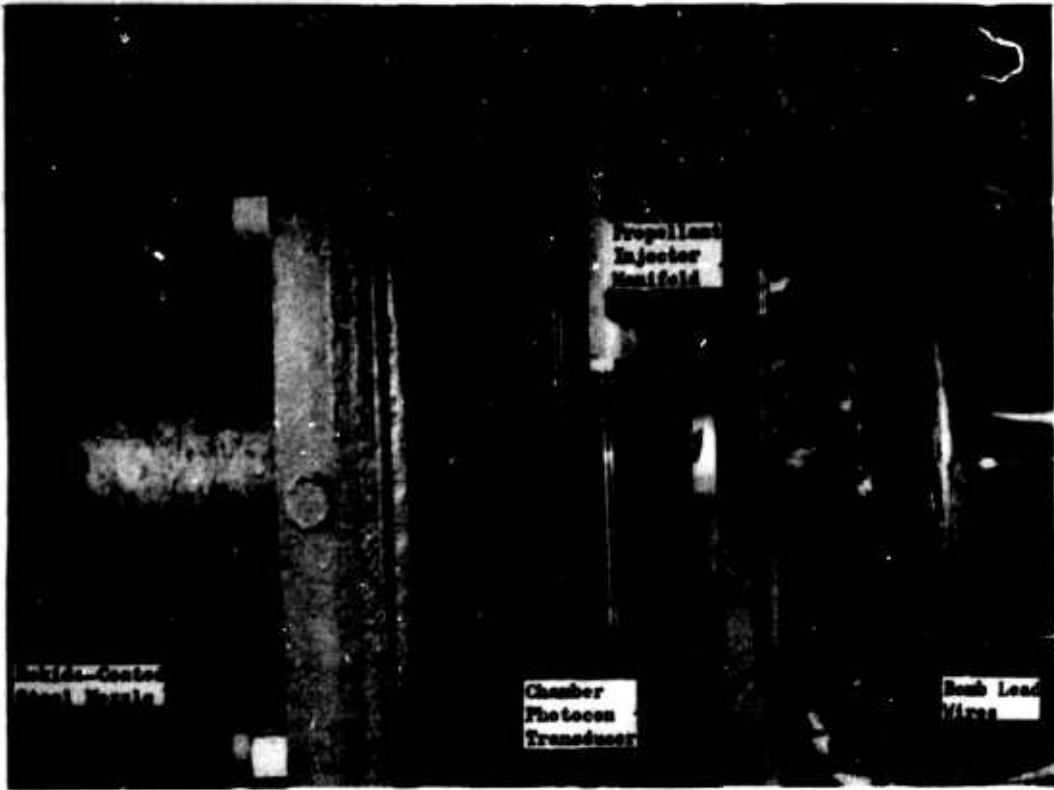
5AE21-2/9/66-81C

a. Side View
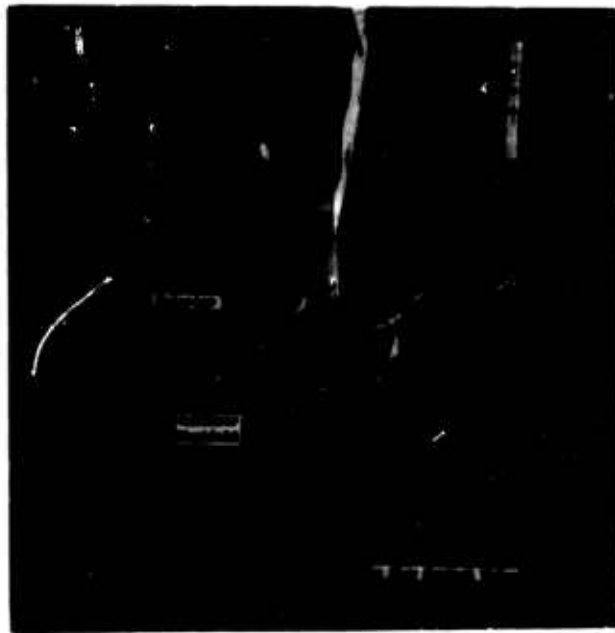
5AE21-2/9/66-81B

b. Injector-End View

Figure 41. Hot-Firing Chamber

128

Figure 42. Combustion Chamber Section With Multiple Pulse and Pressure
Transducer Bosses
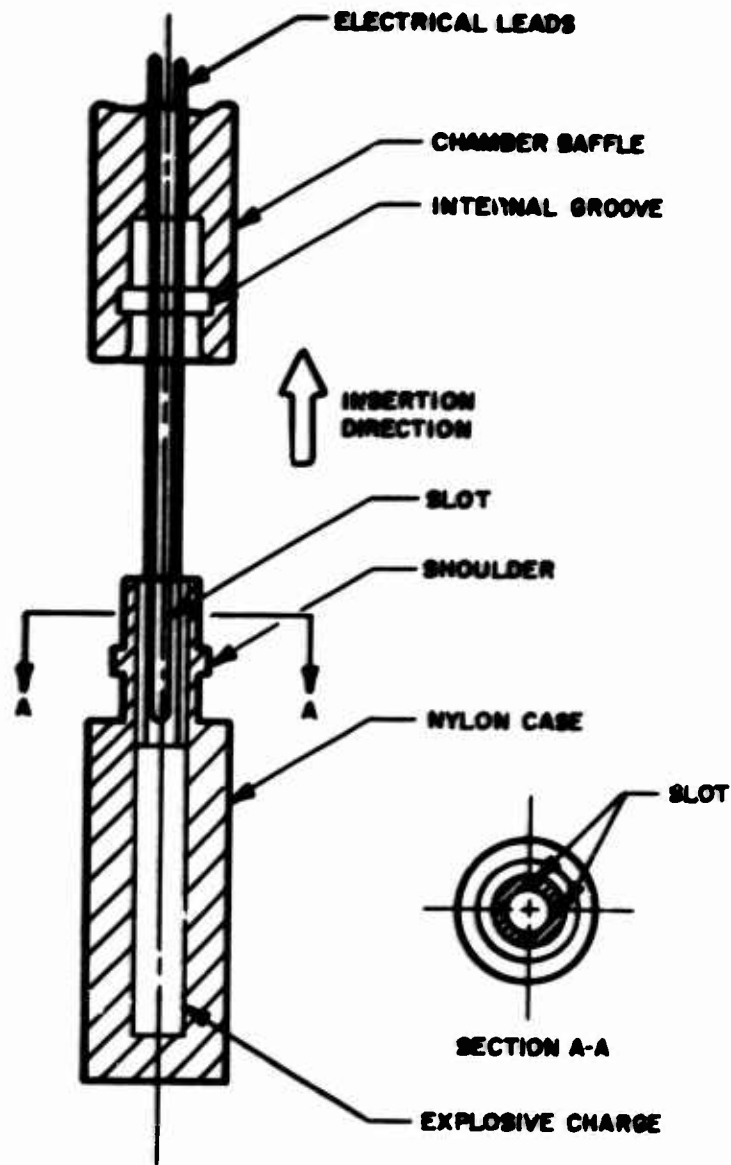
Figure 43.   Snap Attachment Explosive Bomb Case

Several examples of typical bombs are shown in Fig. 44 . Two examples of the snap-action attachment device are shown; one has a threaded end for engaging female threads in the bomb case, and the other has a blind end for plugging bomb-mounting ports that are not in use.

A three-compartment, 1.6-inch-long, uncooled baffle configuration was used. The baffle section was machined from a single copper block and fitted into the machined slots in the copper combustion chamber section (Fig. 42). The baffle blade containing the bomb receptacle holes had an internal drilled channel for conducting the electrical leads through the chamber wall. The leads were externally sealed at the chamber wall with a drilled Teflon compression fitting. The geometrical relationships among the various bosses and baffles are shown in Fig. 45, which is drawn as if the viewer were looking through the injector.

Transparent Chamber. A transparent combustor section was designed to permit photographic visualization of the combustion process. The transparent section was interchangeable with the copper combustor. A photograph of the assembly is given in Fig. 46 . The transparent chamber was machined from Plexiglas and consisted of a cylindrical section with 1-inch-thick walls with serrations machined at both ends for sealing. A radial copper pulse gun boss was attached for one test firing. The walls of the transparent section were slotted to hold the baffle assembly in a manner similar to the solid copper section design. Each transparent combustor was useable for only one short duration test firing.

Nozzle. The nozzle section was of uncooled, Rokide-coated, type 4130 steel construction. Its 1.75-inch-long cylindrical section matched that of the cylindrical combustor section and was followed by convergence to a 7.17-inch diameter throat 15.00 inches from the injector plane. The nominal chamber contraction ratio was 2.54. The nozzle exit was 6.25 inches from the throat with an expansion ratio of 2.35. The nozzle section contained one Photocon instrumentation port and an explosive bomb mounting hole.
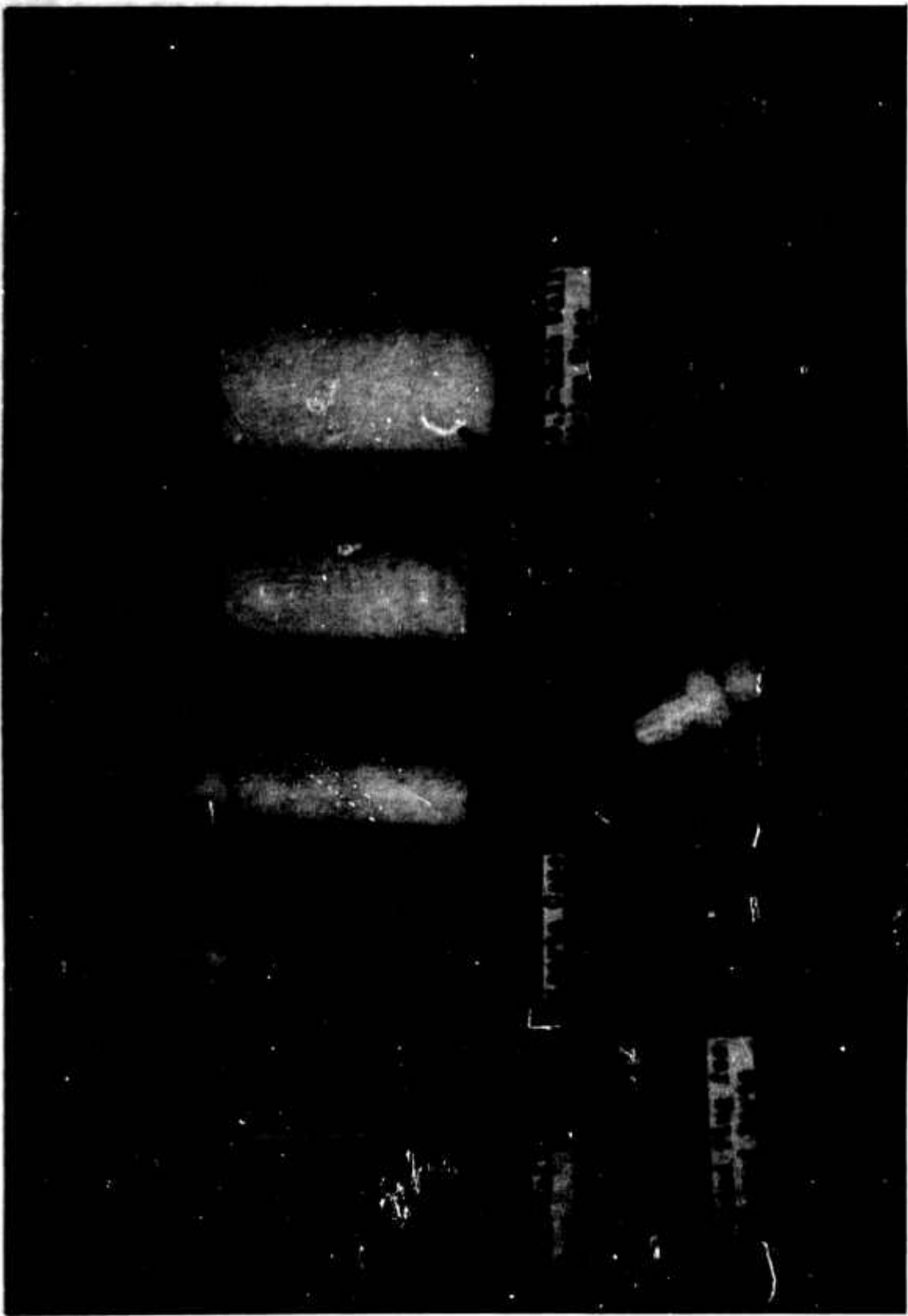
Figure 44. Typical Explosive Bomb Cases and Fixtures
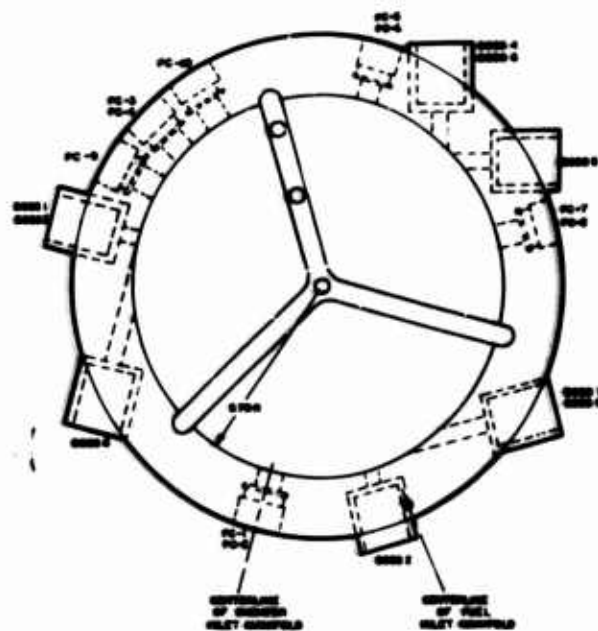
Pulse Boss	Direction, (degrees)	Axial Distance, inches
1	Radial (180)	2.00
2	Radial (180)	3.00
3	Radial (180)	4.00
4.	Chordal (135)	2.00
5	Chordal (135)	3.00
6	Chordal (135)	4.00
7	Tangential (90)	2.00
8	Tangential (90)	3.00
9	Tangential (90)	4.00

Photocon Port	Identification (Test Numbers)	Axial Distance, inches
PC-1	C (03), F (10-37)	1.50
PC-2	B (03), F (38-77, 80-82)	4.00
PC-3	A (01-77, 80-86)	1.50
PC-4		4.00
PC-5	B (01, 02, 04-77, 80-86)	1.50
PC-6		4.00
PC-7	C (01, 02, 04-77, 80-86)	1.50
PC-8		4.00
PC-9	H (80-86)	1.50
PC-10	I (80-86)	1.50
Nozzle	G (59-64, 78, 79)	10.2
Oxidizer Manifold	D (01-09, 78, 79)	NA
Fuel Manifold	E (01-79)	NA

Figure 45. Locations on the Chamber for Pulse Bosses and
Photocon Pressure Transducers

133
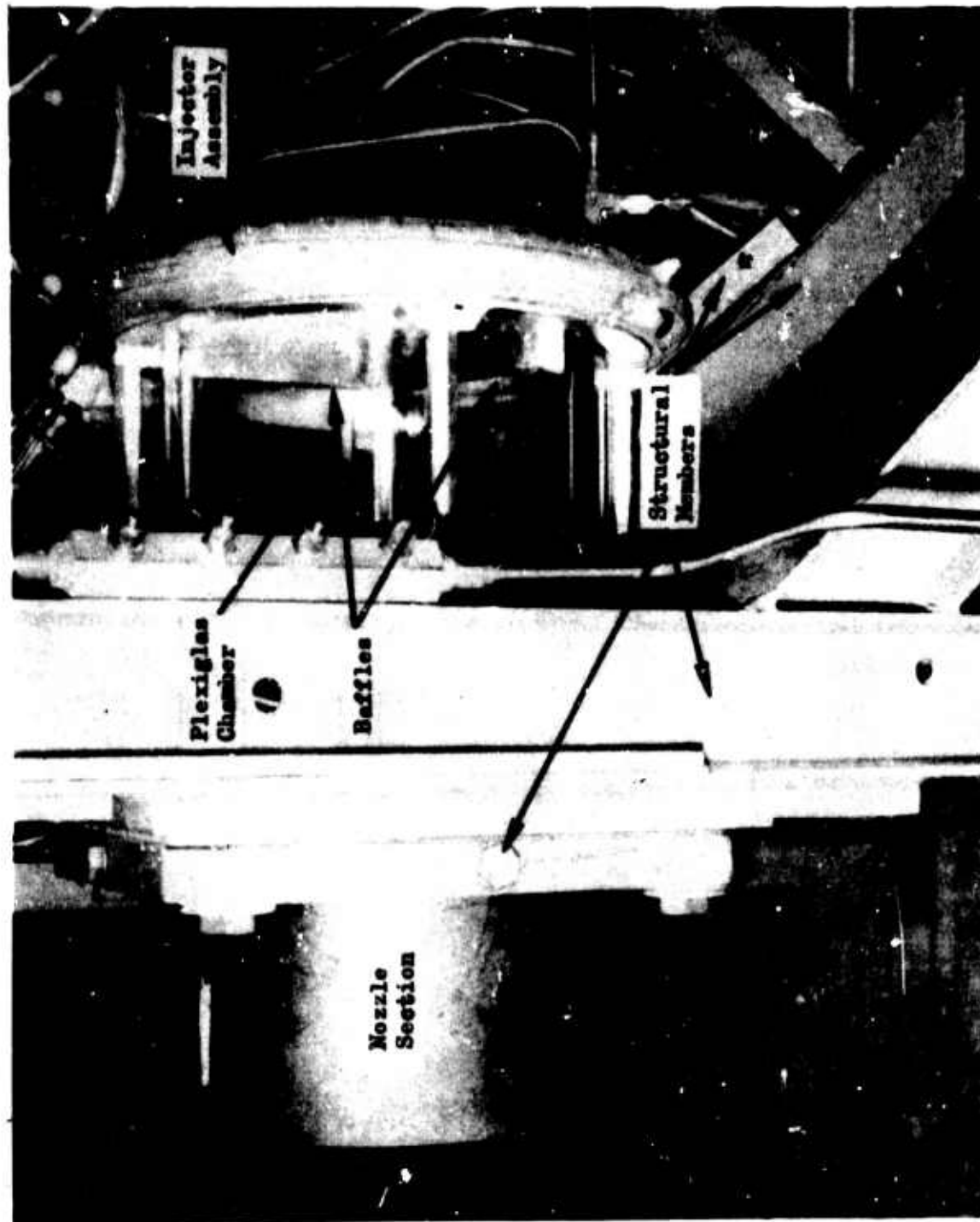
Figure 46. Transparent Combustion Chamber Assembly

Injector Assembly

Structural Members

Plexiglas Chamber

Baffles

Nozzle Section

Transient conduction heat transfer calculations were made and it was predicted that even if the Rokide coating were lost, run durations up to 5-seconds could be made without exceeding the surface melting temperature of the steel nozzle. The Rokide coating started to flake off after about fifteen tests, and no nozzle erosion was experienced.

Injectors. Two different injectors were used; a face-view of one injector with the uncooled copper baffle resting on the triplet pattern is shown in Fig. 47. The other injector, Fig. 48, has a symmetrical pattern of self-impinging doublet (like-on-like) and unlike doublet elements. Examination of Fig. 47 shows that there are four concentric circular rows of triplet elements centered over the oxidizer rings. (Near the center of the injector, a small number of unlike doublet elements provide some propellant injection in corners too small for the triplets.) There are slight variations in hole sizes from ring to ring to balance the propellant mass and mixture ratio distributions. A "typical" triplet element is composed of a single 0.0700-inch-diameter oxidizer injection orifice, drilled normal to the injector face, and a pair of 0.0420-inch-diameter fuel injection orifices drilled at a 55-degree angle to the face to provide symmetrical impingement of both fuel streams on the oxidizer stream at a distance of 0.571-inch from the injector face. Showerhead fuel holes in the outer fuel ring, which originally provided wall film coolant, were plugged by welding over them.

The second injector (Fig. 48) has a symmetrical mixture of self-impinging doublet (like-on-like) and unlike doublet elements. A typical example is 0.0420-inch- and 0.0390-inch-diameter holes for the fuel and oxidizer, respectively, with the self-impinging doublet holes drilled to impinge 0.571 inch from the injector at a 36-degree included angle and the unlike doublets drilled to impinge 0.633 inch from the injector at a 35-degree included angle. To balance the streams' transverse momentum components, 15 degrees of that latter angle is formed by the oxidizer stream and 20 degrees by the fuel stream.
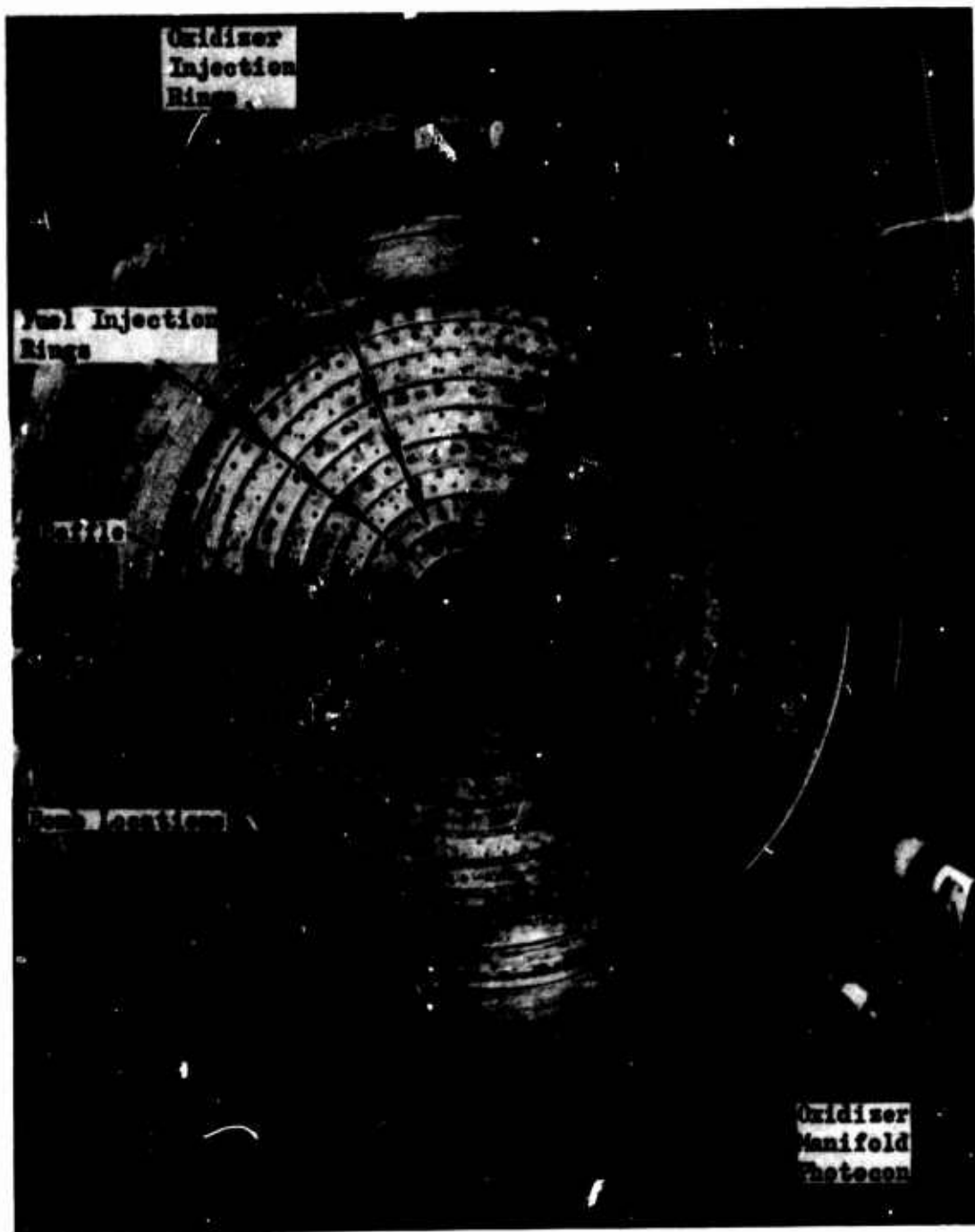
5AE36-3/24/66-S1A

Figure 47. Triplet Pattern Injector
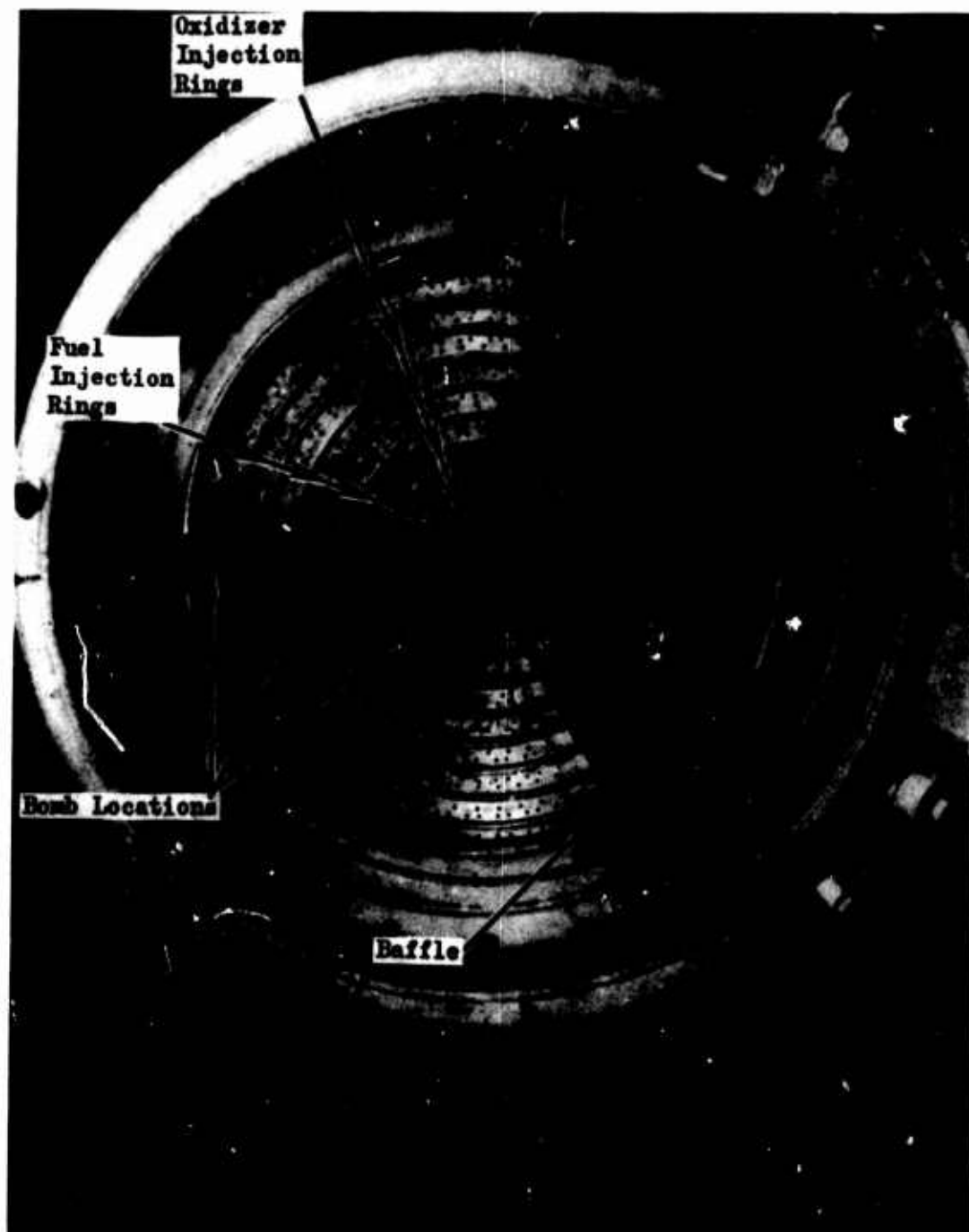
5AE36-3/24/66-S1B

Figure 48. Doublet Pattern Injector

Supporting Test Equipment

The test motor was mounted horizontally within a baffled steel test pit enclosure to provide isolation from the propellant run tanks. A drainage system was installed for water dilution and subsequent runoff of all spilled propellants to a safe area.

Propellant Systems. The NTO was supplied from a 5000-psi, 39-gallon spherical run tank and was pressurized with a 2400-psi gaseous helium bottle bank. The NTO was stored in a 2000-pound forged steel cylinder, and was permanently connected to the run tank. Approximately thirty tests at 150-psia chamber pressure were achieved per cylinder of NTO. The fuel was supplied from a 5000-psi, 33-gallon run tank and was pressurized with 5000-psi gaseous helium. A schematic drawing of the complete system is shown in Fig. 49 . Both propellant systems were plumbed normally closed to prevent atmospheric contamination with vapors. Hand operated vent valves were available on each tank for emergency venting operations.

Each propellant feed system consisted nominally of fifty feet of 1-1/2-inch diameter plumbing and contained two 1-1/2-inch shutoff valves. Average values for the NTO and fuel tank pressurizations were 345 psig and 265 psig, respectively, for 150-psia chamber pressure operation.

Instrumentation. Basically, two kinds of transducer data were acquired from each firing: steady-state operational control data and transient stability data. Steady-state data include propellant flowrates, static pressures in propellant tanks, injection manifolds, the combustion chamber and gas pulse supply system, as well as valve timing and sequence information. These data were recorded with an 18-channel oscillograph and several recording potentiometers.

The primary transient data were rapid pressure fluctuations in the combustion chamber and in the propellant manifolds. These were measured with strategically

138
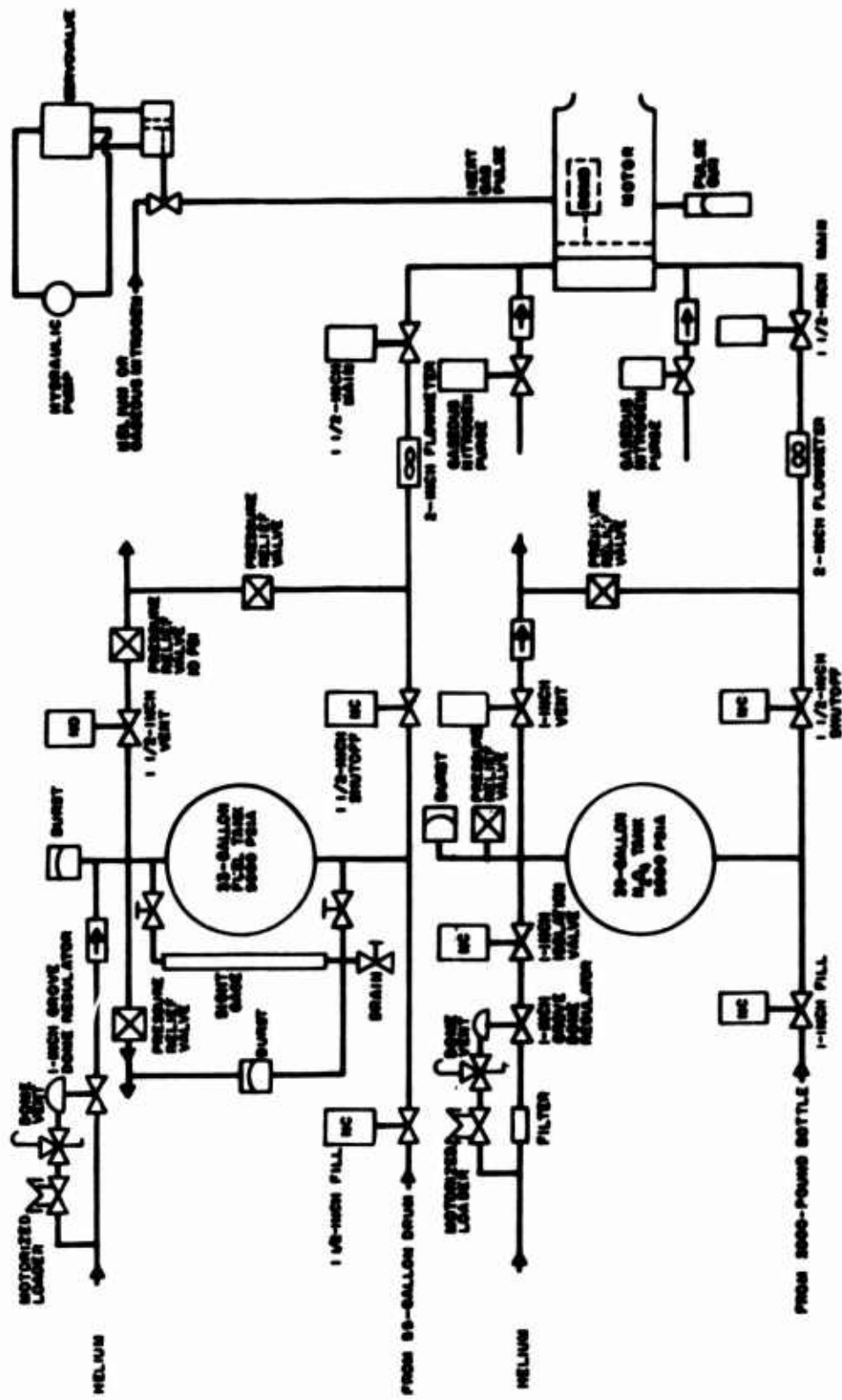
Figure 49. Propellant System

139

located, water-cooled, flush-mounted Photocon pressure transducers.
Photocon locations during each hot firing are shown in Fig. 45.
Model 1345 transducers were used to measure chamber pressure fluc-
tuations. Later in the program, two Model 525 transducers were added
to the chamber in positions H and I. Pressure oscillations in the
propellant manifolds were measured with two Model 775 transducers.

A Rough Combustion Monitor (RCM) system was employed to automatically
terminate each test firing when a certain level of combustion insta-
bility was achieved. The input to the RCM during all solid wall tests
was the signal generated by chamber pressure Photocon A. The output
of fuel manifold Photon E was used during the two transparent wall
motor firings. The RCM unit was calibrated to terminate the test
firing when the Photocon transducer input exceeded 50 psi peak-to-
peak pressure oscillation for 100 milliseconds.

For each test firing, a maximum of five Photocon outputs were recorded
on an Ampex Model FR-100 seven-channel tape recorder. Also recorded
there was the output of an accelerometer mounted on the outside of
the injector plate and a 1000-cps time base that was used for cross-
correlation between recorded data and the streak and motion picture
films.

Test Photography. During the solid-wall chamber tests, high-speed
motion pictures were taken of the exhaust plume with a 16-millimeter
Fastax camera located at one side of the chamber and of the combustion
within the chamber with a Fastax camera positioned beside the exhaust
plume and looking up the exhaust nozzle. The latter camera's field of

140

view covered about one-third of the injector face and usually included
the baffle vane on which the majority of the explosive bombs were
mounted:
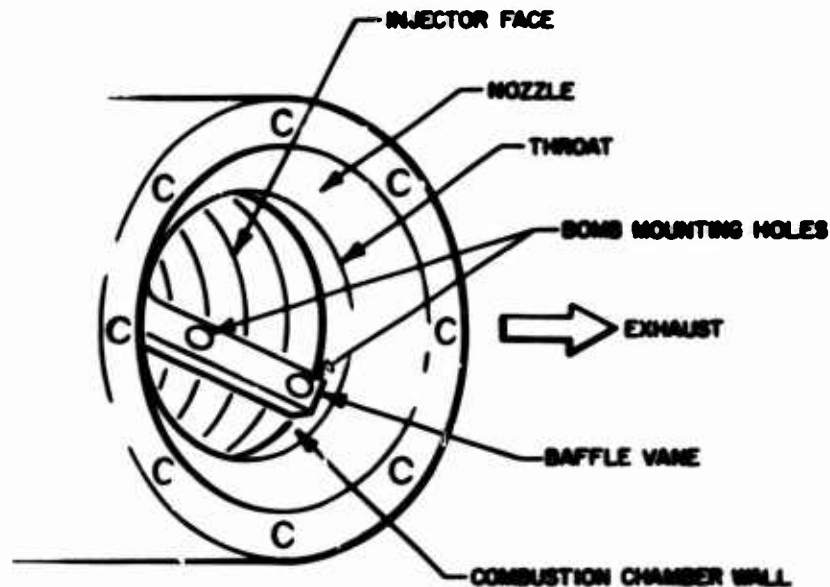
Framing rates up to about 5 to 6000 frames/sec with the standard 16-
millimeter camera and 10 to 12,000 frames/sec with a half-frame camera
were normally taken. The total exposure time for a 400-foot roll of
film was approximately equal to the 2-1/2-second sequenced run duration.

Modified 16 millimeter Fastax cameras were used to obtain nozzle view
streak photographs simultaneously with the motion pictures. The streak
films were taken primarily to obtain continuous records of the luminous
emission from particular narrow fields of view; the films gave data on
the type of chamber instabilities. In the earliest attempts to use this
technique on this program, the camera viewed a circumferential segment
just downstream of the nozzle exhaust plane; no success in instability
mode identification was achieved here. Later, toward the end of the
program, the streak camera was positioned to view portions of the injector
face, just as the motion picture cameras had.

141

The streak films were obtained by removing the framing prisms from the cameras and installing 0.002 to 0.005-inch wide slits at the film plane, perpendicular to the film edges. The rapidly moving film was continuously exposed to the combustion process luminous emission from a narrow field of view of interest. One camera was aligned to provide a field of view parallel to one baffle vane. Another streak camera, containing a circular arc slit, was aligned along the injector periphery for an approximate 100-degree arc segment.

Extended camera coverage was used on the two transparent motor firings. In addition to the two Fastax and two streak cameras previously discussed for the solid-wall chamber tests, three more motion and two more streak cameras were utilized for the transparent motor hot firings. One of the added streak cameras was aligned with its slit field of view parallel to the chamber axis and extending from the baffle tip to a point 4.75 inches downstream. The other streak camera was aligned vertically (or circumferentially) with the narrow field of view located 0.25 inches downstream of the baffle edge. The physical arrangement of the four streak cameras is depicted in Fig. 50 . Two new motion Fastax cameras were added to obtain closeup views of the propellant injection region. The other camera was a 70 millimeter 20 fps device which provided overall views of the transparent chamber firings, Fig. 51.

EXPERIMENTAL RESULTS

A total of 86 hot-firing tests was conducted during this program; 148 combustion chamber disturbances were generated by the rating devices.

Operational Test Results

A minimum number of problems was encountered during operation of the experimental test program. Only two tests resulted in hardware damage,
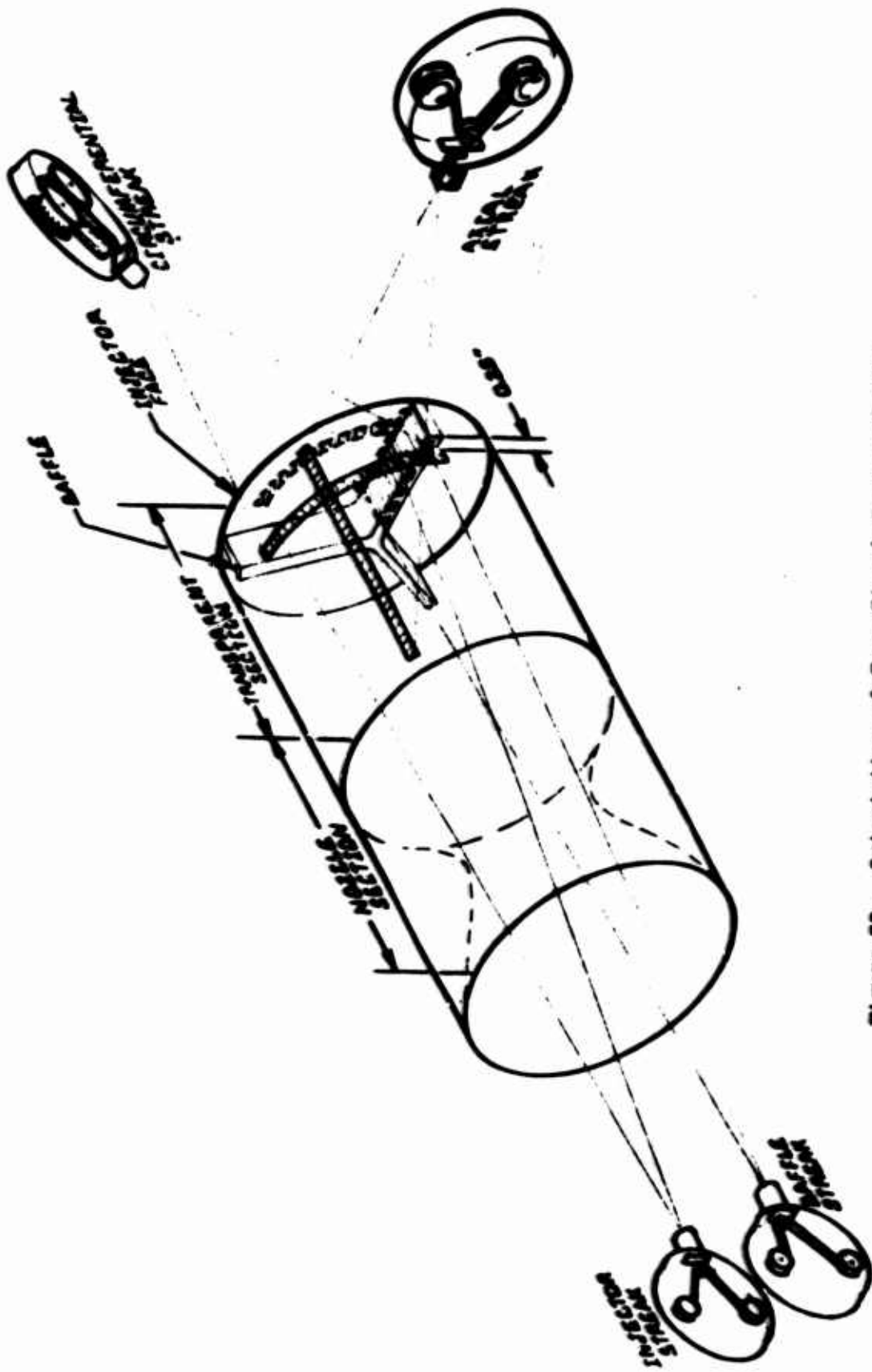
Figure 50. Orientation of Four Streak Cameras During Transparent Chamber Tests
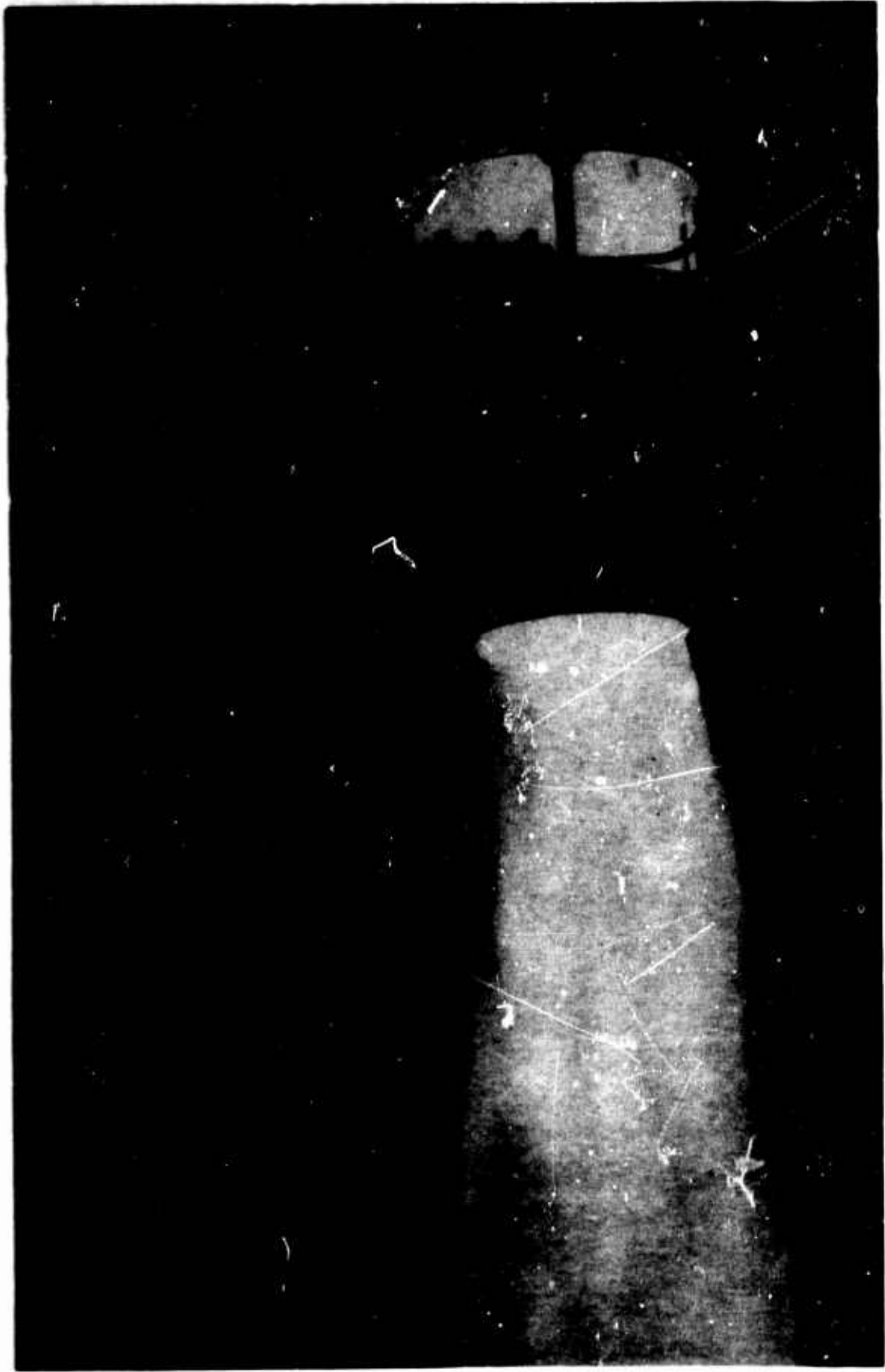
Figure 51. Transparent Chamber Firing

5AA25-6/6/66-S1 2*

144

both were associated with failures of the RCM system. Minor erosion of the uncooled copper baffle assembly resulted on test 003 following a two-second period of sustained instability. A similar failure on test 067 resulted in injector face erosion and subsequent loss of the triplet injector.

Control of the operational test conditions was usually quite satisfactory, although an occasional test exhibited an inordinately low (or high) chamber pressure (or mixture ratio). Pertinent data from each firing are listed in Table 11 . Average values of those parameters which appear in Table 11 as well as some other variables, are given in Table 12 for all firings with both injectors.

The characteristic velocity efficiency data were computed to evaluate the actual percent of theoretical performance achieved. Actual c* performance was calculated by the following equations:

$$c^* = \frac{(Pc)_{ns} A_t g}{\dot{w}_t} \tag{20}$$

where

$$(Pc)_{ns} = (Pc)_{inj} \frac{\left[1 + \frac{(\gamma-1)}{2} M_n^2\right]^{\gamma/\gamma-1}}{1 + \gamma M_n^2} \tag{21}$$

The injector-end chamber pressure, $(Pc)_{inj}$, was measured with a strain-gauge pressure transducer with the tap flush-mounted at the injector face. The c* calculation was based upon the nozzle inlet stagnation pressure $(Pc)_{ns}$ and assumed isentropic flow conditions within the nozzle. The following observations are made with reference to Tables 11 and 12.

The average chamber pressure for the 76 tests with N_2H_4-UDMH (50-50) fuel was 150.76 psia with both the triplet and doublet injectors. The c* efficiency for the triplet was 3 percent higher than with the doublet

145

TABLE 11

ENGINE OPERATIONAL PARAMETERS MEASURED
DURING STABLE COMBUSTION

Test Number	Injector Type	Injector End Chamber Pressure, psia	Mixture Ratio, o/f	Total Propellant Flowrate, lb/sec	Fuel Flowrate, lb/sec	Oxidizer Flowrate, lb/sec	Characteristic Velocity Efficiency, percent
001	Triplet	147	1.38	33.58	14.10	19.48	98.2
002		146	1.56	34.80	13.60	21.20	94.8
003		152	1.57	35.20	13.70	21.50	97.1
004		150	1.56	34.50	13.50	21.00	97.4
005		154	1.57	35.17	13.67	21.50	98.2
006		151					
007		158	1.54	35.47	13.97	21.50	99.7
008		154	1.66	35.41	13.31	22.10	97.3
009		158	1.64	37.76	14.31	23.45	93.8
010		160	1.78	37.24	15.39	23.85	96.2
011		157	1.58	37.11	14.39	22.72	94.8
012		154	1.56	35.77	13.97	21.80	96.7
013		150	1.57	34.61	13.43	21.18	97.4
014		151	1.58	34.99	13.59	21.40	97.2
015		154	1.51	35.18	14.00	21.18	98.4
016		150	1.68	35.98	13.43	22.55	93.8

146

TABLE 11

(Continued)

Test Number	Injector Type	Injector End Chamber Pressure, psia	Mixture Ratio, o/f	Total Propellant Flowrate, lb/sec	Fuel Flowrate, lb/sec	Oxidiser Flowrate, lb/sec	Characteristic Velocity Efficiency, percent
017	Triplet	154	1.57	33.79	13.14	20.65	
018		154	1.46	34.03	13.86	20.17	
019		150	1.40	34.23	14.26	19.97	98.5
020		146	1.47	34.40	13.97	20.43	95.8
021		154	1.48	34.67	13.97	20.70	99.7
022		150	1.50	34.53	13.83	20.70	97.8
023		148	1.51	34.72	13.82	20.90	95.9
024		138	1.31	33.32	13.98	18.34	93.1
025		151	1.50	34.52	13.82	20.70	98.5
026		151	1.51	34.72	13.82	20.90	97.8
027		146	1.51	34.72	13.82	20.90	94.7
028		150	1.60	35.59	13.69	21.90	94.8
029		150	1.58	34.60	13.40	21.20	97.7
030		150	1.50	34.51	13.81	20.70	97.8
031		150	1.61	33.88	12.98	20.90	99.2
032		149	1.60	34.80	13.40	21.40	96.4
033		149	1.58	34.60	13.40	21.20	96.9
034		149	1.60	34.43	13.25	21.18	97.5

TABLE 11
(Continued)

Test Number	Injector Type	Injector End Chamber Pressure, psia	Mixture Ratio, o/f	Total Propellant Flowrate, lb/sec	Fuel Flowrate, lb/sec	Oxidizer Flowrate, lb/sec	Characteristic Velocity Efficiency, percent
035	Triplet	150	1.56	34.32	13.40	20.92	98.4
036		150	1.57	35.44	13.82	21.62	95.3
037		150	1.58	34.83	13.53	21.40	96.8
038	Doublet	143	1.42	32.92	13.62	19.30	97.4
039		160	1.80	36.70	13.10	23.60	97.8
040		159	1.93	37.56	12.81	24.75	94.8
041		151	1.67	35.61	13.33	22.28	95.3
042		152	1.67	36.43	13.65	22.80	93.5
043		150	1.51	35.14	14.02	21.12	95.5
044		152	1.62	35.67	13.62	22.05	95.5
045		152	1.60	36.19	13.94	22.25	94.3
046		148	2.53	35.30	14.09	21.21	94.1
047		150	1.61	36.34	13.92	22.42	92.8
048		155	1.63	36.53	13.88	22.65	95.3
049		152	1.63	36.50	13.87	22.63	93.5
050		156	1.63	36.50	13.87	22.63	95.8
051		156	1.63	36.81	13.98	22.53	96.2
052		152	1.63	36.85	13.98	22.87	92.7

TABLE 11

(Continued)

Test Number	Injector Type	Injector End Chamber Pressure, psia	Mixture Ratio, o/f	Total Propellant Flowrate, lb/sec	Fuel Flowrate, lb/sec	Oxidizer Flowrate, lb/sec	Characteristic Velocity Efficiency, percent
053	Triplet	154	1.56	36.62	14.28	22.34	94.3
054		156	1.58	36.14	14.02	22 12	96.8
055		155	1.61	36.63	14.01	22.62	94 7
056	Doublet	130	1.52	36.23	13.98	21.25	
057		151	1.51	35.75	14.25	21.50	94.8
058		152	1.52	36.23	13.98	21.25	94.2
059		148	1.62	35.97	13.72	22.25	92.2
060		147	1.69	35.78	13.28	22.50	92.2
061		150	1.61	36.49	13.99	22.50	92.2
062		146[1]	1.54	34.78	13.70	21.08	94.0
063		147[1]	1.56	35.02	13.70	21.32	94.0
064		147[1]	1.56	35.02	15.70	21.32	94.0
065		152	1.54	35.45	13.97	21.48	95.8
066		149	1.55	35.36	13.88	21.48	94.7
067	Triplet	155	1.60	36.35	13.95	22.40	96.2
068	Doublet	149	1.51	34.98	13.91[2]	21.07	95.7
069		151	1.53	34.52	13.68[2]	20.84	98.2

[1]Calculated from an assumed c* efficiency.

[2]UDMH fuel

149

TABLE 11

(Concluded)

Test Number	Injector Type	Injector End Chamber Pressure, psia	Mixture Ratio, o/f	Total Propellant Flowrate lb/sec	Fuel Flowrate, lb/sec	Oxidizer Flowrate, lb/sec	Characteristic Velocity Efficiency, percent
070	Doublet	148	1.55	35.44	13.91[2]	21.53	93.7
071		147	1.50	34.58	13.83[2]	20.75	95.4
072		150	1.54	34.59	13.63[2]	20.96	97.3
073		147	1.52	35.11	13.91[2]	21.20	93.8
074		137	1.51	34.98	13.96[2]	21.02	87.8
075		135	1.34	35.72	13.96[2]	18.76	92.7
076		143	1.53	34.92	13.82[2]	21.10	91.7
077		144	1.50	34.82	13.96[2]	20.86	92.7
078[3]		146	1.50	34.98	13.98	21.00	93.8
079[3]		146	1.44	35.99	14.78	21.21	91.1
080[4]		149	1.48	34.50	13.90	20.60	96.7
081[4]		150	1.48	35.21	14.21	21.00	95.3
082[4]		148	1.65	35.48	13.38	22.10	93.7
083[4]		151	1.54	34.90	13.78	21.12	97.1
084[4]		147	1.50	34.89	13.97	20.92	94.3
085[4]		211	1.76	50.17	18.20	31.97	94.4
086[4]		266	1.88	62.50	21.75	40.75	95.4

[2]UDMH fuel
[3]Transparent hot-firing tests
[4]Demonstration hot-firing tests

150

TABLE 11

(Continued)

Test Number	Injector Type	Injector End Chamber Pressure, psia	Mixture Ratio, o/f	Total Propellant Flowrate, lb/sec	Fuel Flowrate, lb/sec	Oxidizer Flowrate, lb/sec	Characteristic Velocity Efficiency, percent
053	Triplet	154	1.56	36.62	14.28	22.34	94.3
054		156	1.58	36.14	14.02	22 12	96.8
055		155	1.61	36.63	14.01	22.62	94 7
056	Doublet	130	1.52	36.23	13.98	21.25	
057		151	1.51	35.75	14.25	21.50	94.8
058		152	1.52	36.23	13.98	21.25	94.2
059		148	1.62	35.97	13.72	22.25	92.2
060		147	1.69	35.78	13.28	22.50	92.2
061		150	1.61	36.49	13.99	22.50	92.2
062		146[1]	1.54	34.78	13.70	21.08	94.0
063		147[1]	1.56	35.02	13.70	21.32	94.0
064		147[1]	1.56	35.02	13.70	21.32	94.0
065		152	1.54	35.45	13.97	21.48	95.8
066		149	1.55	35.36	13.88	21.48	94.7
067	Triplet	155	1.60	36.35	13.95	22.40	95.2
068	Doublet	149	1.51	34.98	13.91[2]	21.07	95.7
069		151	1.53	34.52	13.68[2]	20.84	98.2

[1] Calculated from an assumed c* efficiency.

[2] UDMH fuel

149

TABLE 11
(Concluded)

Test Number	Injector Type	Injector End Chamber Pressure, psia	Mixture Ratio, o/f	Total Propellant Flowrate, lb/sec	Fuel Flowrate, lb/sec	Oxidizer Flowrate, lb/sec	Characteristic Velocity Efficiency, percent
070	Doublet	148	1.55	35.44	13.91[2]	21.53	93.7
071		147	1.50	34.58	13.83[2]	20.75	95.4
072		150	1.54	34.59	13.63[2]	20.96	97.3
073		147	1.52	35.11	13.91[2]	21.20	93.8
074		137	1.51	34.98	13.96[2]	21.02	87.8
075		135	1.34	35.72	13.96[2]	18.76	92.7
076		143	1.53	34.92	13.82[2]	21.10	91.7
077		144	1.50	34.82	13.96[2]	20.86	92.7
078[3]		146	1.50	34.98	13.98	21.00	93.8
079[3]		146	1.44	35.99	14.78	21.21	91.1
080[4]		149	1.48	34.50	13.90	20.60	96.7
081[4]		150	1.48	35.21	14.21	21.00	95.3
082[4]		148	1.65	35.48	13.38	22.10	93.7
083[4]		151	1.54	34.90	13.78	21.12	97.1
084[4]		147	1.50	34.89	13.97	20.92	94.3
085[4]		211	1.76	50.17	18.20	31.97	94.4
086[4]		266	1.88	62.50	21.75	40.75	95.4

[2] UDMH fuel
[3] Transparent hot-firing tests
[4] Demonstration hot-firing tests

TABLE 12

AVERAGE VALUES OF OPERATIONAL PARAMETERS

	Injector Type		
	Triplet	Doublet	
Injection Performance			
Fuel	50-50	50-50	UDMH
Injector End P_c, psia	150.76	150.76	145.10
Characteristic Velocity, ft/sec	5,466	5,295	5,258
Characteristic Velocity Efficiency, percent	97.6 [1]	94.6 [1]	95.6 [2]
Mixture Ratio, o/f	1.54	1.59	1.50
Injection Parameters			
Number Oxidizer Orifices	180	420	420
Number Fuel Orifices	348	420	420
Oxidizer Injector Area, sq in.	0.6519	0.5877	0.5877
Fuel Injector Area, sq in.	0.4661	0.4872	0.4872
Oxidizer Flowrate, lbm/sec	21.09	22.07	20.81
Fuel Flowrate, lbm/sec	13.66	13.80	13.86
Oxidizer Injector Pressure Drop, psi	77.1	102.4	95.4
Fuel Injector Pressure Drop, psi	50.5	49.9	56.7
Oxidizer Discharge Coefficient	0.578	0.584	0.558
Fuel Discharge Coefficient	0.820	0.798	0.803
Oxidizer Injection Velocity, ft/sec	51.3	59.5	56.2
Fuel Injection Velocity, ft/sec	74.3	72.1	83.3

(1) Based upon 5604 ft/sec frozen theoretical characteristic velocity at nozzle inlet stagnation conditions.
(2) Based upon 5500 ft/sec frozen theoretical characteristic velocity at nozzle inlet stagnation conditions.

injector. A slightly higher efficiency was obtained with UDMH fuel than with N_2H_4-UDMH (50-50) fuel. The oxidizer-side injector pressure drop was 25 psi higher with the doublet due to the smaller total orifice injector area.

Stability Results

A total of 148 disturbances by the rating techniques were introduced into the combustion chamber during the 86 hot-firing tests. Three or four disturbances were scheduled to occur within the mainstage portion of each test; if one of the earlier disturbances initiated a sustained instability, the test was usually terminated by the RCM device before the next disturbance was sequenced to occur. Because the nondirectional explosive bombs were susceptible to thermal initiation during their exposure to the high-temperature combustion chamber environment and also because they were likely to be broken or dislodged by even a few cycles of transverse pressure wave motion, only one bomb was installed for a firing and it was always the first sequenced of the rating devices. The directed gas flow rating technique was intended to be used as a standard pulse, with a fixed position of application to the chamber, for establishing both long-term consistency of the combustor's stability and reproducibility. This disturbance was therefore almost invariably sequenced as the last one, with the anticipation of obtaining a rating whenever the combustion process had recovered from all of the earlier disturbances.

Explosive Bombs. A total of 56 bombs all from the high-explosive series, was installed in the combustor. The hot-firing tests which had bombs, the bomb parameters, and their locations in the combustion chamber are presented in Table 13. Also tabulated are the values of the initial disturbance peak pressures recorded from the speed-reduced oscillographs. All except three bombs are believed to have produced valid perturbations.

152

TABLE 13

HIGH-EXPLOSIVE BOMBS USED DURING THE HOT-FIRING

Test No.	Injector Type	Fuel	Bomb Design Parameters			Chamber Locations	
			Charge Weight, grains	Charge L/D Ratio	Case Thickness, inches	Radius, inches	Distance From Injector, inches
002	Triplet	50-50	13.5	2.7	0.170	4.95	2.96
003			5.5	1.3		4.95	3.12
004			5.5	1.3		0	3.12
005			5.5	1.3		0	3.12
006			50	4.0		0	3.85
007			13.5	2.7		4.95	2.15
011			13.5	2.7		4.95	5.67
014			13.5	2.7		2.85	4.48
015			25	4.5		2.85	3.23
016			13.5	2.7		2.85	3.23
017			5.5	1.3		2.85	3.33
018			5.5	1.3		2.85	4.58
019			13.5	2.7		0	3.79
021			5.5	1.3		0	4.6
022			13.5	2.7		0	4.55
023			5.5	1.3		4.95	5.77
025			25	4.5		2.85	5.67
027			5.5	1.3		3.97	4.00
030			5.5	1.3		3.97	4.00
031			3.2	1.0		4.95	3.53
032			3.2	1.0		2.85	3.33
039	Doublet		13.5	2.7	0.280	4.95	3.23
040			13.5	2.7	0.170	4.95	3.23
041			3.2	1.0	0.170	4.95	3.33
042			13.5	2.7	0.280	2.85	3.23
043			13.5	2.7	0.170	2.85	3.23

A

HOT-FIRING PROGRAM

Locations Distance From Injector, inches	Photocon Transducer Initial Pressure, psi							Stability Results	
	A	B	C	F	G	H	I	Modes(1)	Damptime,ms
2.96	154	130	178					2T	11
3.12	83	254	156					2T, 1T-2T, 3T-1R	RCM(2)
3.12								Stable	
3.12								Stable	
3.85								Stable	
2.15	196	187	233					2T, 1T-2T, 1T-3T, 3T-1R	RCM
5.67	159	92	160					2T, 3T-1R	RCM
4.48	170	162	204	200				1T-2T, 2T	5
3.23	239	238	255	280				1T-2T, 1T, 1T-3T, 3T-1R	RCM
3.23	239	234	263	260				1T-2T, 1T-3T, 3T-1R	RCM
3.33	62	81	140	88				1T, 1T-3T, 3T-1R	RCM
4.58	42	43	66	66				1T-2T, 1T-3T, 3T-1R	RCM
3.79	218	220	260	207				1R, 3T-1R	RCM
4.65	43	42	40	41				Stable	
4.55	178	190	140	159				1R, 3T-1R	RCM
5.77	38	39	63	70				1T-2T, 1T, 1T-3T, 3T-1R	RCM
5.67	140	131	178	206				2T, 1T, 1T-3T, 3T-1R	RCM
4.00	130	167	92					UNK, 3T-1R	RCM
4.00	81	63	156	198				UNK, 3T-1R	RCM
3.33	70	70	147	228				2T-1T, 3T-1R	RCM
3.33	74	70	106	94				1T, 1T-3T, 3T-1R	RCM
3.23	207	183	227	305				2T-1T, 1T-3T, 3T	38
3.23	234	189	250	352				2T, 1T, 1T-3T	10
3.33	103	78	194	207				2T-1T, 1T	8
3.23	360	305	382	362				3T, 1T, 1T-3T	14
3.23	295	244	310					3T, 2T-1T, 1T-3T	18

B

TABLE 13

(Continued)

Test No.	Injector Type	Fuel	Bomb Design Parameters			Chamber Locations		P
			Charge Weight, grains	Charge L/D Ratio	Case Thickness, inches	Radius, inches	Distance From Injector, inches	A
044	Doublet	50-50	13.5	2.7	0.280	2.85	3.23	225
045			13.5	2.7	0.170	3.97	4.00	281
046			13.5	2.7	0.170	4.95	5.67	107
047			5.5	1.3	0.170	4.95	5.77	81
048			13.5	2.7	0.170	0	3.79	317
049			13.5	2.7	0.170	4.95	3.23	
050			5.5	1.3	0.170	4.95	3.33	144
051			5.5	1.3	0.170	4.22	4.00	258
052			13.5	2.7	0.170	2.85	4.55	208
053			5.5	1.3	0.170	2.85	3.33	155
054			5.5	1.3	0.170	2.85	5.77	65
055			5.5	1.3	0.280	4.95	3.33	70
060			3.2	1.0	0.170	0	3.33	188
061			13.5	2.7	0.500	4.95	3.23	100
063			13.5	1.0	0.170	4.95	3.40	165
064			13.5	2.7	0.110	3.62	10.2	245
065			13.5	1.0	0.170	2.85	3.40	230
067	Triplet		13.5	2.7	0.110	3.62	10.2	220
068	Doublet	UDMH	13.5	2.7	0.170	4.95	3.23	160
069			13.5	2.7	0.170	0	3.23	304
073			13.5	2.7	0.170	0	3.23	271
075			5.5	1.3	0.170	4.95	3.12	83
077			3.2	1.0	0.170	4.95	3.33	
079		50-50	13.5	2.7	0.110	3.62	10.2	
080			13.5	2.7	0.062	4.95	3.23	200

4

Photocon Transducer Initial Pressure, psi							Stability Results	
A	B	C	F	G	H	I	Modes	Damptime, ms
'25	234	285	272				1T-2T, 1T-3T, 1T, 1T-3T, 3T	33
81	282	219	–				1T, 2T	26
)7	119	165	154				1T-3T, 1T	6
81	69	–	182				1T-2T, 1T, 1T-3T, 3T-1R	RCM
17	260	270	180				1R, 3T-1R	RCM
	192	265	337				2T-6T, 1T, 1T-3T	28
44	131	214					2T-6T, 3T	21
58	308	180					2T-6T, 2T	6
208	196	227					1T	4
55	1 51	273					2T, 1T, 1T-3T, 3T-1R	18
65	75	118					2T, 1T-3T, 3T-1R	RCM
70	85	189					2T-6T, 1T	8
88	217	139	122	68			1R, 3T	RCM
00	195	188	260	133			1T	6
65	197	232	260	125			1T, 1T-3T, 3T-1R	RCM
45	392	220	183				1T, 1T-3T	16
'30	–	240	264				1T, 1T-3T, 3T	20
20	338	144	141				UNK, 3T-1R	RCM
60	208	240	305				2T, 1T, 1T-3T, 3T-1R	RCM
504	287	268	2				1R, 3T-1R	RCM
71	235	26					1R, 2T	RCM
83	92	168					1T-2T, 2T	RCM
	75	136	120				1T-2T, 2T	RCM
				122			1T	22
00	263	280	310			208	1T, 3T	17

154

β

TABLE 13

(Concluded)

Test No.	Injector Type	Fuel	Bomb Design Parameters			Chamber Locations	
			Charge Weight, grains	Charge L/D Ratio	Case Thickness, inches	Radius inches	Distance From Injector, inches
081	Doublet	50-50	13.5	2.7	0.170	4.95	2.55
082			6.9		0.170	4.95	3.33
083			13.5	2.7	0.250	0	3.23
085			13.5	2.7	0.170	4.95	3.23
086			13.5	2.7	0.170	4.95	3.23

[1] T represents a tangential mode

R represents a radial mode

T-R represents coexistent modes

[2] RCM represents premature cutoff due to sustained instabilities

A

tions								Stability Results	
stance From jector, nches	Photocon Transducer Initial Pressure, psi								
	A	B	C	F	G	H	I	Modes	Damptime, ms
2.55	215	245	260	308		254	225	1T-2T,3T-1R	RCM
3.33	137	189	231	223		138	118	1T-2T,1T,3T-1R	RCM
3.23	300	320	315	271		268	344	1R,3T-1R	RCM
3.23	205		295			248	243	1T-2T,3T-1R	22
3.23	213		288			303	265	2T,3T-1R	14

𝐵

The first three bombs installed at the center of the chamber (during Tests No. 004, 005, and 006) were subsequently determined not to have fired within the time increment from bomb fire-signal to the first pulse gun firing. The insulation was presumably melted from the electrical lead wires where they passed under open bomb-installation ports in the baffle assembly so that the bomb-fire signal was shorted; the later practice of putting a blind plug in any of those ports which had lead wires under them eliminated that problem. The bombs in Tests No. 042 and 051 detonated thermally after the nylon case broke loose and slipped off the 13.5-grain blasting cap. The data from these two tests were treated as though the bomb case consisted of zero thickness.

Pressure records from combustion chamber Photocons were examined to determine the combustor's stability response for each perturbation. A typical pressure record is reproduced in Fig. 52 , where it is seen that the stability response may be quite complex. In this case, the initial disturbance triggered a moderately high-amplitude, second tangential acoustic instability. At the same time, however, the propellant sprays which had been burning with a steady-state distribution in the combustion chamber were burned at a much higher than average rate. As a result, the mean chamber pressure was momentarily substantially higher than average. As a further result, the propellant injection rate must have been drastically reduced. The initial second tangential mode found little sustaining energy, and, as the chamber pressure decayed below normal, it was attenuated. Resumption of propellant injection apparently re-established a propellant spray field better able to sustain a first tangential acoustic mode since that mode was seen to arise out of the depth of the chamber pressure's lowest level. After about 5 milliseconds, that mode was replaced by a pair of coexistent acoustic modes: the third tangential (baffle compartment mode) and the first radial. This combination was then sustained to engine cutoff.

156
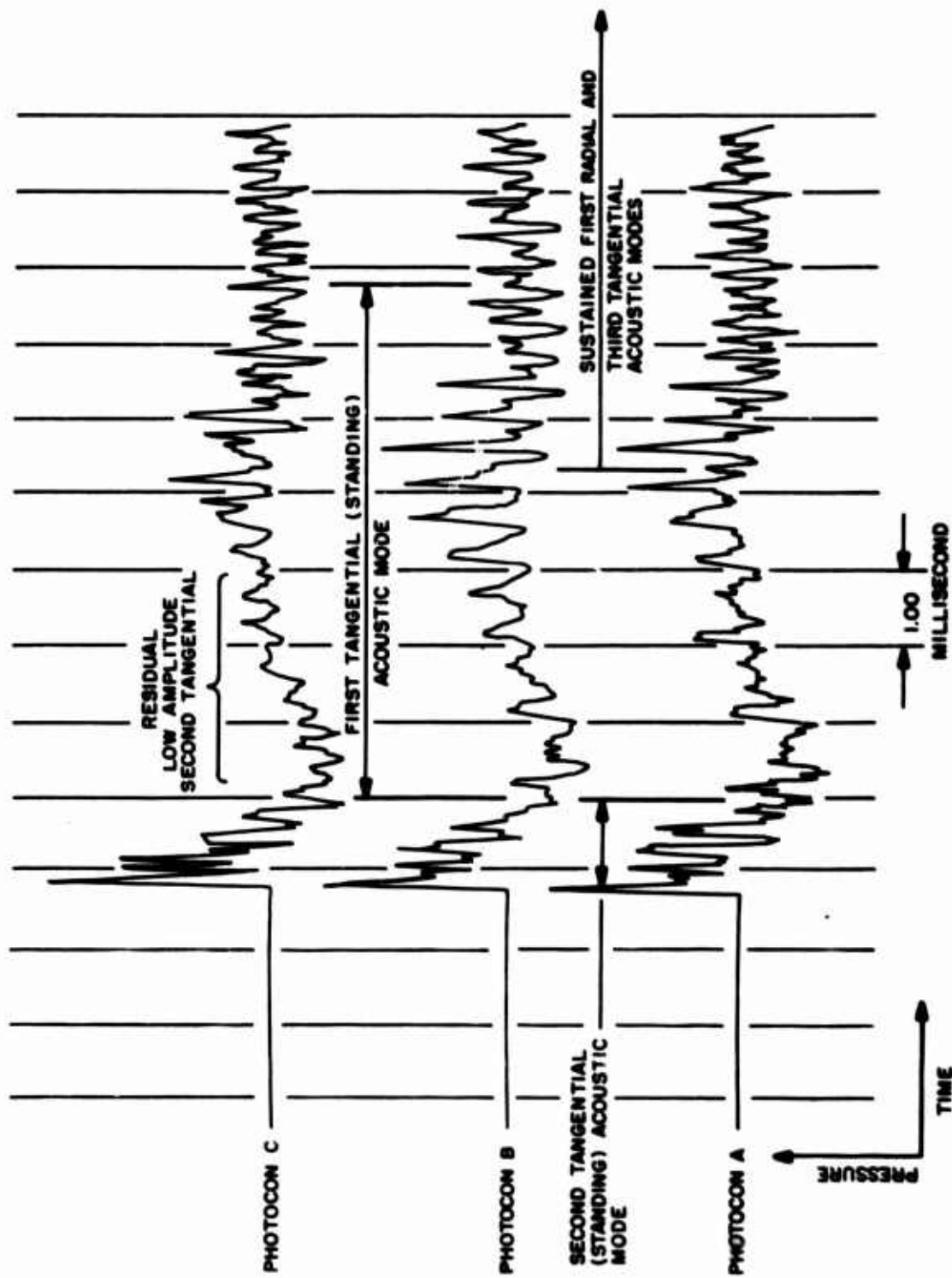
Figure 52. Typical Pressure Record Showing Some
Instability Modal Interrelationships
(Refer to Fig. 45 for transducer locations)

157

The combustor's stability behavior in response to the bombs is summarized
in bar-chart form for the triplet injector in Fig. 53 and the doublet
injector in Fig. 54 . In addition to changes in bomb charge weight and
chamber locations, parametric changes in case material, L/D ratio, wall
thickness and fuel type were made with the doublet injector.

Along the abscissa of these charts are listed increasing values of axial
distance from the injector face to the center of the bomb's explosive
charge for three different values of radial distance from the center of
the chamber to the bomb's cylindrical axis. (Four bombs which were
inserted into the chamber through Photocon ports, Tests No. 027, 030, 045,
and 051, and two bombs inserted near the nozzle, Tests No. 064 and 067
also shown.) The vertical height of each bar represents the explosive
charge weight and the test number appears above the bar.

Stability information, as determined by frequency and phase analysis of
the chamber pressure records, is presented within each bar. The mode
(or modes) of acoustic instability initiated immediately by the bomb is
denoted by the kind of cross-hatching in the bottom 0.2-inch of the bar.
Immediately above that is an indication of whether some other mode replaced
that initially triggered mode. Finally, above that is an indication of
whether an instability was sustained until RCM cutoff (by continued cross-
hatching to the top of the bar) or recovery to stable combustion was
experienced. The height of a particular cross-hatched bar-segment is not
quantitatively related to time. The time required for the combustion
process to recovery to stable operation is tabulated along the abscissa
where applicable.

Pulse Guns. A total of 81 pulse gun charges were fired during the experi-
mental test program. The hot-firing tests in which pulse guns were fired,
the pulse gun charge parameters, the position and direction of blast-wave
entry into the chamber and the initial peak pressures recorded at several
Photocons are presented in Table 14 . All but five of the charges were

158
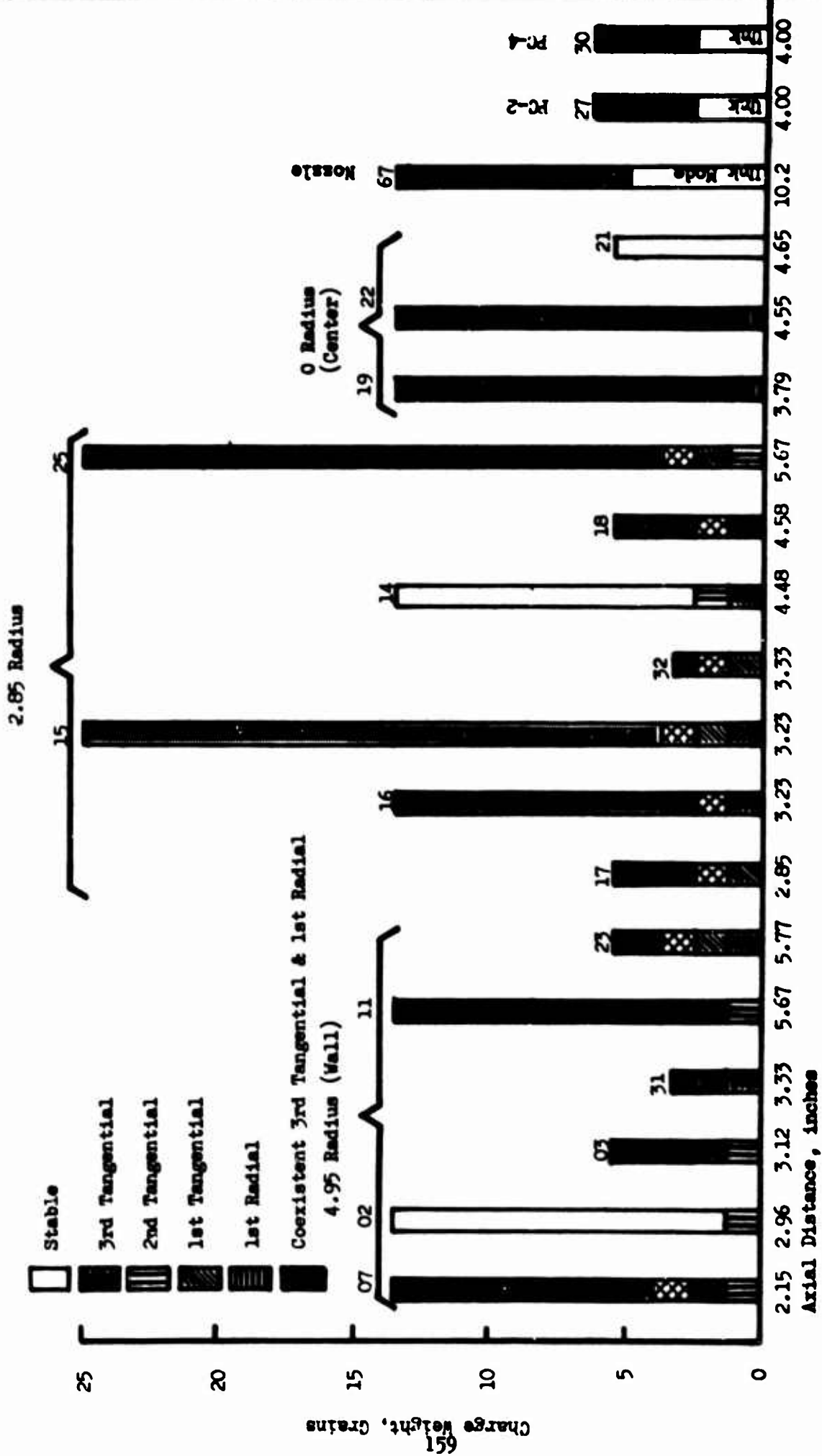
Figure 53. Summary of Hot-Firing Stability Response: Explosive Bombs With Triplet Injector and N_2H_4-UDMH(50-50) Fuel
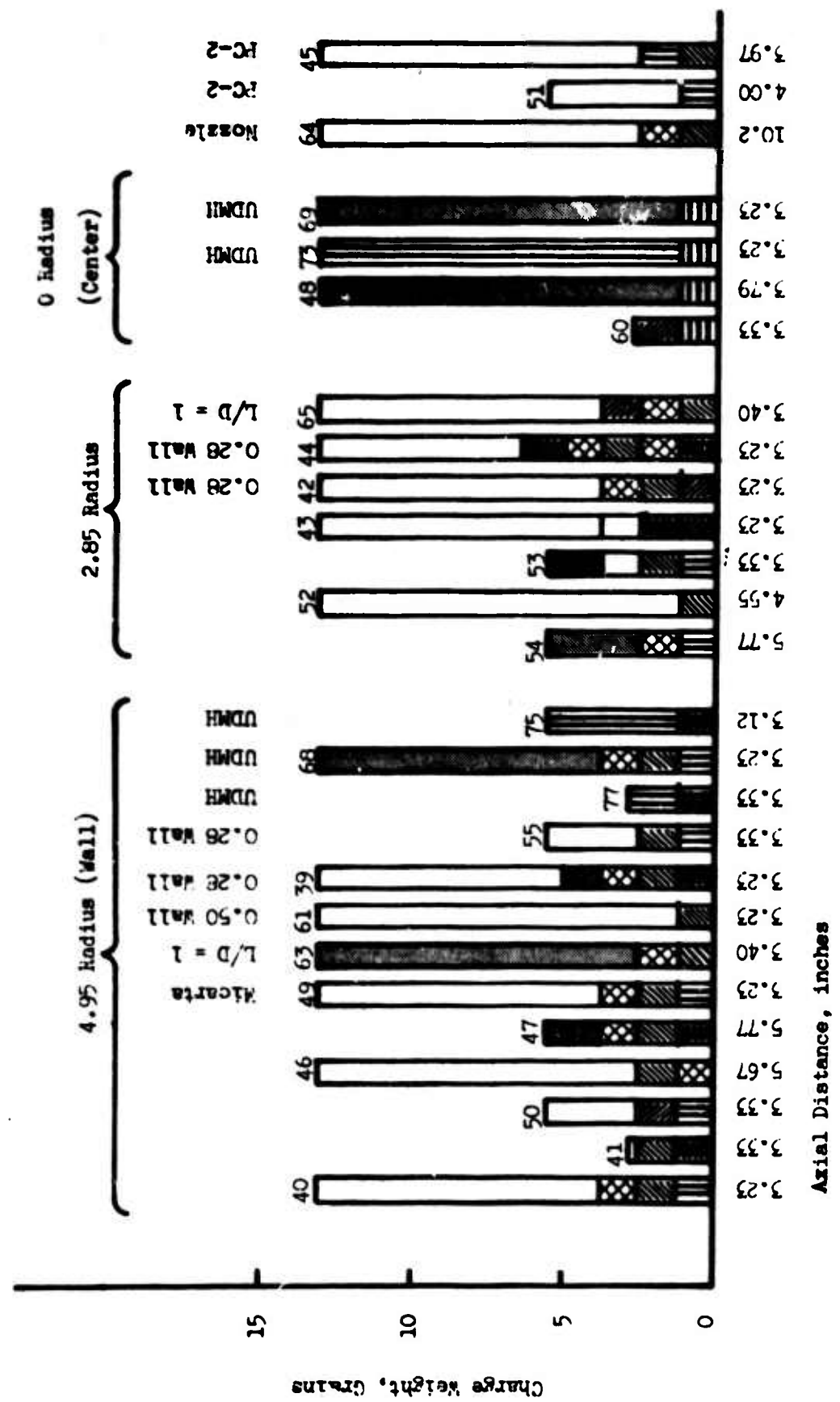
Figure 54. Summary of Hot-Firing Stability Response; Explosive Bombs With Doublet Injector Except as Noted

TABLE 14

PULSE GUNS USED DURING THE HOT-FIRING PROGRAM

Test No.	Injector Type	Fuel	Charge[1] Designation	Boss No.	Direction,[2] degrees	Port Diameter inches	Distance From Injector, inches	Pho Init
003	Triplet	50-50	15HB/10K	1	180	0.515	2.00	
004			40HB/20K	1	180		2.00	1
005			40HB/20K	7	90		2.00	2
006			10HB/7.5K	7	90		2.00	
008			80HB/20K	7	90		2.00	
009[3]			10HB/7.5K	9	90		4.00	
009[3]			30HB/20K	7	90		2.00	
010			15HB/10K	9	90		4.00	
012			10HB/7.5K	8	90		3.00	
012			40HB/20K	7	90		2.00	
013			10HB/7.5K	8	90		3.00	
014			10HB/7.5K	9	90		4.00	
020			40HB/20K	1	180		2.00	
020			40HB/20K	4	135		2.00	
021			10HB/7.5K	1	180		2.00	
022			10HB/7.5K	4	135		2.00	
022			15HB/10K	1	180		2.00	
024			10HB/7.5K	3	180		4.00	
024			20HB/20K	1	180		2.00	
026			10duPN/7.5K					
026			10duPN/7.5K					
028			40HB/20K	4	135		2.00	
028			10HB/7.5K	6	135		4.00	
029			20duPN/20K	4	135		2.00	
029			10HB/7.5K	2	180		3.00	
033			15HB/10K	2	180		3.00	
034			10HB/7.5K	4	135		2.00	
035			15HB/10K	4	135		2.00	

4

NG THE HOT-FIRING PROGRAM

Chamber Inlet Description			Photocon Transducer Initial Pressure psi				Stability Results	
Direction,[2] degrees	Port Diameter inches	Distance From Injector, inches	A	B	C	F	Modes[5]	Damp Time, ms
180	0.515	2.00					Already Unstable	
180		2.00	142	170	242		1T-3T, 1T	7
90		2.00	258	158	78		1T	7
90		2.00	158	52	47		1T, 1T-3T, 3T-1R	RCM
90		2.00	258	240	90		1T, 3T-1R	RCM
90		4.00					1T	6
90		2.00					2T, 1T-2T, 1T-3T, 3T-1R	RCM
90		4.00	240	168	60		1T-3T, 3T-1R	RCM
90		3.00	20	17	17		2T	2
90		2.00	252	223	178		1T, 3T-1R	RCM
90		3.00	116	160	238	80	1T-3T, 3T-1R	RCM
90		4.00	196	178	40	62	1T, 3T-1R	RCM
180		2.00	112	166	178	70	1T-3T, 1T	2
135		2.00	218	182	100	258	1T-3T, 1T	4
180		2.00	88		176	60	1T-3T, 3T-1R	RCM
135		2.00					Already Unstable	
180		2.00	86	132	197	98	1T-3T, 3T-1R	235
180		4.00	10	10	10	10	Stable	
180		2.00	48	148	118	98	1T	2
135		2.00	208	130	97	250	1T	3
135		4.00	10	10	10	10	Stable	
135		2.00					Stable	
180		3.00	38	35	28	22	1T	2
180		3.00	355	254		121	1T-3T, 3T-1R	RCM
135		2.00	155	95	70	240	1T-3T, 3T-1R	RCM
135		2.00	130	108	80	205	1T-3T, 3T-1R	RCM

161

B

TABLE 14

(Continued)

Test No.	Injector Type	Fuel	Charge (1) Designation	Boss No.	Chamber Inlet Description			A
					Direction (2) degrees	Port Diameter inches	Distance From Injector, inches	
036	Triplet	50-50	20HB/20K	4	135	0.515	2.00	168
036			20HB/20K	2	180		3.00	300
037			15HB/10K	3	180		4.00	10
039	Doublet		10HB/7.5K	9	90		4.00	352
039			10HB/7.5K	8	90		3.00	140
040			40HB/20K	7	90		2.00	360
040			10HB/7.5K	1	180		2.00	82
041			20HB/20K	7	90		2.00	400
041			20HB/20K	1	180		2.00	250
042			40HB/20K	1	180		2.00	256
042			40HB/20K	4	135		2.00	190
043			40HB/20K	7	90	0.370	2.00	360
043			20HB/20K	4	135	0.515	2.00	155
044			40HB/20K	7	90	0.430	2.00	366
044			10HB/7.5K	4	135	0.515	2.00	133
045			10HB/7.5K	7	90	0.370	2.00	318
045			10HB/7.5K	6	135	0.515	4.00	90
045			10HB/7.5K	3	180		4.00	32
046			40HB/20K	3	180		4.00	192
046			10HB/7.5K	7	90		2.00	322
049			15HB/10K	3	180		4.00	40
049			40HB/20K	9	90		4.00	358
050			20HB/20K	3	180		4.00	152
050			20HB/20K	9	90		4.00	362
051			40HB/20K	6	135		4.00	46
051			15HB/10K	1	180		2.00	170 (A)
052			15HB/10K	6	135		4.00	152
052			15HB/10K	4	135		2.00	

A

Chamber Inlet Description							Stability Results	
tion (2) rees	Port Diameter inches	Distance From Injector, inches	A	B	C	F	Modes	Damptime, ms
35	0.515	2.00	168	72	75		1T-3T, 1T	10
80		3.00	300	272	135	160	1T, 3T-1R	RCM
0		4.00	10	10	10	10	1T	2
90		4.00	352	225	100	60(4)	1T	7
90		3.00	140	146	282	82	1T	6
90		2.00	360	265	154	208	1T, 1T-3T, 1T, 1T-3T, 1T	28
80		2.00	82	85	190	52	1T-3T, 1T	7
90		2.00	400	252	122	185	2T, 2T-1T	18
180		2.00	250	220	312	194	2T, 2T-1T	5
180		2.00	256	212(4)	280	203	1T	7
135		2.00	190	168	200	372	1T	6
90	0.370	2.00	360	262	132	292(4)	1T	30
135	0.515	2.00	155	180	191	315(4)	1T	7
90	0.430	2.00	366	238	138	190	1T	20
135	0.515	2.00	133	152	150	272	1T, 3T-1R	RCM
90	0.370	2.00	318	210	78		1T	9
135	0.515	4.00	90	70	58		1T, 3T	20
180		4.00	32	25	40		Stable	
180		4.00	192	186	291	127	1T	7
90		2.00	322	231	100	93	1T	8
180		4.00	40	70	78	30(4)	Stable	
90		4.00	358	302	116		1T-2T, 1T, 1T-3T, 3T-1R	RCM
180		4.00	152	208	365		1T-2T	6
90		4.00	362	255	121		1T, 1T-6T, 1T, 3T-1R	RCM
135		4.00	46	44	88		1T, 1T-3T, 1T, 1T-3T, 3T	17
180		2.00	170(4)	155	130		1T	6
135		4.00	152	136	158		1T	5
135		2.00		170	128		1T	7

B

TABLE 14

(Concluded)

Test No.	Injector Type	Fuel (hydrazine/UDMH)	Charge(1) Designation	Chamber Inlet Description			
				Boss No.	Direction,(2) degrees	Port Diameter inches	Distance From Injector, inches
052	Doublet	50-50	15HB/10K	9	90	0.515	4.00
053			15HB/10K	7	90		2.00
055			20HB/20K	6	135		4.00
055			10HB/7.5K	5	135		3.00
056			40HB/10K	7	90		2.00
057			10HB/10K	7	90		2.00
058			20HB/10K	7	90		2.00
059			20duPM/20K	1	180		2.00
061			40duPM/20K	1	180		2.00
062			20duPM/20K	7	90		2.00
062			80duPM/20K	1	180		2.00
064			80duPM/20K	7	90		2.00
065			40duPM/20K	7	90		2.00
070		UDMH	40HB/20K	9	90		4.00
070			40HB/20K	7	90		2.00
070			10HB/7.5K	4	135		2.00
071			15HB/10K	7	90		2.00
072			20HB/20K	9	90		4.00
076			15HB/10K	1	180		2.00
079		50-50	15HB/10K	(1)	180		2.37
080			40HB/20K	5	135		3.00
084			40HB/20K	8	90		3.00
084			40HB/7.5K	5	135		3.00
085			15HB/10K	7	90		2.00
086	↓	↓	15HB/10K	7	90	↓	2.00

(1) The charge designation includes first the charge weight in grains, next the explosive ty[duPont Military) and finally, the burst diaphragm pressure rating in 1000 psi.

(2) Directions of 90, 135, and 180 degrees are referred to elsewhere in this report as tangen respectively.

(3) The gaseous nitrogen flow was admitted to the chamber first during Test 009 and had not b were fired.

(4) Photocon transducer struck by bomb case fragment from previous pulse.

A

Inlet Description		Photocon Transducer Initial Pressure psia						Stability Results	
Port Diameter inches	Distance From Injector, inches	A	B	C	F	H	I	Modes	Damptime, ms
0.515	4.00	372	252	112				1T	7
	2.00	338	250	118				2T,1T,1T-3T,3T-1R	RCM
	4.00	135	97	50				1T,1T-3T,1T,1T-3T,3T	25
	3.00	128	130	70				2T,1T-3T,3T	16
	2.00	390	241	118	118			2T,1T,1T-3T,3T-1R	RCM
	2.00	371	248	106	117			2T,1T,1T-3T,3T-1R	RCM
	2.00	382	238	104	118			1T,1T-3T,3T-1R	RCM
	2.00	140	140	340	120			1T-2T	2
	2.00	90	141	258	88			1T-2T	4
	2.00	322	238		135			1T,1T-3T,3T	34
	2.00	249	249	298	255			1T-3T,1T,3T	14
	2.00	323	268	149	155			1T,1T-3T,3T	23
	2.00	338	267	122	160			1T,1T-3T,3T-1R	RCM
	4.00	365	272	98	222			1T	9
	2.00	318	210	92	128			1T	8
	2.00	15	8	8	6			Stable	
	2.00	292	122	85	118			1T-2T,2T	RCM
	4.00	293	156	90	173			1T-2T	RCM
	2.00	115	82	230	86			1T-2T,2T	RCM
	2.37							UNK	14
	3.00							1T-2T,3T	19
	3.00	253	302	312		217	388	1T	15
	3.00	177	162	150		212	167	1T,3T-1R	23
	2.00	362		170		448	422	1T-2T,1T,3T	14
	2.00	342		138		442	448	1T,3T-1R	63

ns, next the explosive type (HB = Hercules Bullseye No. 2,
ng in 1000 psi.
e in this report as tangential, chordal, and radial,

ing Test 009 and had not been turned off when the pulse guns

pulse.

β

believed to have given valid combustor perturbations. Two of those
(during Tests No. 007 and 022) were fired during previously existing
bomb-initiated instabilities. Three pulse charges made up of duPont
Military powder instead of Hercules Bullseye No. 2 were inadvertently
fired in Tests No. 026 and 029. The 10duPM/7.5K charges failed to burst
their diaphragms. The first 31 charges (including all five of those just
commented upon) were used during hot firings of the triplet injector and
the remaining were with the mixed doublet injector. The combustor's sta-
bility behavior in response to the pulse guns is summarized in bar-chart
form in Fig. 55, 56, and 57. Figure 55 presents the data obtained with
the triplet injector and N_2H_4-UDMH (50-50) fuel. As can be ascertained
by referring to Table 14, only "standard" charge weight/diaphragm strength
combinations of Hercules Bullseye powder are represented there. Figure 56
contains those data from the doublet injector firings which are directly
comparable with the triplet data. Then the other data from the doublet
injector firings (in which variations were made in the pulse gun param-
eters powder burning rate, charge weight/diaphragm strength combination
and barrel port diameter and in the propellant combination) are given in
Fig. 57. The stability information on these charts is presented in the
same manner as that for bombs in Fig. 53 and 54 except that the pulse guns
were directed in three angular directions whereas the bombs were located
at three radial positions.

Directed Gas Flows. Directed flows of gaseous nitrogen and helium failed
to initiate any chamber pressure oscillations during 11 tests. The test
numbers, positions and directions of admission into the chamber and data
on the gas species used and the gaseous flowrate are presented in Table 15.

The maximum flowrate achieved with gaseous nitrogen was 8.08 lb/sec
which corresponded to a linear ramp slope of 300 lb/sec^2. The maximum
helium flowrate was 2.24 lb/sec. Typical ramp profiles are shown in
Fig. 58. All gaseous flows were introduced into the combustion chamber
at an axial distance of 2 inches from the injector face. One test with
the doublet injector utilized a 0.370-diameter port connecting tube; all
others were with a 0.515-inch diameter port.
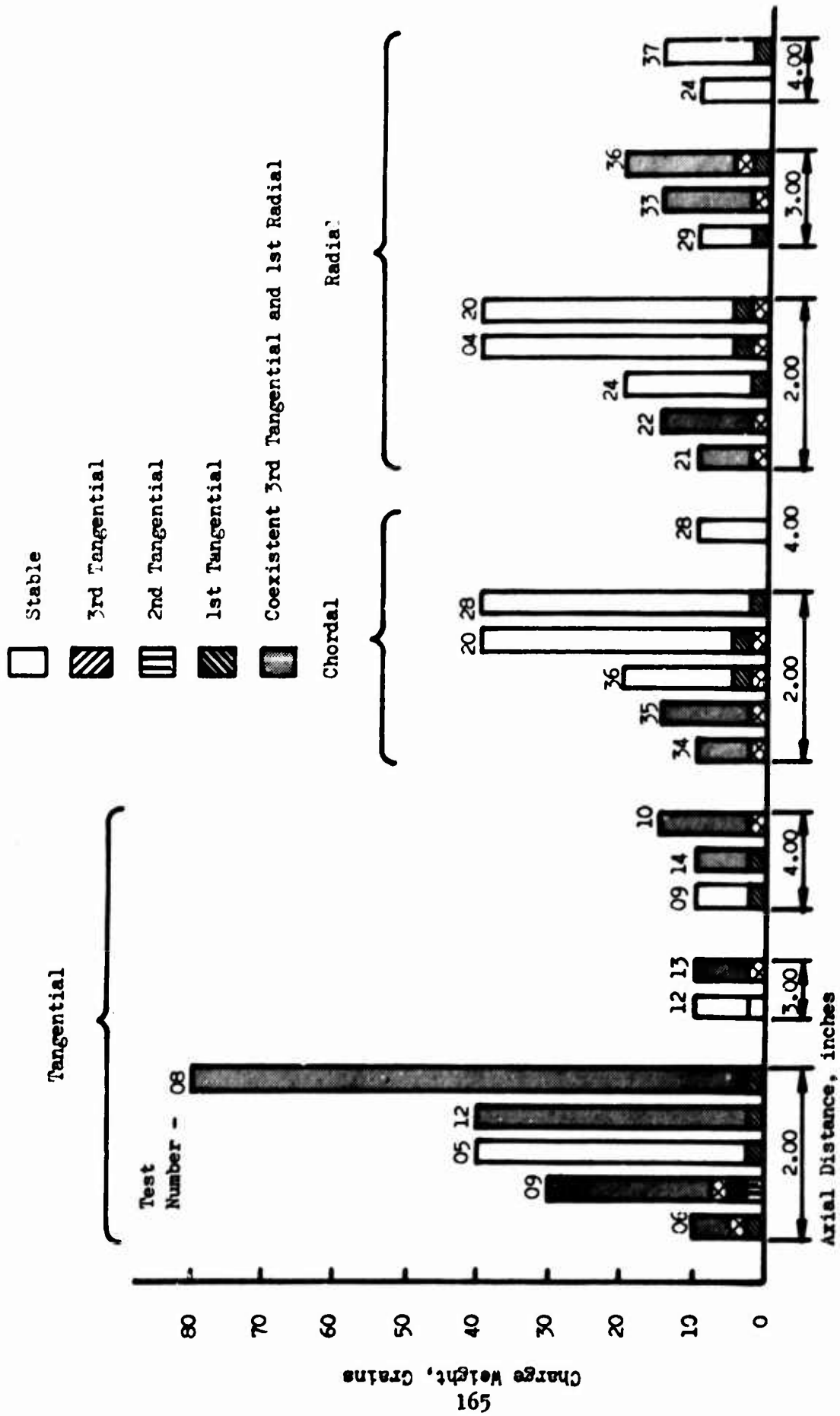
Figure 55. Summary of Hot-Firing Stability Response; Pulse Guns With Triplet Injector and N_2H_4/UDMH (50-50) Fuel
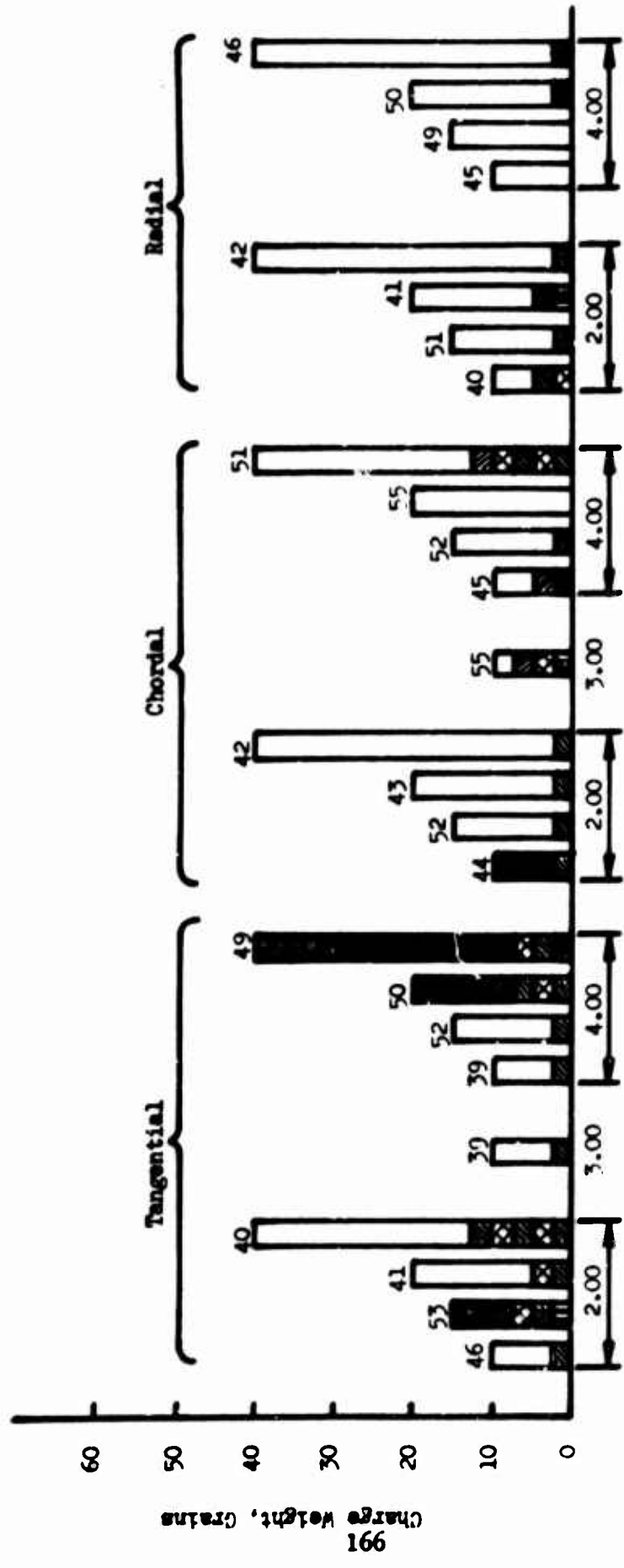
Figure 56. Summary of Hot-Firing Stability Response: Selected Pulse Guns With Doublet Injector and N_2H_4/UDMH(50-50) Fuel

166
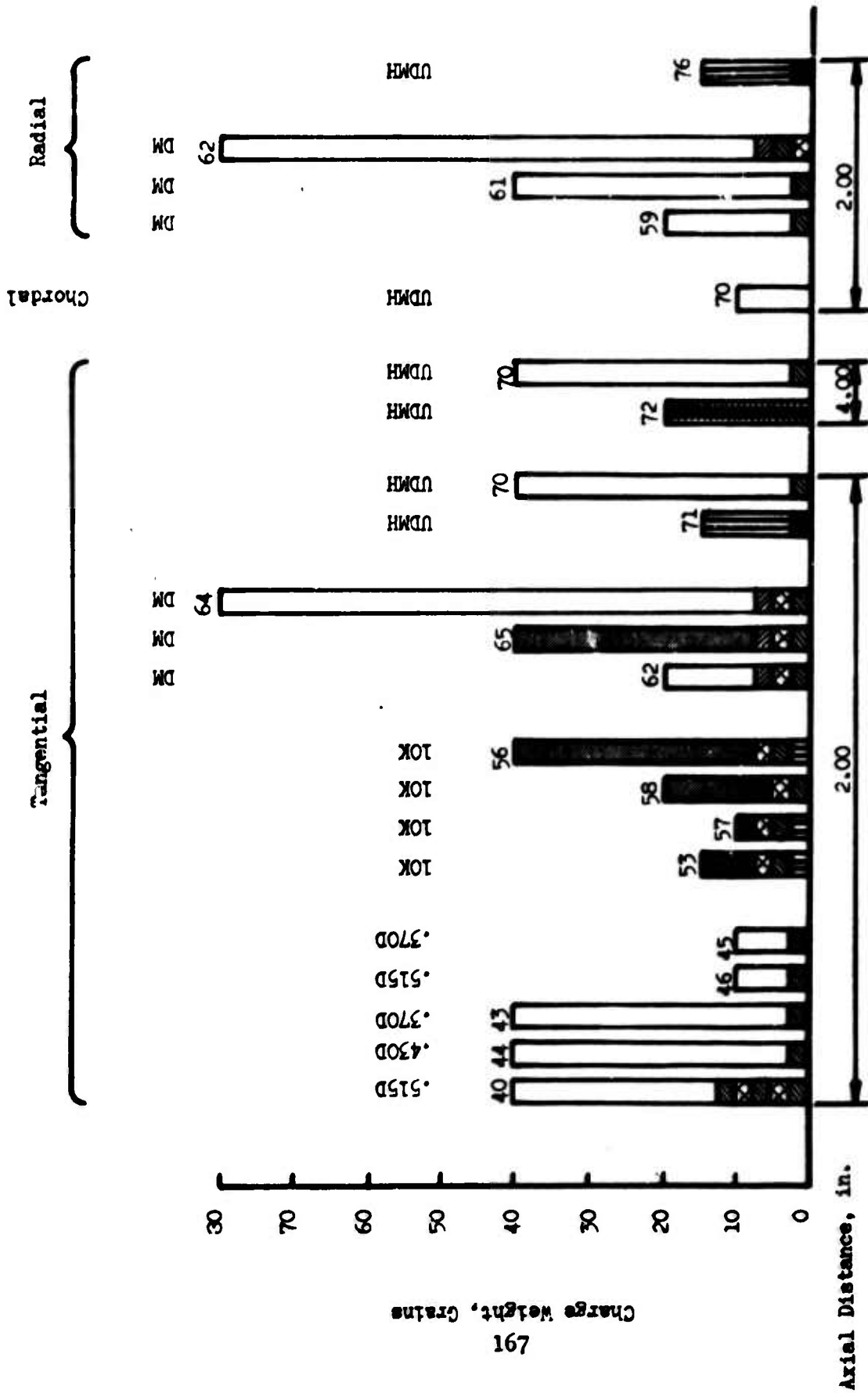
Figure 57. Summary of Hot-Firing Stability Response: Remaining Pulse Guns With Doublet Injector and N_2H_4/UDMH(50-50) Fuel Except as Noted

167

TABLE 15

DIRECTED FLOWS OF GASES USED DURING THE HOT-FIRING PROGRAM

Test No.	Injector Type	Fuel (hydrazine/UDMH)	Chamber Inlet Description				Gas Flow Description			
			Boss No.	Direction, (1)	Port Diameter, inches	Distance From Injector, inches	Species	Valve Opening Time Seconds	Max. Flow, lb/sec	Ramp Slope, lb/sec²
002	Triplet	50-50	7	90	0.515	2.00	Nitrogen	0.570	6.62	11.6
003 (2)			7	90			Nitrogen	-	-	-
004			4	135			Nitrogen	0.560	6.37	12.4
005			4	135			Nitrogen	(3)	-	-
009			4	135			Nitrogen	0.027	8.08	700.0
026			7	90			Nitrogen	0.071	7.12	100.0
028			7	90			Helium	0.079	2.21	28.0
029			7	90			Helium	0.065	2.24	35.6
037 (4)	Doublet		1	180	0.370		Nitrogen	0.060	0.92	15.3
043			1	180			Nitrogen	0.051	6.30	203.0
046			1	180			Nitrogen	(3)	-	-

(1) Directions of 90, 135, and 180 degrees are sometimes referred to as tangential, chordal, and radial, respectively.
(2) Test No. 003 was already unstable when the gas flow was initiated.
(3) The flow ramps during Test No.'s 005 and 046 were nonlinear and the flowrate measurements could not be made reliably.
(4) Two "pops" occurred during the gas flow period during Test No. 037.
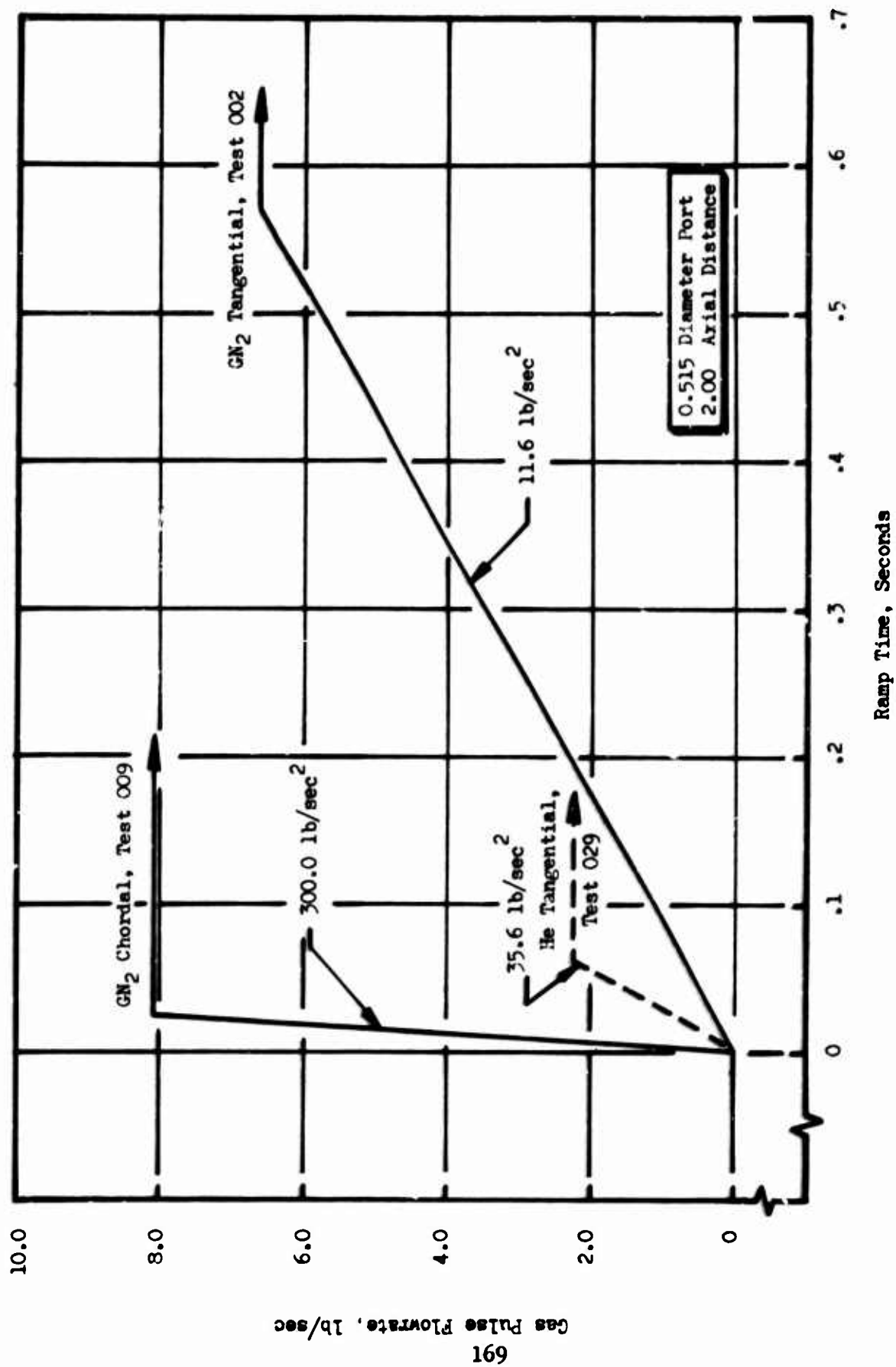
Figure 58. Typical Gas Pulse Ramp Flows With Triplet Injector

On several occasions, a port through which a gas pulse was directed fell within the field of view of the Fastax camera looking up the nozzle into the combustion chamber. The high-speed motion pictures showed clearly that gas flows directed in the chordal or tangential direction resulted in a large circulating eddy motion, or vortex, within the baffle compartment. In terms of the camera's field of view as it was sketched on page 141, a chordally directed pulse produced motion on about the following scale:
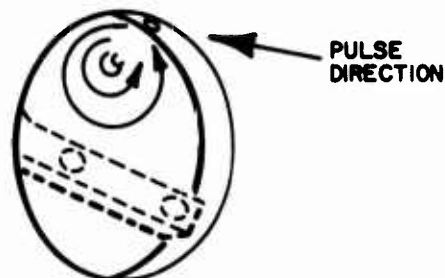
During those tests for which the gas flow ramp was the longest duration, the eddy became more and more distinct as the flowrate increased. During that time, the accelerometer on the injector recorded a vibration that, as shown below, steadily increased in amplitude. There were however, no attendant chamber pressure disturbances or oscillations.
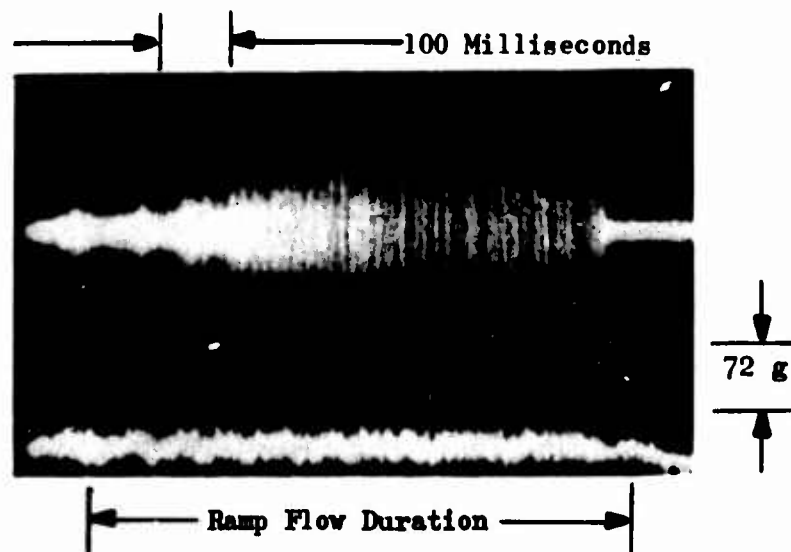
Accelerometer Output During Gas Pulse Flow

170

It is interesting to note that most production-type rocket engine tests utilize accelerometer transducers for rough combustion indicators and often provide a RCM signal for engine cutoff. The accelerations on the above mentioned test exceeded 250 g peak-to-peak and could have been sufficient to generate an erroneous cutoff signal under most normal operating test conditions.

Also observed by the nozzle-end view camera were a few brief flashes of brighter-than-usual combustion products emanating from the general neighborhood of the corner formed by the intersections of the injector face and the baffle with the chamber wall. Two of these were seen during the nitrogen gas flow in Test No. 037 and are listed in Table 15 as "pops". They were first observed in the motion picture and, from their appearance, were immediately thought of in terms of the isolated random pressure disturbances that occur occasionally with N_2O_4 and hydrazine-based propellants. Close examination of the pressure records revealed, however, only very slight disturbances were felt at the nearest Photocon position. In at least one case, the flash of brighter products appeared to penetrate about half the chamber radius at about 1000 ft/sec for about 1/2 millisecond. These results offer a strong indication that the propellant combustion processes with these injectors and propellants are not sensitive to transverse flow disturbances.

Instability Mode Identification and Modal Relationships. The information presented in Fig. 53 through 57 is wholly concerned with the identification of and relationships among particular chamber acoustic modes. For the majority of the tests, these data were derived from examination of the frequency, amplitude, and phase relationships among pressures recorded by the three or four Photocon transducers and displayed by making time-base-expanded oscillographs of the taped data. Data from Photon transducer positions PC1 through PC8 provided positive identification between the first tangential and second tangential acoustic modes. The transducers

171

were located, however, on pressure nodal points for the standing third
tangential mode. Therefore, it was impossible to positively distinguish
between the third tangential and the first radial acoustic modes, since
all pressure oscillations would be in phase for both modes. Based upon a
3550 feet per second acoustic velocity, the following theoretical modal
frequencies were calculated.

TABLE 16

THEORETICAL CHAMBER ACOUSTIC FREQUENCIES

Chamber Acoustic Mode	Theoretical Acoustic Frequency, cps
First Tangential	2188
Second Tangential	3629
Third Tangential	4992
First Radial	4553

It is observed from Table 16 that only 439 cps separate the third tangential
and first radial modes. Additional instrumentation techniques were needed,
therefore, to ascertain conclusively the chamber acoustic behavior. Late
in the firing program, two additional Photocons (H and I) were installed;
each was located 15 degrees on either side of a pressure nodal point for
the third tangential acoustic mode. These transducer output data, in
conjunction with streak film data, indicated that both the first radial
and third tangential modes were coexistent.

172
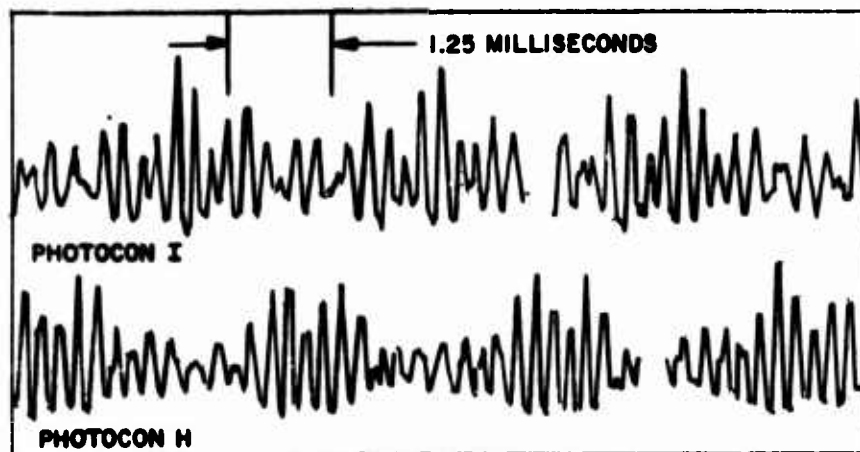
A beat frequency, for example, was recorded on both (H) and (I) Photocons, 180 degrees out of phase, and represented the differential frequency between the two modes. Additional corroborating evidence from the streak photographic records is discussed in a following section.

Transparent Chamber Results

Two hot-firing tests were made with a transparent combustor section using the doublet injector and N_2H_4-UDMH (50-50) fuel. The initial test, run number 078, was nearly nonproductive because the majority of the films were somewhat under exposed and the single scheduled rating disturbance was not activated. A shorting circuit on the explosive bomb firing circuit had not been removed. The second test, run number 079, contained a 13.5-grain bomb located in the nozzle section and a 15HB/10K pulse gun charge directed radially through the transparent side. Both 600-millisecond tests were successful from an operational standpoint.

The most pertinent results of transparent chamber experiments at rocket operating conditions are photographic. Detailed study of high-speed motion pictures can yield semi-quantitative understanding of the combustion processes in depth that is not attainable by any other current means. Unfortunately, in reproducing a few frames of 16 millimeter film for publication, little (if any) of the dynamic quality is transmitted. Some film sequences that are fairly informative when projected in motion may lose all meaning when reproduced as still photographs. Figure 59 shows reproductions of two frames taken with a Fastax camera through the transparent combustor wall during test 079. The axial field of view of the transparent section was 5.56-inches. The first picture, Fig. 59a, was taken several milliseconds prior to initiation of the bomb. The length of the propellant streams during stable combustion is seen to be about 5 to 6 inches. Since the outer injector ring consisted of fuel elements, the observed unburned propellants are probably N_2H_4-UDMH (50-50) fuel fans from the self-impinging doublet elements. Figure 59b shows the interruption of the combustion process several microseconds after the bomb blast. The propellant streams are almost entirely consumed by the

173

a. Steady State Stable Combustion

b. Shock Wave Following Bomb Perturbation

Figure 59. Selected Frames From Motion Photography
of Combustion Process

174

quasi-spherical shock wave generated by the bomb in the nozzle. The fuel spray fans were shortened to about one-half of their original lengths during unstable combustion and when viewed in projected motion, could be seen to oscillate in the transverse directions.

Streak Film Analysis. Streak films, taken for aiding in the identification of instability modes and understanding of the various phenomena that occur when a rating technique is employed, are illustrated in Fig. 60 and 61. Segments of films exposed to light emission through the transparent combustion chamber wall at the time of bomb detonation are shown in Fig. 60. Later-time segments from those same films, when the pulse gun was fired, together with a segment from a baffle-vane-aligned streak film are reproduced in Fig. 61. The geometrical relationships between the streak camera alignments and the chamber are shown in Fig. 50. The nozzle-view streak camera aligned with one baffle vane was obscured behind an NTO cloud during the bomb disturbance and did not produce any useable data until the pulse gun fired.

All streak photographs were correlated with other photographic and tape-recorded data by means of a common 1000-cps reference timing signal. Voltage pulses were simultaneously recorded on the run oscillograph, one channel of the magnetic tape and supplied to each Fastax camera where they powered a timing light for exposing a small portion of the film's edge every millisecond. Cross-correlation was assured by providing a unique blanking or broadening of the voltage pulses during one specific time interval in each test. The pulses to some of the streak cameras were specially shaped to provide more abrupt initiation and termination of lamp luminosity.

Examination of the axial and circumferential streaks in Fig. 60 show the existence of the standing first tangential mode for approximately 7.5 milliseconds following the steep-fronted bomb shock wave. This is typified by the parallel, normally orientated, luminous bars or the axial streaks and the corresponding sinusoidal-like wave appearance in the circumferential

175

streaks. The observed frequency is 2130 cps which compares favorably with the 2188-cps frequency listed in Table 16. During this period the chamber pressure dropped below normal, causing increased injector ΔP's and flowrates, as shown on the axial streak film. About 8 milliseconds after the bomb disturbance, the combustion process recovered from the chug and the chamber pressure reached a high value causing the luminosity to increase as shown. At about this same time a change in the stability behavior can be noted. The frequency increased to 4570 cps. This new wave form can be identified as the first radial acoustic mode and is seen to coexist with the first tangential, particularly on the circumferential streak film. Both modes were damped after 22 milliseconds and stable combustion continued until the pulse gun was fired.

The three streak films taken during the pulse gun disturbance are shown in Fig. 61. In addition to the axial and circumferential orientation, a streak record was obtained with a camera looking up the nozzle with a 0.005-inch-wide slit aligned parallel to a baffle vane. This is shown in Fig. 61c. (The less precise 1000-cps reference time base was recorded on this film and the framing rate was approximately 4100 fps.)

All three films show increased combustion luminosity for about 1.5 milliseconds following the initiation of the pulse gun disturbance. The first tangential mode is again clearly indicated at approximately 2100 cps, primarily on the circumferential streak. A basic difference with the pulse gun disturbance was the presence of the first radial mode immediately following the perturbation. This is again shown by the luminous parallel bars of light on the axial streak and the corresponding saw-toothed pattern observed on the baffle-oriented streak. The instability was damped after 5 milliseconds. The pulse gun did not cause a feed system coupled chugging instability.

...nk Disturbance

|— 0.001 Second —|

Downstream
Edge of Baf...

Flow

Increase Luminosity
Due to Increased
... Chamber Pressure

Time

Circumferential
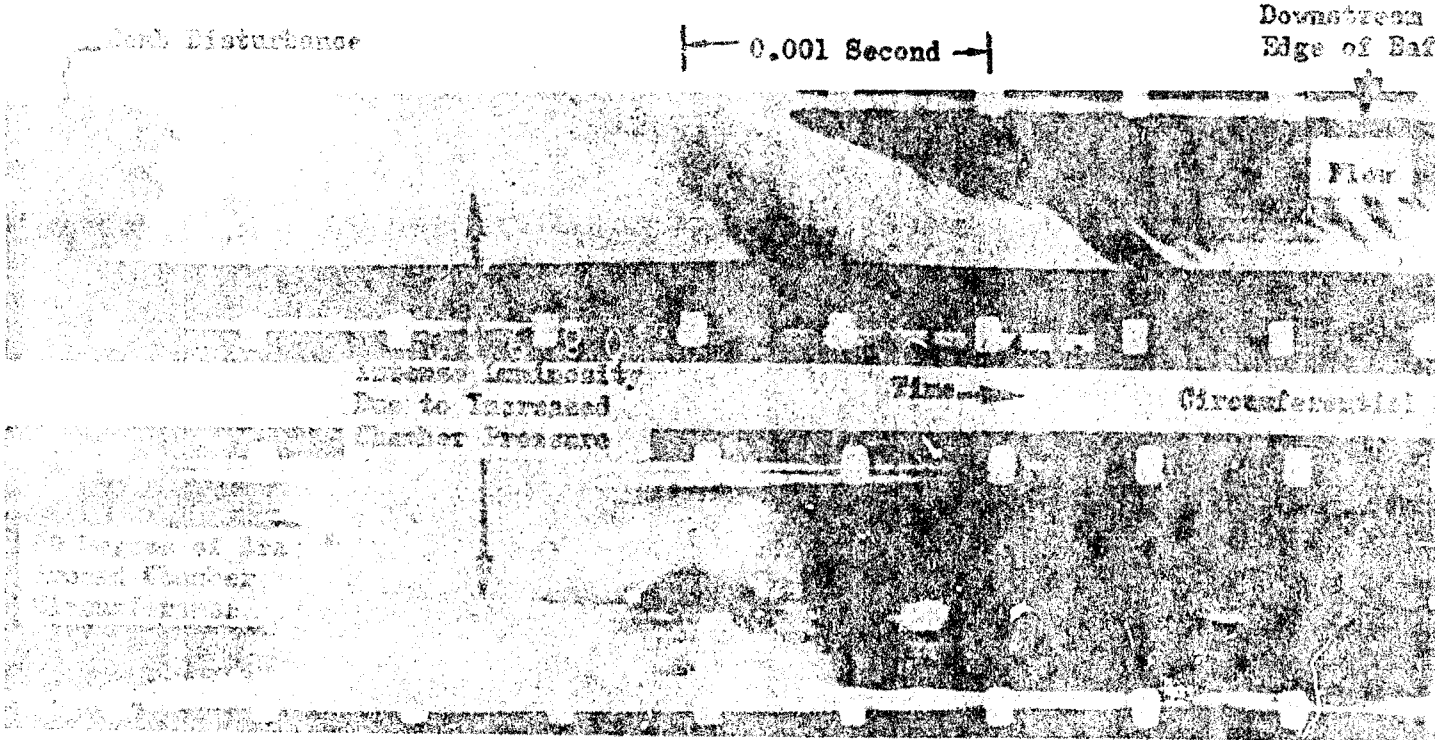
A

Downstream
Edge of Baffle

Axial Streak – Bomb

Accelerating
Propellant Fl

Circumferential Streak – Bomb

Corresponding Pressure
Antinode for First
Tangential Acoustic Mode
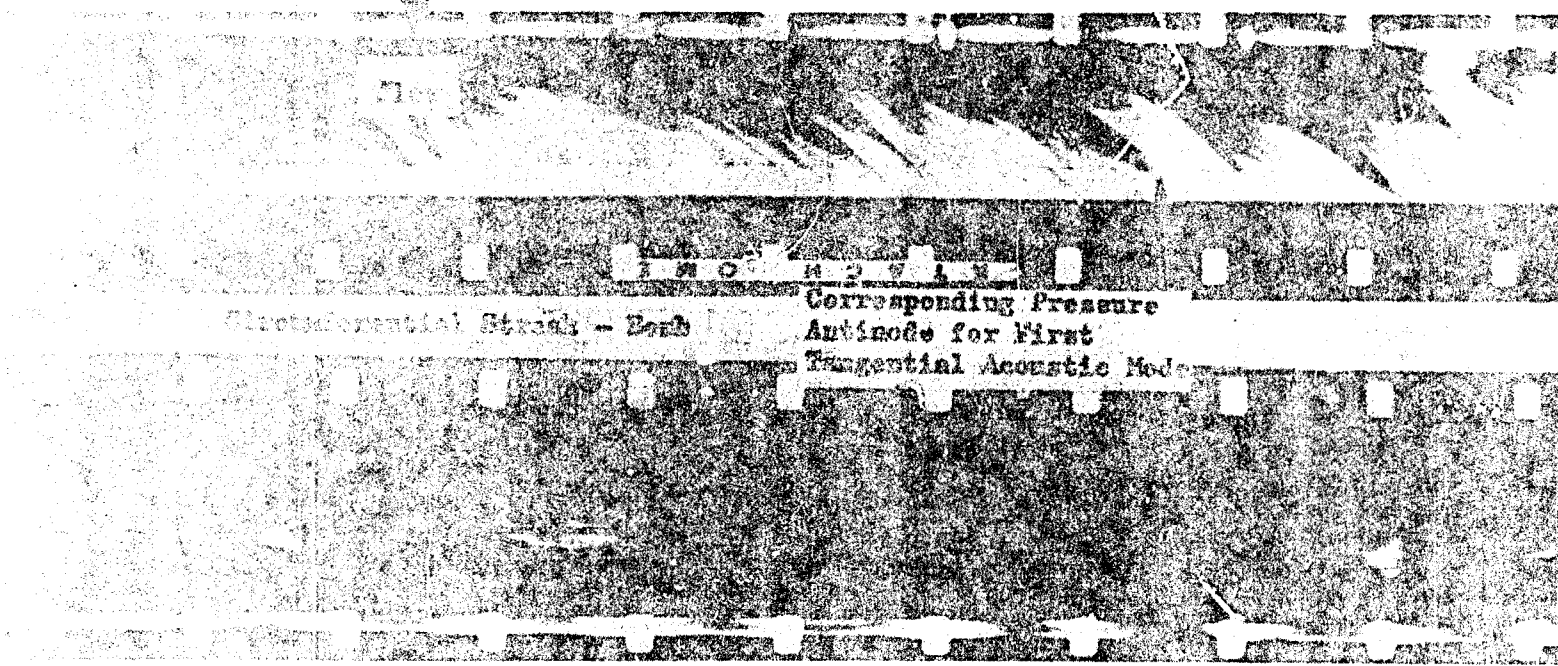
B
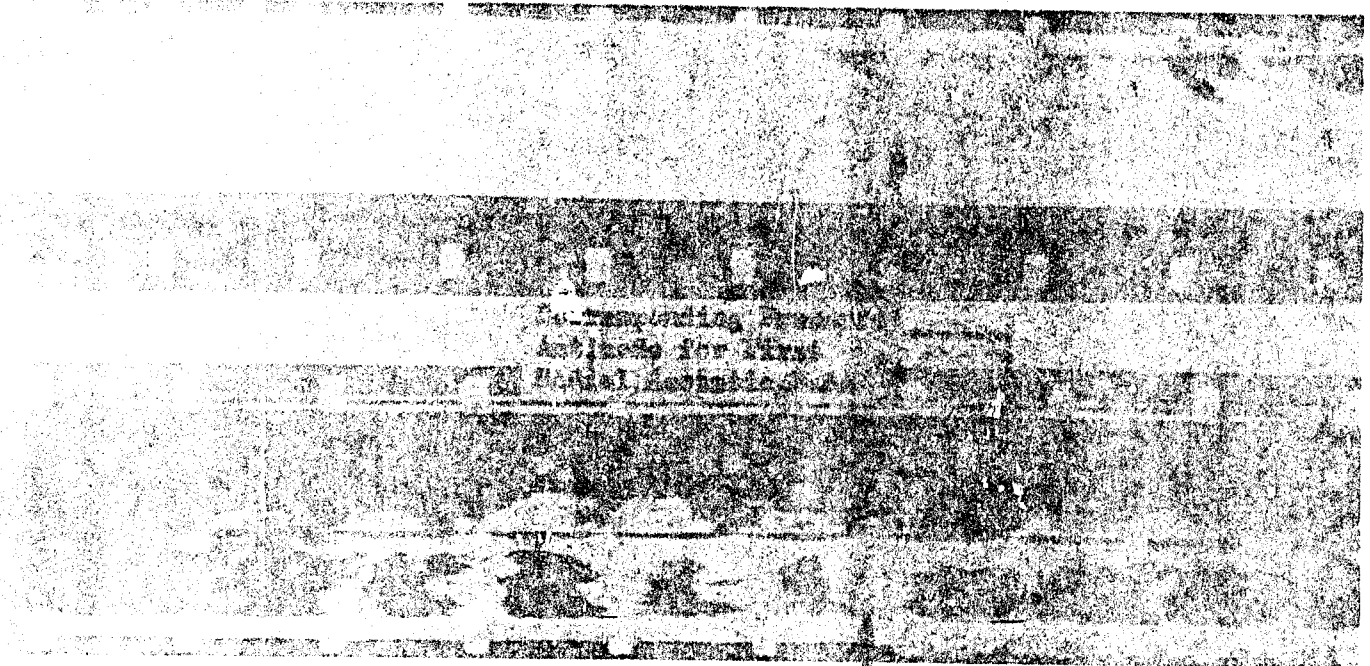
Coexistent First
Tangential Acoustic
Mode

Figure 60. Streak Photographs of Bomb Triggered
Combustion Instability During Test 079

177

C

Axial Streak – Pulse Gun

|← ———— 0.001 Second ————→|
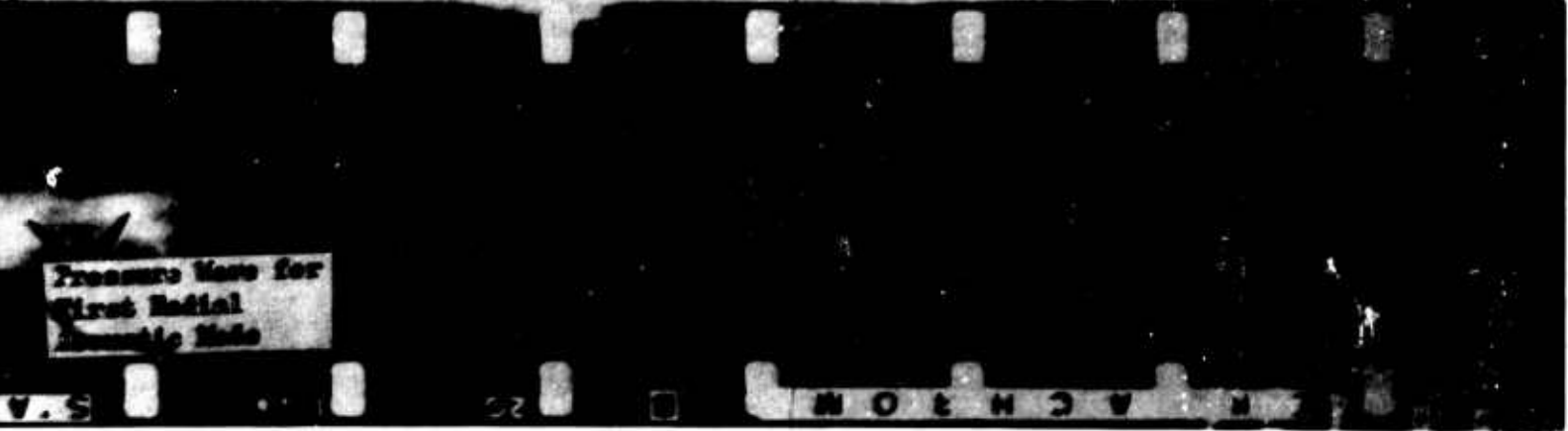
Figure 61. Streak Photographs of Pulse Gun
Triggered Combustion Instability
During Test 079

ANALYSIS AND CORRELATION

COMBUSTOR'S STABILITY RESPONSE

From previous stability experience with the particular rocket system employed, it was anticipated that recovery to stable operation would be experienced with all but a few of the rating devices' perturbations. The projected correlations were based, therefore, on relating the devices' characteristics to response variables such as the initial pressure disturbance amplitude, the recovery or damp time, and the pressure oscillation amplitude decay rate. It was further expected that instances of sustained instability could be clearly related to rating device application variables; e.g., introduction into the chamber at a preferred location for driving a particular mode of instability.

A few tests dispel these promising expectations. The triplet injector, which had previously been found insensitive to bomb perturbations, was found to recover its stability from only a small fraction of the bombs used and only about half of the pulse guns. The least expected revelation was that there was no immediately apparent relationship between the rating device parameters varied and the ultimate stability of the combustor. In other words, recovery to stable operation appeared to occur randomly. Thoughtful examination of Fig. 52, 53 and 55 will clearly reveal the complexity that the first several tests began to reveal.

The projected correlation technique was not appropriate for the stability responses experienced. In view of the responses' complexity, an alternate correlation approach was devised which was based on conceptual interrelationships among characteristics and responses as depicted in Fig. 62. There the correlation is broken down into several separate steps, each of which forms a logical stepping stone for relating the rating device to the combustor's ultimate stability behavior. This approach has a great advantage over a simple beginning-to-end correlation: If the ultimate stability is unrelated to the rating techniques' variations, it should be possible to determine at which point an hypothesized relationship breaks down.

179

Combustor Design
and
Operating Conditions

Propellant Spray
Combustion Process
Characteristics

Propellant Feed
System Designs
and
Response Characteristics

Output: Rating
Device Characteristics

Step 2
Initial Response of
Combustion Processes

Output: Initial
Pressure Wave
Amplitude

Step 3
Continued Response
of
Combustion Processes

Output: Initial
Mode of Pressure
Oscillation

Step 4
Establishment of

Step 1
Cold Flow
Experiments

Rating Device
Input
Parameters

Rating Device Application:
Position or Orientation
In Combustion Chamber

4

Figure 62. Relationships Among Various Sets of Characteristics and Combustion Process Responses

180

β

The cold characterization, step (1), has already been discussed at length. As indicated by the dashed line input to step (2), it is conceivable that direct correlation of the input parameters may be desirable or required, but use of the characteristics should lead to a more fundamental understanding of the processes involved.

This section is concerned with the analysis and correlation of information regarding steps (2), (3), and (4). Each of these is shown in Fig. 62 as having the propellant spray combustion characteristics as an input; these were certainly not determined, but were considered to be held constant for three distinct groups of tests (viz., the triplet injector, the doublet injector, and the doublet injector with UDMH fuel).

In step (2), quantitative correlations were sought between the rating techniques and the initial response of the combustion processes. Since the gas flow disturbances did not induce any measurable pressure disturbances, no further consideration will be given that technique here. For the bomb and pulse gun techniques, the correlations are in terms of the initial pressure wave amplitude.

The continued response, following the establishment of an initial pressure wave, is interpreted in step (3) as the driving of an initial mode of combustion instability. The available information has been related qualitatively, and somewhat heuristically, to the position and orientation of the rating device in the combustor but the quantitative correlation appears to break down at this step.

The ultimate stability is discussed in step (4) in terms of interactions between the initial mode, a low-frequency chug, and subsequent instability modes. Again, quantitative correlations are lacking.

Initial Wave Amplitudes

The direct analog pressure records were analyzed to obtain quantitative data on the initial bomb and pulse gun-initiated blast wave amplitudes

181

as functions of time and distance from the source. Correlation of these data on the initial overpressure to the devices' cold-flow characteristics or to their descriptive parameters was the principal goal of this effort. The magnitude of the overpressure and its growth or decay were also of interest as providing possible explanations for the types of acoustic modes initiated, their amplitudes, and perhaps the ultimate dynamic stability of the tests.

Explosive Bombs. The way in which the bomb position was described in the analysis is illustrated in Fig. 63 . The axial distance of the bomb from the injector face, denoted by l, varied from 2.95 to 10.2 inches. The radial distance r of the bomb from the chamber axis had values of zero (bomb at the center), 2.85 inches (bomb at the midradius), and 4.95 inches (bomb near the chamber wall) for the tests included in the correlation.

The Photocons were located at axial distances x from the injector face of 1.5 and 4 inches at several different positions around the circumference of the chamber (Fig. 45). The positions were characterized in terms of the projected distance y from the bomb to the Photocon; that is, the distance from the Photocon (A in Fig. 63) to the projection of the bomb into the Photocon plane (D in the figure). The direct distance from the bomb to the Photocon is $z = \sqrt{y^2 + (l - x)^2}$. Of subsequent interest in the analysis is the angle α between the lines $\overline{CA}$ and $\overline{AB}$. The former is the normal to the Photocon face and the latter is the direction of propagation of the initial shock wave from the bomb. The cosine of this angle which may be obtained from the side lengths of the triangle ABC, is given by

$$\cos \alpha = \frac{(5.75)^2 + z^2 - r^2 - (l - x)^2}{2 (5.75) z} \tag{22}$$

where

5.75 inches is the chamber radius $\overline{CA}$ and $\sqrt{r^2 + (l - x)^2}$ is the distance from B to C.
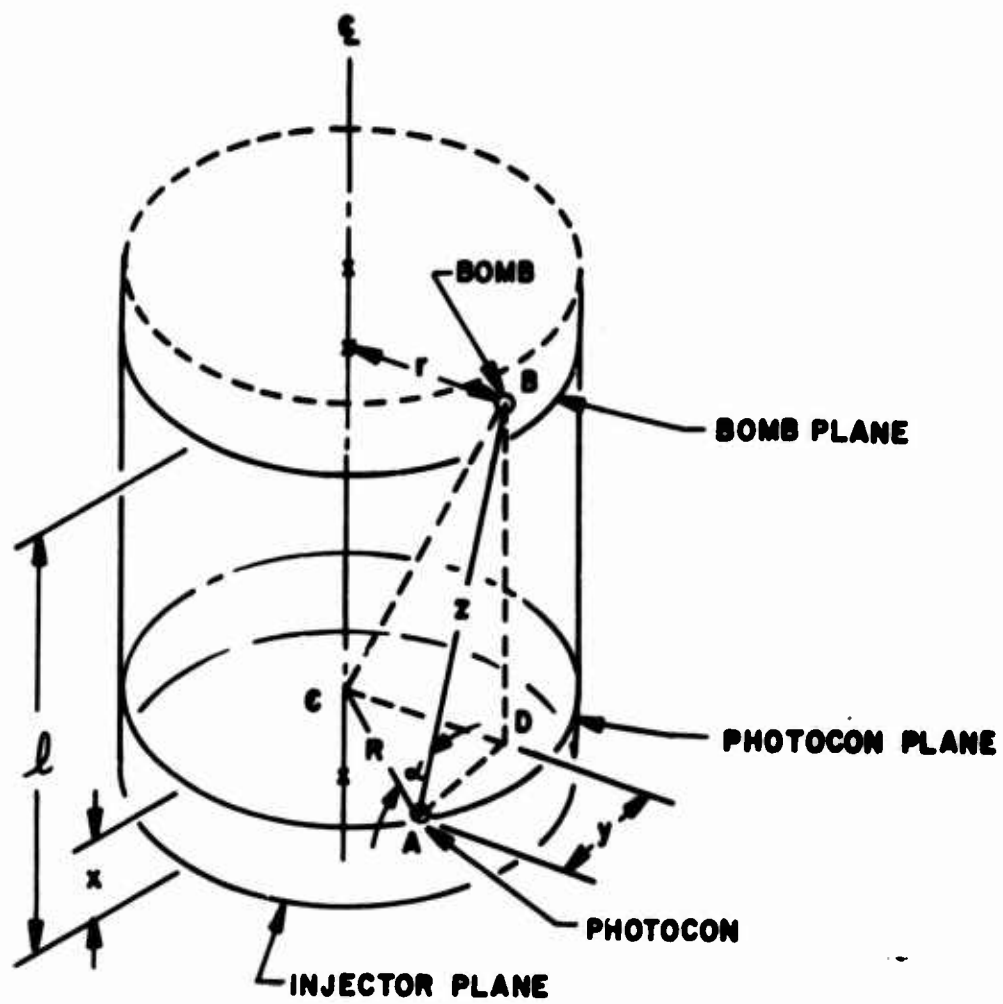
Figure 63. Chamber Geometrical Relationships for Correlations

In the next few pages, data on the combustor's response to bombs are discussed and extensively cross-plotted to present a good overview of the results. Occasionally some data from the demonstration tests, described later, are drawn in to emphasize a point. Demonstration test data were not used in the statistical correlation of the bomb data, however. The initially developed correlations were based on the as-measured transducer data, as are the following cross-plots. The final correlations are seen to be much simpler when the data are treated with a pseudo-reflection coefficient.

It was originally anticipated that the disturbance from the bombs would propagate symmetrically in all directions; i.e., that the bombs are non-directional. This hypthosis was tested by observing the response to bombs mounted on the baffle at the chamber axis $(r = 0)$. Figure 64 shows this to be reasonably valid for the 5.5-grain bombs. The degree of scatter for the 13.5-grain bombs indicates that the pressure measured at a distance of one chamber radius (5.75 inches) from the bombs had a mean deviation of ±10 percent from the average value.

Further indication of departure from a truly symmetrical initial wave is evidenced by an overall average difference in the initial overpressure at Photocons A and B of about 11 percent. These pressure transducers were symmetrically located with respect to all baffle-mounted bombs. Asymmetry of the initial wave was particularly marked with the thickest (0.500-inch wall) bomb case tested.

The varying distances from the bombs to the different pressure transducers provided a means of determining the rate of growth or decay of the initial pressure wave. However, the inhomogeneity of the combustion environment posed a problem as to the correct distance to use. In one limit, a homogeneous bipropellant spray could be assumed to be distributed quite far down the chamber, in which case the overpressure was plotted as a function of the direct distance, z, from bomb to Photocon. As another limit, the actual combustion zone could be assumed to be thin in the axial direction and located near the injector. It is convenient to assume that it is in the plane of Photocons A, B, C (and, also, F for triplet injector runs)
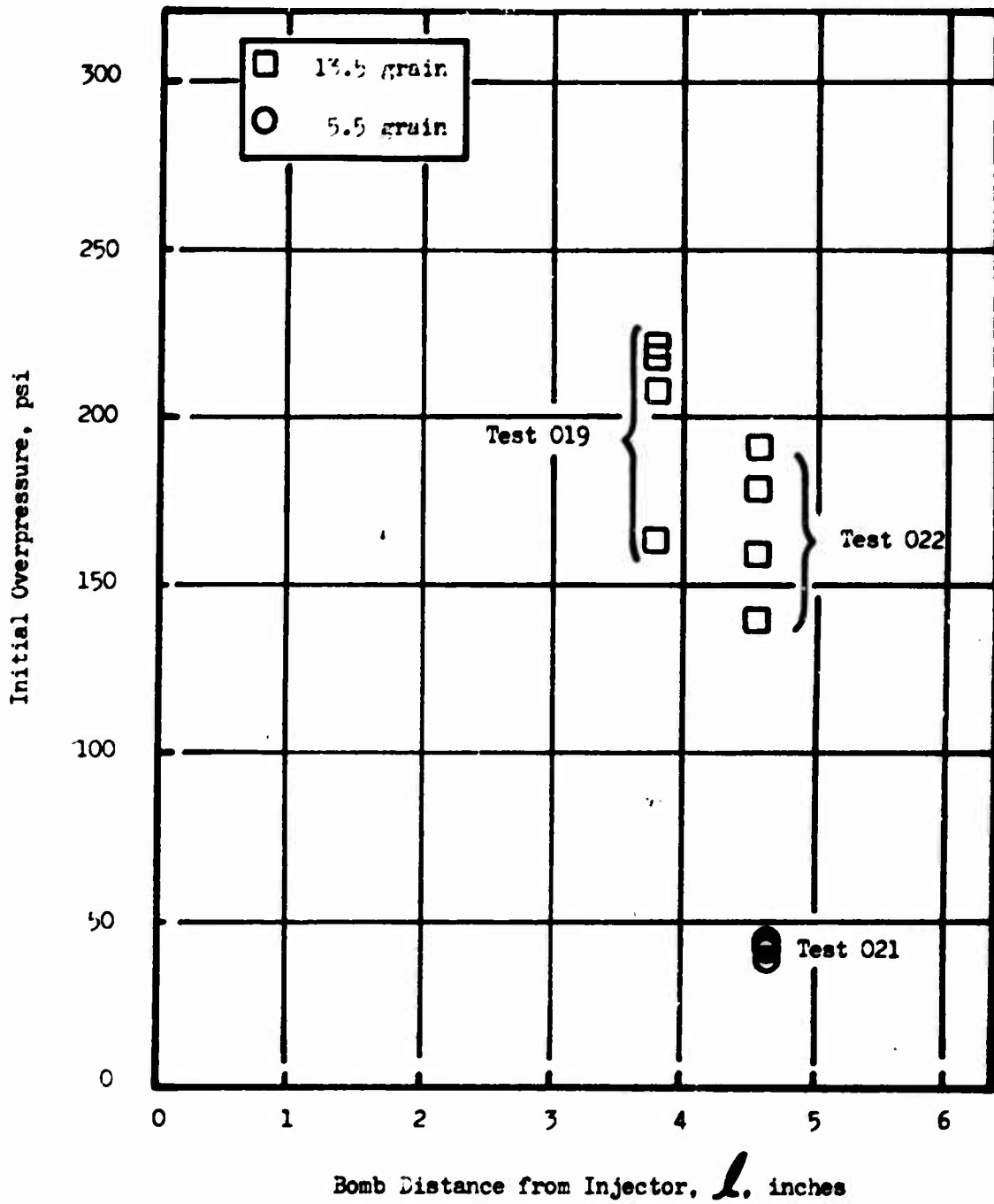
Figure 64. Initial Overpressures From Bombs at the Chamber Axis
(Triplet Injector, N_2H_4–UDMH(50–50) Fuel)

at 1.5 inches from the injector. In this case the shock wave from the bomb (which was always at least 2.15 inches downstream of the injector) would decay until it reached the burning zone, wherein it would then be amplified. In the latter case, the growth would occur only over the projected distance from bomb to Photocon, or y (Fig. 63). The actual physical situation should lie between these two extremes with a burning zone of finite width concentrated reasonably near the injector and attenuating in intensity further downstream.

The initial overpressure data were plotted against both y and z for each run. In most cases the curves were more nearly linear as a function of z than as a function of y. Otherwise, the two parameters indicated similar trends. Typical curves in terms of z only are shown in Fig. 65 through 68. In all cases the wave strength increased as it traveled through the burning spray. Most of the curves tended to level out at y or z distances bet* n about 6 and 10 inches. Notable exceptions to this were the curves for the doublet injector with the bombs near the chamber wall. In this case, for both N_2H_4-UDMH(50-50) (Fig. 67), and UDMH fuels, the curves which exceeded 150 psi at y or z of about 3 inches showed an increasing slope with distance (concave upward); while, if the overpressure at 3 inches was below about 150 psi, the curves were concave downward. Another exception was the case of the bomb mounted in the converging position of the nozzle (see run 064 which is superimposed on Fig. 68 containing "mid-radial" bombs). The wave strengthened abruptly as it moved into the vicinity of the injector.

To examine the effect of bomb size, shape, case thickness, and bomb location on the initial wave, a single value of overpressure for each test was obtained. The points arbitrarily selected were those taken from the initial overpressure curves at z = 5.75 inches, or one chamber radius from the bomb. The effects of varying only axial location of the bomb (ℓ), radial position of the bomb (r), bomb charge weight (W), and bomb case thickness (T_c) were investigated. The latter two are illustrated in Fig. 69 and 70.
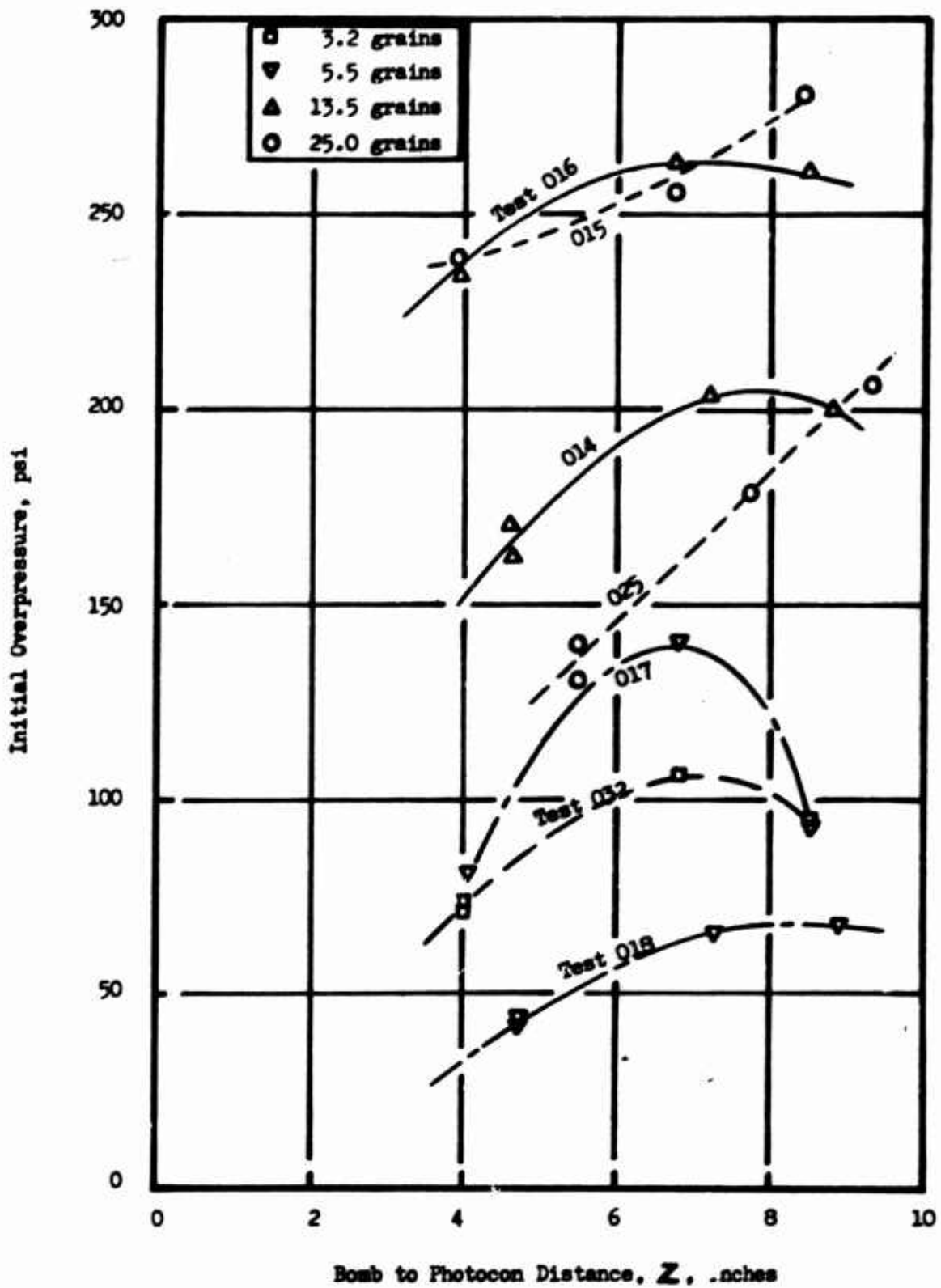
Figure 65.   Initial Overpressures From Bombs at 2.85-Inch Radius
(Triplet Injector, N_2H_4-UDMH(50-50) Fuel)
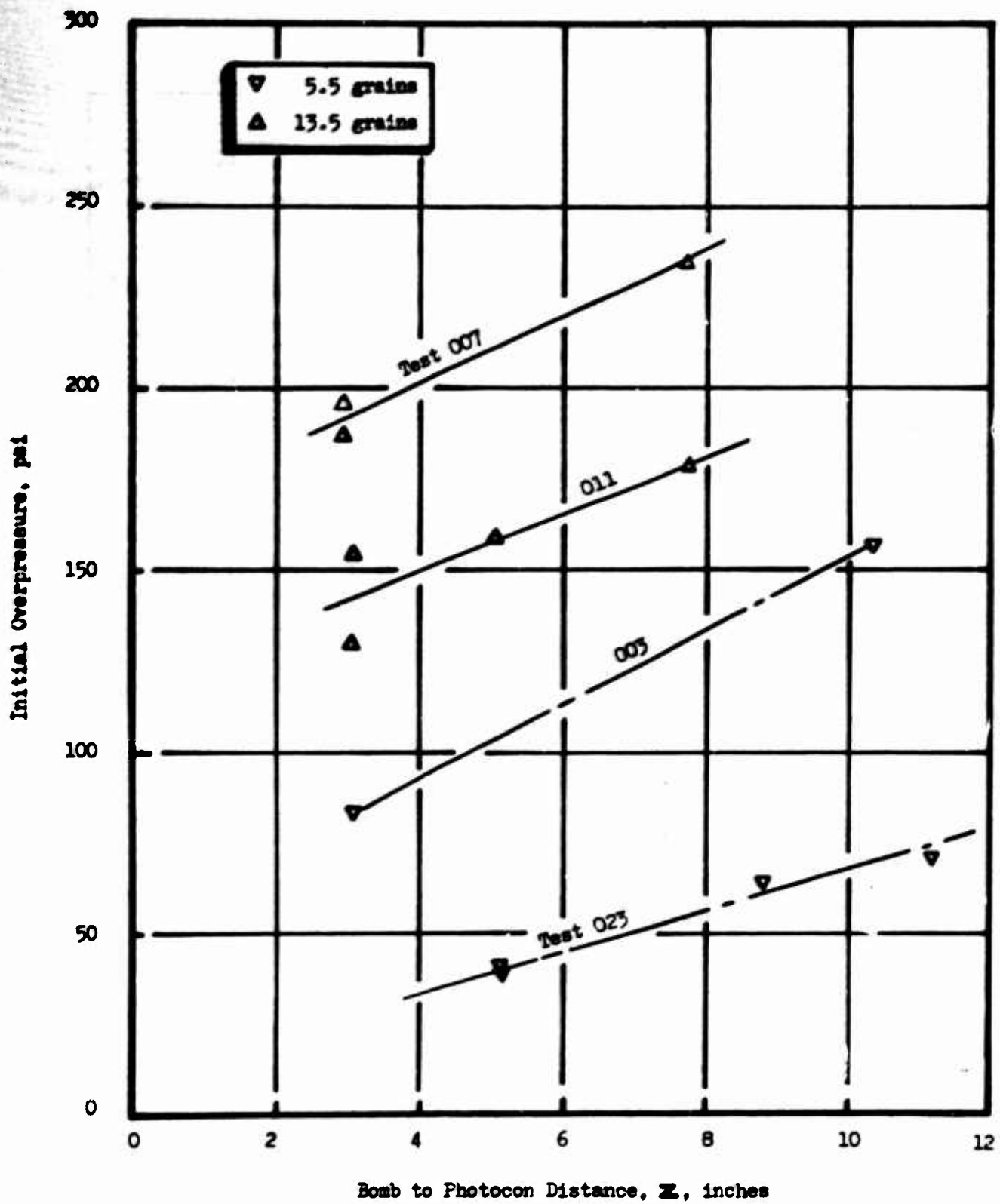
Figure 66. Initial Overpressure From Bombs at 4.95-Inch Radius (Triplet Injector, N_2H_4-UDMH(50-50) Fuel)

188
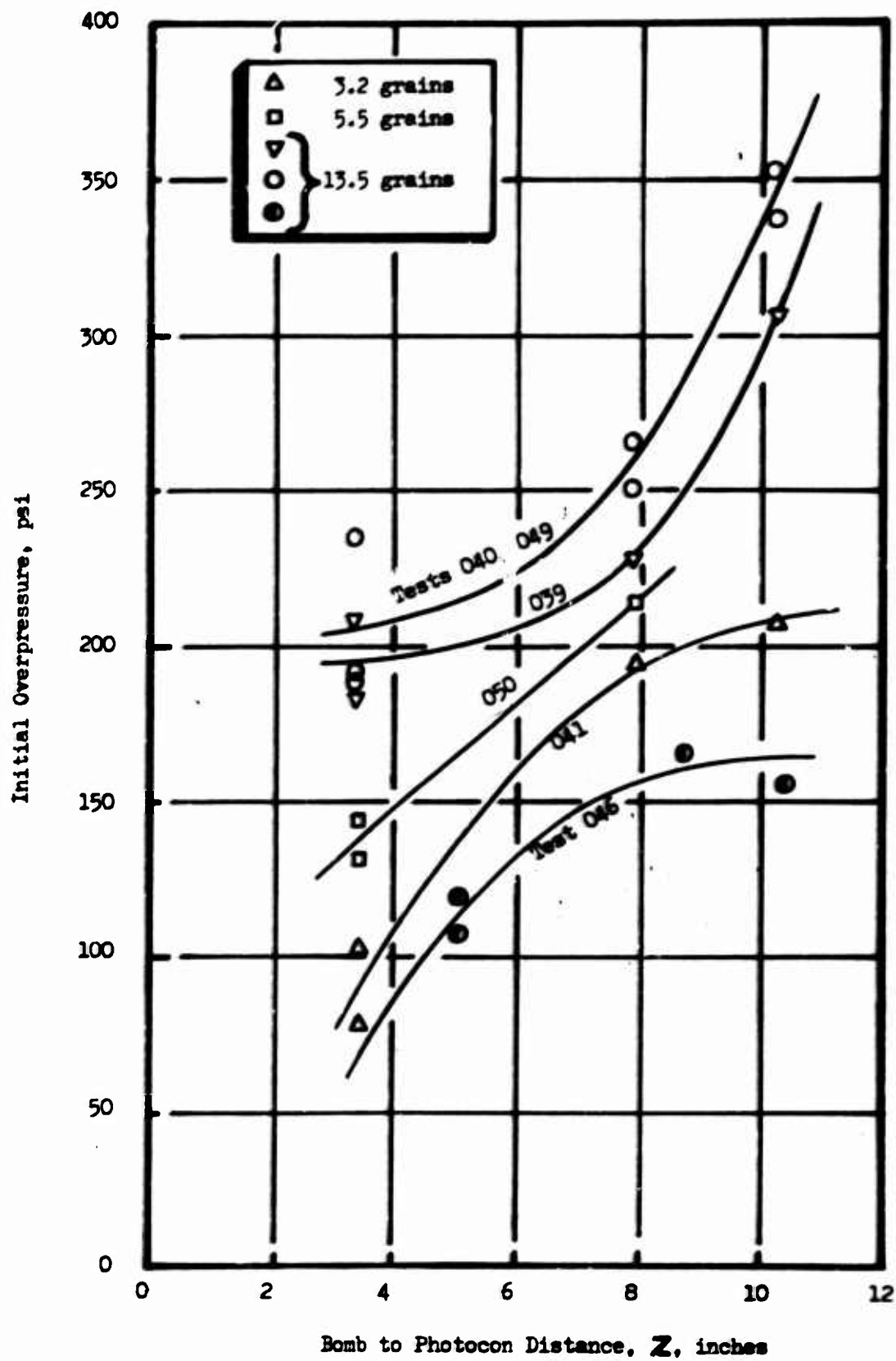
Figure 67. Initial Overpressures From Bombs at 4.95-Inch Radius (Doublet Injector, N_2H_4-UDMH(50-50) Fuel)
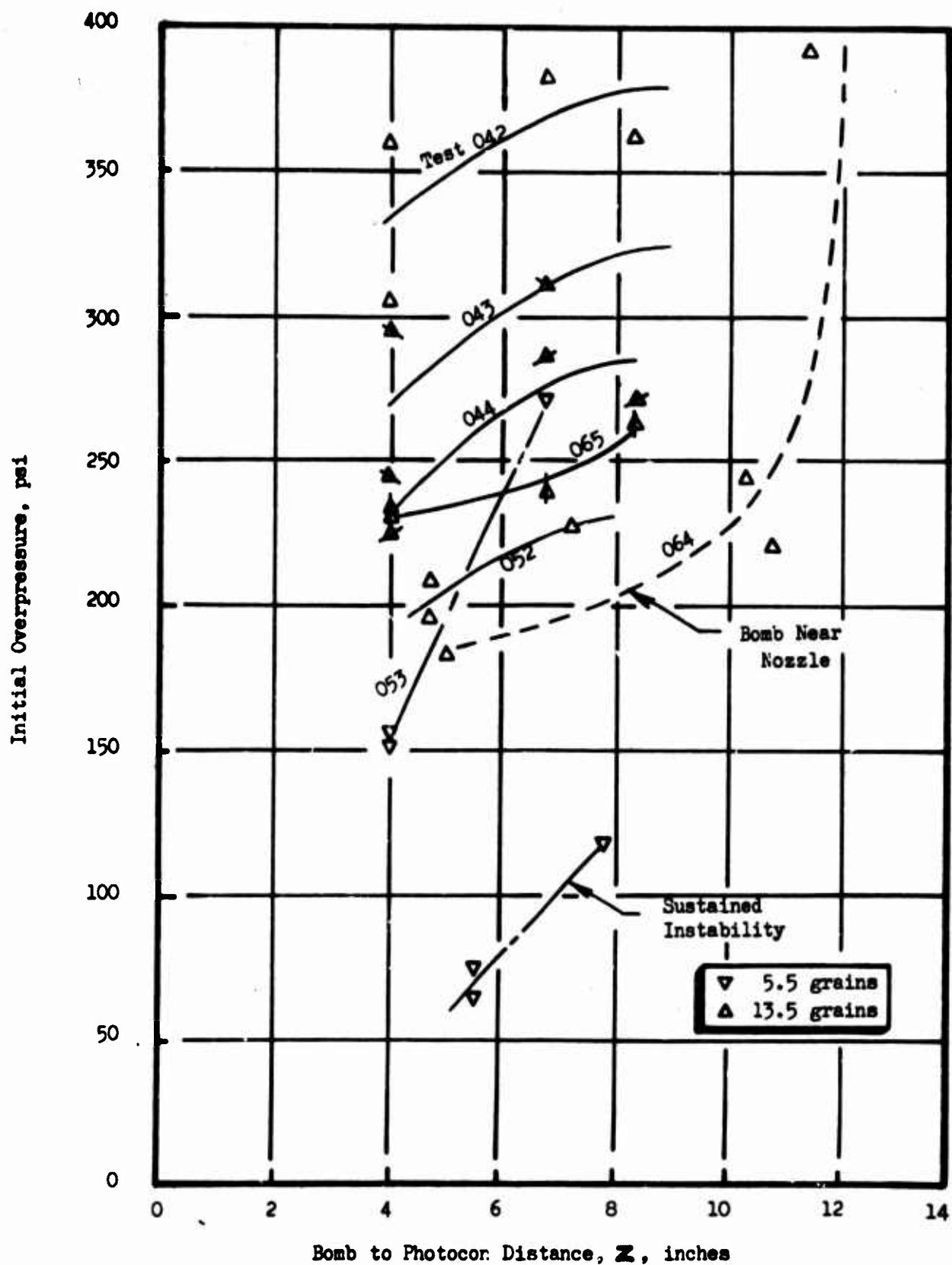
Figure 68. Initial Overpressures From Bombs at 2.85-Inch Radius (Doublet Injector, N_2H_4-UDMH(50-50) Fuel)
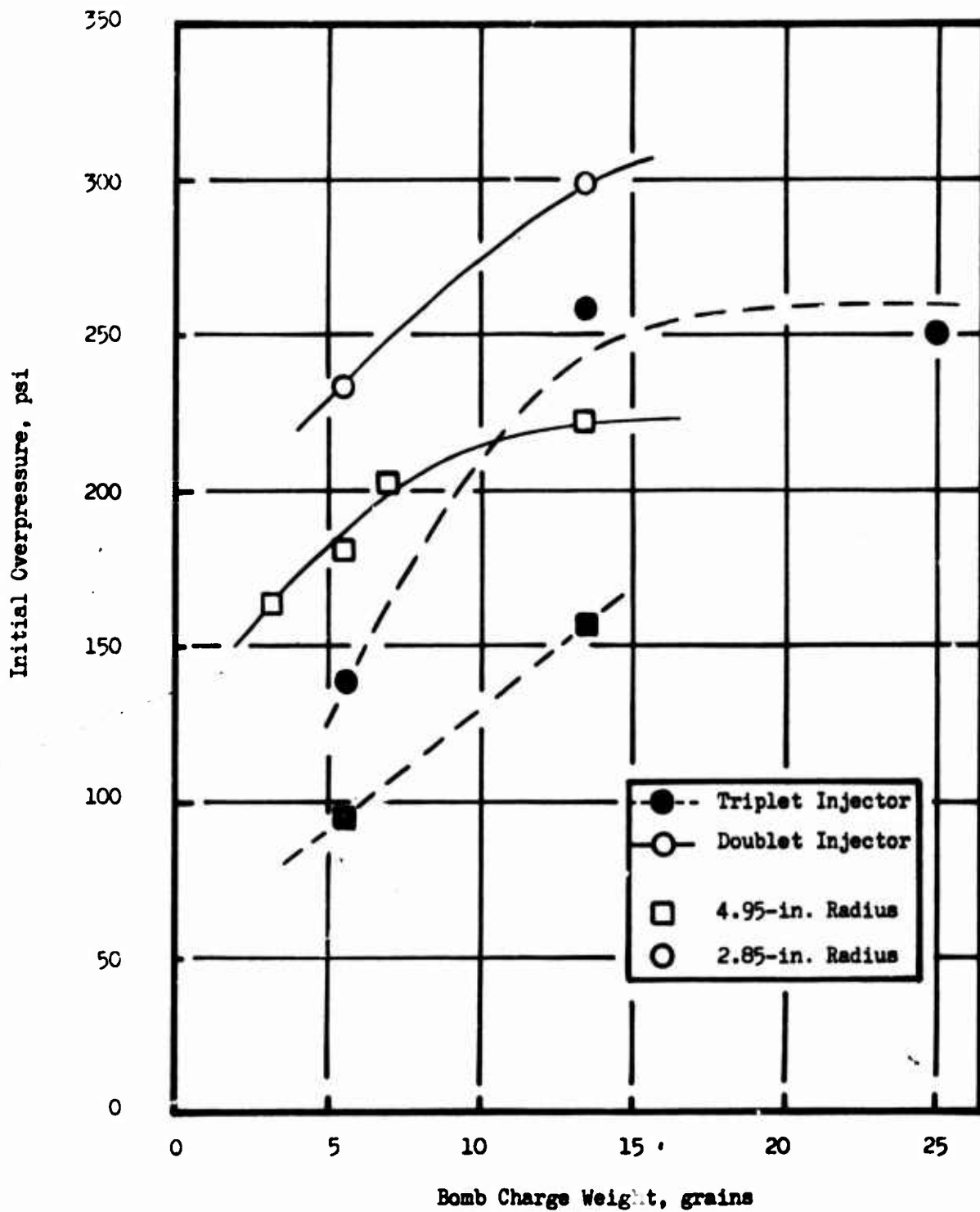
Figure 69. Initial Overpressure From Bombs Having 0.17-Inch
Case Thickness (Z = 5.75 inches)

191
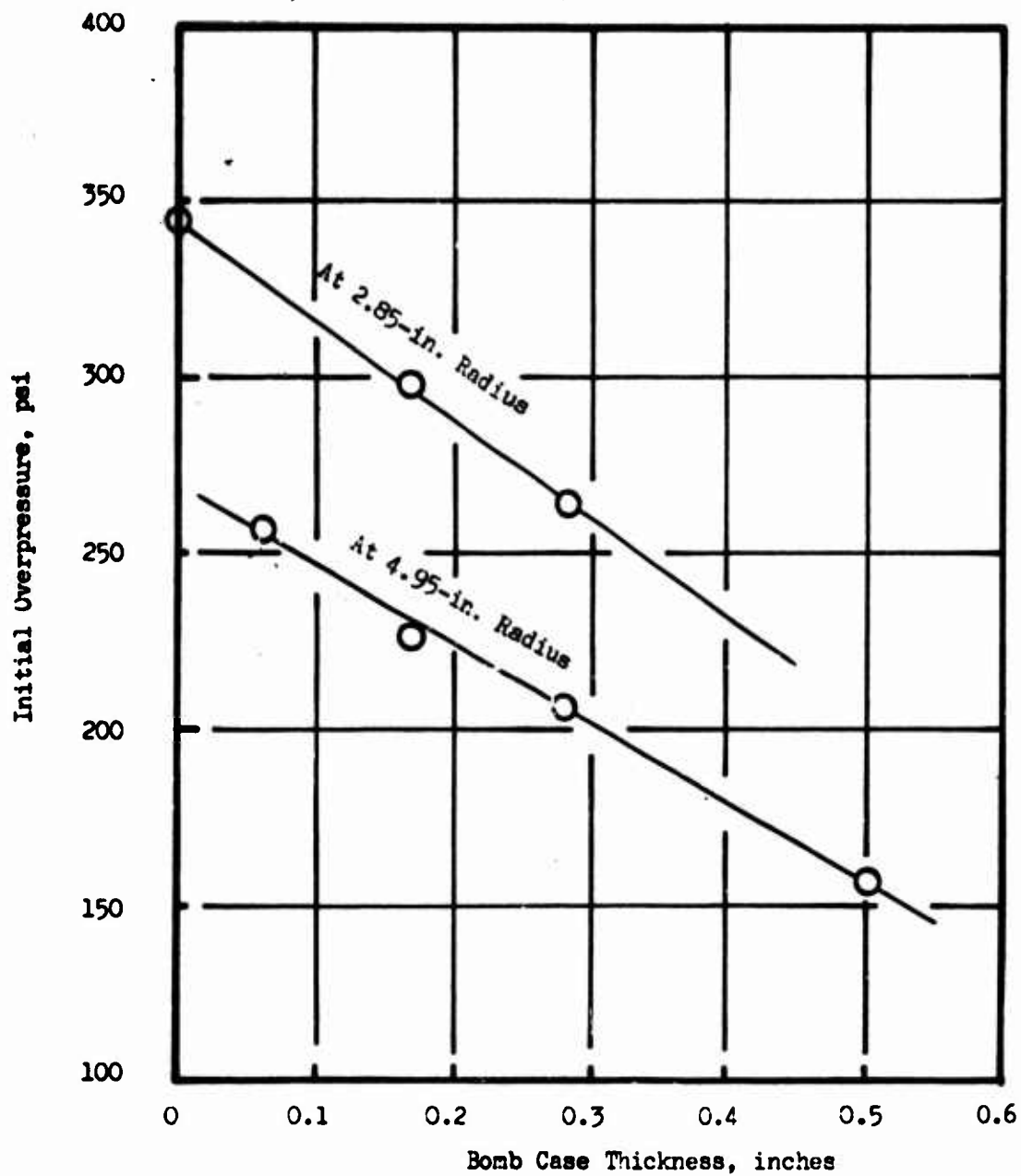
Figure 70. Effects of Bomb Case Thickness on Initial Overpressure From 13.5-Grain Bombs (Doublet Injector)

Two tests (040 and 049) show that changing the bomb case material from nylon to Micarta had negligible effect on the initial wave. Comparison of tests 040 and 041 with 068 and 077, respectively, showed a slightly stronger initial wave with N_2H_4-UDMH(50-50) fuel than with UDMH. As expected, increasing chamber pressure increased the initial wave strength. This is illustrated, together with the effect of using UDMH, in Fig. 71. In general, the initial overpressures were greater with the doublet injector than with the triplet, which is somewhat surprising in view of the higher incidence of sustained instability with the latter.

A regression analysis was performed to obtain mathematical models correlating the experimental initial overpressure data with the bomb input parameters.

Descriptive Correlations. It was hoped that one model would be sufficient to describe all of the initial peak pressure data from the motor hot-firings. It was found, however, that different models were required for the doublet and triplet injectors. In particular the projected distance y which appears as a quadratic expression in both models has opposite curvature in the two cases. For both injectors, number of descriptive models with a number of different types of terms were tried. Among the best models (i.e., highest multiple correlation coefficient and lowest standard deviation) for the triplet and doublet injector, respectively, were the following:

$$P = -2.11\ W + 1.47\ W^2 - 2.12\ W\ell\quad + 32.1\ y - 2.25\ y^2$$
$$+ 210\ \ell - 108\ \ell^2 + 13.2\ \ell^3 + 52.3\ r - 16.6\ r^2 \qquad (23)$$

$$P = 200 + 3.98\ W/T_c - 0.022\ (W/T_c)^2 + 21\ n - 29.7\ y$$
$$+ 4.04\ y^2 - 13.4\ x - 4.45\ \ell^2 - 2.49\ r^2 \qquad (24)$$

The variable n in the model for the doublet assumes the value 1 for nylon-case bombs and the value 0 for Micarta. The variable thickness
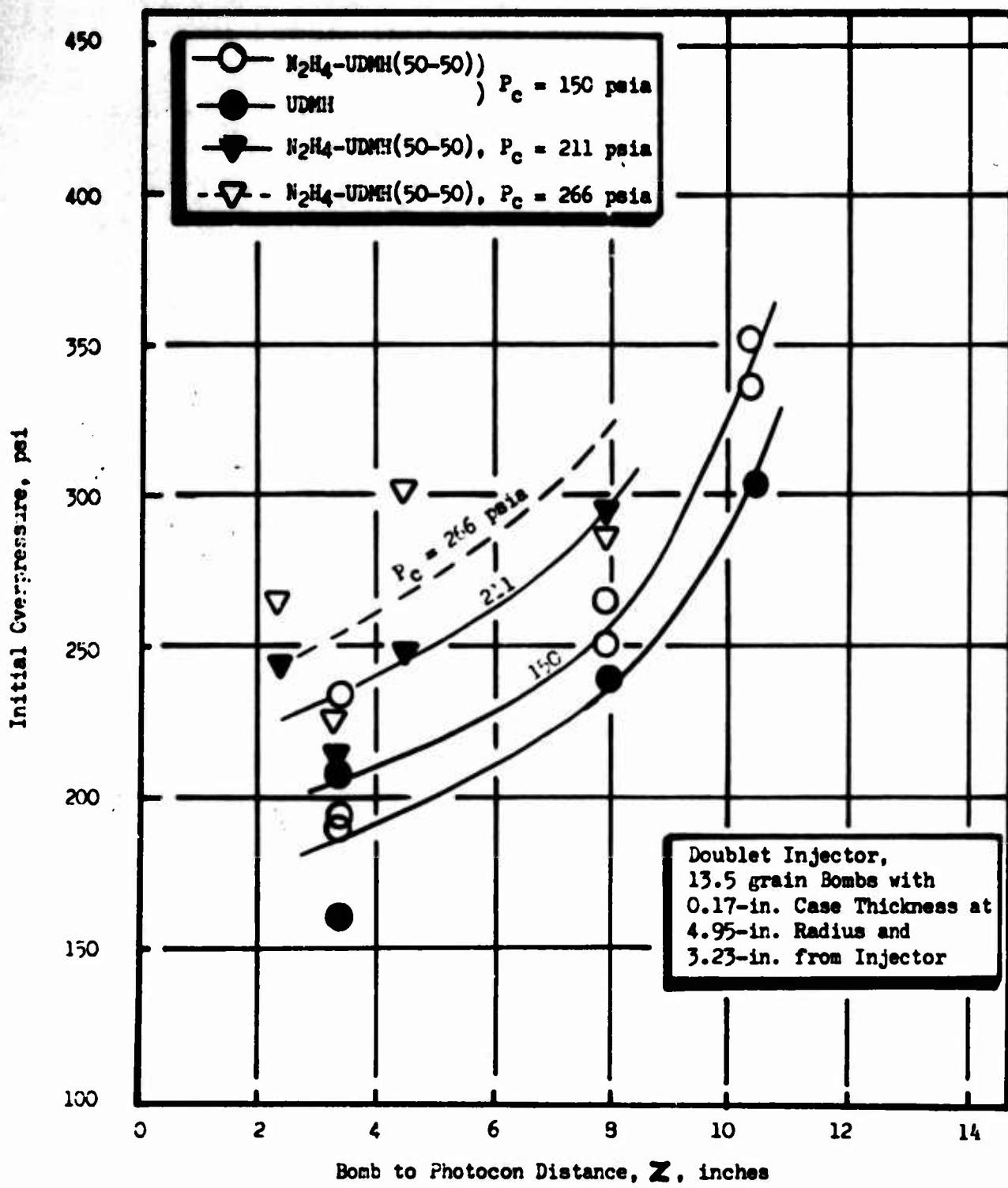
Figure 71. Effects of Chamber Pressure and Fuel on Initial Overpressures From Bombs

194

(T_c), case material (n) and Photocon axial position (x) were held constant in the tests with the triplet injector; hence, do not appear in the mathematical model. Other terms which appear in other models tried include the direct transducer to bomb distance s, more powers of W, y, ℓ, and r, and such terms as W^3/T_c.

Some of the experimental data were not included in the analytical models: the 25-grain bombs with the triplet injector and data with the doublet injector which introduced an additional factor (different orientation of bomb, different type fuel, etc.). Cross plotting the data had indicated that for bombs smaller than 13.5-grams peak pressure increased with increasing weight but an asymptotic value was approached with larger charges. Because of the large number of independent bomb parameters it was not feasible to introduce a model which would allow for asymptotic effects. Instead, peak pressures were calculated from the model using the test conditions for the 25-grain bombs but assuming a weight of 13.5 grains. These were, in fact, higher than the observed values which tend to confirm the asymptotic assumption. The same procedure, i.e., comparing predicted and observed values, was used when additional factors were introduced with the doublet injector. In all cases the two values were sufficiently different to believe that each factor had an effect on the process. This could not be explored more thoroughly without more data.

Correction for Direction of Incidence Effects. A number of anomalies appeared in the raw peak pressure data which were difficult to attribute to chance variation. For example, the models contained a number of terms in the geometrical variables ℓ, y, x, and r. Cross-plots of P vs y showed different curvature effects as a function of transducer position x. Although the models given above are quite useful for smoothing the data and predicting peak pressures for future tests with the same system, they give no physical insight into the growth of the pressure wave in the chamber.

In an attempt to obtain more realistic models, the raw data were corrected by means of a simplified wave incidence coefficient. In lieu of making

195

laborious calculations, it was assumed that the incidence coefficient would be equal to unity plus the cosine of the angle between the path of the blast and the normal to the transducer (the angle α in Fig. 63). The corrected pressures, obtained by dividing the observed pressure by the incidence coefficient, are tabulated for 16 tests with the doublet injector and 12 tests for the triplet injector in Table 17. These data were correlated to give the following model for the doublet injector:

$$\frac{P}{1 + \cos \alpha} = 124 + 5.25 \, W - 147 \, T_c + 5.0 \, y - 18.6 \, \ell + 3.3 \, r \quad (25)$$

The standard error of this model was 16.7 psi, which is comparable to that obtained with the more complicated model for uncorrected pressure, Eq. 24. There is no evidence of curvature with W, y, or T_c. The effect of thickness appears the same at each charge weight, so that an interaction term is unnecessary. It is important to note that y is preferred to z and ℓ to $(\ell - x)$ as correlating variables. Thus, peak pressure grows slightly in the radial direction but there is no apparent effect of transducer axial location, x. If a bomb is exploded at a position further downstream, its shock front is weaker and this effect cannot be explained solely in terms of the distance from the bomb to the sensor.

For the triplet injector data, the resulting model with incidence co-efficients was:

$$\frac{P}{1 + \cos \alpha} = 46.3 + 7.63 \, W - 10.4 \, \ell \quad (26)$$

The multiple correlation coefficient and residual standard deviation resulting from the model are 0.94 and 14.2 psi, respectively. The variables z, y, and $(\ell - x)$ were not at all significant. There is no effect of the radial position of the bomb nor curvature in the effect of ℓ.

The effect of W in Eq. 26 requires some comment. The data from 25-grain bombs were not used in the analysis, since, as was noted earlier, they appear to be essentially the same as those for 13.5-grain bombs due to

TABLE 17

REDUCTION OF INITIAL WAVE AMPLITUDES BY
INCIDENCE COEFFICIENTS FOR BOMBS

Test No.	Transducer	Observed Pressure Amplitude, psi	Corrected Pressure Amplitude, psi
		Doublet Injector	
039	A and B	196	136.5
	C	227	129.9
	F	305	155.4
040	A and B	247	172.0
	C	250	143.1
	F	352	179.3
041	A and B	90	63.0
	C	194	111.1
	F	260	132.4
043	A and B	270	147.9
	C	310	165.7
044	A and B	230	126.0
	C	285	152.3
	F	272	137.3
046	A and B	113	87.7
	C	165	98.6
047	A and B	75	58.4
	F	182	93.3
048	A, B, and C	282	146.2
	F	180	90.0
049	B	192	133.7
	C	265	151.6
050	A and B	138	96.7
	C	214	122.6

TABLE 17

(Continued)

Test No.	Transducer	Observed Pressure Amplitude, psi	Corrected Pressure Amplitude, psi
Doublet Injector			
052	A and B	202	118.9
	C	227	125.0
053	A and B	153	84.2
	C	273	146.2
054	A and B	70	44.0
	C	118	67.3
055	A and B	78	54.6
	C	189	108.3
060	A, B, and C	181	92.7
	F	122	61.2
061	A and B	148	103.1
	C	188	107.6
	F	260	132.5
Triplet Injector			
002	A and B	142	95.9
	C	178	101.1
007	A	196	131.0
	C	233	132.1
011	A and B	126	97.8
	C	160	95.6
	F	135	71.3
014	A and B	166	97.4
	C	204	112.1
	F	200	103.7
016	A and B	236	129.3
	C	263	140.6
	F	260	132.3

TABLE 17
(Concluded)

Test No.	Transducer	Observed Pressure Amplitude, psi	Corrected Pressure Amplitude, psi
		Triplet Injector	
017	A and B	72	39.7
	F	88	43.0
018	A and B	42	24.8
	C	66	36.4
	F	66	34.3
019	A, B, C and F	226	117.2
021	A and B	42	22.4
022	A, B, C and F	167	88.7
023	A	38	29.6
	C	63	37.7
	F	70	37.0
032	A and B	72	39.6
	C	106	56.8
	F	94	47.9

an asymptotic effect. An attempt was made to insert a W^2 term into Eq. 26 to model this effect. The W^2 term was statistically significant, but its sign was positive, which was an unexpected result. Examination of the raw data showed that the curvature was due to unusually low peak pressures for the 5.5-grain bomb used in test 018. Therefore, the linear model is preferred.

Somewhat surprising is the fact that for a bomb in a fixed axial position, no significant radial amplification of the initial peak overpressure was observed from 2 to 10 inches from the bomb. This contrasts with the results from the more stable doublet injector, in which radial wave growth was observed. Thus, difference in wave growth does not appear to relate to the stability characteristics of the two injectors.

Correlation With Cold-Characteristics. The preceding correlating models related the stability response directly to the rating techniques' parameters, rather than to their characteristics established in the cold flow experiments. The latter correlations would be of more fundamental value to the understanding of the rating techniques' effects and in comparing one technique to another.

Since the decay in initial peak pressure of a blast wave in air will in general be totally different than the blast wave behavior in a chamber full of burning propellants, the cold flow equations were used to find the initial peak pressure at the bomb surface. First, Eq. 12 was used to compute $\ln c_s$ at the bomb surface for each bomb used in the engine firings. Then the shock Hugoniot relation (Eq. 3) was used to convert to pressure. The predicted bomb initial pressures are as follows:

Weight	Thickness	$\ln c_s$	P_i, psi
13.5	0.17	-3.035	199.1
13.5	0.28	-3.312	113.3
13.5	0.50	-3.635	58.3
5.5	0.17	-3.199	142.5
5.5	0.28	-3.477	80.8
3.2	0.17	-3.299	116.4

Because of the simplicity of the models obtained using them, the pressure
data modified by incidence coefficients will be used. The bombs used
with the triplet injector varied only in charge weight. For the three
charge weights used, the equation $W = 3.67 - 0.0793 P_i + 0.000646 P_i^2$
holds. This may be substituted directly into Eq. 26 to obtain the
model:

$$\frac{P}{1 + \cos \alpha} = 74.3 - 0.605 P_i + 0.00493 P_i^2 - 10.4 \ell \qquad (27)$$

Due to the inclusion of the curvature term in P_i, this model is hard to
visualize immediately. The peak pressure predicted at $\ell = 3$ inches for
$P_i = 200$ is 120 psi and for $P_i = 50$ is 25 psi. At the midpoint $P_i = 125$,
the prediction is 45 psi, which is considerably less than the result of
72 psi obtained by linear interpolation between the two extremes.

The behavior of bombs in the doublet injector tests was described by a
somewhat more complex model because the bomb case thickness was allowed
to vary. Therefore a direct substitution into Eq. 25 is not possible.
Instead, a new correlation was computed using the predicted peak pressure
as a substitute for charge weight and case thickness. The resulting model
is as follows:

$$\frac{P}{1 + \cos \alpha} = 106.7 + 0.406 P_i + 5.84 y - 22.2 \ell \qquad (28)$$

Examination of the results indicated a residual effect of case thickness
apart from the effect of P_i. Therefore the following additional model
containing a T_c term plus the effect of radial position was computed:

$$\frac{P}{1 + \cos \alpha} = 26.0 + 0.643 \left(P_i + 244 T_c\right) + 5.17 y - 21.1 \ell + 3.03 r \qquad (29)$$

The multiple correlation coefficient and residual standard deviation for
this model are 0.87 and 18.8 psi, respectively.

The failure of the bomb's characteristic initial pressure to account completely for the effect of case thickness in the engine tests may be interpreted in several ways. The simplest is to assume that the case thickness is reduced by ablation before the bomb is fired, thereby giving results corresponding to a thinner case. To check this hypothesis, the composite term $(P + 244\ T_c)$ was evaluated for each bomb configuration to obtain an effective cold-characterization pressure. This was converted to velocity and used in Eq. 12, the cold-characterization equation, to compute an effective case thickness. For the six bomb types, these are as follows:

Charge Weight	Case Thickness	Effective Case Thickness
13.5	0.17	0.13
13.5	0.28	0.17
13.5	0.50	0.17
5.5	0.17	0.12
5.5	0.28	0.13
3.2	0.17	0.12

Although there is a great deal of error in approximating an ablation rate in this way, these data seem not to support the hypothesis. First, they indicate an excessively high ablation rate. Second, the reduction in thickness is not a constant for the six bombs. The discrepancy for the 0.50-inch case may be discounted as possibly due to a nonlinearity in the effect of case thickness, but even the remaining data do not support the assumption. The effect of ablation may be present, but it cannot account for the magnitude of observed anomalies.

Within the range of bombs considered, thickness has a very important effect on cold initial pressure. Therefore, another possible explanation is that the thickness term is expressing a nonlinearity in the model. Such a nonlinearity could arise from the fact that the cold characterizations were done at ambient pressure whereas the engine tests had a chamber pressure of 150 psi. Such a change had a minor effect on the cold-flow characteristics of the pulse gun, but was not examined experimentally for bombs.

<u>Bomb Orientation Effects</u>. In addition to the usual method of mounting the bombs from the baffle at different radial distances from the chamber axis, some tests were also made with the bombs installed with their cylindrical axes perpendicular to the chamber wall surface. Four tests (027, 030, 045, and 051) were run with the explosive bombs inserted through Photocon ports; two tests each with the triplet and doublet injectors, respectively.

No significant difference could be noted in the observed initial overpressures with respect to this different orientation. A difference was observed, however, with respect to the acoustic modal behavior. The first several cycles of instability with the triplet injector could not be identified in terms of any fundamental acoustic mode. The ultimate sustained instability, however, was the familiar coexistent third tangential and first radial modes. Slightly different results were observed with the doublet injector; the sustained instability initiated by bombs in Photocon ports was the second tangential mode for both firings. It will be noted that a similar behavior was obtained with the doublet injector and UDMH fuel. No apparent explanation can be given at this time.

Three doublet injector firings (064, 067, and 079) were made with bombs installed in the nozzle convergent section, 10.2 inches downstream of the injector face. A transparent combustor section was used on the last test, so that only one Photocon pressure measurement was obtained and that one was in the nozzle section. Results from the other two tests were considerably different from those obtained with baffle-mounted bombs.

The observed experimental values of initial overpressure were approximately five times greater than those calculated by Eq. 25. Obviously, the same correlation does not hold for the nozzle-mounted bombs as for bombs only half as far from the injector. Although no direct explanation for this effect was apparent, it is thought that it may be due either to reinforcement of the initial blast wave by a higher velocity nozzle-reflected shock or simply to a cumulative effect from the initial waves having propagated through burning sprays over a longer path. Whatever the reason for the phenomenon, it deserves further study since it is sometimes found—much to the investigators' confusion—that bombs placed in the nozzle are more effective in initiating instability than those located near the injector (Ref. 4).

203

<u>Pulse Guns</u>. The amplitudes of the initial disturbances generated by the pulse gun charges have also been reduced from the time-base expanded oscillographs. Some pressure data have been plotted in Fig. 72 through 80 vs the direct distance x from the chamber entry port to the Photocons. The solid data points represent those tests with sustained instabilities. The following trends are observed with respect to the initial wave growth.

Figure 72, 73, and 74 show the effect of the pulse gun charge size and axial distance from the injector upon the initial wave growth for the three different angular directions. Typical data are plotted for two charge sizes; 40 HB/20K and 10 HB/7.5K for the doublet injector. In all cases with the dynamically stable or unstable tests, the initial wave amplitude increased with distance from the transducer. and reached a maximum value diametrically opposite the point of entry of the disturbance. Negligible wave growth was observed for completely stable tests. A test was considered to be dynamically stable if it recovered from a rating device disturbance in less than 100 milliseconds. The initial pressure wave growth was attributed to energy addition from accelerated combustion as the wave traveled through the burning sprays. A definite trend was shown for the larger pulse charge sizes to generate higher combustion chamber initial peak pressures. This trend was most pronounced with radially and chordally directed pulse guns; differences observed near the pulse entry point with tangential pulse direction were effectively obscured by the time the initial waves had propagated across the chamber. The size of the disturbance, however, had no apparent relationship to the ultimate stability of the system.

With the exception of a few anomalous data from tangentially directed pulses with the triplet injector, weaker initial peak pressures were generated with pulse entry ports at distances further downstream from the injector face. This suggests that less unburned propellants were available at increased axial distances to support and amplify the disturbances.

In some instances the test-to-test reproducibility was poor. For example, two repeat pulse gun firings were made with 40 HB/20K charges during Test No. 005 and 012. The initial waves started out at greatly different
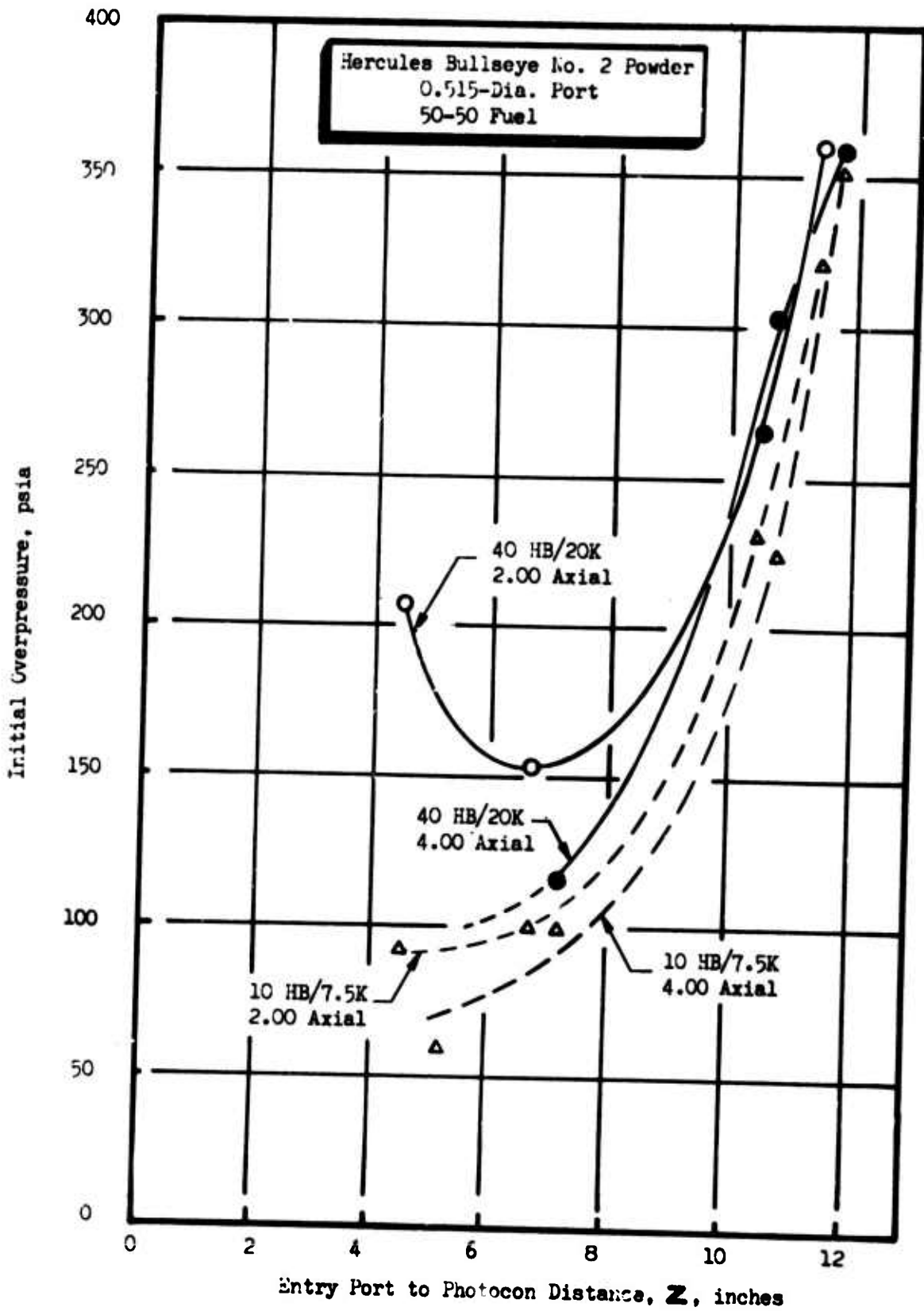
Figure 72. Initial Overpressure From Pulse Guns With Doublet Injector and Tangential Entry

205
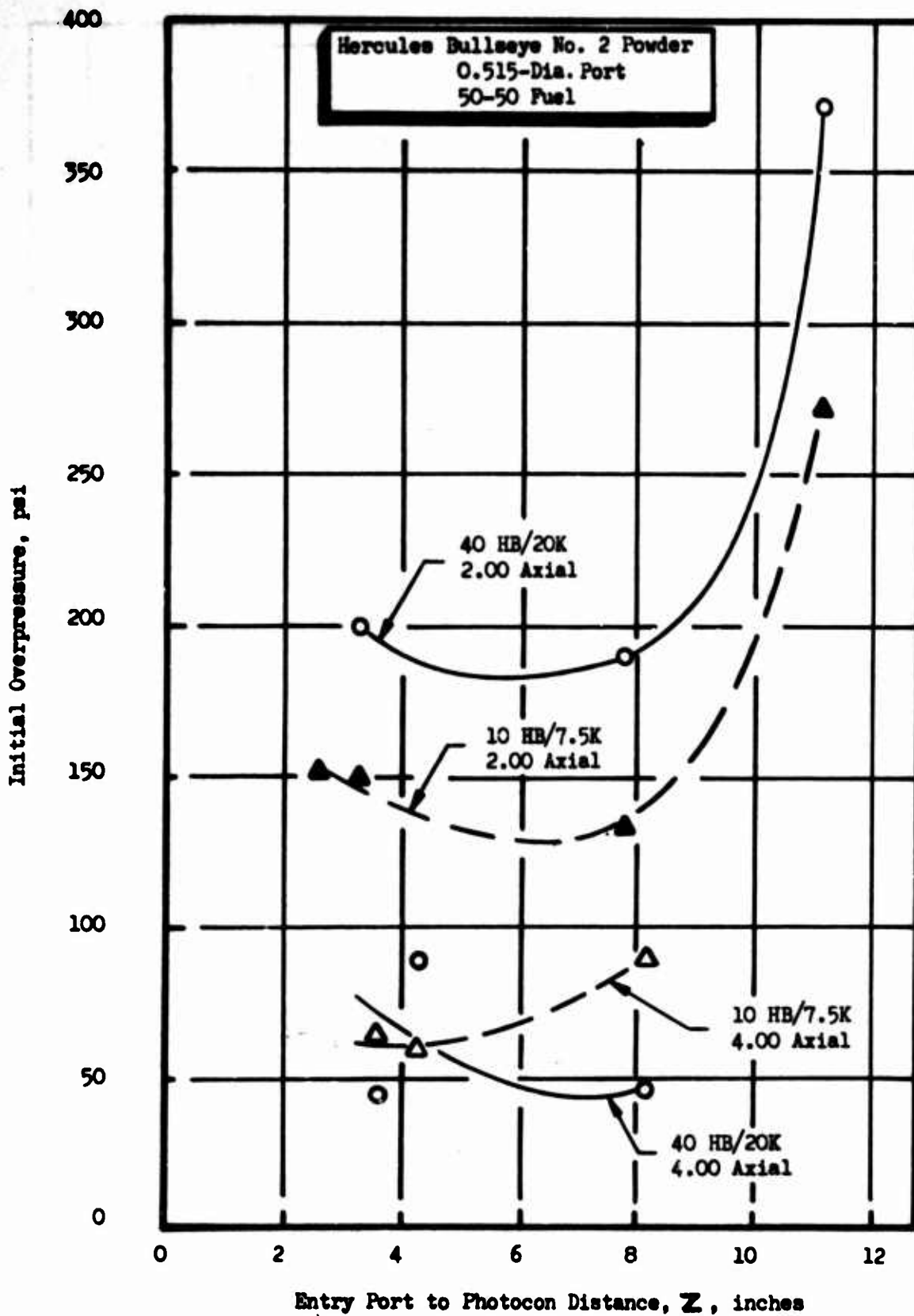
Figure 73. Initial Overpressures From Pulse Guns With Doublet Injector and Chordal Entry
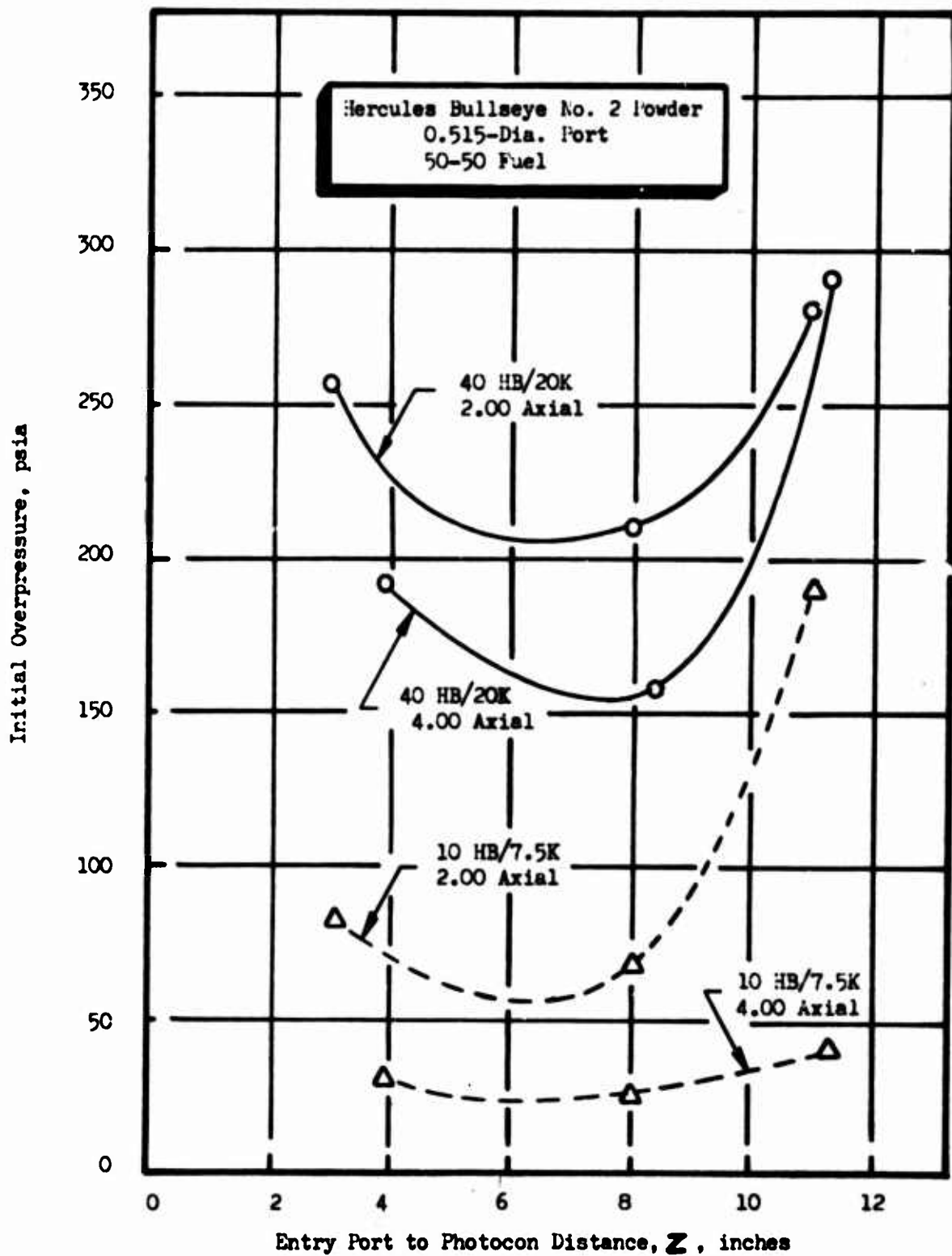
Figure 74. Initial Overpressures From Pulse Guns With Doublet
Injector and Radial Entry

207
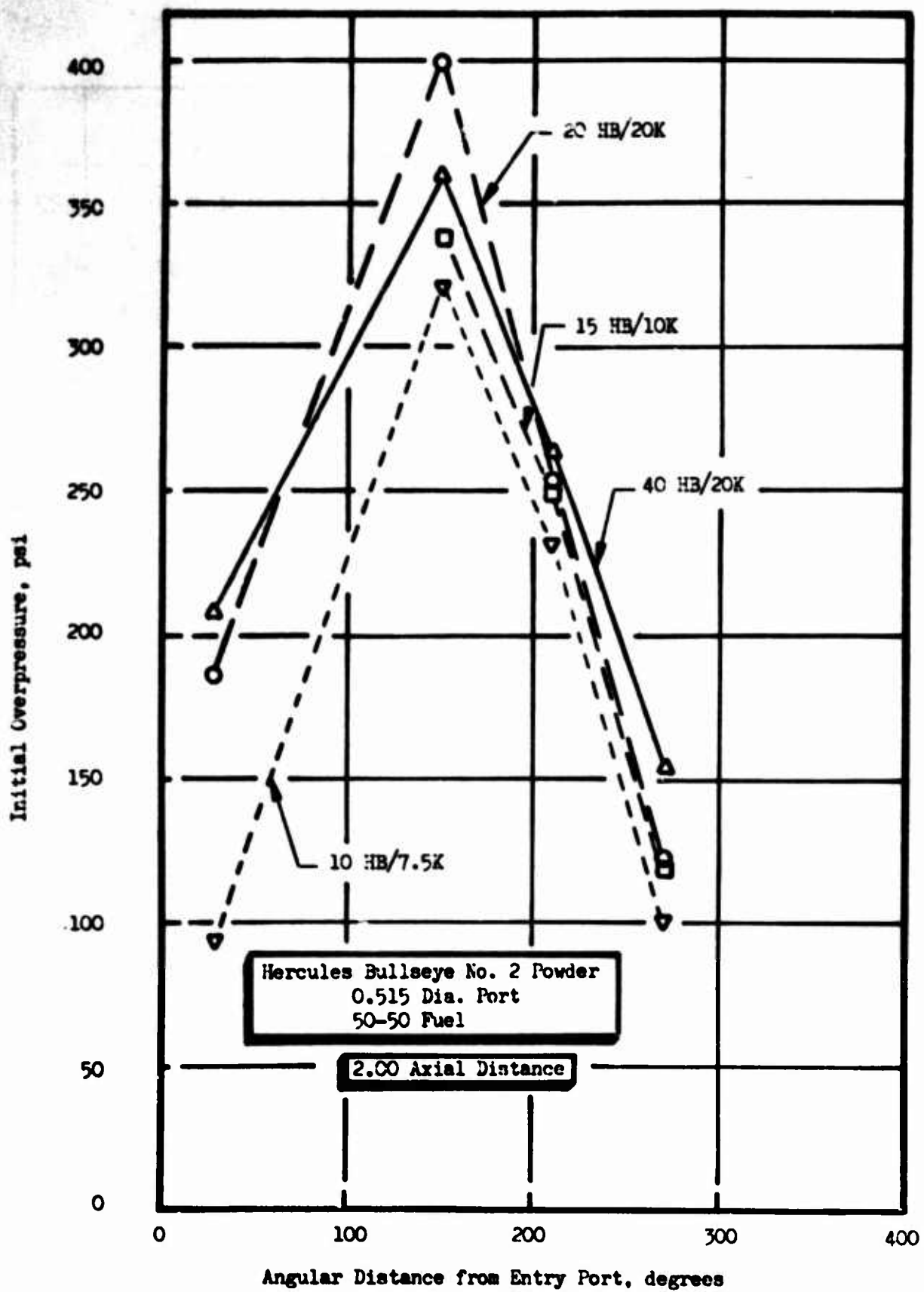
Figure 75. Initial Directional Pulse Gun Disturbance Wave Growth
With Doublet Injector and Tangential Entry

208
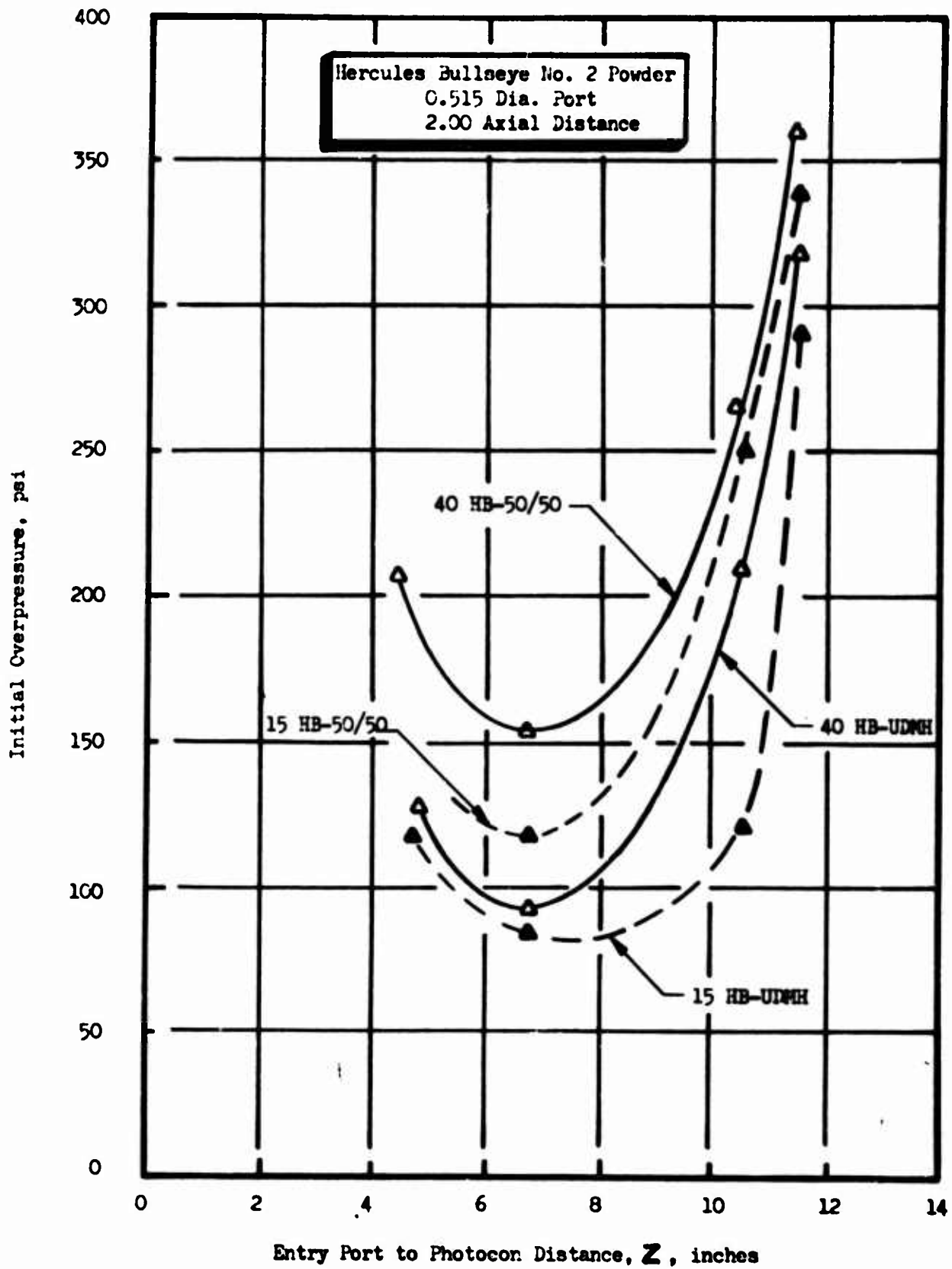
Figure 76. Effect of Fuel Type on Initial Overpressure From Pulse
Guns With Doublet Injector and Tangential Entry

209
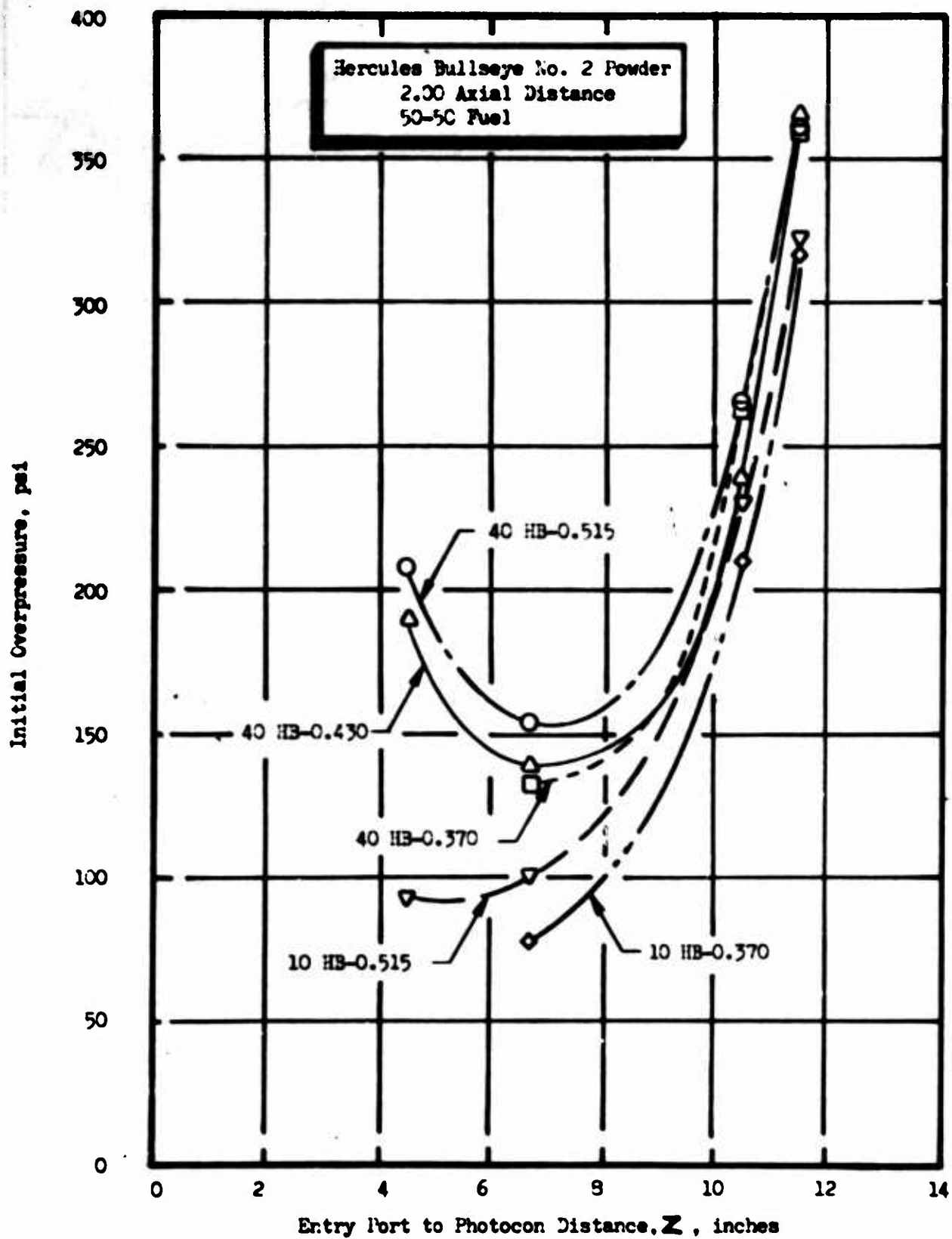
Figure 77. Effect of Port Size on Initial Overpressures From Pulse Guns With Doublet Injector and Tangential Entry
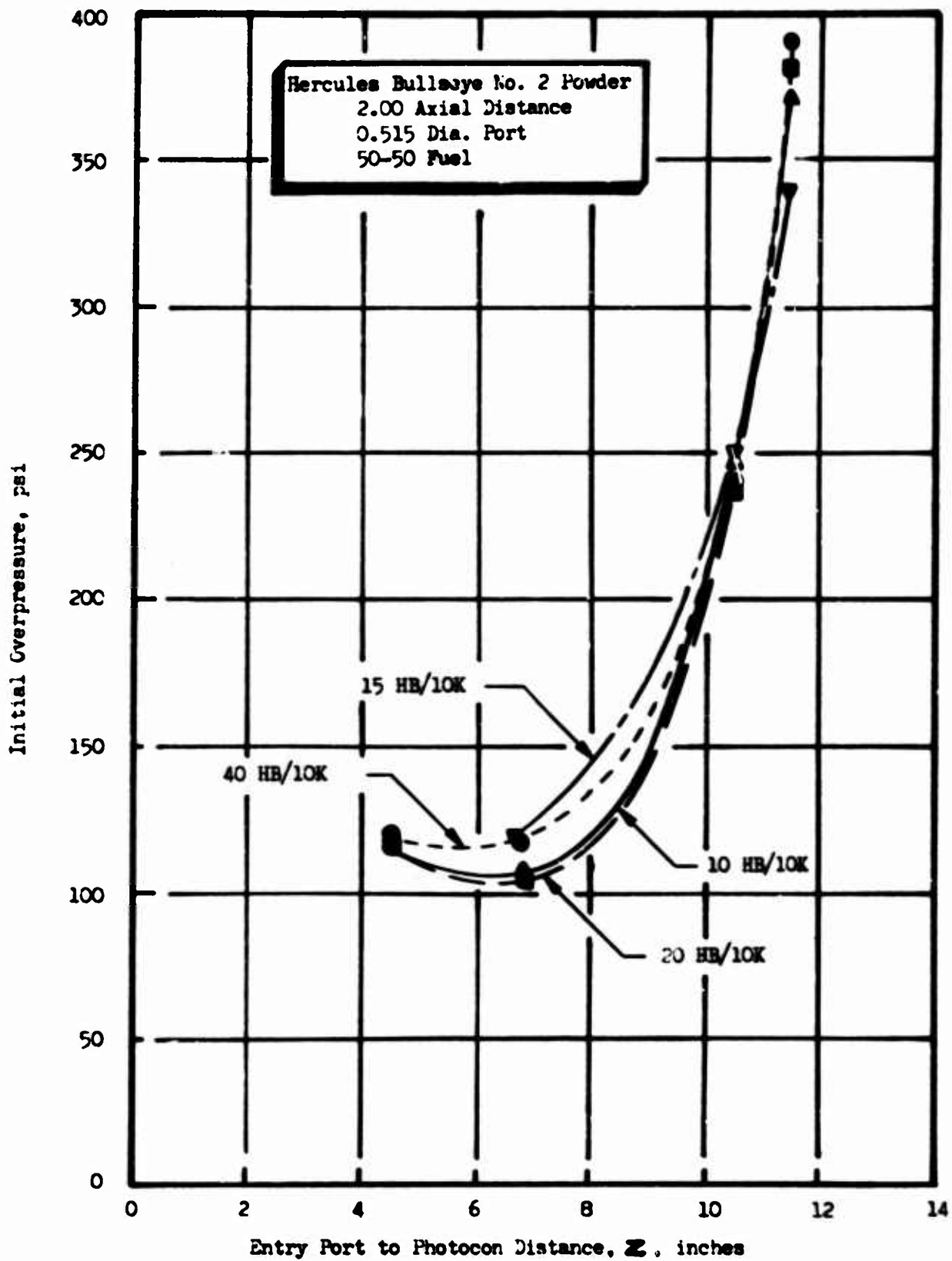
Figure 78. Effect of Mixed Charge Sizes on Initial Overpressures
From Pulse Guns With Doublet Injector and Tangential
Entry

211
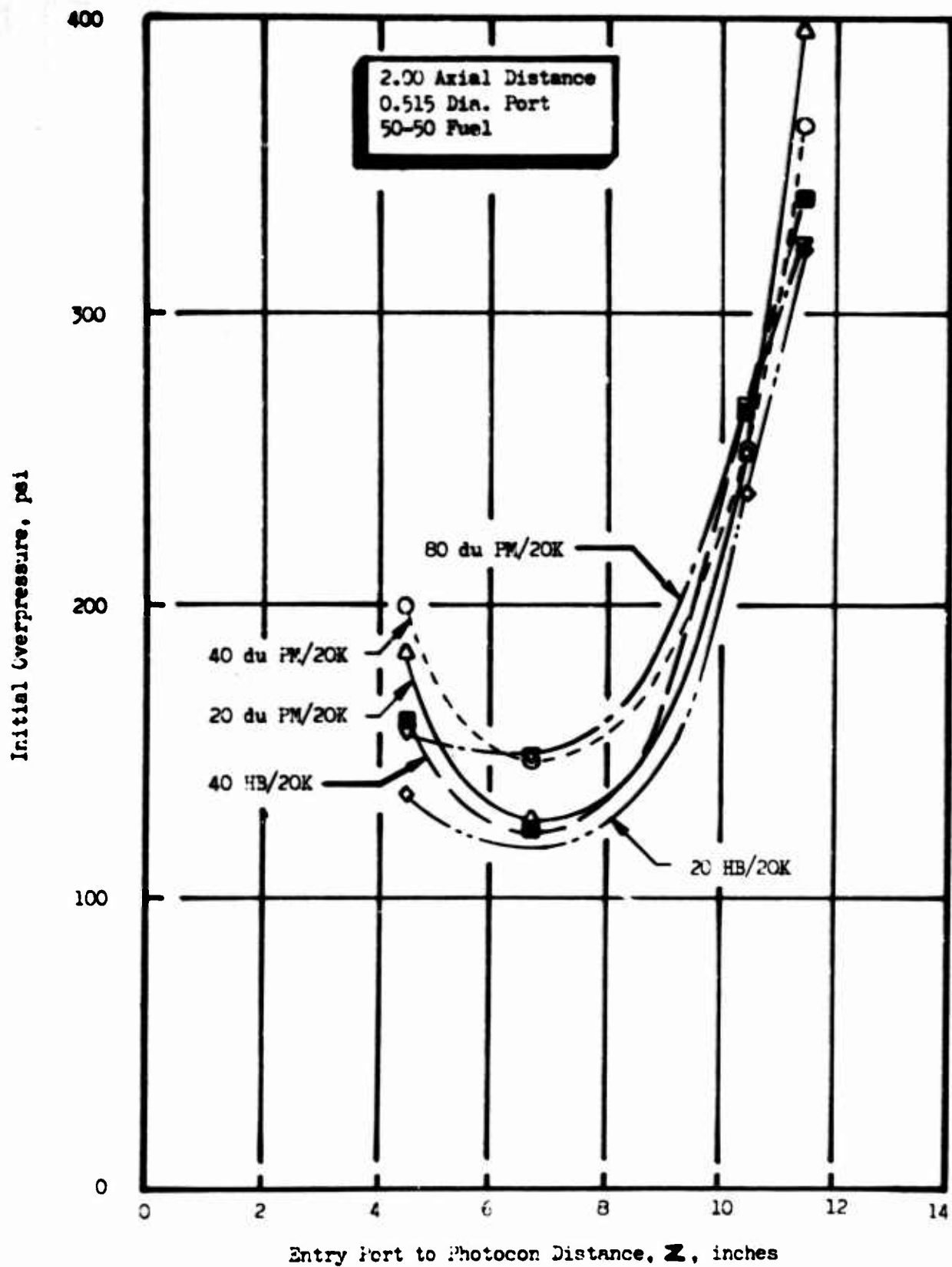
Figure 79. Effect of Powder Type on Initial Overpressures From
Pulse Guns With Doublet Injector and Tangential Entry
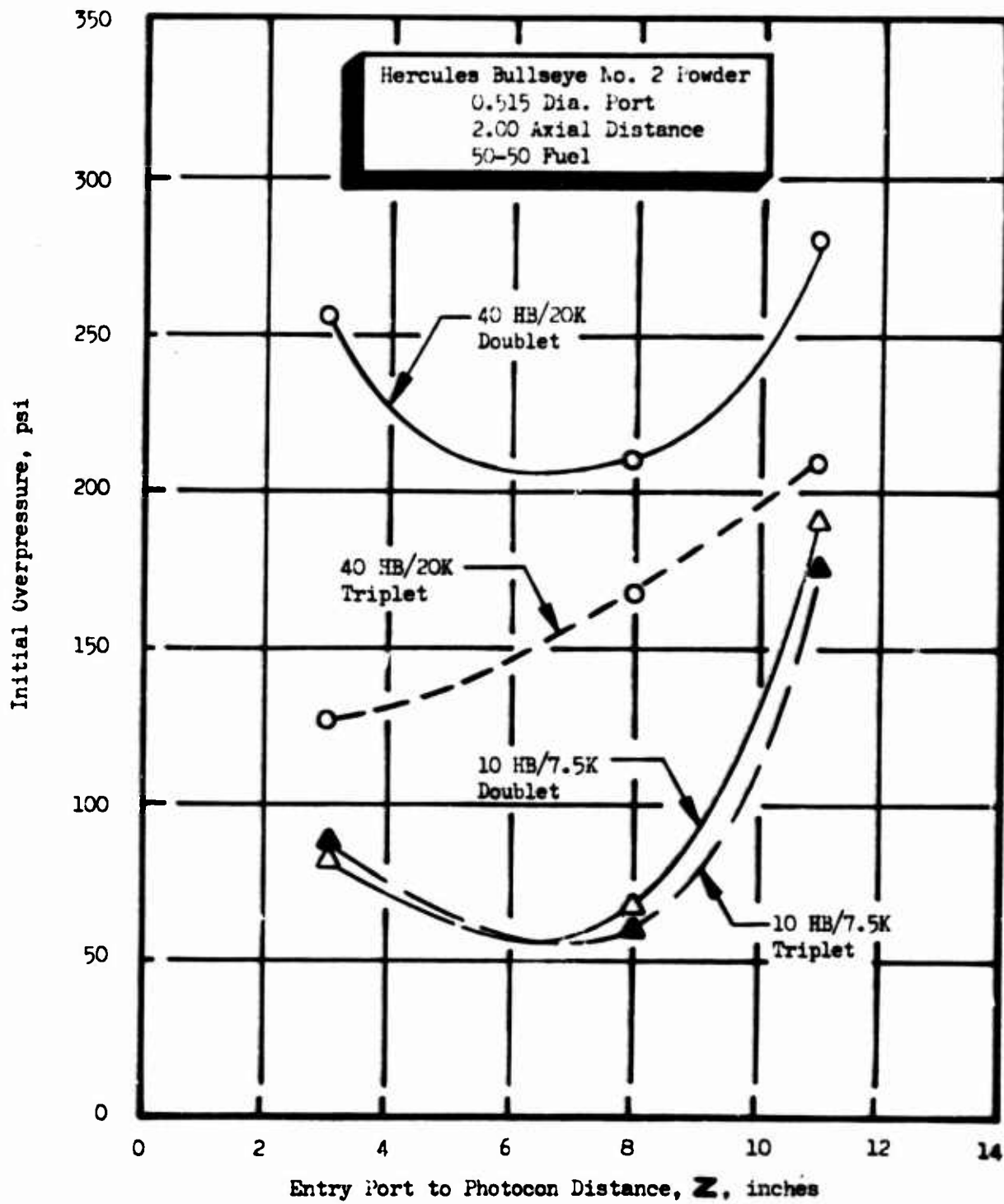
Figure 80. Effect of Injector Type on Initial Overpressures From
Pulse Guns With Radial Entry

213

amplitudes (about 80 and 180 psi, respectively), but eventually converged to the same value at a point opposite the shock entry. The mathematical correlations were difficult to obtain with the pulse guns due to the large data scatter. Nevertheless, generalizations can be drawn based upon the experimental results.

Initial wave growth from the tangentially orientated pulse gun propagated both spherically and circumferentially from the entrance port. The directionality effect is shown in Fig. 75. The angular displacement of each Photocon from the point of entry of the disturbance into the chamber, measured in the direction of wave propagations, is plotted as the abscissa. Thus, 180 degrees represents a wave travel half way around the chamber, or to a point diametrically opposite the point of introduction of the disturbance. As indicated previously, this point on the chamber represents the region of maximum wave growth.

As shown in Fig. 76, higher initial wave amplitudes were demonstrated with N_2H_4-UDMH(50-50) fuel than with UDMH. This is in agreement with the bomb results. Larger disturbances resulted with increased pulse gun barrel and port diameters as graphically illustrated in Fig. 77. This was probably caused by the increased attenuation of the blast wave as it propagated out of a smaller bore barrel into the chamber.

Three tests were made with mixed pulse gun charge sizes; 10,000 pound burst diaphragms were used for all tests. The standard charge consisted of a 1ᶠ ℬB/10K cartridge; the other three charges were 10 ℍB/10K, 20 ℍB/10K, and 40 HB/10K cartridges. No significant differences in the initial pulse amplitude were attributed to the variation in charge size with a fixed burst diaphragm, as shown in Fig. 78. Six hot-firing tests were made using charges of the slower burning duPont Military powder; results from three firings made at the 2-inch tangential boss are shown in Fig. 79. For comparison purposes, two similar test results are shown with Hercules Bullseye powder. The minor differences observed probably are not significant. Interestingly, all the charges plotted in Fig. 79 were with 20,000 psi burst diaphragms. Comparison with Fig. 78 suggests the possibility that the initial pressure wave amplitude is determined

214

solely by the burst diaphragm strength (and the propellant spray combustion field characteristics). This possibility is particularly intriguing when it is recalled that both the initial shock wave and the maximum blast wave pressure were reduced by a factor of 2 when the Hercules powder was replaced by the duPont powder in the cold-characterization testing.

A cross-plot of the data from both injectors using the radial entry pulse gun port is shown in Fig. 80. Almost identical wave growth behavior was obtained with the smaller 10 HB/7.5K pulse gun charges with the triplet and doublet injectors. Increased wave growth was observed with the doublet injector with the larger 40 HB/20K charges.

Descriptive Correlations. As with the bombs, the initial peak pressure in the rocket chamber due to the pulse gun firings have been studied as a function of pulse gun and engine parameters. In addition to the parameters which describe the charge (charge weight and burst diaphragm rating), the following additional parameters were included in the hot-firing experiment:

1. Pulse Gun-Transducer Angle θ, degrees/180

2. Axial Distance ℓ, inches

3. Pulse Gun Diameter D_{gun}, inches

4. Pulse Gun Chamber Angle β, degrees/180

The angle β between the pulse gun and the chamber is equal to 90 degrees for tangential bosses, 180 degrees for radially directed bosses, and 135 degrees for the intermediate (chordal) bosses. The barrel lengths, BL, (the distance from the burst diaphragm to point of chamber entry) associated with these three angles were 7.25, 5.69, and 6.12 inches, respectively. Both these variables cannot be used in the correlations since they are so closely related. Because barrel length is the more easily quantified, it was chosen as the independent variable. The pulse gun-transducer angle was measured from the center of the chamber and normalized by dividing by 180 degrees.

215
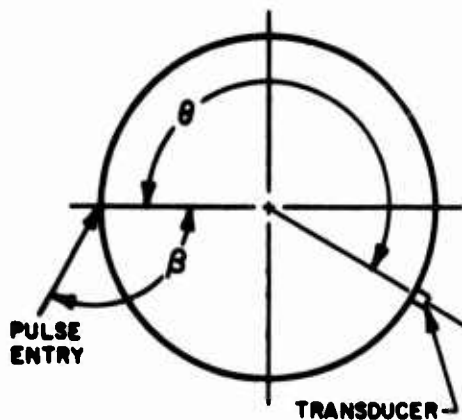
As one would expect from the results using bombs, the pressure wave resulting from the pulse-gun firings behaved differently with the two injectors. From the shape of the data, logarithmic models were chosen to represent the initial peak overpressure. The model found to best represent the triplet injector data is as follows:

$$\ln P = 32.4 - 12.0 \ln z + 0.459 (\ln z)^2 + 0.189 \ln W$$

$$- 15.4 \ln BL - 2.98 \ln BL \ln \theta + 6.11 BL \ln z + 5.47 \ln \theta \tag{30}$$

The multiple correlation coefficient is 0.92; the residual standard deviation is 0.215.

The only parameter in Eq. 30 that is a function solely of the pulse gun is the charge weight W. Over the range of variation of this parameter, from 10 to 80 grains, a 50-percent increase in ΔP was produced. This is a considerably smaller effect of charge weight than was observed with a much smaller range of charges for bombs. The burst diaphragm strength was not included in the model because it was not varied independently.

Unlike the bomb model, the pulse gun model contains no term in l, the axial position of the triggering device. Although it does not show up in Eq. 30, the results of the data plots consistently agree that the

216

initial waves from pulse guns at 4 inches from the injector had lower amplitudes than those from guns at 2 inches.

The effect of transducer distance z is complex, as it was in the bomb models before employing incidence coefficients. An examination of the three terms involving ln z suggests that there is pressure growth away from the pulse entry port. This effect is further complicated by the presence of the angle between the pulse gun and the transducer. For some ports, hence for some barrel lengths, the transducer distance z and transducer angle θ are nearly linearly related. It seems plausible, therefore, that the three terms involving barrel length are simply further manifestation of the effect of transducer distance.

It was hoped that modifying the raw peak pressure data by incidence coefficients would clear up the complexities of the model as it did with the bomb data. If the propagation of the shock wave is essentially spherical from the pulse entry port, then the incidence coefficients are calculated in exactly the same way as for bombs. The following model was fit using the pressure data adjusted in this way:

$$\ln \left(\frac{P}{1 + \cos \alpha} \right) = 3.69 + 0.183 \ln W + 0.0804 \, \ell - 0.259 \, z$$
$$+ 0.0223 \, y^2 + 0.650 \, \beta \tag{31}$$

The residual standard deviation, which should be smaller by a factor of $1/(1 + \bar{c})$, where $\bar{c} = 0.64$ is the average value of the cosine of the angle α, has increased from 0.215 to 0.27, and the multiple correlation coefficient has correspondingly decreased from 92 percent to 77 percent. Further, the signs on some of the terms appear to be of questionable validity.

Modification of the data by the simple incidence coefficients used for bombs thus does not permit a good fit with a simple model. We conclude, therefore, that with the triplet injector the pressure waves produced by pulse guns have a strong directional effect, rather than being

217

essentially spherical with only a slight distortion in the direction of the barrel. A further analysis of the angle with which the shock front hit each transducer would be difficult and tenuous based on the data made available by this program.

The model which best fits the uncorrected pulse-gun data using the doublet injector, 50-50 fuel, and Hercules Bullseye powder is as follows:

$$\ln P = 50.8 + 1.40 \ln W - 0.244 (\ln W)^2 + 0.0728 \ln W \ln P_{db}$$

$$- 4.92 \ln s + 1.56 (\ln s)^2 + 0.512 \ln BL$$

$$- 0.104 \ln \ell - 9.31 \ln BL \ln \theta \tag{32}$$

The multiple correlation coefficient and residual standard deviation using the model are 93 percent and 0.19, respectively.

The terms involving the gun parameters are the same as those which appear in the fits of the cold characterization data. The way in which they appear differs from the cold results in two respects: (1) The magnitude of the influe e of these parameters on the pressure is much less (an increase in char_e weight from 10 to 40 grains produced nearly a fourfold increase in pressure during the cold tests but only about a 25-percent increase during engine firings), and (2) the coefficients on the ln W and $(\ln W)^2$ terms have reversed in sign. The curve still has positive slope, but the curvature has reversed. Thus, we are seeing an asymptotic effect of charge weight.

The involvement of the transducer distance and angle terms in Eq. 32 is much less than for the triplet-injector model. The general appearance of the terms in s, BL, and θ suggests that the pressure waves may be much more nearly spherical with the doublet than with the triplet injector. Although, these look like good data with which to continue evaluation of the incidence coefficient concept, this was not accomplished in the current program.

218

Correlation with Cold Characteristics. The parameters which have
to do with the pulse after it arrives in the chamber and which were
therefore allowed to remain in the models are: z, θ, ℓ, D_{gun} (which
was not varied in the cold-flow experiments), β, and fuel type F. The
data for the pulse gun characteristics were estimated using Eq. 16, 17,
and 18 and the hot-firing input parameter values were taken from the
previous analysis. For each injector design, empirical models were com-
puted using each of the estimated pulse gun characteristics peak pressure,
impulse, and velocity. In Table 18 the estimated coefficients for all
three cases are entered with the coefficient for the pulse gun character-
istic heading the corresponding column. Each column of the table may
easily be converted into an equation. For example, the first column be-
comes $\ln P = 0.5867 \ln P_{max} + 4.70 \ln z + 0.4746 \ln \theta + $ etc. The multiple
correlation coefficients were all over 93 percent, indicating that about
87 percent of the variations in $\ln P$ are explained by hot firing input
parameters and pulse gun characteristics. The standard errors about the
regression lines were 0.214, 0.221, and 0.217 for columns one, two, and
three, respectively.

Since the peak pressure, positive impulse, and shock wave velocity were
so highly related, the three equations are very similar, except for the
constant term. The constant is different from model to model because
the three parameters are measured in different units. Once again, the
models contain an abundance of terms in z, θ, and β, which were used in
these models in place of BL and reflection coefficients.

Similar results were obtained for the doublet injector as shown in
Table 19. The data for duPont Military powder and for the UDMH fuel
were included in the analysis. The fits are somewhat worse than for the
triplet. The standard errors are 0.209, 0.204, and 0.202 for the three
models, respectively; the multiple correlation coefficients are all over
0.85.

219

TABLE 18

COEFFICIENTS FOR TERMS IN EQUATIONS RELATING
INITIAL PRESSURE AMPLITUDE TO PULSE GUN
CHARACTERISTICS

(TRIPLET INJECTOR)

Coefficient / Term	Characteristics		
	Maximum Blast Pressure	Positive Impulse	Shock Wave Velocity
ln (Characteristic)	0.5867	0.1542	0.1570
Constant	0.0	-6.48	-8.75
ln z	4.70	-3.15	-3.12
ln θ	0.4746	0.4812	0.4846
ln l	3.12	3.09	3.12
ln β	1.71	1.79	1.69
$(\ln z)^2$	0.8749	0.8799	0.8706
$(\ln l)^2$	-2.51	-2.49	-2.54
ln z · ln l	0.8368	0.8397	0.8546
ln z · ln β	-0.6580	-0.6663	-0.6523
ln θ · ln l	-0.6430	-0.6465	-0.6543

220

TABLE 19

COEFFICIENTS FOR TERMS IN EQUATIONS RELATING
INITIAL PRESSURE AMPLITUDE TO PULSE GUN
CHARACTERISTICS

(DOUBLET INJECTOR)

Coefficient / Term	Characteristics		
	Maximum Blast Pressure	Positive Impulse	Shock Wave Velocity
ln (Characteristic)	0.8785	0.2327	0.2593
Constant	0.0	6.38	8.75
ln z	-4.89	-4.93	-4.98
ln θ	0.0	-0.1785	-0.1756
ln β	-0.1446	-0.0926	-0.1185
$F^{(1)}$	0.217	0.248	0.251
$(\ln z)^2$	1.54	1.58	1.57
ln $\theta \cdot$ ln ℓ	-0.1725	0.0	0.0

[1] The fuel factor F was set equal to 1.0 for N_2H_4-UDMH (50-50) fuel and to 0.0 for UDMH/fuel

221

Initial Instability Modes

Consideration of the first few cycles of instability initiated by bombs suggests that there are at least four categories of initial behavior which may be identified:

1. Bombs in the center of the combustion chamber initiated the first radial acoustic mode.

2. The smallest bombs, near the wall or at the midradius, sometimes initiated the first tangential acoustic mode.

3. Other bombs in these locations initiated the second tangential acoustic mode.

4. Some bombs near the wall and at the midradius initiated coexistent first and second tangential acoustic modes.

Similarly, the initial instabilities caused by the pulse gun disturbances can be categorized as follows:

1. Pulse guns directed tangentially with both injectors initiated predominantly the spinning first tangential acoustic mode.

2. Pulse guns directed chordally with the triplet injector initiated coexistent first and third tangential acoustic modes.

3. Pulse guns directed chordally with the doublet injector initiated either the spinning first or standing second tangential acoustic modes.

4. Pulse guns directed radially with both injectors initiated either the standing first, second, or third tangential acoustic modes, singularly or coexistent.

222

Subsequent Modes

The propagation of a moderately high amplitude bomb or pulse gun pressure
wave through the steadily burning propellant combustion medium may so
alter the burning rate of that medium that it is rapidly consumed. Such
higher-than-steady-state combustion gas generation raises the mean chamber
pressure. This leads (through the same mechanisms that dominate the
occurrence, frequency and amplitude of chugging instability) to one or
more cyclical oscillations in mean chamber pressure about the steady-
state value.

These low frequency oscillations are apparent in pressure traces such
as Fig. 52 and streak photographs, Fig. 60 and 61, but are not in-
dicated in the bar-chart stability summaries of Fig. 53 through 57.
There is some evidence that the variations in predominant acoustic modes
shown there may be associated with particular times in the low-frequency
pressure oscillations. The initial mode of acoustic instability, for
example, usually decays rapidly during the pressure decay that follows
the initial steady-state spray burnout. Then, as the mean pressure falls
below the steady-state value and the propellant injection rates begin to
exceed their average values, the conditions that ultimately determine
whether an instability will be sustained or not are apparently established.
During this time, the rate of amplification for the first tangential
acoustic mode (whether or not it was evident before) appears to be crucial.

Whenever an instability was sustained following a bomb or pulse gun dis-
turbance during these experiments, the initially triggered mode and any

intermediate modes were replaced within a few milliseconds by coexistent third tangential and first radial acoustic modes. Because the third tangential is the lowest order tangential acoustic mode whose velocity nodal pattern matches the boundary conditions imposed by a three-vane baffle configuration, it is the one sustained and, since the first radial mode is so near in frequency and can also match the baffle boundary conditions, it is excited, too. With the exception of the first radial mode initiated by bombs at the chamber's axis, the sustained third tangential mode appears to have been driven only by the first tangential mode having been amplified above some threshold amplitude before the low-frequency, mean pressure oscillations had decayed and converged on an equilibrium mean chamber pressure. Once the crucial point was passed and it was established that the third tangential mode would be sustained, the first tangential mode was more or less rapidly damped and disappeared. An interesting corollary of this observation that the first tangential mode cannot survive the presence of the third tangential is suggested by several of the pulse gun tests: if the third tangential mode were present in the initial pressure oscillations, it appeared to prevent the first tangential mode from being amplified enough to drive a sustained third tangential mode following the low-frequency oscillation in mean pressure.

When the doublet injector was fired with UDMH fuel, the second tangential mode was a predominant contributor to about half of the instances of sustained instability. The reason for this tendency was not discerned.

The occurrence of at least some conflicting evidence in such a program is inevitable. As an example, the pressure records following explosion of 20HB/20K pulse gun charges during Tests No. 005 and 012 are superimposed on each other in Fig. 81. These tests were essentially precise replicates (Table 11) and the pressure traces are nearly identical for about 4 milliseconds after pulse gun initiation. Then the spinning first tangential acoustic mode during Test No. 005 decayed while that in Test No. 012 continued to be amplified and, after about 3 more milliseconds, drove the combined third tangential and first radial modes.
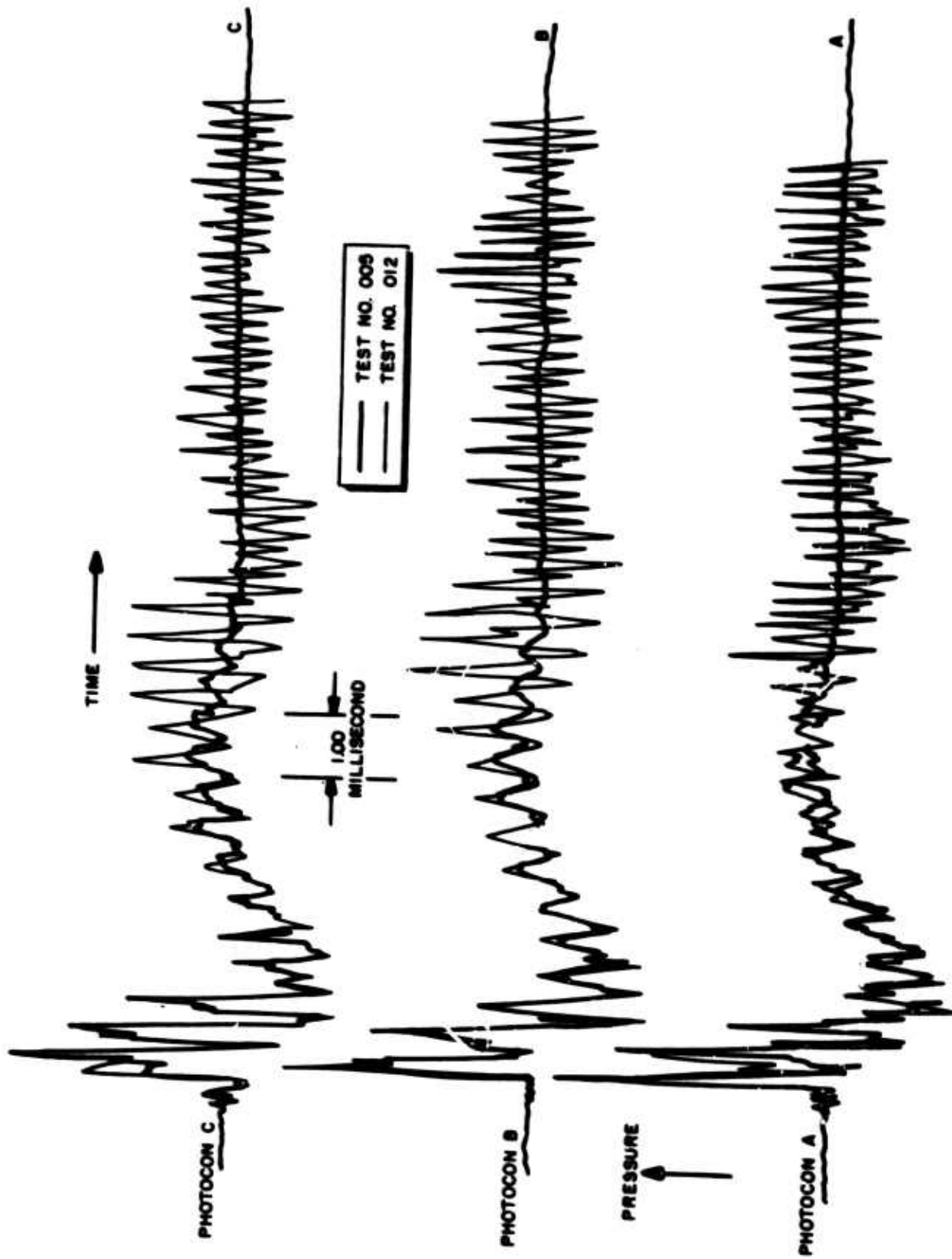
Figure 81. Pressure Traces Superimposed From Two Tests With 40MB 20K Pulse Gun Charges

225

<u>Sustain or Damp Characteristics</u>. It would be highly desirable to be able to predict dynamic stability of the motor as a function of the location and/or characteristic of the rating device; for example, the magnitude of the initial overpressure in the chamber. With the pulse gun disturbances, there appeared to be a threshold value of peak overpressure of 40 psia, below which the combustion process remained stable and was insensitive to wave amplification. Such was not the case with bombs. Once the initial threshold was exceeded with pulse guns such a relationship to ultimate stability ceased. The darkened points on Fig. 72 through 80 represent those tests with sustained combustion instabilities. The unstable tests occurred randomly without regard to the initial peak pressures.

The only parameters having an unambiguous effect on ultimate stability as determined by bombs were injector type and fuel. With the triplet injector the bomb-induced disturbances damped only 4 times in 18 tests, whereas 19 of 26 tests damped with the doublet injector. With UDMH fuel, all 5 bomb tests led to sustained oscillations. The ultimate damp/sustain behavior of the bomb-induced disturbances is shown in Fig. 82.

The pulse gun-induced disturbance with the triplet damped 19 times in 31 tests. Similiarly, 39 tests in 50 recovered with the doublet injector. Using UDMH fuel, 3 of 6 tests with pulse guns recovered. Combustor damp/ sustain behavior with pulse guns is summarized in Fig. 83.

For the triplet injector, the dynamic stability with bombs depended randomly on bomb parameters (W and T_c), bomb radial (r) and axial (ℓ) coordinates, and on the magnitude of the initial overpressure. This is implied by the fact that for any dynamically stable test, tests with sustained instabilities can be found with higher or lower bomb sizes and greater or smaller ℓ's or r's.

The same can be said for the doublet injector with the following exception. All three bombs on the chamber axis caused sustained instabilities. It appeared reasonable that this was a most sensitive location for the
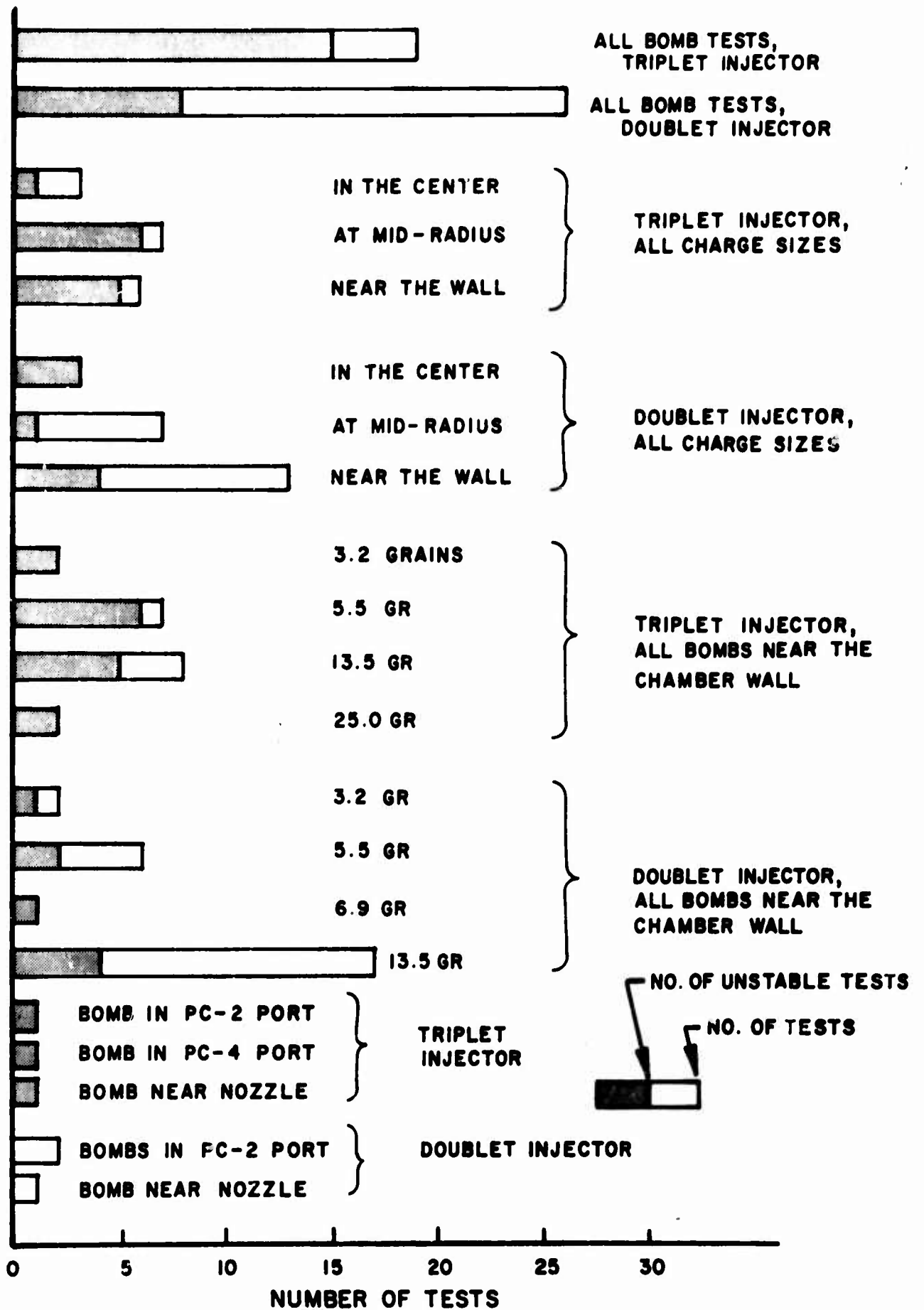
Figure 82. Stability of Tests With Bombs (50-50 Fuel)

227
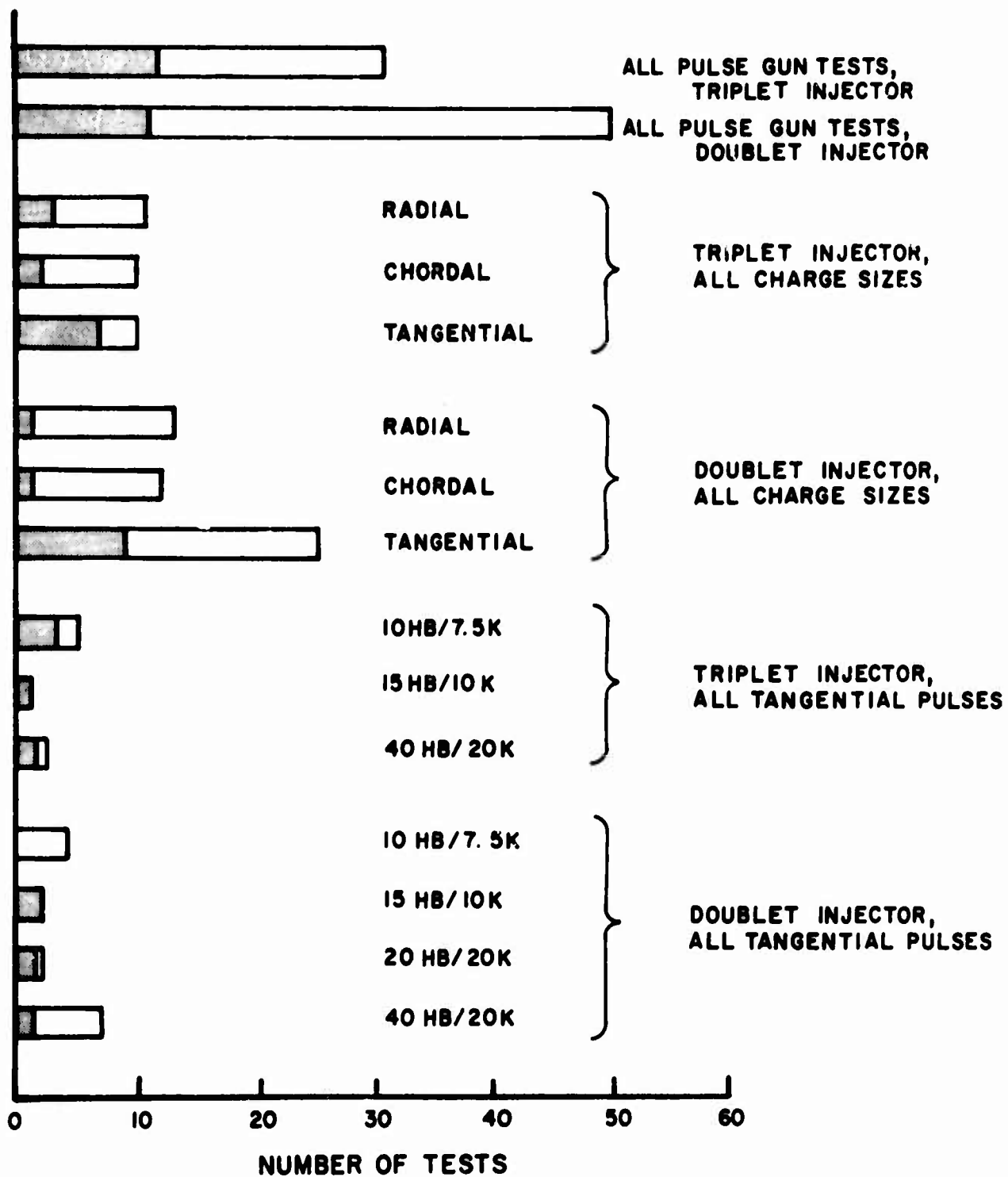
Figure 83. Stability of Tests With Pulse Guns (50-50 Fuel)

228

disturbance since for the doublet injector the first radial mode which was immediately initiated by such bombs, survived the chug and thus drove sustained coexistent first radial and third tangential modes. The incidence of sustained oscillations was only slightly less for mid-radial bombs than for those near the wall (14.3 vs 23 percent). In addition to the effect of radial position, moving the bomb further downstream led to sustained instability in two cases (compare run 053 [stable] vs 054 and run 050 [stable] vs 047).

This was in spite of the fact that the initial overpressures were weaker for the downstream bombs.

In general, the magnitude of initial overpressure could not be correlated with damping or sustaining instability. In Fig. 84 , damp times are plotted against initial overpressures (as would be seen by a pressure transducer one chamber radius away from the bomb axis). The scatter is obvious, although for the stable tests the damp times fall below an envelope which increases with pressure. Sustained instabilities occurred over the entire range of overpressure, however. One interesting incident is that of the seven mid-radial bombs (doublet injector), only the one generating the weakest initial disturbance (Fig. 68) failed to damp. This "upper threshold" did not occur for radial bombs and is not considered significant. Attempts to correlate damp time with bomb position failed.

The highest incidence of triplet instability with the pulse guns occurred with the 15HB/10K charge sizes; four out of five tests resulted in sustained instabilities. Seven out of ten tests with the triplet remained unstable with the pulse gun fired tangentially.

In every case of a sustained instability with both injectors and with N_2H_4-UDMH(50-50) fuel, the first radial and/or third tangential mode prevailed. Among eight doublet tests with UDMH fuel in which instability was sustained, two bomb and three pulse gun firings resulted in a sustained second tangential mode.

229
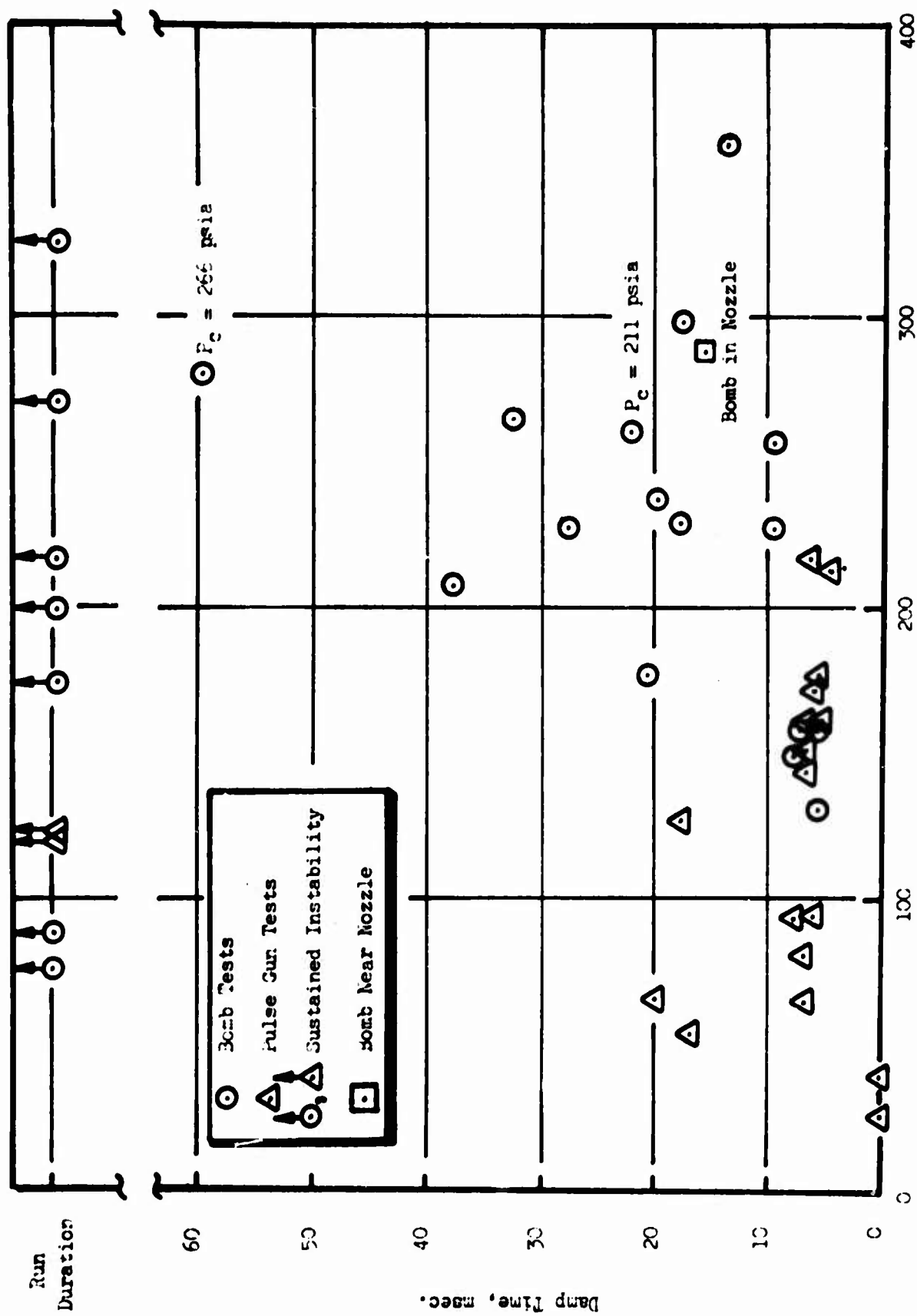
Figure 84. Pressure Oscillation Damp Times for Bombs and Pulse Guns, Doublet Injector (50-50 Fuel)

Amplitudes of Sustained Instabilities. The amplitudes of sustained in-
stabilities with both injectors and fuel types are compared in Fig. 85 .
For each run, estimated average oscillation amplitudes were measured
with Photocons at two axial positions. In each case these transducers
were located essentially on the third tangential mode nodal points so it
is primarily the amplitude of the accompanying first radial mode that is
measured. For three runs with the doublet injector (047, 048, 082) with
N_2H_4-UDMH(50-50) fuel, the agreement is within the accuracy of measuring
the average amplitude (± 10 psi). This seems to verify the concept that
the amplitude of the sustained mode is dependent only on the run conditions
and not the initiating disturbance. UDMH fuel with the doublet injector
and N_2H_4-UDMH(50-50) fuel with the triplet injector gave amplitudes of
the sustained instabilities which were higher than those with N_2H_4-UDMH(50-50)
and the doublet injector. These data are consistent with the same UDMH
and triplet tests having exhibited lower initial pressure wave amplitudes.
Both phenomena probably stem from more concentrated combustion nearer to
the injector.

As described previously, in all sustained instabilities with N_2H_4-UDMH(50-50)
fuel, coexisting first radial and third tangential modes are believed to
be present. Analysis of the records of Photocons H and I* in runs 080
through 083 indicates that the sustained peak-to-peak-oscillation amplitude
of the first radial mode was about 81 psi while that of the third tangential
mode was about 164 psi. Photocons A, B, and C (which are supposedly on
the third tangential node and measure only the first radial) average about
90 psi peak-to-peak which may be due to their "seeing" a little of the
third tangential mode.

---

*Photocons H and I show a distinct "beat" which has a frequency close to
the difference in the theoretical frequencies of the first radial and
third tangential modes. Applying simple sinusoidal analysis, the beat
maximum is the sum of the amplitudes of the two modes, while the beat
minimum is the difference of the respective amplitudes. Since these
transducers were midway between the third tangential nodes and antinodes,
the third tangential amplitude calculated still had to be corrected to
its value at the antinode.
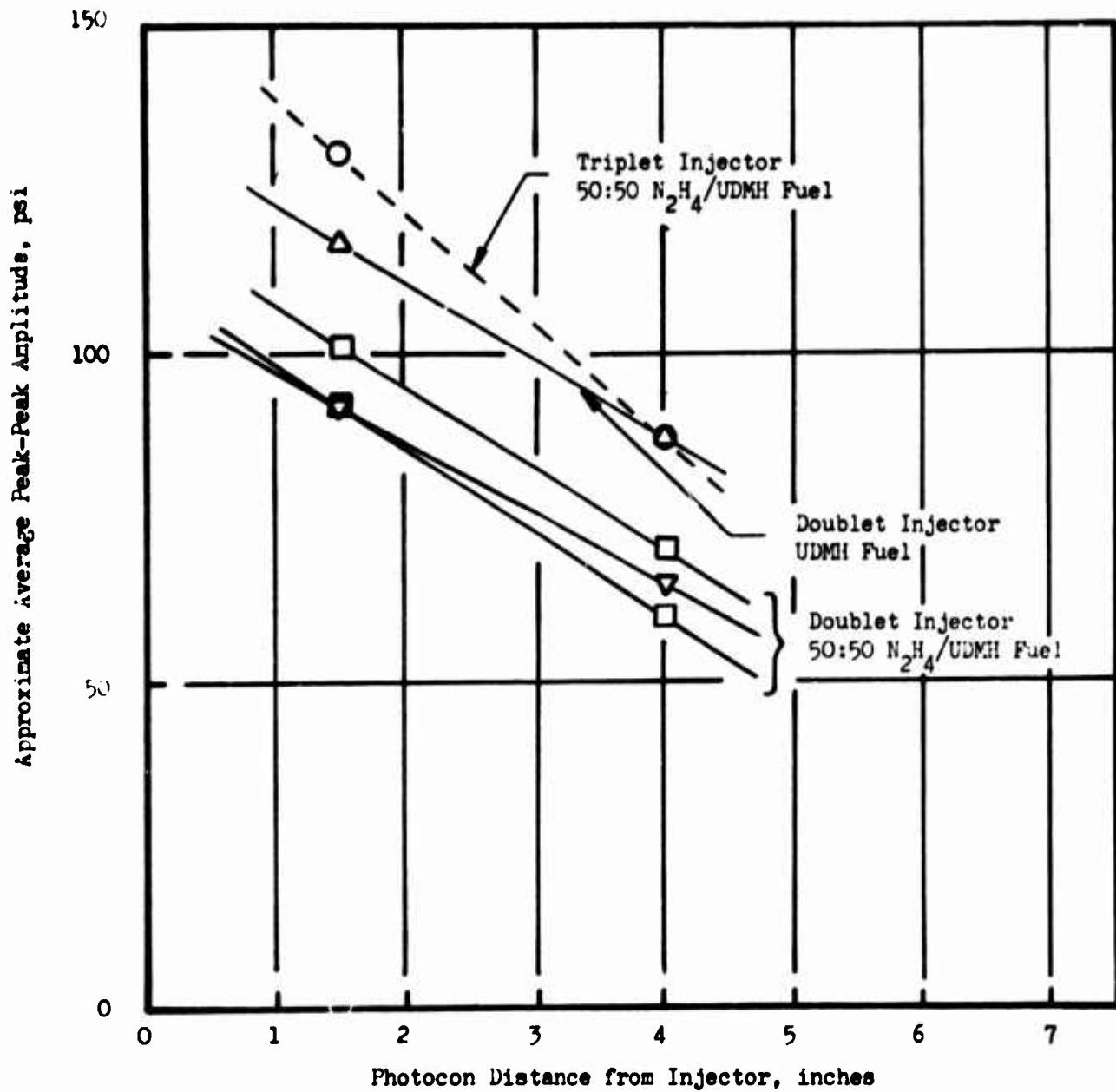
Figure 85. Amplitudes of Sustained Instabilities

Demonstration Tests

Based upon the data obtained during the experimental hot-firing program, analytical models were developed that correlated the combustor response (in terms of the initial peak overpressure) to the rating device's input parameters or characteristics. A short series of additional hot-firings using the doublet injector and N_2H_4-UDMH(50-50) fuel were made to demonstrate the accuracy of the analytical models. The triplet injector was damaged earlier in the program and therefore could not be used during the demonstration firings. The correlations obtained (Eq. 25 and 32) during the analysis were used to predict the motor's initial disturbance pressure growth for rating devices' parameters or motor conditions not previously tested.

A total of seven demonstration tests were made; six bombs were fired, two at elevated chamber pressures of 211 and 266 psia, respectively. Four pulse gun charges were fired with two at the higher chamber pressures. The input parameters varied for the demonstration firings are listed in Table 20 . A complete description of the rating device parameters were given in Tables 13 and 14.

In addition to the parametric changes made in the rating devices, two new chamber Photocons were installed with different values of transducer distance, z. In some instances, a Photocon used in the demonstration firings was as close as 1.80 inches from the disturbance. The correlations were based upon data with Photocons no closer than 2.95 and 2.60 inches for the bombs and pulse guns, respectively. Those points below 2.60 inches, therefore, represent input conditions outside of the range upon which the model was based.

The demonstration firing results are shown in Fig. 86 through 89 . A correlating line has been drawn through the individual predicted points (solid) for each test. The experimental points are also plotted. The percent error between the predicted values and the actual experimental data were calculated at several discrete values of z by the following equation.

233

TABLE 20

RATING DEVICE PARAMETERS FOR DEMONSTRATION FIRINGS*

Test No.	Device	Reason for Selection
080	Bomb	The wall thickness was 0.062-inch, which was half the thickness of the nylon cases previously fired.
081	Bomb	The axial distance was 2.55 inches, which was closer to the doublet injector face than bombs previously tested.
082	Bomb	The charge size was 6.9-grains of PETN, which was intermediate between the previous charge sizes of 5.5 and 13.5 grains.
083	Bomb	The wall thickness was 0.250 inch, which was intermediate between the previous 0.170- and 0.280-inch nylon wall case thickness.
084-8**	Pulse Gun	The axial distance was 3.00 inches, which was intermediate between 2.00 and 4.00 inches for previous tests with 40HB/20K charges and tangential entry.
084-5	Pulse Gun	The axial distance was 3.00 inches, which was intermediate and also the charge size 40HB/7.5K was mixed.
085	Bomb	A repeat charge size of 13.5-grains with a 3.23-inch axial distance was made at 211-psia chamber pressure.
085-7	Pulse Gun	A repeat charge size of 15HB/10K and 2.00-inch axial distance was made at 211-psia chamber pressure.
086	Bomb	Same as 085 except at 266-psia chamber pressure.
086-7	Pulse Gun	Same as 085 except at 266-psia chamber pressure.

*Complete descriptions are given in Tables 13 and 14

**The dash number refers to the boss orientation (Fig. 45)
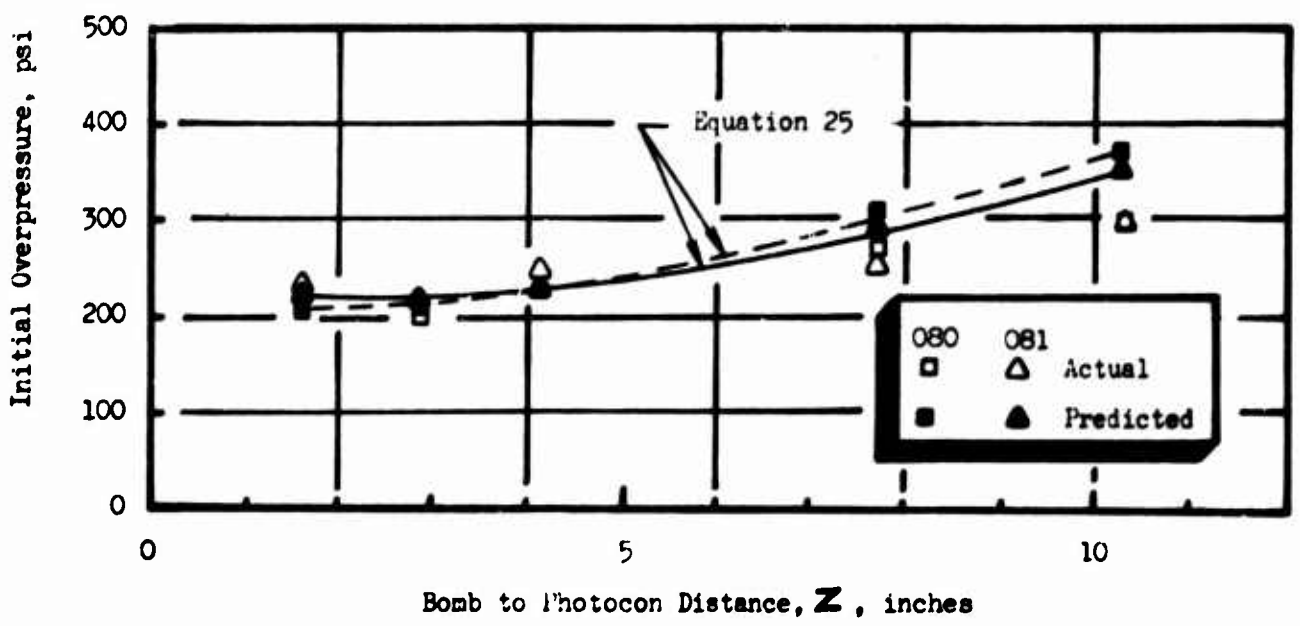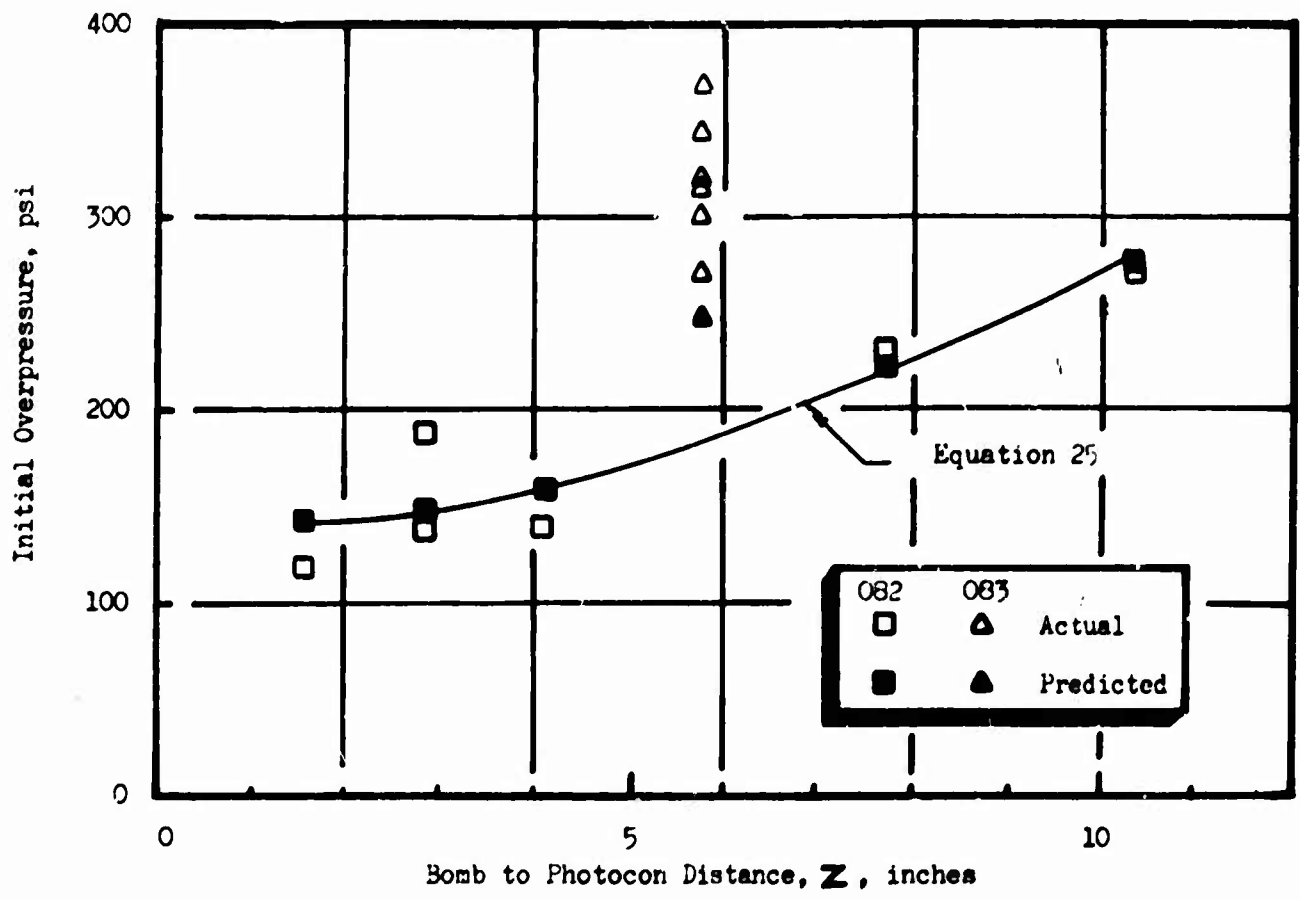
Figure 86. Demonstration Hot-Firing Results With Bombs
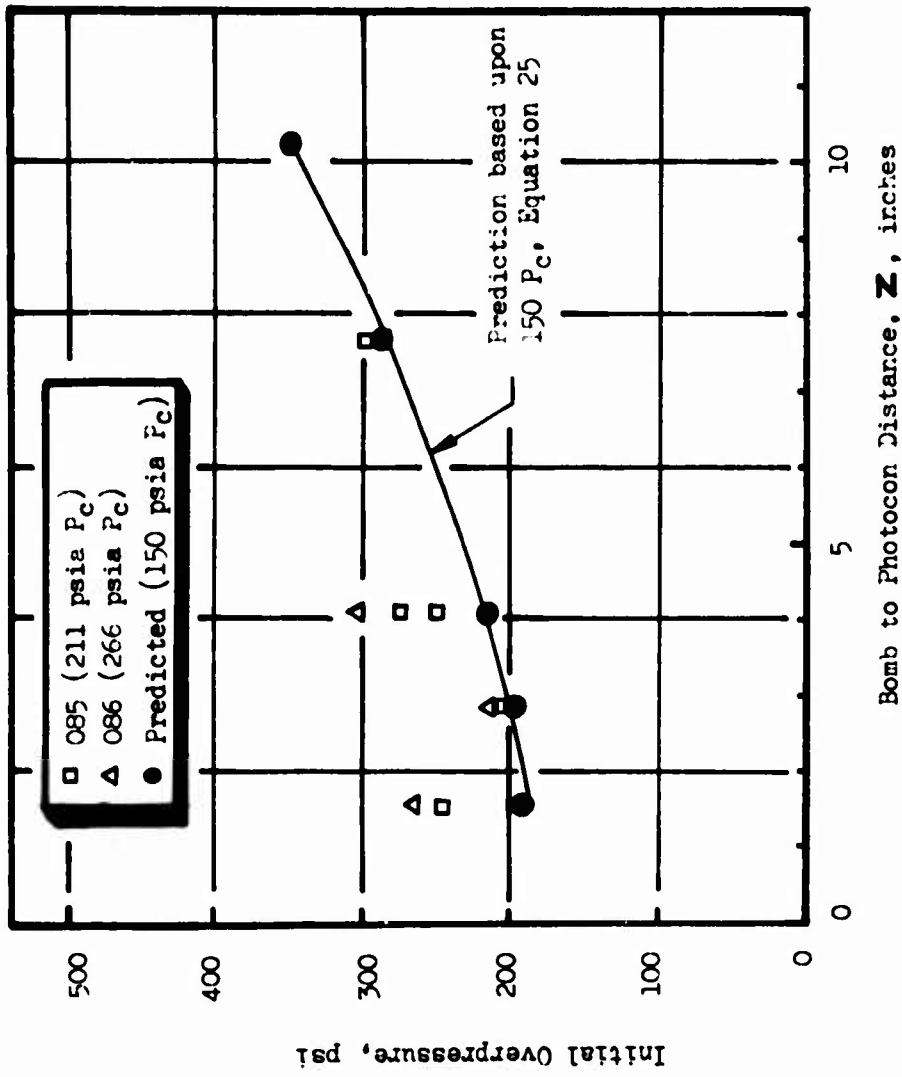
Figure 87. Demonstration Hot-Firing Results With Bomb at Elevated Chamber Pressures

236
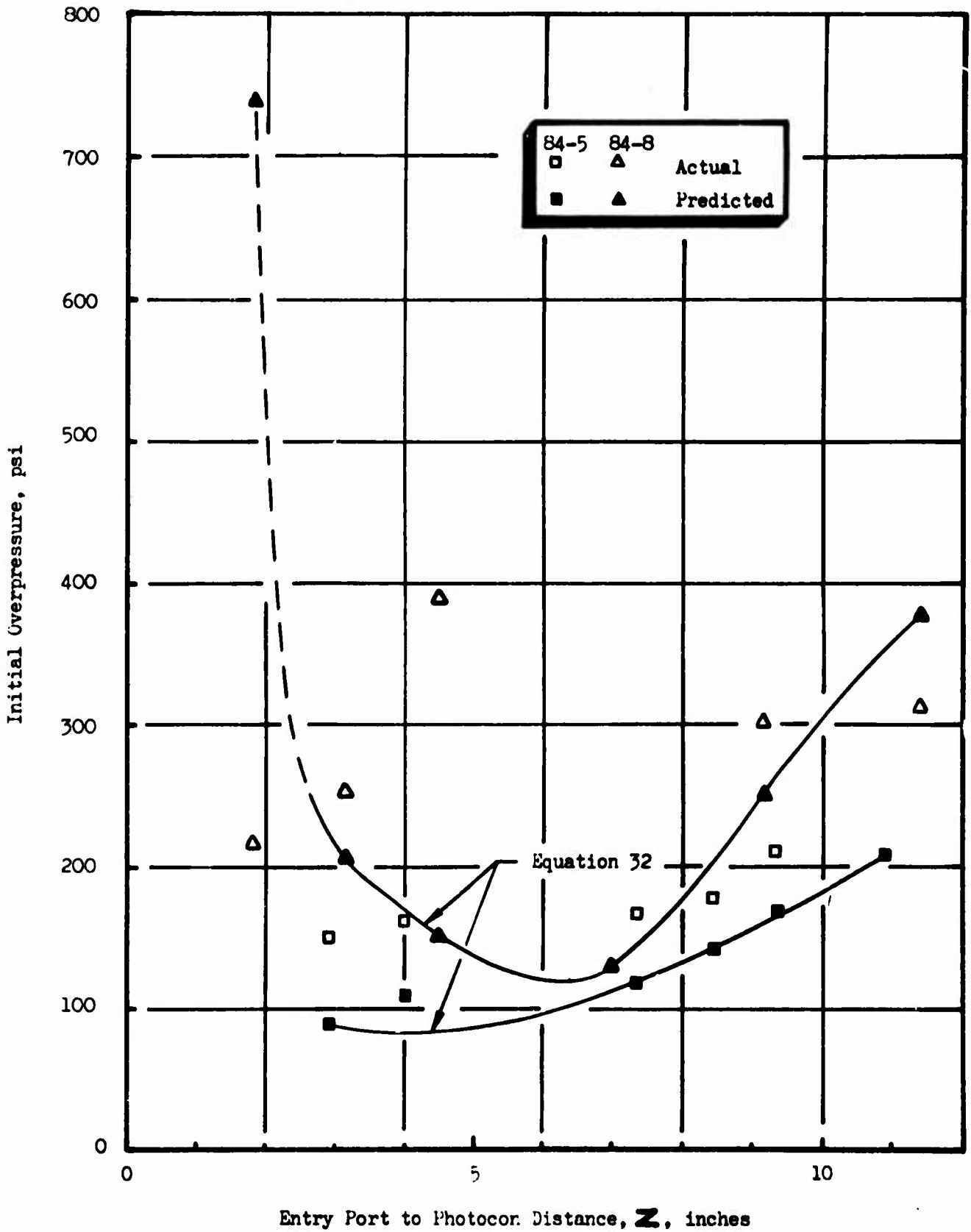
Figure 88. Demonstration Hot-Firing Results With Pulse Guns

237
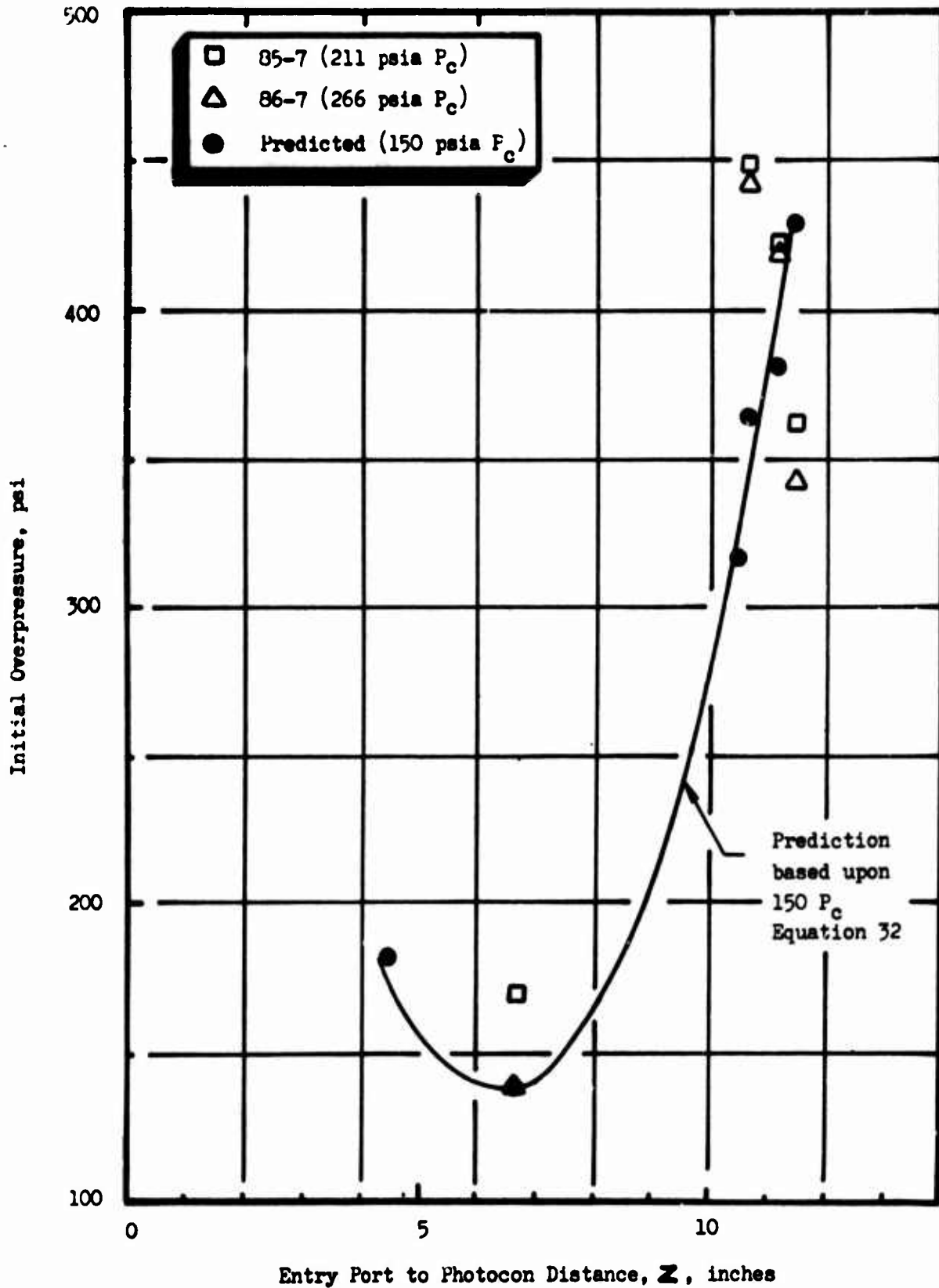
Figure 89. Demonstration Hot-Firing Results With Pulse Guns at Elevated Chamber Pressures

$$\text{Percent Error} = \frac{|\text{Predicted Value} - \text{Experimental Value}|}{\text{Predicted Value}} \quad (100)$$

These data are presented in Table 21.

The negative signs indicate that the predicted values of peak overpressure were less than the experimental values. Results from the first four tests with bombs are shown in Fig. 86 . The actual data obtained on tests 080, 081, and 082 were on the average, within 10.3 to 12.5 percent of the predictions. With a bomb (0.280-inch wall thickness) located at the chamber center for test 083, the percent error increased to 28.0 percent. The effects of chamber pressure upon the initial wave amplitudes are shown in Fig. 87 . In all instances the actual run values were higher than the predictions based upon 150-psia chamber pressure. The percent deviation from the correlation line, however, was not significantly higher than the data obtained for only changes in the bomb parameters. Thus, a clear trend is not indicated for the effect of chamber pressure upon the initial wave growth of the disturbance. (Refer also to Fig. 71.)

A larger data scatter was obtained for the pulse gun results as shown in Fig. 88 . The model is highly suspect below a z value of 2.60 inches. A data point at 4.50 inches for the -8 location (tangential) was considered in error and was not included in the average data. The average percent error for the -5 location (chordal) was 44.6 compared to only 19.8 for the -8. The more accurate prediction for the latter is probably due to the fact that only one pulse gun parameter was varied from those on which the correlation was based, i.e., axial distance. For test 084-5 both the axial distance and the pulse gun charge weight/diaphragm size were changed.

The effect of chamber pressure on the pulse gun initial wave growth is shown in Fig. 89 . The actual data points were scattered about the 150-psia chamber pressure correlating line. No definite effect of chamber pressure on initial wave amplitude can be noted.

TABLE 21

DEMONSTRATION FIRING RESULTS

Test No.	Device	Percent Error in Prediction				
		$z = 2$ to 4	$z = 4$ to 7	$z = 7$ to 10	$z = 10$ to 11.5	Average
080	Bomb	9.1		10.8	17.6	12.5
081	Bomb	4.0	0	16.1	16.5	12.2
082	Bomb	5.5	13.2	-4.0	18.6	10.3
083	Bomb		-28.0			28.0
084-8	Pulse Gun	-22.2	-157.1*	-19.8	17.3	19.8
084-5	Pulse Gun	-58.9		-30.4		44.6
085	Bomb	-4.1	-22.0	-3.1		9.7
085-7	Pulse Gun		-23.2	-23.2	-5.1	14.1
086	Bomb	-8.1	-42.2	0		25.1
086-7	Pulse Gun		0		-10.5	10.5

*Data point not included in average value

COMPREHENSIVE COMPARISON OF RATING TECHNIQUES

The three combustion stability rating techniques investigated have been
found to affect the propellant spray combustion field in two fundamentally
different ways. The bomb and pulse gun techniques introduce, primarily,
finite amplitude pressure disturbances and their ratings reveal the com-
bustion field's pressure sensitivity. The gas flow technique, on the
other hand, primarily introduces flow velocity or propellant displacement
disturbances and its ratings are based on the combustion field's displace-
ment sensitivity. Such a fundamental distinction has often been alluded
to but, prior to this program, the two fundamental effects had not been
shown to be separable and independent.

The N_2O_4/N_2H_4-UDMH(50-50) and N_2O_4/UDMH propellant combinations, under
the conditions tested, had no demonstrable displacement sensitivity.
As a result, the gas flow rating technique was at a great disadvantage
in this comparative program. With other propellant combinations (or
perhaps at other conditions), displacement sensitivity may be an important
contributor to initiation of combustion instabilities and the gas flow
technique thus may be a valuable investigative tool. Discussions in-
cluded in this section of the gas flow technique's effectiveness and re-
peatability are based, therefore, on previous experience with LOX/RP-1
propellants.

The flow of explosion products that follows the initial blast wave out
of the pulse gun's barrel may be thought to make this rating device one
that acts upon both the pressure sensitivity and displacement sensitivity.
The flow of explosion product gases, however, persists no longer than the
positive pressure duration. That characteristic was seen in the cold-flow
studies to be of the order of a millisecond for the pulse guns. While
this is about three times longer than the bombs' positive pressure dura-
tions, it is one to two orders of magnitude shorter than the initiation
of flow to initiation of instability typically observed with the gas
flow rating technique. It seems likely, therefore, that the pulse gun
and bomb techniques both fulfill the singular role of pressure disturbance
sources.

241

COMPARISON OF MERITS AND LIMITATIONS

The three rating techniques are critically compared in this section in
terms of specific individual attributes. When a single attribute is
considered, one technique may appear to exhibit distinct advantages over
the other techniques. In order to arrive at a choice of the technique(s)
to be used for a particular rocket engine rating, however, merits and
limitations in terms of all the attributes must be taken into account.
A listing of merits and limitations is given in Table 22 to place the
following in sharper perspective.

Applicability and Physical Size

The rating technique attribute termed applicability is concerned with
the suitability of the technique for a particular engine rating. Questions
concerned with the length of the projected test series, time available
for preparations, the physical size of the rating device, the type of
combustion chamber to be rated, potential engine damage, and the devices'
external and internal engine access requirements must be considered.

If the projected test series is necessarily short, the gas flow rating
technique's potential for obtaining comparative ratings in a very few
tests may be important. Again, however, its use is restricted to pro-
pellants and conditions exhibiting displacement sensitivity. The pulse
gun, similarly, can potentially supply ratings in a limited number of
tests through use of several graduated size charges fired sequentially
during each test. The requirement of a separate chamber access port may
impose a limitation on how rapidly the rating may be obtained. By con-
trast, only a single bomb can usually be scheduled for use in each test
because of the likelihood that a few cycles of wave motion induced by
one bomb would dislodge any additional bombs.

Concerning time available for preparation before a rating program is
to begin, the techniques would normally be ranked: bombs, pulse guns,
gas flows. Bombs can be prepared quite quickly because they require

TABLE 22

MERITS AND LIMITATIONS OF RATING TECHNIQUES

	Bombs	Pulse Guns	Gas Flows
Merits	Rate pressure sensitivity Best correlated technique Small size Minimum external access required Wants permit many positions from a port Best access for regeneratively cooled combustion chambers Materials readily available at modest cost Position versatility, i.e., not restricted to wall Disturbances are nondirectional	Rate pressure sensitivity Charges protected from heat Multiple guns per test possible Charges not fired in a test are not discarded Precise fire control (timing) Modest size Directionality permits forcing particular modes Handling hazards are minimized No chamber flow disruption	Rate displacement sensitivity Potential for quick rating in a few tests Does not disrupt chamber flow Limited hazard to chamber (no shrapnel) Possibility of chemical effects Precise control Good reproducibility Limited handling hazards
Limitations	Shrapnel damage to engine parts Initiation needs electrical circuit with external access May disrupt normal chamber flow Heat transfer to case may change structural and explosive characteristics Liable to thermal detonation Subject to structural failure; limited to one per test Orientation affects sensitivity Hazardous to handle Must dispose of live bombs not exploded during a test Possibility of ejecting live bombs from chamber	Requires access to positions external to engine Multiple bosses are required for multiple pulses or varying locations Limited to chamber wall applications Limited availability of some components Complex wave form is produced Poor reproducibility (cold flow) Ports may affect stability as acoustic cavities	Does not rate pressure sensitivity Not known to simulate natural triggering mechanisms Multiple bosses required for varying location Limited to chamber wall application Extensive supply and flow control system may be required Large quantities of gas may be needed for triggering Ports may affect stability as acoustic cavities

243

minimal amounts of simple machining operations and they are constructed of readily available materials; preparing the combustor to receive tnem may require the longest time. Preparation of pulse gun equipment requires somewhat longer times than bombs. More complex machining operations and case hardening processes are used in fabricating a pulse gun. Further, the burst diaphragms required may not be immediately available. (Some of the orders placed during this program were delivered in six to eight weeks.) An adequate gas flow system may be the slowest prepared because an extensive gas supply system and the attendant flow control systems are needed even before calibration tests can begin.

The rating devices' physical size is important in relationship to the external and internal engine access required. The gas flow apparatus is certainly the largest of the techniques but it usually can be mounted in some unobtrusive location within a few feet of the combustor. Its only required connection to the engine is usually a simple flow line which, unless the flow entry point is varied from test to test, does not require continuous accessibility. Bombs and pulse guns, on the other hand, must be removed from the combustor and rebuilt after each test. This requires that each entry port be readily accessible from the outside of the engine, a requirement which may severely limit selection of application points and the number of pulse guns that may be used. If there is good access to the inside of the combustor, external access problem for bombs may be avoided by installing them inside the chamber. Minimum external access for making electrical connections is then needed.

With regeneratively cooled combustion chambers, installation of rating technique application ports may be very difficult, very expensive or even prohibited. Bombs enjoy clear advantages over the other devices in this regard. As just noted, they may be mounted wholly within the combustion chamber with only an electrical connection port required. (Even the electrical connection may be eliminated if thermal initiation and its random variation in explosion time are acceptable.) Further, some variation in bomb chamber position can be achieved from an individual attachment point by means of extension wands.

244

Bombs in regeneratively cooled combustions chambers have a distinct disadvantage, however, in that their shrapnel may distort, or even penetrate and cause leakage from thin-walled structures. A similar potential for damaging injector components exists but it is usually not of as much concern as is regeneratively cooled wall damage. Other combustor damage potential comes from the disruption of the normal propellant flow paths. When any of the techniques is admitted through the chamber wall, increased turbulence may lead to wall melting or erosion downstream of the entry port. Again this may be minimized for bombs by mounting them on injector or baffle components and making the flow disruption a free-stream rather than a wall effect.

Effectiveness

How effective a rating device is for delineating a particular engine's instability traits depends, as has been seen, on the propellant combination, propellant injection pattern, combustor configuration and operating conditions. Additionally, there is strong dependency upon the devices' directionality (or lack of it) and versatility in the location of application.

The evaluation of a device's effectiveness may also vary from one application to another with differences in the rating goal. A greater effectiveness would surely be ascribed to pulse guns, for example, to be used for a study of tangential acoustic instability of an unbaffled injector than those used for general evaluation of any instabilities that might occur at a baffled engine's normal operating point. In the latter instance, a pulse gun might not effectively initiate baffle compartment or longitudinal acoustic resonances nor give any clues to a potential feed system coupled (chug or buzz) instability problem. (Only the effective initiation of wave motion within the chamber will be considered here.)

For general purpose stability investigations, bombs may be more effective than gas flows or pulse guns because of the nearly spherical, essentially

245

nondirectional pressure waves generated by bombs; this permits (conceivably at least) initiation of the longitudinal acoustic mode. In the current experiments, where no longitudinal mode was observed, radially directed pulse guns were apparently as effective as bombs positioned near the chamber wall and initiated the same standing acoustic modes. Chordally and tangentially directed pulse guns, however, nearly invariably initiated the spinning first tangential mode. While the ultimate stability appeared to be critically dependent upon the behavior of the first tangential mode, there was no evidence linking that effect preferentially to either the spinning or standing mode.

Direct initiation of the first radial acoustic mode occurred only with bombs mounted at the center of the combustion chamber, a strong pressure anti-node for that mode. Its initiation with bombs in other positions and pulse guns was indirect, i.e., by the third tangential mode, and appeared not to be related to the rating techniques. Again, the bomb technique's versatility in mounting locations gives it a clear advantage over the pulse guns, which are restricted to applications at the combustor's wall.

The gas flow technique is similarly limited to applications near the wall. This technique's effectiveness may be enhanced by using a gas that is chemically reactive with one or both propellants; this was not investigated in the current program.

The apparent advantages in effectiveness of bombs are lessened somewhat by the fact that bomb orientation did affect initial wave growth in this program. This suggests that bomb blast waves do have some directional characteristics.

Repeatability

Somewhat facetiously, it might be said that the gas flow method was the most repeatable of the rating techniques investigated--not very applicable, but consistent and repeatable. From previous studies, it is noted

246

that this technique has a reputation for precise control and good repro-
ducibility, e.g., ratings have been established with individual values
falling within about ±5 to 10 percent of the mean value.

Few replicate tests with the explosive devices were attempted in this
hot-firing program. Among five sets of replicate pulse gun firings,
four sets exhibited comparable initial wave amplitudes (within about ±10
percent) and the other gave completely conflicting data (i.e., only a
very low amplitude wave was produced in one case). With the exception
of that same set, the initial modes triggered were also duplicated.
Ultimate stability was duplicated in three of the five sets; in view of
the apparent lack of correlation of ultimate stability to the rating
techniques, this is perhaps surprisingly good repeatability. The fact
that the amplitudes of the initial waves were moderately well correlated
to the variations of pulse gun parameters is further evidence of reasonably
acceptable pulse gun repeatability.

Pulse gun repeatability appeared to be better in the hot-firing tests
than in cold-characterization experiments. It seems reasonable that im-
proving the device to reduce data scatter in the latter would also improve
the former as well. Another potential source of scatter in the hot-firing
tests was that the burst diaphragms were exposed to heat transfer from
the combustion gases for varied lengths of time and may have undergone
changes in their burst pressures.

That the initial pressure wave amplitudes produced by bombs were corre-
lated even more closely to the bomb parameters than those from pulse guns
is convincing evidence of bomb repeatability. They were also quite con-
sistent in the initial modes of instability induced. The correlations
were based on averages, however, and each average value represented some
degree of scatter. An indication of repeatability was given by several
bombs mounted at the center of the chamber. Depending upon the charge
weight, some random variations in amplitude were observed among the
pressure transducers in each test and from test-to-test that were not

apparently related to the injector pattern. This was believed to be a result of non-uniform case rupture; fabrication variability, such as eccentric or off-center cavities in the cases, or operational variability, such as asymmetric heating (softening) or ablation, might be the cause.

It is apparent from the foregoing that repeatability was not very well established in this program but that it was not so poor for either pulse guns or bombs as to represent a major obstacle to fulfilling the program objectives.

Reliability

Gas pulse technique reliability is determined primarily by the reliability of the electronic and servo control systems for producing the desired flowrate-time function. With the full servo control of flowrate system used in the hot-firing program, non-linear ramps were produced in two of eleven tests, an inordinately high 18 percent. That system was used as an expedient; for considerably greater versatility and essentially complete reliability, the indirect flow control using the function generator is preferred.

The protective case design for explosive bombs has a strong influence on bomb reliability. Being mounted within the combustion chamber, bombs are subjected to the high temperature environment and if the case is too thin, may be prematurely detonated due to thermal sensitivity of the explosive charge. Only one instance of thermal detonation occurred in this test series but it has been common enough in other programs that it is some-times relied upon for bomb initiation when routing of lead wires out of the chamber has appeared particularly inconvenient or difficult. Internal mounting also exposes bombs to the stresses of transverse combustion gas flow and any pressure wave motion within the combustor. This has usually meant that only one bomb could be used in each test because the first sequenced bomb is likely to break or dislodge any others. Structural failure of a single bomb (e.g., by a brief disturbance such as a transient instability during the engine start sequence) could then mean that no bomb rating data would be obtained from that test.

248

Inadequate protection of detonator lead wires as they were routed out of the combustor caused three bombs to fail to detonate and another was aborted by a disconnected lead wire terminal. Thus, components throughout the bomb design and fire circuit affect its reliability.

By comparison, the pulse gun was found to be relatively trouble-free and reliable. Some difficulties were experienced in the cold-flow experiments with diaphragm leakage prior to its rupture and with firing pin jamming and breakage. These problems were overcome by devoting more careful attention to tightening and cleaning operations and were not experienced during the hot-firing tests. The burst diaphragms apparently offer adequate protection to the explosive charges; no problem with thermal initiation was experienced.

Handling Characteristics

Some discussion pertinent to the handling characteristics of each rating device has been given earlier. The relative effort required to effect changes or replacement between tests and the hazards associated with each technique are discussed briefly here.

Once the basic flow system has been installed for the gas pulse apparatus, very little additional handling is required. The only test hardware preparation consists of relocating the connecting line between the control valve and the appropriate chamber boss. The operation of the device, however, requires additional preparation. This includes the manipulation of numerous valves and the pressurization of the source tank to the desired valve. Other than personnel association with high pressure gas systems, no particular hazard is associated with the gas pulsing equipment.

The bomb and pulse gun devices both contain small amounts of high explosives. Safety with explosives requires knowledge of the hazards involved and rigid adherence to the proper methods of performing each function. The greatest hazards to be guarded against are stray currents, static

electricity, frictional heat, impact and carelessness. Pulse guns are less hazardous than bombs because the cartridge-loaded charges and the unidirectional blast make it easier to avoid direct personal exposure.

Following a hot-firing test, any bombs that have not been detonated must be disposed of immediately. Extra precautions are called for because of the potentially higher sensitivity of explosives that have been heated; this work should be performed by personnel specifically trained in explosives disposal techniques. Residual pulse gun charges, on the other hand, may simply be returned to storage and used in a subsequent test (unless there is external evidence of excessive heating of the pulse gun assembly).

Another hazard associated with bombs is the possibility that one may be dislodged and ejected from the combustion chamber as a live bomb. This is even more hazardous than having a residual bomb in the combustor; personnel may be completely unaware of its presence and so may unwittingly detonate it without benefit of protective equipment. Periodically, the test area should be searched thoroughly and a specific search should be conducted whenever there is not positive evidence that a bomb actually detonated in the combustor.

RATING TECHNIQUE SELECTION FOR CURRENT USAGE

From the foregoing comparisons, it is apparent that there is not a single stability rating technique that is universally applicable, effective, reliable, etc., for use in any and all engine rating studies. Rather, the particular engine, with its particular injection pattern, combustor geometry and propellant combination, must be considered in terms of the various rating devices' characteristics and attributes and a particular single device (or combination of devices) selected for use.

The choice of a rating technique is also influenced by the goals established for the rating program. From previous experience, for example,

it may be well known that an engine is especially sensitive to one par-
ticular acoustic mode of instability. A short rating program's goal
might well be an evaluation of how that sensitivity is affected by a
change in injection pattern (or by an acoustic liner or baffle assembly).
The rating device that is best suited to initiation of that particular
mode of instability would probably be selected, even though another tech-
nique might initiate more and other modes with better repeatability or
reliability.

Another rating program might have as its goal the establishment, with
reasonable assurance, that no destructive instabilities can be initiated
within the engine's normal operating range. The rating technique selected
might then be a complementary combination of devices, utilizing both bombs
and pulse guns. For a cylindrical chamber, this should certainly include
tangentially directed pulse guns, bombs at the chamber's axis and bombs
near the exhaust nozzle. For other chamber configurations, there may be
other specific modal triggering requirements to account for by combina-
tions of rating techniques.

This latter example fits in the category of dynamic stability evaluation
or demonstration. Among the rating techniques, there exist today suffi-
cient versatility and range of experience to accomplish such ratings
rapidly and efficiently. It appears that such ratings may best be
accomplished by making more use of complementary combinations of rating
techniques.

RECOMMENDATIONS FOR IMPROVED RATING TECHNIQUE

It has been shown in this study that certain of the parameters and charac-
teristics of explosive bombs and pulse guns can be quantitatively corre-
lated with some aspects of the stability response of an operating liquid
rocket combustor to them. Each of the rating techniques has been found
to have specific advantages and limitations; some minor design changes
should be investigated as means of enhancing the advantages and reducing
the limitations. It does not now appear that such improvements will
advance either device to a position of general applicability. For that
reason, it is recommended that some alternate devices be designed to
incorporate as many of the advantages and as few of the limitations of
the existing rating techniques as possible and evaluated in terms of
the attributes required of a generally applicable rating technique.

Additional Correlations

Somewhat expanded statistical correlations of the data obtained in this
program might include the effects of pulse gun initial shock wave amplitude,
effects of powder burning rate, and effects of improved models for the
wave incidence coefficient at each transducer. Some additional data
would be required to ensure statistical significance; e.g., small bombs,
bombs closer to the injector and pulse guns farther from the injector.
Detailed spectral analysis could conceivably give initial mode of insta-
bility data for quantitative correlation to the initial wave information.
The validity and value of the results would be enhanced greatly if a por-
tion of the additional experimental data correlated were obtained from
another program, such as those conducted in recent years at AFRPL.

Improvements for Bombs and Pulse Guns

Bombs would be considerably more useful if their reliability were improved. In particular, their susceptibility to thermal detonation and physical failure under stress need to be eliminated. The possibility of using more than one bomb per test and of reliable scheduling of the explosion are highly desirable goals. Simultaneously, however, the potential for chamber damage should be reduced by designing the case to produce less shrapnel. Finally, if the bomb is to be a truly non-directional disturbance, the directional effects introduced by the cylindrical charge design should be investigated and eliminated.

Pulse guns should be improved by determining and correcting the causes of the excessive variability in pressure amplitude and impulse among replicate charges observed in the cold-flow tests. Means could also be determined for eliminating the complex wave form and providing a single, clean pressure wave. Better correlations might be obtained if the pressure wave amplitude just outside the muzzle of the gun were determined; the streak photographic techniques used in the current bomb characterization should be directly applicable here.

Investigation of Other Rating Technique Concepts

By combining the beneficial attributes of the various rating techniques, several candidate rating systems can be conceived, one or more of which might be developed into a single device with universal applicability. In the preceding section, it was recommended that a combination of bombs and pulse guns be used for general stability rating and that the combination be selected by considering the characteristics of the engine system to be rated. Perhaps this is too permissive; continued investigation might show that one particular combination is adequate for general rating use. In that case, a single integrated design should be developed.

The possibility of bringing the gas flow technique back into the picture by initiating its flow with a high amplitude shock wave is intriguing. Both pressure sensitive and displacement sensitive mechanisms would be perturbed. The shock wave could be provided by mechanically rupturing a diaphragm sealing a prepressurized high pressure gas from the chamber or by simply plumbing the gas flow through a modified pulse gun.

Another concept worthy of investigation is the repetitive generation of pressure pulses, perhaps by a chemically fueled shock or detonation tube, to establish ratings based on the minimum sensitivity that occurs in a given time interval as opposed to the instantaneous sensitivity at the instant of detonation of a single charge.

Finally, means of achieving the versatility in chamber position now available for bombs need to be developed so that the improved, more generally applicable devices may, indeed, be applied more generally.

APPENDIX A

THE APPLICATION OF STATISTICAL CORRELATION ANALYSIS

In applying multiple correlation or regression methods, one begins by
listing potentially important independent variables, each suitably quan-
tified. Dependent variables or responses are selected which describe the
physical process under investigation as completely as possible. Then from
previous experimental experience, knowledge of underlying physical prin-
ciples, or judicious application of physical intuition, one hypothesizes
specific algebraic forms or models relating each dependent variable with
the independent variables. The parameters of these models (i.e., the
coefficients and exponents in the algebraic expressions) are generally un-
known, however, and it is the basic purpose of the statistical correlation
to obtain best estimates for these parameters.

Generally speaking, a satisfactory model is one which can account for
most of the variation in the dependent variable. It should include only
those functions of the independent variables which have importance in
describing the dependent variable. When such a model has been determined,
it is possible to describe past test results from a quantitative point
of view and, in addition, make statistically qualified estimates of the
behavior of the dependent variable for any combination of the independent
variables within the general test ranges.

More specifically, two distinct types of models have been developed and
reported in the course of this program. The first, which might be called
descriptive models, are designed to fit the available data as well as
possible. Descriptive equations generally contain many terms, any one
of which may have only a small effect, in order to model well the peculi-
arities of a particular data set. The criterion for the inclusion of a
specific term is whether it will help, rather than hurt, the fit. Such
models may therefore contain terms which appear to be meaningless or of
the wrong sign on physical grounds, but which do serve to reduce a
certain amount of variation in the data. If one is interested in

255

predicting the future performance of the same system from which the
original data set is obtained, and if no extrapolation is made beyond
the original ranges of the independent variables, then such a model is
probably the most useful for prediction. It is sure to contain all the
really important effects, even though they be small.

The second class consists of what we will call interpretive models. A
term is included in such a model only if the evidence of its reality is
overwhelming in a statistical sense. Statistical methods called tests
of hypotheses are generally used to assess the significance of terms in
such models. If one wishes to generalize the results of experimental
work to different systems or to extrapolate the results on the same
system, such models should be used. Only those terms which are sure to
be real should be employed; for example, one will often avoid the "whiplash"
effect caused by extrapolating on the basis of spurious curvature terms.

All the correlations determined in this program were obtained by using
the Rocketdyne Stepwise Regression Routine, a computer program for which
a card deck is on file at Rocketdyne's computer facility. This program
can be used for any model which either is linear or some transformation
of it is linear in the unknown parameters. By a stepwise procedure
functional variables are added or deleted until a final multiple linear
regression equation is obtained. This model will include only those
functional variables which have a significant effect on the dependent
variable. By specifying in advance the confidence levels used to include
or delete terms, one can obtain either a descriptive or interpretive
correlation.

To determine whether a useful correlation has been obtained, the multiple
correlation coefficient is evaluated. The square of this index is the
fraction of the total variation in the dependent variable which has been
accounted for by the independent variables using the chosen model. For
example, a coefficient of 0.8 indicates that 64 percent of the variation
can be attributed to the variables used in the model. The other 36 percent
may be identified with other variables not included in the analysis, in-
consistencies in the data, a poor choice of the original model, and/or

256

simply "random error." The maximum value of this coefficient is unity
which corresponds to perfect correlation. Thus a correlation coefficient
close to one indicates that the correlation is of significant practical
value.

The model predictions should not differ greatly from the corresponding
observed values. A measure of these deviations is given by the standard
error about the fit or residual standard deviation. This is defined as
the root mean square of the deviations of the actual data from this pre-
diction based on the model, with an adjustment factor depending on the
number of terms in the model. When the logarithm of the response is used
as the dependent variable then the standard error is roughly the percent
error in the response. Thus, if the standard error for ln y is 0.05,
then the deviations between observed values and predicted values of y
are approximately 5 percent.

NOMENCLATURE

a, A, b, B, c, d, e, f	=	arbitrary constants
A	=	area, sq in.
BL	=	pulse gun barrel length, inch
c^*	=	characteristic exhaust velocity, ft/sec
c_s	=	shock or blast wave velocity, ft/sec or in./microsec
$(c_s)_o$	=	initial value of c_s at the blast source
c_o	=	velocity of sound in the undisturbed medium, ft/sec or in./microsec
d	=	duration of gas flow ramp, sec
D	=	diameter, inch
$\exp[\ ]$	=	$e^{[\ ]}$ where e = 2.71828 (base for Naperian logarithms)
F	=	a correlating parameter for fuel type, Table 19
I	=	impulse, lbf-sec or lbf-microsec
I_u	=	unit impulse, psi-sec or psi-microsec
ℓ	=	axial distance from the injector face to the centerline of a rating device, inch
L	=	length of a cylindrical explosive charge, inch
L/D	=	length to diameter ratio of a cylindrical explosive charge
M	=	shock or blast wave Mach number $(= c_s/c_o)$
P	=	pressure, psia
P_b	=	back pressure downstream of a pulse gun, psig
P_o	=	initial pressure in the undisturbed medium, psia
PT	=	explosive powder type correlating parameter
ΔP	=	shock or blast wave overpressure, psi
r	=	radial position, inch (Fig. 63)
R	=	radius, inch or feet
t	=	time, sec or microsec

259

Δt	=	time interval or duration, sec or microsec
T_+	=	duration of the positive pressure portion of a blast wave, sec or microsec
T_c	=	bomb case thickness, inch
V	=	velocity, ft/sec
V_T	=	surge tank volume, ft^3
$\dot{w}$	=	weight flowrate, lbm/sec
W	=	explosive charge weight, grains or pounds
x	=	axial distance from the injector face to the centerline of a pressure transducer, inch
X	=	axial distance from pulse gun diaphragm to the centerline of a pressure transducer, inch
y	=	projected transverse distance between the centerline of a bomb and a pressure transducer, in (Fig. 63)
z	=	straight line distance between the center of a bomb charge and a pressure transducer, inch (Fig. 63)
Z	=	blast wave correlating parameter ($= RW^{-1/3}$)

Greek Symbols

α	=	approximate angle of blast wave incidence on a pressure transducer (Fig. 63)
β	=	angle between pulse gun's centerline and the chamber radius which intersects it at the chamber wall
γ	=	ratio of specific heats (c_p/c_v) for air or combustion gases
ρ	=	density, lbm/ft^3
θ	=	projected angle between combustion chamber radii which intersect the pulse gun's centerline at the wall and intersect the center of a pressure transducer (measured in the pulse direction)

Subscripts

numeral	=	value of a parameter at that distance, in inches, from a blast source
b	=	value for a base explosive charge
c	=	value for an explosive charge
d	=	value for an explosive detonator
db	=	value for a burst diaphragm
f	=	final value
gun	-	value for a pulse gun (barrel)
i	=	initial value
inj	=	injection value or at the injector
max	=	maximum value
n	=	value at the nozzle inlet
ns	=	nozzle stagnation conditions value
R	=	value at a radial distance from a source
t	=	value at the nozzle thrust
+	=	positive value

REFERENCES

1. Goodman, H. J.: <u>Compiled Free-Air Blast Data on Bare Spherical Pentolite</u>, Report No. 1092, Ballistic Research Laboratories, 1960.

2. Ruetenik, J. R. and S.D. Lewis: <u>Pressure Probe and System for Measuring Large Blast Waves</u>, Massachusetts Institute of Technology, Cambridge, Massachusetts, Technical Report AFFDL-TDR-65-35, June 1965.

3. Savit, J. and R. H. F. Stresau: <u>J. Appl. Phys.</u>, Vol. 25, 1954, 89.

4. <u>An Experimental Investigation of Combustion Stability Characteristics at High Chamber Pressure</u>, Interim Report 11741-I, Aerojet-General Corp., Sacramento, California, September 1965.

5. Peoples, R. G. and P. D. Baker: <u>Stability Rating Techniques</u>, WSS/CI Paper No. 64-11, Western States Section, The Combustion Institute, 1964 Spring Meeting, Stanford University, Palo Alto, California, April 1964.

6. Combs, L. P.: "A Summary of Experience With Combustion Stability Rating Techniques," <u>ICRPG Second Combustion Conference, Volume 2</u>, CPIA Publ. No. 105, Chemical Propulsion Information Agency, Silver Spring, Maryland, May 1966.

DOCUMENT CONTROL DATA · R&D

(Security classification of title, body of abstract and indexing annotation must be entered when the overall report is classified)

1. ORIGINATING ACTIVITY (Corporate author)	2a. REPORT SECURITY CLASSIFICATION
Rocketdyne, a Division of North American Aviation, Inc., 6633 Canoga Avenue, Canoga Park, California	UNCLASSIFIED
	2b. GROUP

3. REPORT TITLE

COMBUSTION STABILITY RATING TECHNIQUES

4. DESCRIPTIVE NOTES (Type of report and inclusive dates)

5. AUTHOR(S) (Last name, first name, initial)

Combs, L. P., Hoehn, F. W., Webb, S. R.

6. REPORT DATE	7a. TOTAL NO. OF PAGES	7b. NO. OF REFS
September 1966	296	6

8a. CONTRACT OR GRANT NO.	9a. ORIGINATOR'S REPORT NUMBER(S)
AF04(611)-10811	R-6355-4
b. PROJECT NO. 3058	
c.	9b. OTHER REPORT NO(S) (Any other numbers that may be assigned this report)
d.	AFRPL-TR-66-229

10. AVAILABILITY/LIMITATION NOTICES

This document is subject to special export controls and each transmittal to foreign governments or foreign nationals may be made only with prior approval of AFRPL (RPPR/STINFO), Edwards, California 93523

11. SUPPLEMENTARY NOTES	12. SPONSORING MILITARY ACTIVITY
	Air Force Rocket Propulsion Laboratory Research and Technology Division Edwards, California

13. ABSTRACT

The objectives of a comprehensive investigation of three techniques for rating the combustion stability of liquid-propellant rocket engines were the establishment of the characteristics of the techniques and of their intercorrelations. The techniques studied were: (1) nondirected explosive bombs, (2) directed explosive pulse guns, and (3) directed flows of inert gases. Characterization was accomplished through cold-flow experiments; each rating device's output pressure, impulse, velocity, etc., were quantitatively correlated to variations of its descriptive parameters, e.g., explosive charge weight, explosive type, burst diaphragm strength, bomb case thickness, etc. Correlations among techniques were sought by applying them at various positions and directions to an operating rocket and measuring the combustor's stability response. Two different propellant injectors were tested with N_2O_4/N_2H_4-UDMH (50-50) propellants; one of the injectors was tested with N_2O_4/UDMH propellants. It was discovered that combustion with these propellants and operating conditions is insensitive to transverse velocity or displacement perturbations; the gas-flow technique initiated no chamber pressure disturbances. However, considerable sensitivity to pressure disturbances from bombs and pulse guns was observed. The combustor's ultimate stability following a pressure perturbation could not be correlated to either bomb or pulse gun parameters or characteristics; recovery to stable operation occurred randomly. The amplitude of the initial pressure wave was correlated quantitatively to both the rating devices' parameters and characteristics.

DD FORM 1473 JAN 64

14. KEY WORDS	LINK A		LINK B		LINK C	
	ROLE	WT	ROLE	WT	ROLE	WT
Rocket Engines Injectors Combustion Stability Rating Techniques Explosive Bombs Explosive Pulses Cold-Flow Testing						

INSTRUCTIONS

1. **ORIGINATING ACTIVITY:** Enter the name and address of the contractor, subcontractor, grantee, Department of Defense activity or other organization (corporate author) issuing the report.

2a. **REPORT SECURITY CLASSIFICATION:** Enter the overall security classification of the report. Indicate whether "Restricted Data" is included. Marking is to be in accordance with appropriate security regulations.

2b. **GROUP:** Automatic downgrading is specified in DoD Directive 5200.10 and Armed Forces Industrial Manual. Enter the group number. Also, when applicable, show that optional markings have been used for Group 3 and Group 4 as authorized.

3. **REPORT TITLE:** Enter the complete report title in all capital letters. Titles in all cases should be unclassified. If a meaningful title cannot be selected without classification, show title classification in all capitals in parenthesis immediately following the title.

4. **DESCRIPTIVE NOTES:** If appropriate, enter the type of report, e.g., interim, progress, summary, annual, or final. Give the inclusive dates when a specific reporting period is covered.

5. **AUTHOR(S):** Enter the name(s) of author(s) as shown on or in the report. Enter last name, first name, middle initial. If military, show rank and branch of service. The name of the principal author is an absolute minimum requirement.

6. **REPORT DATE:** Enter the date of the report as day, month, year; or month, year. If more than one date appears on the report, use date of publication.

7a. **TOTAL NUMBER OF PAGES:** The total page count should follow normal pagination procedures, i.e., enter the number of pages containing information.

7b. **NUMBER OF REFERENCES:** Enter the total number of references cited in the report.

8a. **CONTRACT OR GRANT NUMBER:** If appropriate, enter the applicable number of the contract or grant under which the report was written.

8b, 8c, & 8d. **PROJECT NUMBER:** Enter the appropriate military department identification, such as project number, subproject number, system numbers, task number, etc.

9a. **ORIGINATOR'S REPORT NUMBER(S):** Enter the official report number by which the document will be identified and controlled by the originating activity. This number must be unique to this report.

9b. **OTHER REPORT NUMBER(S):** If the report has been assigned any other report numbers (either by the originator or by the sponsor), also enter this number(s).

10. **AVAILABILITY/LIMITATION NOTICES:** Enter any limitations on further dissemination of the report, other than those imposed by security classification, using standard statements such as:

(1) "Qualified requesters may obtain copies of this report from DDC."

(2) "Foreign announcement and dissemination of this report by DDC is not authorized."

(3) "U. S. Government agencies may obtain copies of this report directly from DDC. Other qualified DDC users shall request through
_____."

(4) "U. S. military agencies may obtain copies of this report directly from DDC. Other qualified users shall request through
_____."

(5) "All distribution of this report is controlled. Qualified DDC users shall request through
_____."

If the report has been furnished to the Office of Technical Services, Department of Commerce, for sale to the public, indicate this fact and enter the price, if known.

11. **SUPPLEMENTARY NOTES:** Use for additional explanatory notes.

12. **SPONSORING MILITARY ACTIVITY:** Enter the name of the departmental project office or laboratory sponsoring (paying for) the research and development. Include address.

13. **ABSTRACT:** Enter an abstract giving a brief and factual summary of the document indicative of the report, even though it may also appear elsewhere in the body of the technical report. If additional space is required, a continuation sheet shall be attached.

It is highly desirable that the abstract of classified reports be unclassified. Each paragraph of the abstract shall end with an indication of the military security classification of the information in the paragraph, represented as (TS), (S), (C), or (U).

There is no limitation on the length of the abstract. However, the suggested length is from 150 to 225 words.

14. **KEY WORDS:** Key words are technically meaningful terms or short phrases that characterize a report and may be used as index entries for cataloging the report. Key words must be selected so that no security classification is required. Identifiers, such as equipment model designation, trade name, military project code name, geographic location, may be used as key words but will be followed by an indication of technical context. The assignment of links, rules, and weights is optional.